

**STABILIZATION OF BENTONITE AND KAOLINITE CLAYS
USING RECYCLED GYPSUM AND LIQUID SODIUM SILICATE**

by

Mehmet Sagnak

A thesis submitted to the Faculty of the University of Delaware in partial fulfillment of the requirements for the degree of Master of Civil Engineering

Winter 2018

© 2018 Mehmet Sagnak
All Rights Reserved

**STABILIZATION OF BENTONITE AND KAOLINITE CLAYS
USING RECYCLED GYPSUM AND LIQUID SODIUM SILICATE**

by

Mehmet Sagnak

Approved: _____
Christopher L. Meehan, Ph.D.
Professor in charge of thesis on behalf of the Advisory Committee

Approved: _____
Sue McNeil, Ph.D.
Chair of the Department of Civil and Environmental Engineering

Approved: _____
Babatunde A. Ogunnaike, Ph.D.
Dean of the College of Engineering

Approved: _____
Ann L. Ardis, Ph.D.
Senior Vice Provost for Graduate and Professional Education

ACKNOWLEDGMENTS

Firstly, I would like to express my profound gratitude to my advisor Prof. Christopher L. Meehan for his intellectual suggestions, kind guidance, supports, and encouragements in the classes and this research.

I want to thank faculty members at the Department of Geotechnical Engineering who entitled my engineering skills by teaching advanced solution techniques regarding the geotechnical engineering problems.

I cannot resist expressing one of the special thanks to Turkish government, the Ministry of Education, and particularly General Directorate of State Hydraulic Works “DSI” for their financial support, and all the members of DSI who have solved all problems once I have faced during my education at the University of Delaware. Thanks to their efforts, my dream is to become true.

I would like to express my appreciations to my officemates, and friends, Cenk Demir, Ahmet Ates, Mesut Karakoc, Bora Karanfil and Turkish community members living in Newark for their priceless supports, delicious dinner events and camping activities organized by H. Turgut Guclu, East Coast Turkish Association president.

I am greatly indebted to my family including my cousin, Vedat Aybar, and his family for their boundless supports and encouragements that help me every step during my life.

The last, but not the least, so many thanks to Dr. Hatice Çilsalar who not only has become part of my life and miracle but also has made my life enjoyable. Thank you for your supports, endless love, and boundless smiles.

With all my love and gratitude,

To my country

To my family

And

To Hatice

“Science is the most reliable guide for civilization, for life, for success in the world. Searching a guide other than the science is meaning carelessness, ignorance, and heresy.”

Mustafa Kemal Atatürk
The Founder of Turkish Republic

TABLE OF CONTENTS

LIST OF TABLES	xi
LIST OF FIGURES	xii
LIST OF ABBREVIATIONS	xx
ABSTRACT	xxii

Chapter

1	INTRODUCTION	1
1.1	Soil Stabilization	1
1.2	Objectives	5
2	LITERATURE REVIEW	7
2.1	Methods of Soil Stabilization	7
2.1.1	Mechanical Soil Stabilization	7
2.1.2	Biological Soil Stabilization	8
2.1.3	Chemical Stabilization	8
2.2	Mechanism of Soil Stabilization	10
2.2.1	Cation Exchange	10
2.2.2	Flocculation and Agglomeration	12
2.2.3	Pozzolanic Reaction	12
2.2.4	Alkali Activated Geopolymerization	14
2.2.5	Stabilization Mechanism of Alkali Activated Geopolymers	15
2.3	Review of Soil Stabilization with Gypsum and Alkali Activation	25
2.3.1	An Overview of Recycled Gypsum and Sodium Silicate Stabilization	48
3	EXPERIMENTAL APPROACH	57
3.1	Soils and Stabilizers	57
3.1.1	Soils	57
3.1.1.1	Stabilizer Liquid Sodium Silicate	57
3.1.1.2	Recycled Gypsum	58
3.2	Macrostructural Soil Characterization	58

3.2.1	Moisture Content	58
3.2.2	Particle Size Distribution.....	58
3.2.3	Liquid Limit, Plastic Limit, and Plasticity Index	59
3.2.4	Classification of Soils for Engineering Purpose.....	59
3.2.5	Specific Gravity.....	60
3.2.6	Acidity/ Alkalinity (pH) Testing	60
3.2.7	Laboratory Compaction Testing.....	61
3.2.8	The Unconfined Compressive Strength Test.....	61
3.3	Microstructural Soil Characterization	62
3.3.1	X-Ray Fluorescence (XRF).....	62
3.3.2	X-Ray Diffraction, (XRD).....	62
3.3.3	FTIR-ATR Spectroscopy.....	64
3.3.4	FESEM/EDAX Analysis	65
3.3.5	N ₂ -BET Surface Area Analysis	65
3.4	Methods for Preparing and Testing Specimens.....	66
3.4.1	Process of Mixing Soil and Stabilizer	67
3.4.1.1	Soil and Stabilizer Mix Design.....	67
3.4.2	Curing Conditions	68
3.4.2.1	Curing Temperature and Humidity	68
3.4.2.2	Curing Time.....	69
3.4.3	Sample Preparation and Extraction Procedure for the Strength Testing	69
4	TEST RESULTS AND DISCUSSIONS	73
4.1	Material Characterizations.....	73
4.1.1	Soil Descriptions	73
4.2	The pH Test Results of Stabilized Soils	77
4.2.1	Bentonite Clay	78
4.2.1.1	Mixture of Recycled Gypsum and Bentonite	78
4.2.1.2	Mixture of Sodium Silicate solution and Bentonite	79
4.2.1.3	Mixture of Recycled Gypsum, Sodium Silicate Solution, and Bentonite	81

4.2.2	Kaolinite Clay.....	82
4.2.2.1	Mixture of Recycled Gypsum and Kaolinite.....	82
4.2.2.2	Mixture of Sodium Silicate Solution and Kaolinite	83
4.2.2.3	Mixture of Kaolinite, Recycled Gypsum and Sodium Silicate Solution.....	85
4.2.3	Effect of Additives on Standard Compaction Results of Bentonite.....	86
4.2.4	Effect of Additives on Standard Compaction Results of Kaolinite	90
4.3	Unconfined Compressive Strength Test Results of Stabilized Soils-	93
4.3.1	Effect of Recycled Gypsum on Soils.....	94
4.3.1.1	Bentonite Clay	94
4.3.1.2	Kaolinite Clay.....	97
4.3.2	Effect of Sodium Silicate on Soils.....	99
4.3.2.1	Bentonite Clay	100
4.3.2.2	Kaolinite Clay.....	103
4.3.3	Effect of the Admixture of Recycled Gypsum and Liquid Sodium Silicate on Soils.....	106
4.3.3.1	Bentonite Clay	106
4.3.3.2	Kaolinite Clay.....	109
4.4	X-Ray Diffraction Results of Stabilized Soils.....	113
4.4.1	Effect of Recycled Gypsum on Soils.....	116
4.4.1.1	Bentonite and Recycled Gypsum	116
4.4.1.2	Kaolinite and Recycled Gypsum	119
4.4.2	Effect of Sodium Silicate Solution on Soils	122
4.4.2.1	Bentonite and Sodium Silicate Solution.....	122
4.4.2.2	Kaolinite and Sodium Silicate solution	125
4.4.3	Effect of the Admixture of Recycled Gypsum and Liquid Sodium Silicate on Soils.....	128

4.4.3.1	Bentonite and the Mixture of Recycled Gypsum and Sodium Silicate Solution	128
4.4.3.2	Kaolinite and the Mixture of recycled Gypsum and Sodium Silicate Solution	132
4.5	FESEM/EDAX Analysis of Stabilized Soils.....	136
4.5.1	Effect of Recycled Gypsum on Soils.....	139
4.5.1.1	Bentonite and Recycled Gypsum	139
4.5.1.2	Kaolinite and Recycled Gypsum	147
4.5.2	Effect of Sodium Silicate Solution on Soils	156
4.5.2.1	Bentonite and Sodium Silicate Solution.....	156
4.5.2.2	Kaolinite and Sodium Silicate Solution	164
4.5.3	Effect of Recycled Gypsum and Sodium Silicate Solution on Soils	172
4.5.3.1	Bentonite and Recycled Gypsum and Sodium Silicate Solution.....	172
4.5.3.2	Kaolinite and Recycled Gypsum and Sodium Silicate Solution.....	181
4.6	FTIR Test Results of Stabilized	189
4.6.1	Effect of Recycled Gypsum on Soils.....	192
4.6.1.1	Bentonite Clay and Recycled Gypsum.....	192
4.6.1.2	Kaolinite Clay and Recycled Gypsum	194
4.6.2	Effect of the Alkali Activator Liquid Sodium Silicate in Soils.	196
4.6.2.1	Bentonite Clay and Sodium Silicate Solution	196
4.6.2.2	Kaolinite Clay and Sodium Silicate Solution.....	199
4.6.3	Effect of Recycled Gypsum and Liquid Sodium Silicate in Soils	202
4.6.3.1	Bentonite Clay with Recycled Gypsum and Sodium Silicate Solution.....	202
4.6.3.2	Kaolinite Clay with Recycled Gypsum and Sodium Silicate solution	204

4.7	The Nitrogen-Based Brunauer-Emmett-Teller (N ₂ -BET) Surface Area Test Results of Stabilized Soils	206
4.7.1	Effect of Recycled Gypsum on Soils.....	207
4.7.2	Effect of Sodium Silicate Solution on Soils	209
4.7.3	Effect of Recycled Gypsum and Sodium Silicate Solution on Soils	211
5	SUMMARY AND CONCLUSIONS.....	214
	REFERENCES	233
	Appendix	250
	PERMISSION LETTERS	250

LIST OF TABLES

Table 2.1 Effect of recycled gypsum and alkaline activation on the engineering properties of various soil types.....	51
Table 4.1 Geotechnical engineering characteristics of Bentonite and Kaolinite.....	76
Table 4.2 Chemical composition of tested clays	76
Table 4.3 Chemical composition of additives	77

LIST OF FIGURES

Figure 2.1. Reactions of chemical stabilization: (a) cation exchange; (b) flocculation-agglomeration, and (c) pozzolanic reaction (Prusinski and Bhattacharja, 1999, reproduced with the permission).	14
Figure 2.2. Computer molecular graphics of polymeric M_n -(-Si-O-Al-O-) $_n$ poly(silicate) and M_n -(-Si-O-Al-O-Si-O-) $_n$ poly(sialate-siloxo), and related frameworks. (Davidovits, 1991, reproduced with the permission).	18
Figure 2.3. Reaction mechanism of exothermic polymerization (Davidovits, 1991, reproduced with the permission).	20
Figure 2.4 The geopolymer reactions mechanism of an alkali activation process (modified after Guo et al., 2016).	22
Figure 3.1 Reflection of X-ray from the plane in a solid.	63
Figure 3.2 Curing bath utilized to achieve proper humidity condition.	69
Figure 3.3 Dimensions of manufactured mold for preparation of the UCS test specimens.	71
Figure 4.1 The grain size distribution of tested bentonite and kaolinite clays.	74
Figure 4.2 pH values of bentonite-recycled gypsum mixture (BG) at various additive contents and curing time intervals.	79
Figure 4.3 pH values of bentonite-sodium silicate solution admixture, (BS), at various additive contents, and curing time intervals.	80
Figure 4.4 pH values of gypsum, recycled gypsum, and sodium silicate mixtures (BGS), at various additive contents and curing time intervals.	82
Figure 4.5 initial pH values of recycled gypsum-kaolinite mixture, (KG), at various content and curing time intervals.	83
Figure 4.6 pH values of kaolinite- sodium silicate-mixture (KS), at various additive content and curing time intervals.	84
Figure 4.7 pH values of kaolinite, gypsum, sodium silicate, (KGS), 50%:50%, at various additive contents, and curing intervals.	85

Figure 4.8 Compaction tests for untreated and stabilized Bentonite: (a) Bentonite-Gypsum (BG), (b) Bentonite-Sodium Silicate (BS), and (c) Bentonite-Gypsum-Sodium Silicate (BGS).	88
Figure 4.9 Compaction test results for untreated and stabilized Kaolinite: a) Kaolinite-Gypsum (KG), b) Kaolinite-Sodium Silicate (KS), and c) Kaolinite-Gypsum-Sodium Silicate (KGS).....	92
Figure 4.10 The effect of curing time on the unconfined compressive strength of bentonite-recycled gypsum mixtures (BG) at different additive contents.....	95
Figure 4.11 The effect of curing time on the unconfined compressive strength of kaolinite-recycled gypsum mixtures (KG) at different additive contents.....	97
Figure 4.12 The effect of curing times on the unconfined compressive strength of bentonite-sodium silicate (BS) at different additive contents.	101
Figure 4.13 The effect of curing times on the unconfined compressive strength of kaolinite-sodium silicate mixtures (KS) at different additive contents.	104
Figure 4.14 The effect of curing time on the unconfined compressive strength of bentonite-recycled gypsum-sodium silicate mixtures (BGS) at different additive contents.	108
Figure 4.15 The effect of curing time on the unconfined compressive strength of kaolinite-recycled gypsum-sodium silicate mixtures (KGS) at different additive contents.	110
Figure 4.16 X-ray diffraction patterns for untreated, (a) Kaolinite, and (b) Bentonite.	115
Figure 4.17 X-ray diffraction patterns for bentonite stabilized with recycled gypsum (BG) at the same additive content and different curing times.	118
Figure 4.18 X-ray diffraction patterns for kaolinite stabilized with recycled gypsum (KG) at the same additive content and different curing times.	121
Figure 4.19 X-ray diffraction patterns for bentonite stabilized with sodium silicate (BS) at the same additive content and different curing times.	124
Figure 4.20 X-ray diffraction patterns for kaolinite stabilized with sodium silicate (KS) at the same additive content and different curing times.	127

Figure 4.21 X-ray diffraction patterns for bentonite stabilized with recycled gypsum and sodium silicate (BGS) at the same additive content and different curing times.	131
Figure 4.22 X-ray diffraction patterns for kaolinite stabilized with recycled gypsum and sodium silicate (KGS) at the same additive content and different curing times.	135
Figure 4.23a FESEM micrograph images and EDAX results of untreated bentonite. (ETH=8.00kV; WD= 7.2 mm, Mag=11.00KX). (Element legend: Na: Sodium, Si: Silicate, Al; Aluminum, Fe: Iron, Mg: Magnesium, Au: Gold, Pd: Palladium).	137
Figure 4.23b FESEM micrograph images and EDAX results of untreated kaolinite. (ETH=3.00kV; WD= 7.1 mm, Mag=9.69KX). (Element legend: Na: Sodium, Ca: Calcium, Si: Silicate, K: Potassium, Al; Aluminum, O: Oxygen, Mg: Magnesium, Au: Gold, Pd: Palladium).	138
Figure 4.24 FESEM-EDAX image, B3G3. (ETH=8.00kV; WD= 6.7 mm, Mag=15.00 KX). (Element/compound legend, CASH = Calcium Sodium Aluminum Silicate Hydrate, Si:Silicate, Al:Aluminum, Ca: Calcium, S: Sulfate).	140
Figure 4.25 FESEM-EDAX image, B3G3. (ETH=8.00kV; WD= 6.0 mm, Mag=10.10 KX). (Element/compound legend: CNASH = Calcium Sodium Aluminum Silicate Hydrate, Si: Silicon, Al: Aluminum, Ca: Calcium, Na: Sodium, Fe: Iron, Mg: Magnesium, S: Sulfate).	141
Figure 4.26 FESEM-EDAX image, B14G3. (ETH=8.00kV; WD= 6.8 mm, Mag=10.00 KX). (Element/compound legend: NASH = Sodium Aluminum Silicate Hydrate, Si:Silicon, Al:Aluminum, Ca: Calcium, Na: Sodium, Mg:Magnesium, S: Sulfate, Pd: Palladium, Au: Gold)....	142
Figure 4.27 FESEM-EDAX image, B14G3. (ETH=8.00kV; WD= 6.8 mm, Mag=10.00 KX). (Element/compound legend: CASH= Calcium Aluminum Silicate Hydrates; Si: Silicon; Al: Aluminum; Ca: Calcium; Na: Sodium; Mg: Magnesium; K: Potassium; Fe: Iron; S: Sulfate; Pd: Palladium; Au: Gold).....	143
Figure 4.28 FESEM-EDAX image, B28G3. (ETH=8.00kV; WD= 6.0 mm, Mag=15.00 KX). (Element/compound legend: CASH= Calcium Aluminum Silicate Hydrate, Si:Silicon, Al:Aluminum;Ca: Calcium; Na: Sodium; Fe: Iron; Mg:Magnesium; S: Sulfate; Pd: Palladium; Au: Gold).....	144

Figure 4.29 FESEM-EDAX image, B28G3. (ETH=8.00kV; WD= 6.7 mm, Mag=10.00 KX). (Element/compound legend: CNASH= Calcium (Sodium) Aluminum Silicate Hydrate; Si:Silicon; Al:Aluminum;Ca: Calcium; Na: Sodium; Fe: Iron; Mg: Magnesium; S: Sulfate; Pd: Palladium; Au: Gold).	145
Figure 4.30 FESEM-EDAX image, K14G12. (ETH=8.00kV; WD= 7.0 mm, Mag=2.02 KX). (Element/compound legend: CASH = Calcium Aluminum Silicate Hydrate, Si:Silicon, Al: Aluminum, Ca: Calcium, S: Sulfate, Pd: Palladium, and Au: Gold).....	150
Figure 4.31 FESEM-EDAX image, K14G12. (ETH=8.00kV; WD= 6.7 mm, Mag=10.00 KX). (Element/compound legend: CASH = Calcium Aluminum Silicate Hydrate, Si:Silicon, Al: Aluminum, Ca: Calcium; S: Sulfate, Pd: Palladium, Au: Gold).	151
Figure 4.32 FESEM-EDAX image, K28G12. (ETH=8.00kV; WD= 7.1 mm, Mag=5.00 KX). (Element/compound legend: CNAS = Calcium Sodium Aluminum Silicate Hydrate, Si:Silicon, Al: Aluminum, Ca: Calcium, Na: Sodium, Mg:Magnesium, Pd: Palladium, Au: Gold).....	152
Figure 4.33 FESEM-EDAX image, K28G12. (ETH=3.00kV; WD= 7.3 mm, Mag=10.75 KX). (Element/compound legend: CNASH= Calcium Sodium Aluminum Silicate Hydrate, Si:Silicon, Al: Aluminum, Ca: Calcium, Na: Sodium, S: Sulfate, Pd: Palladium, Au: Gold).....	153
Figure 4.34 FESEM-EDAX images for K56G12. (ETH=8.00kV; WD= 7.1 mm, Mag=10.00 KX). (Element/compound legend: CNASH= Calcium (Sodium) Aluminum Silicate, Si:Silicon, Al: Aluminum; Ca: Calcium; Na: Sodium, S: Sulfate; Pd: Palladium; Au: Gold).....	154
Figure 4.35 FESEM-EDAX images for K56G12. (ETH=8.00kV; WD= 7.1 mm, Mag=10.00 KX). (Element/compound legend: NMASH= Sodium Magnesium Aluminum Silicate Hydrate, Si:Silicate, Al: Aluminum, Ca: Calcium, Na: Sodium, Mg:Magnesium, S: Sulfate, Pd: Palladium, Au: Gold).....	155
Figure 4.36 FESEM/EDAX image, B3S12. (ETH=8.00kV; WD= 6.9 mm, Mag=10.00 KX). (Element/compound legend: CNASH= Calcium Sodium Aluminum Silicate Hydrate, Na: Sodium, Al: Aluminum, Si: Silicate, O: Oxygen, Pd: Palladium, Au: Gold).	158

Figure 4.37 FESEM/EDAX image, B3S12. (ETH=8.00kV; WD= 4.7 mm, Mag=10.00 KX). (Element/compound legend: NCASH= Sodium Calcium Aluminum Silicate Hydrate, Na: Sodium, Al: Aluminum, Si: Silicate, O: Oxygen).....	159
Figure 4.38 FESEM/EDAX image, B7S12. (ETH=8.00kV; WD= 4.7 mm, Mag=10.00 KX). (Element/compound legend: NASH= Sodium Aluminate Silicate Hydrate, Na: Sodium, Al: Aluminum, Si: Silicate, C: Carbon, Pd: Palladium, Au: Gold).....	160
Figure 4.39 FESEM/EDAX image, B7S12. (ETH=8.00kV; WD= 4.7 mm, Mag=10.00 KX). (Element/compound legend: NCAS= Sodium Calcium Aluminum Silicate Hydrate, Na: Sodium, Al: Aluminum, Si: Silicate, C: Carbon, Pd: Palladium, Au: Gold).....	161
Figure 4.40 FESEM/EDAX image, B14S12. (ETH=8.00kV; WD= 6.9 mm, Mag= 5.00 KX). (Element/compound legend: NASH= Sodium Aluminate Silicate Hydrate, Na: Sodium, Al: Aluminum, Si: Silicate, Au: Gold, Pd: Palladium).	162
Figure 4.41 FESEM/EDAX image, B14S12. (ETH=8.00kV; WD= 6.9 mm, Mag= 15.00 KX). (Element/compound legend: NCAS= Sodium Calcium Aluminate Silicate Hydrate, Na: Sodium, Ca: Calcium, Al: Aluminum, Si: Silicate, Au: Gold, Pd: Palladium).	163
Figure 4.42 FESEM/EDAX images K3S6. (ETH=8.00kV; WD= 6.4 mm, Mag= 15.00 KX). (Element/compound legend: NASH= Sodium Aluminum Silicate Hydrates, Na: Sodium, Au: Gold, C: Carbon, O: Oxygen).....	166
Figure 4.43 FESEM/EDAX image, K3S6. (ETH=8.00kV; WD= 6.4 mm, Mag= 15.00 KX). (Element/compound legend: NASH= Sodium Aluminum Silicate Hydrate, Mg: Magnesium, Fe: Iron, K: Potassium, Fe: Iron, Au: Gold, O: Oxygen).	167
Figure 4.44 FESEM/EDAX image, K7S6. (ETH=8.00kV; WD= 6.5 mm, Mag= 15.00 KX). (Element/compound legend: CASH= Calcium Aluminum Silicate Hydrate, Ca: Calcium, Au: Gold, O: Oxygen, C: Carbon).	168
Figure 4.45 FESEM/EDAX image, K7S6. (ETH=8.00kV; WD= 7.9 mm, Mag= 25.00 KX). (Element/compound legend: CASH= Calcium Aluminum Silicate Hydrate, Al: Aluminum, Si: Silicate, Na: Sodium, Au: Gold, Pd: Palladium, O: Oxygen, C: Carbon).....	169

Figure 4.46 FESEM/EDAX images, K56S6. (ETH=8.00kV; WD= 6.4 mm, Mag= 20.00 KX).. (Element/compound legend: NASH= Sodium Aluminum Silicate Hydrate, Na: Sodium, Al: Aluminum, Si: Silicate, Au: Gold, Pd: Palladium, O: Oxygen; C: Carbon).....	170
Figure 4.47 FESEM/EDAX image, K56S6. (ETH=8.00kV, WD= 5.4 mm, Mag= 10.00 KX). (Element/compound legend: NASH= Sodium Aluminum Silicate Hydrate, Al: Aluminum, Si: Silicate, Na: Sodium, Au: Gold, Pd: Palladium, O: Oxygen, C: Carbon).....	171
Figure 4.48 FESEM/EDAX images, B3GS6. (ETH=8.00kV, WD= 6.6 mm, Mag= 10.00 KX). (Element/compound legend: NCASH= Sodium Calcium Aluminate Silicate Hydrate, Na: Sodium, Al: Aluminum, Ca: Calcium, Au: Gold, Pd: Palladium).....	175
Figure 4.49 FESEM/EDAX images, B3GS6. (ETH=8.00kV, WD= 5.6 mm, Mag= 7.50 KX). (Element/compound legend: NCASH= Sodium Calcium aluminate Silicate Hydrate, Na: Sodium, Ca: Calcium, Al: Aluminum, Si: Silicate, P: Phosphorus, Au: Gold, Pd: Palladium).....	176
Figure 4.50 FESEM/EDAX images, B14GS6. (ETH=8.00kV, WD= 6.5 mm, Mag= 2.00 KX). (Element/compound legend: CASH= Calcium Aluminate Silicate Hydrate, Al: Aluminum, Si: Silicate, Ca: Calcium, S: Sulfate, Au: Gold, Pd: Palladium).	177
Figure 4.51 FESEM/EDAX images, B56GS6. (ETH=8.00kV, WD= 8.9 mm, Mag= 5.00 KX). (Element/compound legend: NMCAS= Sodium Magnesium Calcium Aluminate Silicate Hydrate, Na: Sodium, Ca: Calcium, Fe: Iron, Mg: Magnesium, K: Potassium, Mn: Manganese, Au: Gold, Pd: Palladium).	178
Figure 4.52 FESEM/EDAX images, B56GS6. (ETH=8.00kV, WD= 7.5 mm, Mag= 10.00 KX). (Element/compound legend: NCASH= Sodium-Magnesium-Calcium Aluminate Silicate Hydrate, Na: Sodium, Mg: Magnesium, Al: Aluminum, Ca: Calcium, Au: Gold, Pd: Palladium, C: Carbon).	179
Figure 4.53 FESEM/EDAX images, B56GS6. (ETH=8.00kV, WD= 7.5 mm, Mag= 10.00 KX). (Element/compound legend: CASH= Calcium Aluminate Silicate Hydrate, Al: Aluminum, Si: Silicate, S: Sulfate, Ca: Calcium, Au: Gold, Pd: Palladium).	180

Figure 4.54 FESEM/EDAX images, K3GS6. (ETH=8.00kV, WD= 7.9 mm, Mag= 13.87 KX). (Element/compound legend= CAS Calcium Aluminate Silicate (Hydrates), Al: Aluminum, Si: Silicate, S: Sulfate, Ti: Titanium: Au Gold, Pd: Palladium).	183
Figure 4.55 FESEM/EDAX images, K7GS6. (ETH=8.00kV, WD= 7.9 mm, Mag= 20.17 KX). (Element/compound legend: NASH= Sodium Aluminum Silicate Hydrates, Na: Sodium, Mg: Magnesium, Al: Aluminum, Si: Silicate, S: Sulfate, K: Potassium, Ca: Calcium, Au: Gold, Pd: Palladium).	184
Figure 4.56 FESEM/EDAX images, K28GS6. (ETH=8.00kV, WD= 5.4 mm, Mag= 15.00 KX). (Element/compound legend: CNASH= Calcium (Sodium) Aluminate Silicate Hydrate, Na: Sodium, Al: Aluminum, Si: Silicate, Ca: Calcium. S: Sulfate, Au: Gold, Pd: Palladium).	185
Figure 4.57 FESEM/EDAX images, K28GS6. (ETH=8.00kV, WD= 7.5 mm, Mag= 32.25 KX). (Element/compound legend: NCASH= Sodium Calcium Aluminate Silicate Hydrate, Na: Sodium, Ca: Calcium, K: Potassium, Au: Gold, Pd: Palladium).	186
Figure 4.58 FESEM/EDAX images, K56GS6. (ETH=8.00kV, WD= 7.4 mm, Mag= 40.07 KX). (Element/compound legend: NCASH= Sodium Calcium Aluminate Silicate Hydrate, Na: Sodium, Mg: Magnesium, Al: Aluminum, Si: Silicate, S: Sulfate, Mg: Magnesium, Au: Gold, Pd: Palladium).	187
Figure 4.59 FESEM/EDAX images K56GS6. (ETH=8.00kV, WD= 7.4 mm, Mag= 25.49 KX). (Element/compound legend: NASH= Sodium Aluminate Silicate Hydrate, Na: Sodium, Mg: Magesium, Au: Gold).	188
Figure 4.60 FTIR spectra of the primary absorption region in the untreated Kaolinite, (KUNT), and Bentonite (BUNT).	189
Figure 4.61 FTIR spectra of the primary absorption region in recycled gypsum.	191
Figure 4.62 FTIR spectra of untreated (BUNT) and stabilized kaolinite with 3% recycled gypsum (BG3), at different curing times.	192
Figure 4.63 FTIR spectra of untreated (KUNT) and stabilized kaolinite with 12% recycled gypsum (KG12), at different curing times.	194
Figure 4.64 FTIR spectra of untreated (BUNT) and stabilized bentonite with 12% sodium silicate (BS12), at different curing times.	197

Figure 4.65 FTIR spectra of untreated (KUNT) and stabilized kaolinite with 6% sodium silicate (KS6), at different curing times.....	200
Figure 4.66 FTIR spectra of untreated (BUNT) and stabilized bentonite with 6% mixture (50:50) of recycled gypsum and sodium silicate (BGS6), at different curing times.	203
Figure 4.67 FTIR spectra of untreated (KUNT) and stabilized Kaolinite with 6% mixture (50:50) of recycled gypsum and sodium silicate (KGS6), at different curing times.	205
Figure 4.68 N ₂ -BET results for untreated (BUNT) and stabilized bentonite with 3% recycled gypsum (BG3), at different curing times.	208
Figure 4.69 N ₂ -BET results for untreated (KUNT) and stabilized kaolinite with 12% recycled gypsum (KG12), at different curing times.	209
Figure 4.70 N ₂ -BET results for untreated (BUNT) and stabilized bentonite with 12% sodium silicate solution (BS12), at different curing times.....	210
Figure 4.71 N ₂ -BET results for untreated and stabilized kaolinite with 6% sodium silicate solution samples (KS6), at different curing times.....	211
Figure 4.72 N ₂ -BET results for untreated (BUNT) and stabilized bentonite with a 6% admixture (50:50) of recycled gypsum and sodium silicate (BGS6), at different curing times.	213
Figure 4.73 N ₂ -BET results for untreated (KUNT) and stabilized kaolinite with a 6% admixture (50:50) of recycled gypsum and sodium silicate (KGS6), at different curing times.....	213

LIST OF ABBREVIATIONS

ASTM	American Society of Testing and Materials
ATR-FTIR	Fourier transform infrared spectroscopy
BG	Bentonite-Recycled Gypsum
BGS	Bentonite-Recycled Gypsum-Sodium Silicate
BS	Bentonite-Sodium Silicate
BUNT	Untreated Bentonite
B6GS7	Bentonite and 6% Gypsum-Sodium Silicate with 7 Days Curing Age
C-A-H	Calcium Aluminate Hydrate
C-S-H	Calcium Silicate Hydrate
C-A-S-H	Calcium Aluminate Silicate Hydrate
Ca-OH	Calcium Hydrate
G	Gypsum
KG	Kaolinite-Recycled Gypsum
KS	Kaolinite-Sodium Silicate
KGS	Kaolinite-Recycled Gypsum-Sodium Silicate
KUNT	Untreated Kaolinite
K3GS3	Kaolinite and 3% Gypsum and Sodium silicate with 3 Days Curing Age
Na ₂ SiO ₃	Sodium Silicate
N-(C)-A-S-H	Sodium (Calcium) Aluminate Silicate Hydrate
N ₂ -BET	Nitrogen Based Brunauer-Emmett-Teller (N ₂ -BET) Surface Area Test

FESEM-EDX	Field Emission Scanning Electron Microscopy-Energy Dispersive Spectrometry
OMC	Optimum Moisture Content
SP	Standard Proctor Compaction Test
SS	Sodium Silicate
UCS	Unconfined Compressive Strength
USGS	United States Geological Survey
XRD	X-ray Diffraction
XRF	X-ray Fluorescence
γ_{dry}	Maximum Dry Unit Weight

ABSTRACT

Sustainable soil stabilization of clays utilizing chemical agents relies primarily on chemical reactions between additives and soil materials to attain the desired geotechnical properties such as strength, compressibility, and durability. In this regard, the use of chemicals for ground stabilization is one of the most favorable soil improvement techniques to improve weak engineering properties of soils by combining unbound materials through fabricated cementation products. A variety of soil stabilizers are available for ground stabilization and are categorized as “traditional” (Portland cement, fly ash, hydrated lime) and “non-traditional” (liquid alkali activators, sodium silicate, polymers, enzymes). The production of traditional additives (such as Portland cement or hydrated lime) emits large amounts of greenhouse gases (CO₂) into the atmosphere worldwide. As a separate problem, an excessive amount of waste materials are produced from the construction and demolition of civil engineering projects around the world, and the disposal cost of the associated waste materials is high. As a result, more recently, the use of nontraditional additives (such as sodium silicate) and recycled materials (such as gypsum) in earthwork projects has become attractive as a replacement for traditional stabilization agents due to their economic and environmental benefits for society.

Blending soil and alkaline solutions fabricates new cementation materials named geopolymers, achieving a sustainable improvement in the engineering properties of soils, which produces similar mechanical performance relative to traditional stabilizers

such as Portland cement. Geopolymers can be synthesized using a variety of sources including industrial waste as well as fine materials such as natural clays.

This research investigates the use of two nontraditional stabilizers, recycled gypsum produced from wall plasters (sometimes referred to as “sheetrock” in the United States), and a sodium silicate solution, to enhance the strength of two types of clay soils, Bentonite and Kaolinite. Three different stabilizer combinations are assessed during this study: (1) “gypsum only”, (2) “sodium silicate only”, and (3) a 50/50 combination of “gypsum and sodium silicate”. For both of the clay minerals that were stabilized, as well as the three stabilizer combinations that are denoted above, four levels of additive stabilization were explored, at 3%, 6%, 9% and 12%. After stabilization, specimens were subjected to various curing intervals, including 0, 3, 7, 14, 28 and 56 days of curing, and unconfined compressive strength (UCS) testing was conducted to determine the strength development with curing time for each of the stabilized soil mixtures. The change in the pH values of the additive-soil mixtures at different curing periods was monitored. Additional microstructural characterization tests including x-ray diffraction (XRD), field emission scanning microscopy (FESEM), energy-dispersive X-ray analysis (EDAX), fourier transform infrared spectrometry (FTIR), and the nitrogen-based Brunauer-Emmet-Teller (N₂-BET) test were all used to explore and assess changes in the soil microstructure as soil stabilization progressed with curing time.

The UCS test results demonstrate that the use of powdered recycled gypsum, a sodium silicate solution, and their combination all considerably increased the strength of both stabilized clay soils. Strength increases measured for gypsum stabilized

bentonite and kaolinite were 4 and 2.5 times greater than the strengths measured for the corresponding untreated clays, respectively, at all stabilizer mix ratios and curing times that were assessed. Similarly, strength increases measured for sodium silicate stabilized kaolinite and bentonite were 3.5 and 3.5 times greater than the strengths measured for the corresponding untreated clays, respectively. Strength increases measured for gypsum and sodium silicate (50/50) stabilized kaolinite and bentonite were 3.5 and 2.5 times greater than the strengths measured for the corresponding untreated clays, respectively. It should be noted that these strength multipliers are the lower bound of the observed strength gain, and that many of the tested specimens exhibited significantly higher strengths at various stabilizer concentrations and curing times.

The required optimum additive content of stabilizers depended upon the type of soils, and was different for different curing times. In this study, the optimum stabilizer contents were determined based upon the stabilizer mix ratio that yielded the largest gain in strength in the treated specimens after 56 days of curing. The optimum additive contents for bentonite stabilized with gypsum, sodium silicate, and a 50/50 mixture of gypsum and sodium silicate were 3, 12, and 6, respectively. The optimum additive contents for kaolinite stabilized with gypsum, sodium silicate, and a 50/50 mixture of gypsum and sodium silicate were 12, 6, and 6, respectively. As shown, in general, the kaolinite clay needed a higher content of recycled gypsum relative to the bentonite clay, whereas the sodium silicate stabilized kaolinite required a lower content of sodium silicate relative to the bentonite. The combination of recycled gypsum and sodium silicate was found to have benefits regarding the improvement of engineering properties

of both soils, with the same amount of admixture (6%) yielding the greatest strength gain for both soils. The observed chemical reactions for all of the soil stabilization processes were time-dependent, especially for the bentonite treated with the combination of recycled gypsum and sodium silicate.

The XRD tests show the formation of new cementation products via the appearance of new diffraction peaks, along with a reduction of the intensities of the peaks corresponding to the aluminum silicate minerals for both of the tested clays. The FESEM tests showed the transformation/modification of the soil microstructure and clay particle surfaces for both of the clays that were tested, and for the three stabilizer combinations that were utilized. Moreover, new crystalline gel (geopolymer) phases of cementation were observed. Alteration of the chemical composition of both treated soils was validated using energy-dispersive X-ray analysis (EDAX). The modifications of the functional groups of both clay minerals were confirmed utilizing Fourier transform infrared spectrometry (FTIR). In general, the nitrogen-based Brunauer-Emmet-Teller (N₂-BET) tests showed a decrease in the surface area of both stabilized clays in the long-term for the different stabilizers that were assessed, as cementation products were created and the pore space between the specimens was filled. At some of the intermediate curing times, increases in surface area of the treated specimen were observed; this behavior is attributed to dissolution of the base materials prior to formation of stabilizing cementitious compounds. These N₂-BET surface area results are generally consistent with the UCS test results as the strength reported for

intermediate curing times is sometimes lower than the initial strengths that were measured.

From the results of this study, it is believed that the combination of recycled gypsum and sodium silicate improves the soil strength properties significantly, offering positive benefit for long-term soil stabilization. The potential for beneficial reuse of waste gypsum can reduce the quantity of this material that ends up in landfills, and the replacement of traditional Portland cement and lime stabilizers with the combination of gypsum and sodium silicate could serve to decrease the emission of greenhouse gases that are associated with the production of these more traditional soil stabilizers.

Chapter 1

INTRODUCTION

1.1 Soil Stabilization

Associated with the acceleration of civilization and urbanization, the use of land for society's living and transportation needs has been significantly increasing for decades all over the globe. More and more buildings, earth dams, levees, tunnels, and highways have been constructed, and even more are going to build in the future. In many locations, favorable construction sites have become less available, and it has become necessary to perform construction on relatively unsuitable sites to fulfill unmet construction needs (Han, 2015). On many sites, unfavorable subgrade conditions that have the potential to create geotechnical problems and challenges exist, such as (1) water seepage and soil erosion, (2) stability problems including slope failure, bearing capacity, and excavation collapse, or (3) movement-related problems such as large total or differential settlements, lateral movement of walls and braced excavations, or "lateral squeeze" of foundation soils, foundation and embankment treatment (e.g., Horpibulsuk et al., 2009, 2010; Chinkulkijniwate et al., 2015) Consequently, soil improvement solutions designed to address unfavorable geotechnical conditions have become a necessity for many projects, to avoid possible failures that can result in loss of human life or significant financial loss (Lee and Karunaratne, 2007; Turkoz, 2011).

In an attempt to handle problematic geotechnical conditions, engineers have developed a variety of approaches for conducting “ground improvement” at a given field site, in order to achieve more desirable engineering properties for a given soil (Zaliha et al., 2013). The term “ground improvement” is the most common term in practice and in the literature, but “soil stabilization”, “ground/soil treatment”, and “ground modification” are also commonly used in practice (Han, 2015). Improvement of geomaterials can be achieved by treating soils chemically, biologically, or mechanically; in some cases, more than one approach is used concurrently to achieve the desired results (e.g., Horpibulsuk et al., 2006; Arulrajah et al., 2013, Bo et al., 2014; Du et al., 2013, 2014; Wu et al., 2015; Latifi et al., 2016).

One example of biological ground improvement is the use of denitrifying bacteria, which can be utilized to decrease the degree of saturation of sand by producing tiny nitrogen bubbles that minimize the chance of liquefaction during earthquake shaking (Han, 2015). Mechanical stabilization includes commonly employed techniques such as soil compaction, mixing, and geo-reinforcement at the macro-scale; micro-scale fiber-reinforcement is an emerging technique that can also be used to improve the ground without altering its chemical properties (e.g., Molenaar, 2005; Caterpillar, 2006). Chemical soil stabilization using “traditional” stabilizers involves the use of additives such as cement, lime, bituminous materials, or industry by-products such as fly ash, calcium carbide residue, or granulated blast furnace slag. “Nontraditional” chemical stabilization involves the use of enzymes, polymers, resins, acids, silicates, ions, or lignins that exist in nature or which can be produced through a

natural process; these chemical additives can generally be provided in a liquid or powder form” (Rashid et al., 2017). These additives are typically mixed, injected, or otherwise introduced to the soils in a fashion that allows chemical stabilization to occur (Ma et al., 2015). Like mechanical stabilization, chemical stabilization is fairly common, particularly using cheap and readily available cementitious additives such as Portland cement or lime. Ground improvement using chemical, mechanical, or biological means can be utilized for a multiple purposes, such as achieving a desired soil load-bearing capacity, reducing soil permeability, allowing for soil filtration and drainage, mitigating undesirable soil swelling properties, or enhancing a soil’s shear strength and/or stiffness to meet the specific needs of a project (e.g., Bergado et al., 1996; Prabakar et al., 2004; Koliass et al., 2005; Zaliha et al., 2013).

Recent increases in demand for ground improvement on various projects has led to accelerating production of ordinary Portland cement (Guo et al, 2010). It has provoked to release huge amounts of greenhouse gases, carbon dioxide (CO₂), into the atmosphere. To produce 1 ton of ordinary Portland cement is approximately equivalent to releasing 1-ton of carbon dioxide (CO₂) into the air (Neville, 2012; Sukmak et al., 2013; Pavithra et al., 2016). According to USGS (2014), annual cement production across the globe is 4.0 billion tonnes and annually increasing at 4%. In parallel, production of waste materials has globally increased in the construction and infrastructure sectors (e.g., Guleria and Dutta, 2011; Kamei et al., 2013; Ahmed et al., 2015). For instance, production, construction, and demolition of gypsum wall plasterboard has annually produced about 12-25 million tonnes of waste material all

over the world, and according to the U.S Geological Survey, it is estimated to reach 40 million tons by 2020 (Kuttah and Sato, 2015).

The use of gypsum as a chemical stabilizer for ground improvement would achieve three positive outcomes: (1) effective soil stabilization for the benefit of many projects, (2) effective reduction of the volume of this waste material that is directed to straight to landfills on an annual basis, and (3) effective reduction of the associated production of Portland cement or lime that would likely have been used a the low-cost stabilizer of choice instead of gypsum on many projects (Yilmaz and Civelekoglu, 2009; Ahmed, 2015; Kuttah and Sato, 2015). This also would indirectly allow Portland cement to be reserved for the production of Portland cement concrete, an area where it fulfills a more valuable need (Kobayahi et al., 2013).

Hence, the use of waste materials has increasingly become popular for stabilization, owing to both their environmental and cost benefits relative to traditional soil stabilization approaches such as the application of Portland cement. As noted previously, production of ordinary Portland cement requires high energy consumption and releases large amounts of greenhouse gases. Thus, recently, another class of soil stabilizers has emerged as an alternative to traditional stabilization approaches; these stabilizers are produced from various alumino-silicate materials, including kaolinite, and various industrial wastes, such as fly ash, or ground granulated blast furnace slag. These cementing materials, which are activated in high alkaline solutions, are commonly referred to as “Geopolymers”, and soils stabilized with these materials possess similar mechanical performance and appearance to those stabilized with

ordinary Portland cement. Geopolymers are also touted for their low carbon release, reduced energy consumption in the production process, and common use of industrial wastes as a precursor in the polymerization process (Guo et al., 2010). It is reported that geopolymer based materials can in some cases yield higher compressive strength and durability than cement-based materials (e.g., Bignozzi et al., 2014; Reig et al., 2014; Hoy et al., 2016).

1.2 Objectives

The goal of the current study is to examine the potential utility of sodium silicate and recycled gypsum wall plasterboard for improvement of unfavorable soils via a combined use of these stabilizers. The suitability of these chemicals for stabilization of two pure clay minerals, bentonite and kaolinite, was examined. The current study focuses on increases in soil strength, changes in surface area at the micro-level within the specimen, and the formation of new cementitious material compounds such as geopolymers and zeolitic structures within the soil structure that occur due to the addition of the chemical stabilizing agents. Assessment of the chemical additives was performed at various curing intervals to examine the rate of strength gain during the stabilization process; this information is of critical importance for construction engineers that may seek to deploy these stabilizers in a time-constrained environment in the field. The formation of geopolymer gels and/or zeolites will be examined by combining a liquid alkali activator and waste gypsum wall plaster; it is hoped that this

combination will improve the soil strength gain and development of favorable microstructural features.

Chapter 2

LITERATURE REVIEW

2.1 Methods of Soil Stabilization

Soil stabilization is a process which increases strength and improves the stability of soil by mechanical, biological, or chemical, means. Noted that the main objective of this review herein focuses on chemical stabilization technique.

2.1.1 Mechanical Soil Stabilization

As mentioned in the previous section, mechanical stabilization is a technique which enhances the stability and shear strength of a soil without altering its chemical properties. Mechanical stabilization approaches include using induced compaction or vibration to densify a soil, or by incorporating other mechanical reinforcement elements such as nailing, reinforcement, barriers, or columnar inclusions. Common methods of mechanical stabilization in the field include soil compaction, in-place mixing of chemical or mechanical binding or reinforcement elements that act at the micro-level within the soil, and applying geosynthetic reinforcement (e.g., Caterpillar, 2006). For instance, fibers can be mechanically mixed with sand or clays soils to form a fiber-reinforced soil (Han, 2015). Mechanical stabilization is not a primary subject of this thesis, and consequently, will not be discussed in additional detail in this literature review. Interested readers are referred to Mitchell (1981), Hausmann (1990), and Ye et al. (1994) for more discussion in this area.

2.1.2 Biological Soil Stabilization

More recently, the use of biological treatment techniques for soil stabilization has emerged as a new and potentially environmentally friendly option for engineering projects. The most common of these approaches that have been studied to date is the use of bacteria to stimulate microbial carbonate cementation for soil stabilization (e.g., Levrel et al., 1999; Bianco and Madonia, 2007; Ozdogan, 2010). Similar biologically-induced cementation processes have also been used for various other civil engineering projects, such as filling cracks in concrete or granite (e.g., Gollapuded et al., 1995). Some of these approaches have been touted for their ability to “heal” cracked concrete infrastructure post-installation in the field (e.g., Ramachandran et al., 2001; Canakci and Cabalar, 2003). In a similar fashion to mechanical compaction, as biological soil stabilization is not the focus of the current thesis, it will not be discussed further in the current literature review. Interested readers are referred to Bang et al. (2001), Dejong et al. (2006), Ramakrishnan (2007), and Jonkers et al. (2008) for more discussion in this area.

2.1.3 Chemical Stabilization

Chemical stabilization is the process of altering soil properties through the use of binding chemical additives. Various chemical additives have been added to base soil materials to modify their engineering properties such as improving strength, reducing compressibility, reducing plasticity, changing shrink/swell behavior, and altering their permeability. The effect of additives may be unique for a given soil, and depends heavily

on the type of chemical additive that is used. Soil stabilization agents have historically been classified into either two or three main groups, including “traditional”, “non-traditional”, and “by-product” stabilizers, according to Petry and Little (2002); Eisazadeh, (2010); Rashid et al., 2017.

- **Traditional stabilizers;** Portland cement, hydrated lime, fly ash, and bituminous materials
- **Non-traditional stabilizers;** silicates ions, liquid polymer-based products, sulfonated oils, ions, ammonium chloride, acids, enzymes, lignin derivatives,
- **By-product stabilizers;** a third category that is sometimes used, which contains byproducts of various manufacturing or industrial processes. Examples include: cement kiln dust, calcium carbide residue, lime kiln dust and other forms of lime by-products. In some cases, fly ash can also be considered in this category, since it is a by-product of coal combustion.

The primary reaction mechanism of many calcium-based “traditional” stabilizers is calcium exchange and pozzolanic reactions, which is also the mechanism for stabilization of a number of the commonly used “by-product” stabilizers (e.g, Tingle et al., 2007). Non-traditional stabilizers, by comparison, typically have different stabilization mechanisms than their more traditional counterparts. For instance, sulfonated oils achieve soil improvement via penetration of hydrogen ions into the clay

lattice, with the hydrogen altering the water-retention capacity of the structure of the clay (Tingle et al., 2007). Enzyme stabilizers instantly react with the clay particles, and are not consumed by the reactions that occur since enzymes are organic materials catalyzing very specific chemical reactions (e.g., Petry and Little, 2002; Tingle et al., 2007). Polymer-based products, such as geopolymer gels, have been attractive for various interdisciplinary applications, such as in new cement concrete, stabilization of toxic and radioactive deposit fills, and structural heat and fire resistance, since geopolymer gels have some advantages relative to cement-based materials (e.g., Komnitsas and Zaharaki 2007; Sukmak et al., 2013; Reig et al., 2014). For instance, geopolymer-based materials can in some cases provide higher strength and durability against sulfate attack than cement based materials (Hoy et al., 2016).

2.2 Mechanism of Soil Stabilization

All chemical stabilization agents blended with soils are able to develop new cementation materials as a result of chemical reactions between the base soil and the stabilizing agent. Thus, the product of chemical stabilization can improve soils and modify their properties through chemical reactions such as cation exchange, flocculation and agglomeration, and pozzolanic reactions.

2.2.1 Cation Exchange

In clays, exchangeable cations like Ca^{2+} , Mg^{2+} , Na^+ , and K^+ are tightly detained by the negatively charged clay particles. The type of absorbed cations depends on

environmental conditions such as the temperature and pH, and the chemical and biological content of the water in the pore space. A negative charge develops on the surface of clay particles due to unbalanced valence charges at the edge of the clay crystal lattice. Cations floating in the clay matrix are attracted to the clay surface, which has a neutralizing effect on the negative surface charge imposed by the clay's crystal structure. Charge deficiencies differ from clay to clay, and therefore the exchangeable cations have different behavioral tendencies. As expected, replacement of the cations illustrated in Figure 1(a) can occur to a partial degree or completely in response to changes in environmental conditions at the microlevel. Via cation exchange, the structure of clay particles might not be altered, yet a significant modification in the physical and physicochemical properties of the soil can occur as a result of the exchange process. The replacement of cations relies on diverse factors, in particular the valence of cations. Higher valence cations quickly exchange with cations of lower valence. Exchangeability of cations occurs in the following priority order (Mitchell and Soga, 2005);



These cations might be naturally occurring in the pore water, or can be artificially provided by a variety of stabilizers, such as waste gypsum plaster boards, lime, cement, kiln dust, fly ash, etc.

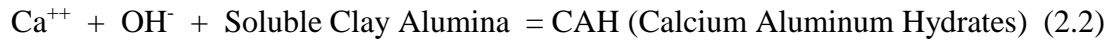
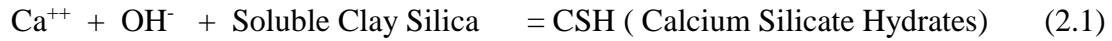
2.2.2 Flocculation and Agglomeration

Flocculation and agglomeration are a modification of clay particles corresponding to a cation exchange process which reforms the texture of clays from fine grained to a more friable and granular phase (Holtz and Kovac, 1981). Flocculation is a process where particles contact in the solution, and adhere each other to form flakes, flocks or clumps of clay, silt or sand particles in soil matrix, and flocculation and agglomeration are synonymous terms (Chibowski 2011). Clay particles can be randomly oriented in the pore space, or can have a more aligned (i.e., parallel) orientation; the flocculation process transfers the clay microstructure from a more aligned orientation to a more random orientation by altering their smooth texture, as shown in Figure 1(b). The process of flocculation begins with cation exchange. Agglomeration is believed in forming at the edge of the clay surface due to weak bonds and deposition of fabrication materials among clay particle interfaces (Tran et al., 2014).

2.2.3 Pozzolanic Reaction

The pozzolanic reaction is a critical reaction that occurs as part of the concrete curing process, and in many soil improvement applications, depending upon the stabilizer that is used (Little, 1995). The pozzolonic reactions shown in Eqs. 2.1 and 2.2 involve a chemical process between an added stabilizer (such as Portland cement, lime or fly ash, to name a few common examples), a base material that is being stabilized such as concrete aggregate or natural soil particles (i.e., naturally occurring

clays, silts, sands, etc.), and water (Petry and Little, 2002; Little et al., 2010; Makusa, 2012; Troni et al., 2013; Firoozi et al., 2017). The reaction can be followed as;



The nature of the reaction that occurs tends to form strong bonds between the particles in the matrix over time, a stabilization process which happens over an extended period, which is affected by chemical and mineralogical composition of the soil and temperature. During the reaction process, a high pH is required to dissolve the existing aluminosilicate minerals in the clay lattice. Dissolved silicate and aluminum ions react with free Ca^+ or Na^+ ions to manufacture cementitious hydration compounds such as calcium silicate hydrates (CSH), calcium aluminate hydrates (CAH), and calcium (or sodium) aluminate hydrates (C(N)AH), which cause increases in the strength of a stabilized soil over time, as shown Figure 2.1(c). It should be noted that the abbreviations in the previous sentence are as follows: C is CaO, S is SiO_2 , A is Al_2O_3 , N is NaO, and, and H is H_2O (Tasong, 1999; Prusinski and Bhattacharja, 1999; Little and Nair, 2009; Mohn, 2015).

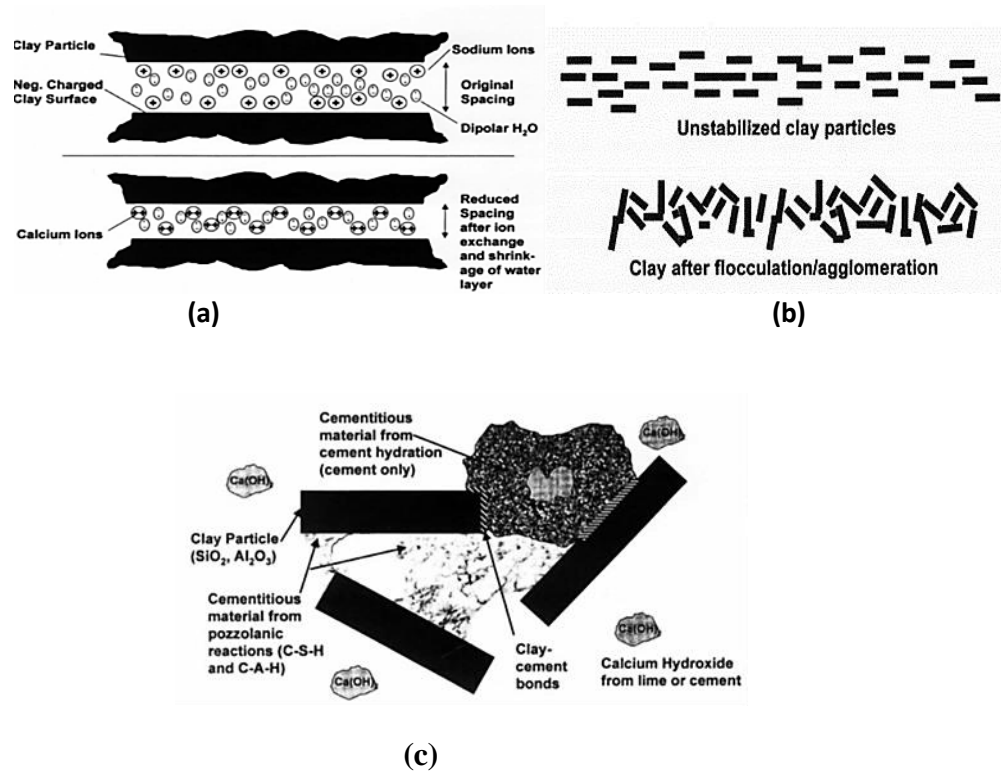


Figure 2.1. Reactions of chemical stabilization: (a) cation exchange; (b) flocculation-agglomeration, and (c) pozzolanic reaction (Prusinski and Bhattacharja, 1999, reproduced with the permission).

2.2.4 Alkali Activated Geopolymerization

More recently, alkali activation of aluminate minerals or polymerization have seen increased interest by researchers as possible alternatives to Portland cement stabilization of soil. Alternatives to Portland cement are desirable because the process of cement production emits significant amounts of carbon dioxide (CO_2) into the atmosphere, which contributes to the phenomenon of global warming (e.g., Guo et al.,

2010; Sukmak et al., 2013; Zaliha et al., 2013; Bignozzi et al., 2014; Reig et al., 2014;). Successful application of geopolymer technology for soil stabilization has the potential to reduce CO₂ emissions for this application by up to 80% according to Rowles and O'Connor (2003). The production expenses associated with geopolymer manufacturing are relatively low in comparison with the production of ordinary Portland cement, as they can be created with naturally existing materials using a combination of alkali solutions and water (Smith and Comrie, 1988).

For the production of geopolymers, sodium silicate has often been utilized for creating an alkaline solution, though sodium hydroxide, potassium silicate, and other chemical solutions are in some cases preferable. (Rowles and O'Connor, 2003; Zaliha et al., 2013) The application of sodium silicate can be used to stiffen problematic soils and/or as a treatment to augment their load-bearing capacity, to reduce settlement and lateral movement in poor foundation soils, and to mitigate problems with seepage flow in earth structure projects such as dams, levees, tunnels, and excavations (OxyChem, 2003). Major benefits of alkali activated geo-polymers are cost-effectiveness, a general ease of application, a short curing process, relatively fast strength development compared to traditional stabilizers, and a reduction in stabilized soil permeability (Kamnitsas and Zaharaki, 2007; Bignozzi et al., 2014).

2.2.5 Stabilization Mechanism of Alkali Activated Geopolymers

Geopolymers (mineral polymers formed by geochemistry), first named by Davidovits, (1972), are inorganic compounds that are synthesized in a highly alkali

medium to react with rich in alumina-silicates to yield amorphous, semi-crystalline, and crystalline 3-D structures, as shown in Figure 2.2.

The process of sodium silicate stabilization may be divided into four basic chemical reaction mechanisms, as noted by Nigussie (2011):

- **Hydration/ Dehydration:** Glassy nature of silicates exhibits strong and rigid properties. Bonds formed by hydration/dehydration process can be dissolved by any pore water that is present. The formation of silicate gel is driven by the formation of silicate structures, which can occur up to temperatures of 250°C.
- **Surface Charge Modification:** Dissolved sodium silicate ions in the pore fluid interact with other charged materials, in particular, aluminum silicate which is present in the base material that is to be stabilized. This interaction causes the sodium and aluminum silicate on the surface of the base material particles to ionize; these ions then interact with the ions in the pore fluid to form cementing agent bonds between particles. In conjunction with this process, the relative repulsion and or attraction of various ions can lead to localized dispersion and flocculation behavior, which can change the pore structure of the stabilized material at the micro-scale.
- **Metal Ion Reaction:** Silicates can react with many metal ions such as Magnesium, Iron, Magnesium, Calcium, Potassium, Aluminum, and facilitate those metals into insoluble and inactive products that improve the long-term stability of soil.

- **Precipitation/Gelation Reaction:** This reaction mechanism occurs as a result of adding extra acid into the binder system, once the pH values of the pore fluid solution fall below approximately 10.7. This approach is a more energy efficient alternative than heating silicates to over 250°C, in order to form new cementing bonds in the soil matrix.

Chemical classification of geopolymers depends upon the quantity of silicon-oxo-aluminate, and the nature of a bonding network known as poly(sialate), which is a structure of existing SiO₄ and AlO₄ tetrahedra that are linked alternately by sharing the oxygen molecules that are present (Davidson, 1991; Komnitsas and Zaharaki, 2007; Pavithra et al. 2016). The negative charge of Al⁺³ is balanced by positive ions, Na⁺, K⁺, Ca⁺⁺, Li⁺, NH⁴⁺⁺ displaying in the polymer framework cavities, which refers to physical bonding mechanism. The empirical formula of the poly(sialates) chain and ring polymers with Si⁺⁴ and Al⁺⁴ in 4-fold coordination with oxygen is given as Davidovist, (1991); Xu and Van Deventer, (2000):



Where z is 1,2 and 3, M is a monovalent cation such as Na⁺, K⁺, Ca⁺⁺ and n is a degree of polycondensation. The type of poly(sialates) and related frameworks for Zeolite identified by Davidovits, (1991) are displayed in Figure 2.2. The structure unit of Zeolite A is indistinguishable from that Na-poly(sialate) and is built Sodalite-framework, Na-PS. As can be illustrated in Figure 2.2, zeolite phases exhibit perfectly

crystallized structures depending on the chemical composition of additives; however, industrially developed polymer compounds present non-crystalline phases (amorphous or glass structures) (Davidovots, (1991).

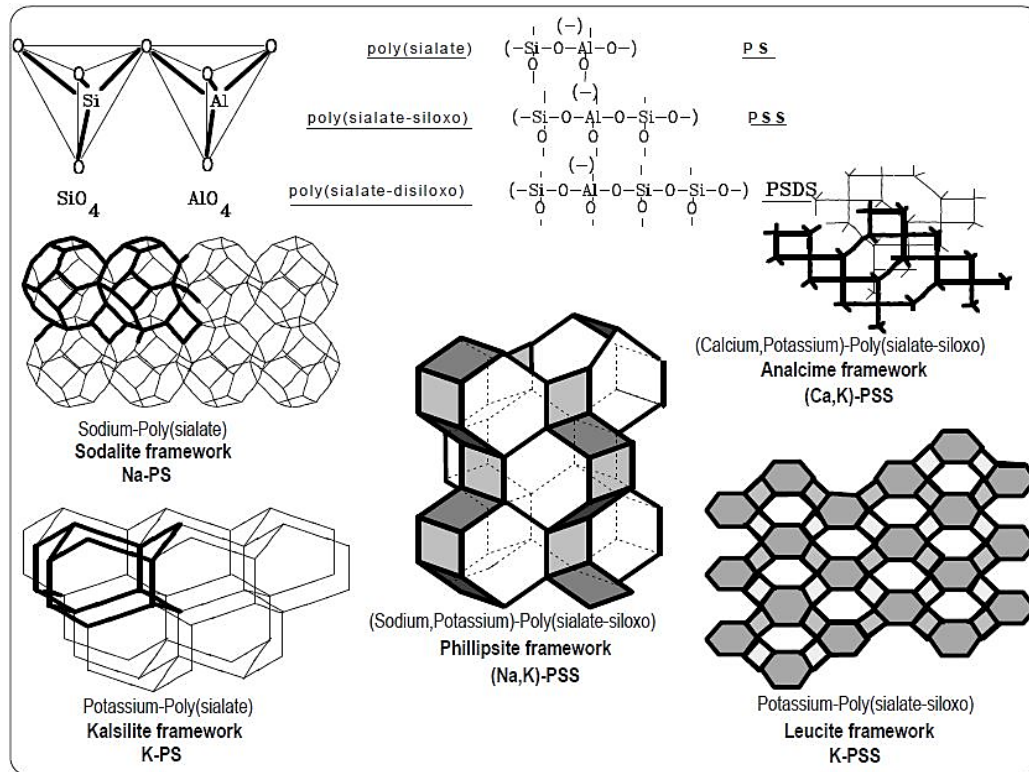


Figure 2.2. Computer molecular graphics of polymeric $M_n-(-\text{Si}-\text{O}-\text{Al}-\text{O}-)_n$ poly(silicate) and $M_n-(-\text{Si}-\text{O}-\text{Al}-\text{O}-\text{Si}-\text{O}-)_n$ poly(sialate-siloxo), and related frameworks. (Davidovits, 1991, reproduced with the permission).

The structure of complex geopolymers is categorized as chains, sheet-like and three-dimensional networks, combining a variety of SiO_4 and AlO_4 tetrahedra (Singh et al., 2005). Amorphous to semi-crystalline three-dimensional aluminate-silicate structures are poly (Sialate) $M_n-(-\text{Si}-\text{O}-\text{Al}-\text{O}-)_n$, Poly(sialate-siloxo) $M_n-(-\text{Si}-\text{O}-\text{Al}-\text{O}-$

SI-O)_n and Poly(Sialate-disil-oxo) Mn-(-Si-O-Al-O-Si-O-Si-O)_n emerging as a result of hydrothermal setting conditions. Geopolymerizations ordinarily do not complete under this condition due to their formation of non-crystalline (amorphous or glassy) structures (Davidovist, 1991).

Amorphous poly(sialate-siloxo) (-Si-O-Al-O-Si-O) binders are a hardening mechanism associated with alumino-silicate oxides (Al⁺³ in IV-fold coordination) and alkali polysilicates providing Si-O-Al bonds in the matrix. According to Davidovits, (1991), manufacture of (Si₂O₅, Al₂O₂)_n is accomplished by the following phases;

- Calcining alumino-silicate hydroxides, (CASH)
- Sodium alumino-silicate hydroxides, (NASH)
- Condensation of SiO and Al₂O vapors
- Calcining Silicate Hydrates, (CSH)

Geopolymerization is also an exothermic chemical reaction between various alumino-silicate oxides (Al³⁺ in IV-V fold coordination) with silicates under the highly alkaline conditions, resulting in polymeric Si-O-Al-O bonds, which is schematized in Figure 2.3 as the result of polycondensation of still hypothetical monomers, the orthosialate ions as follows the reactions by (Davidovits, 1991);

interested readers are referred to representative works by Xu and Van Deventer (1999), Komnitsas and Zaharaki (2007), and Metha and Siddique (2016) for more information in this area (among many others). As these studies are heavily focused on chemical engineering processes, additional discussion in this area is beyond the scope of the current thesis. Overall, it is important to note that effective dissolution of an aluminate silicate source plays a critical role in the final geopolymer fabrication (Davidovits, 1991).

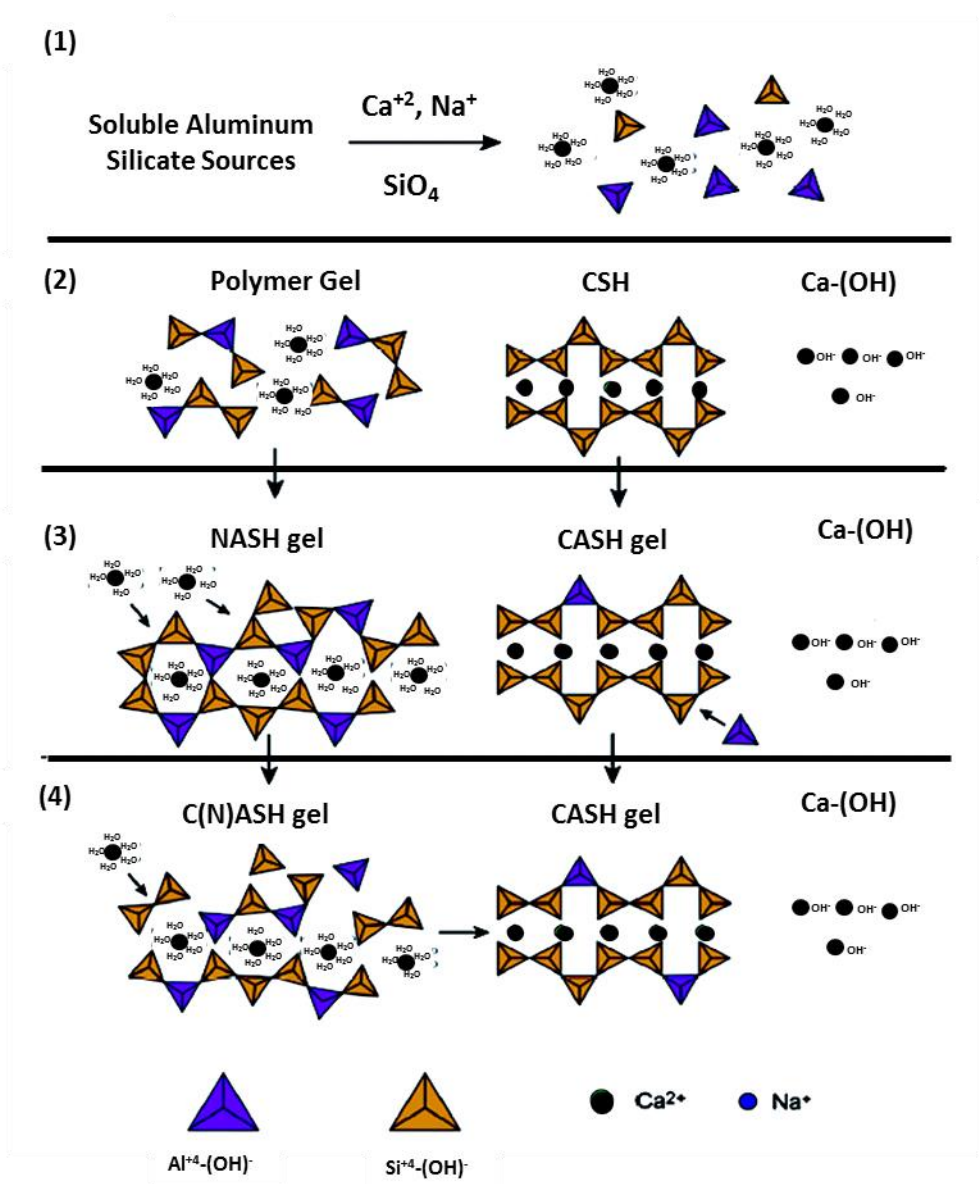


Figure 2.4 The geopolymer reactions mechanism of an alkali activation process (modified after Guo et al., 2016).

Geopolymer gels act as crystalline zeolite minerals hardening the soil polymer structures, providing an excellent mechanical improvement in strength. Additionally,

the process of chemical reactions for zeolites, e.g., hydroxisodalite, calclite, and analcime are similar to the aforementioned polymerization reaction, yielding products that have different structures and components (Phair, 2001; Komnitsas and Zaharaki, 2007).

The fundamental needs to synthesize geopolymer binders are raw materials, inactive filler, and geopolymer liquor (Phair, 2001). Raw materials can be aluminosilicate minerals or industrial wastes. The inactive filler is mostly kaolinite or metakolinite, yielding Al^{+3} through polymerization (Xu and Van Deventer, 2000). Geopolymer liquor is an alkaline solution that works to encourage the dissolution of raw materials, after which point the sodium silicate solution behaves as a binder, alkali activator, and dispersant or plasticiser (Ikeda, 1998; Phair, 2001; Komnitsas and Zaharaki, 2007).

Throughout the polymerization process, chemical reactions occur quickly in the soil matrix once the alkaline solution is mixed with aluminosilicate sources such as kaolinite or metakaolinite. As a result of that quick response, the alkaline solution changes into a rigid polymer. It should be noted that time and space are both curtailing effects on growing well-crystallized minerals (i.e., zeolites) in the soil matrix (Xu and Van Deventer, 2000); this is an essential distinction between zeolites and geopolymer gels, even though the mechanism of chemical reactions likewise involve each other. The formation of geopolymer gels is a substantially faster reaction, however, which results in an amorphous to semi-crystalline matrix relative to the highly crystalline and regular zeolitic structures which can be formed if sufficient space and time are available, and if

the environmental factors such as temperature are favorable at a given location in the microstructure. It has been proposed that geo-polymers are the amorphous indication of zeolitic crystals since the influence of crystalline zeolite syntheses in the matrices are temperature, pH, and cations (sodium, calcium, aluminum etc.) (Davidovits, 1991; Davidovits, 1999; Xu, 2001). It should be noted that the exact process of geopolymer setting and hardening that occurs is not entirely understood. Most conventional hypothesized mechanisms predict steps involving dissolution, transportation or orientation, and polycondensation (reprecipitation) (Xu and Van Deventer, 2000). An aspect of the curing condition, fabrication of geopolymers requires lower curing temperature than the manufacture of zeolites in the binder since growing aluminosilicate polymers (gels) from a solution can occur up to 120 °C (Komnitsas and Zaharaki, 2007). In other words, zeolites can develop over 120 °C, whereas geopolymer requires a lower degree of curing temperature. Thus, temperature controls the type of cementation products that develop during the polymerization. The associated curing conditions will consequently regulate the reaction kinetics by combining or delaying crystal growth and nucleation (Sindhunata, 2006). The cooperation of zeolites and polymers have been investigated in metakaolin (Palomo and Glasser, 1992; Palomo et al., 1999a), and in fly ash-based geopolymers (Palomo et al., 1996b; Bakharev, 2005).

Waste-based materials such as fly ash have been utilized to synthesize geopolymers or zeolites due to their low production costs and beneficial chemical composition and/or material characteristics. In an attempt to immobilize toxic metals, Lin and His (1995) derived fly ash based zeolites which may be utilized in tailings dam

projects. In their research, fly-ash having a low calcium content was chosen to fabricate higher amorphous aluminosilicate phases since lower calcium content, and higher Al and Si develops a better workability and excellent reactivity. In addition, Bell and Maud (1994) proposed the use of gypsum as a stabilizing material for dispersive soils, especially in earth dam construction, owing to its reasonable solubility in water, and the fact that it can be finely pulverized at a low cost. The texture of zeolites depends on the composition of the silicon and aluminum, alkali concentration, and curing temperature (Murayama et al., 2002). In practice, these stabilizers can be mixed with each other, or can be combined with a wide range of waste materials such as recycled gypsum plasterboard, tire chips, fly ash, building residues (i.e., waste materials from building demolition), and high-pozzolan wastes such as cement kiln dust or iron slag, to achieve the desired engineering properties for use on a construction site. Much of the research to date has utilized the aforementioned source materials on a random basis without consideration of their respective mineral compositions (e.g., Khater, 2012; Reig et al., 2014).

2.3 Review of Soil Stabilization with Gypsum and Alkali Activation

The primary objective of this section is to outline and combine the behavior of chemically stabilized/treated soils with various traditional and non-traditional additives utilized in experimental studies where researchers have used these materials to enhance the physical and chemical properties of weak, soft subgrades or clays. The effect of stabilizers as either waste materials or alkali solutions has been investigated by itself or

combined with other stabilizing materials to enhance the development of strength and cementation compound formation within the soil matrix. This section evaluates the use of various non-traditional additives such as liquid sodium silicate, recycled gypsum, and other additives for stabilization of various subsoils, with different stabilizer contents and curing periods being a focal point in most of the studies that have been conducted.

Yilmaz and Civelekoglu (2009) investigated the effect of adding various amounts of pure gypsum to an expansive clay (Bentonite), and reported results from unconfined compressive strength, swelling potential, and plasticity index tests. Yilmaz and Civelekoglu (2009) noted that gypsum-treated soil had improved swell behavior and strength properties, for specimens stabilized with gypsum contents up to 10% by dry mass, which were cured for up to 60 days. The optimum gain in strength was observed to occur at a 5% gypsum content. Overall compressive strengths increased the most rapidly in the first 7 days of curing, with much smaller gains in strength occurring from 7 to 60 days of curing. The swelling potential of treated clay significantly decreased at a 5% gypsum content; this behavior was attributed to replacement of the Na⁺ ions in the bentonite by the calcium ions from the gypsum. A considerable reduction in plasticity index was also observed at a 5% gypsum content. Exchange of monovalent sodium by calcium ions in the clay lattice led to a decrease in the liquid and plastic limits. This study indicates that gypsum may be a viable alternative as a stabilizing additive for highly expansive clays.

Jha and Sivipullaiah (2014) also examined the change in montmorillonite soil that occurred after stabilization with various amounts of gypsum. In this study, X-ray

diffraction analysis, SEM-EDX, pH, unconfined compressive strength, and compaction tests were carried out to understand the micro- and macro-structural changes that occurred to the stabilized soil over different curing periods at room temperature. The authors reported that the acidity of the soil was immediately increased by the addition of gypsum (i.e., a decrease in pH), however, the level of acidity decreased as the curing period increased due to the replacement of ions. Also, increases in the amount of gypsum that were used for stabilization caused immediate strength reduction due to a loss of cohesion in the samples. Development in short-term strength was attributed to the availability of calcium ions for cation exchange since the increase in curing time reduces the solubility of calcium ions and the acidity of the soil. The increases in long-term strength were due to mineralogical and microstructural changes in the clay indicated by new cementation peaks, which were observed in the XRD results, such as calcium sulfate hydrate ($\text{CaSO}_4 \cdot 0.67\text{H}_2\text{O}$) - bassanite ($\text{CaSO}_4 \cdot 0.5\text{H}_2\text{O}$), and formation of new minerals, i.e., zeolite. The SEM results indicated that the voids in the soil were filled with the dissolution of gypsum, with some images revealing sulfate coated around the native minerals. The dry unit weight of the stabilized soil decreased while the optimum moisture content increased; the authors attribute this behavior to the lower specific gravity of the stabilizer relative to the base soil, and the ionic interactions that occur between the stabilizer and base material in the presence of the pore fluid.

Ahmed et al. (2011) examined the effect of combining various additives into a single stabilizing additive mixture, which included: recycled bassanite produced from wallboard, waste plastic trays, and Portland cement; this combined stabilizing mixture

was then used to stabilize a poorly graded sandy soil. Recycle bassanite in various quantities (5, 10, 15 and 20%) was investigated as a stabilizing agent that was utilized to enhance the compressive strength, and plastic waste tray shreds were selected to improve the splitting tensile strength. A small amount of cement, 3% of the dry soil mass, was mixed with the native soil and bassanite, and then water was added to the mixture; cement was utilized in this study to prevent later dissolution of bassanite in the presence of water (i.e., post-stabilization). The primary reasons for conducting compressive strength and tensile strength is that the UCS test is one of the most significant engineering parameters for earth projects. And, tensile strength gives vital shear strength properties especially embankments, highways and heavy moving loads. The findings of the study concluded that additional gypsum slightly increases the dry unit weight of treated soil, and significantly increases the OMC. The use of recycled bassanite significantly improved the compressive strength, particularly in the early stage of curing of the soil (i.e., in the first 14 days) relative to the splitting tensile strength of cured samples. The addition of plastic waste tray shreds (2.5, 5 and 10 mm) to the stabilized soil with recycled gypsum enhanced the splitting strength more than the compressive strength. The influence of curing time is significant, especially in the first 14 curing days, with the curing time being relatively insignificant in improving the strength after 14 days. These results agreed in general with those of Yilmaz and Civelekoglu (2009).

Guleria and Dutta (2012) prepared a reference fly ash geopolymer mix by combining fly ash (the source material of the geopolymer) with 8% lime, and 0.9%

gypsum. This reference mix was also reinforced with wet/dry tire chip contents ranging from 5 to 15%, and the effect of 7, 28, 90, and 180 days of curing on the strength enhancement was then assessed. Standard compaction, unconfined compressive strength (UCS), and scanning electron microscopy (SEM) tests were conducted for this research. The research findings state that small portions of gypsum (i.e., less than 1%) do not have any effect on the optimum water content and the dry unit weight. Not surprisingly, the dry unit weight of the reference mix decreases with the increase in tire chip ratio due to the low specific gravity of tire chips. The result of the UCS increases with increase in curing period for all of the specimens that were tested. The UCS values with wet, tire chips yielded higher strengths relative to dry tire chips. This behavior is associated with the improvement in bonding and formation of cementation products that is believed to occur in a wet environment. Observed strength gains were attributed to the reaction between fly ash particles fabricating ettringite needles, calcium aluminum sulfate minerals, and developed bonding of tire chips during the curing ages. Nevertheless, the UCS decreases with the increase in the dry tire chips content (5-10%) in the soil. This could be attributed to dry tire chips having a tendency for capturing air during the mixing process. Consequently, the proposed reference mix prepared using various waste materials can be used for soil stabilization for heavy traffic load embankments, providing beneficial reuse of multiple waste streams.

Sato et al. (2012) explored the behavior of two different type of soils stabilized using basanite and cement: (1) Decomposed granite soil, which has a uniform grain size and (2) dewatering cake, a fine-grained soil containing organic materials, which was

obtained from construction sites in Japan. These two soils were stabilized by adding 10% and 15% basanite and cement mixtures. The test results state that the strength of stabilized decomposed granite soil was unable to be improved significantly by the addition of basanite, whereas the mixture of basanite and cement could provide a significant improvement in the strength, even after 7 days of curing. Beyond 7 days of curing, additional increases in strength were more gradual. These results were in general agreement with those of Kuttah and Sato (2015). The presence of organic materials tended to inhibit the strength of dewatering cake soil in all stabilizer agents. The usage of the only basanite in this research was not effective; however, an admixture of cement and basanite exhibited considerable improvements in strength.

Kobayashi et al. (2013) utilized recycled gypsum waste plasterboard and Portland cement to improve two different type of cohesionless soil, (1) a fine sand, and (2) a silty soil. A series of standard Proctor compaction and unconfined compressive strength tests were conducted with up to 15% recycled gypsum and 3% cement by soil mass. The effect of the curing time was also investigated at various time intervals. During curing, the temperature was held constant at 21 ± 1 °C, and specimens were preserved at over 90% relative humidity to prevent significant loss of moisture in the treated soils throughout the curing process. Researchers observed that the optimum moisture content and dry unit weight of the stabilized soils increased following increases in the recycled gypsum content. The high content of recycled gypsum significantly impacts the improvement in strength properties of both soils. Curing period affected the development of strength, especially in the early stages of curing. The majority of

strength improvement of treated samples was observed to occur in the first seven days of curing (Yilmaz and Civelekoglu, 2009; Ahmed et al., 2011; Sato et al. 2012; Kuttah and Sato, 2015), whereas the rate of strength gain was slow and insignificant after 14 days of curing. The early strength improvement offers a significant benefit, as rapid curing times are beneficial for some geotechnical engineering projects, such as embankments.

Sivapullaiah and Jha (2014) studied the effect of gypsum upon an expansive soil stabilized with a fly ash-lime admixture for up to 90 curing days. The change of strength mechanism was explored through macrostructural, mineralogical, and alkalinity tests (i.e., pH). Sivapullaiah and Jha (2014) concluded that the dry unit weight of fly-ash-lime stabilized soil with additional gypsum decreased as the optimum moisture content increased, behavior which was attributed to augmenting the binding of particles which occurred in the presence of gypsum. The initial pH value of the fly-ash-lime and gypsum mixture was higher than the fly-ash-lime mixture that did not contain gypsum. It is believed that the additional calcium in the presence of gypsum may increase the pH value. Additional gypsum in the soil matrix increased the strength at 7 and 14 days of curing, relative to the stabilized soil mixture that did not contain gypsum. This study observes that binding gypsum and soil accelerates early strength gains. Moreover, it is believed that the cementation/ polymerization components such as CSH, CSAH (and dissolution of Al and Si) increase the strength of soil while filling the voids of the matrix (Metha 1973; Dermatas 1995; Little et al. 2009; Puppala et al. 2005).

Kiliç et al. (2015) stabilized a highly plastic clayey soil by mixing 3, 6, 9, 12 and 15% of a lime/gypsum mixture into the base soil. For stabilization purposes, a consistent 1:1 lime to gypsum ratio was maintained during the stabilizer preparation process, and specimens were tested at curing periods of 7, 28 and 90 days. For comparison purposes, 100% lime and 100% gypsum mixtures were also prepared at the same stabilizer percentages mentioned above. Unconfined compressive strength tests and swelling tests were performed on the stabilized clayey soil. Results indicated that the mixture of gypsum and lime at all percentages improved the strength of soil more effectively than only recycled gypsum. The highest strength was obtained by the 15% all-lime stabilized mixture. The use of only recycled gypsum resulted in the lowest strength gain at all stabilizer mix percentages for 7 and 28 days, which is why the optimum ratio of gypsum was not proposed for those curing intervals due to the low rate of strength improvement. It was noted that gypsum was not suggested as a soil stabilizer due to yielding weaker strength values when it was utilized alone. The optimum additive rate (i.e., the most beneficial strength gain with the smallest amount of stabilizer added) was for the 100% all-lime stabilizer at a stabilizer percentage of 6%, which resulted in a considerable reduction in the swell percentage and associated swelling pressures. The 50%/50% mixture of lime and gypsum yielded middle-ground performance among the others in terms of swell percentage, swell pressure, and unconfined compressive strength. It was concluded that the effect of gypsum and lime on this clay yielded results that were between those of the 100% lime and 100% gypsum stabilizers.

Ahmed (2015) studied the microstructure and mineralogical composition of soft clay treated with recycled basanite derived from gypsum waste material. Additive mixture of the basanite was prepared at different ratios with cement and lime (1:1, 2:1, and 3:1), respectively, which leads to reduced solidification of basanite, and cured for three different intervals (3, 7, and 28 days) to investigate their impact on the compressive strength and formation of cementation compounds. The result of tests shows that adding basanite into soft clay augments the strength of the soft clay, for all of the admixture ratios that were assessed. Nonetheless, increasing the basanite-cement mixture content has a negative effect on the strength gain process. Gradual strength increases were observed with the addition of the basanite-cement mixture, at the various curing stages, whereas the mixture of basanite-lime resulted in enhancing the maximum strength in 7 and 28 days of curing. The XRD and the SEM analyses detected a number of cementation products such as the formation of ettringite (C-A-S-H), calcite forming during carbonation, and calcium hydroxide as a result of binding additives with the soil. Ettringite is one of the well-defined cementation materials leading to gain strength for stabilized soils that utilize calcium based additives (Khoury et al., 2003).

Jha and Sivapullaiah (2015) examined the role of gypsum on the strength of the lime-stabilized soil after an extended period of curing times. The content of gypsum and lime ranges from 0, 2, 4, and 6% for up 28 days curing in the short term. The experiment extended up to 365 days to investigate the effect of stabilizers over a long-term curing period. The conclusions highlighted in the study are the admixture of gypsum and lime (4%) accelerated the early strength gain up to 14 days, whereas the improvement in

strength at 28 days of curing yielded a lower value. The strength was, afterward, recovered for 90 days of curing, but the development of the strength for 180 and 365 days of curing was generally fluctuating in nature. Additional gypsum results in the reduction of the strength depending on the curing period. Alteration in strength was associated with the high content of gypsum compared to lime content. The initial pH values increased with the increase of curing time, but additional fluctuation was observed with increasing additive content and curing time. The microstructural analysis of the stabilized soil reveals the formation of ettringite compounds, C-S-H, C-S-A-H, C-(S)-A-H. Different quantities of ettringite and unreacted additives cause serious changes in the ground at various admixture contents and curing times. The formation of cementation products was found to be clearly related to the additive content and curing time.

Ahmed and El Naggar (2016) investigated the use of recycled bassanite gathered from plasterboard waste mixed with lime and furnace cement at a 2:1 ratio with bentonite at 3%, 6%, 9%, and 12% by dry weight. They performed compressive strength tests, mineralogical and microstructural composition tests, and environmental property tests (pH) to observe the effect of basanite admixture stabilization. The XRD results indicated a decreasing intensity of montmorillonite with the increasing percentage of additives in the soil, as the montmorillonite was consumed by stabilizers in the soil matrix. The ultimate compressive strength and dry unit weight of the tested bentonite increased depending on the admixture content, which is related to dewatering and flocculation controlling the improvement in strength. Not only do dewatering and

flocculation improve the strength of soils, but the development of new cementation/polymerization compounds also occur due to pozzolanic reactions that occur, i.e., carbonation and cation exchange. However, new cementation compounds such as ettringite were not detected through the XRD and SEM investigation. The lack of new compounds may be related to the formation of calcite, a product of carbonation, delaying the formation of ettringite. The study shows that the pH also has a significant effect on cementation products forming in the soil matrix depending on curing time because consumption of calcium ions in the soil matrix accelerates the reduction of pH in the bentonite mixture over time, as soil stabilization occurs.

Kamei et al. (2013) investigated the use of recycled bassanite obtained from gypsum waste plasterboard and coal ash as stabilizer material for a very soft clay (kaolinite). Strength increases were measured using a series of unconfined compression tests. Treated specimens were cured up to 28 days at room temperature ($21\pm 1^\circ\text{C}$). The combination of bassanite that was derived from recycled gypsum and coal ash positively improved the mechanical properties (strength and durability) of soft clay, although the use of only coal ash had a smaller beneficial effect on the improvement in strength. Significant strength development quickly occurred from 1 to 7 days; afterward, the strength gradually increased for all specimens. The initial stages of curing are therefore much more significant than the later curing times for gains in the stabilized soil strength. The dry unit weight of treated soil decreased with the increase in bassanite-coal ash ratio. In addition, the OMC was reduced for increasing bassanite-coal ash ratios due to the tendency of bassanite to absorb water. SEM analysis states that the growth in the

presence of bassanite-coal ash accelerates to form ettringite minerals in the soil mixture. It is noted that the use of waste materials contributes to improving a sustainable society by diminishing solid wastes, while producing useful construction materials.

El-Afi and Gado (2016) performed research using kaolin, marble sludge, and gypsum to produce a calcium sulfoaluminate-belite cement face that provided an alternative to Portland cement due to low production cost and beneficial environmental effects. Treated samples at different curing temperatures (1150, 1200 and 1250°C were characterized through microstructural techniques including Fourier transform infrared spectroscopy (FTIR), X-ray diffraction (XRD), and scanning electron microscopy (SEM). The XRD patterns indicate that the primary hydration products were ettringite, calcium sulfoaluminate hydrate (CSAH), calcium silicate hydrate phase (C-S-H), and Portlandite. Ettringite is deficient in early age treated samples due to the lack of gypsum content through the hydration process. Such hydration products, Stratlingite, Katoite, manocarboaluminate, and hydrogarnet, may be observed in calcium sulfoaluminate cement, and further investigation regarding their chemistry is proposed as a future area of research study. The chemical composition of cement hydration products was detected using the spectroscopic method (FTIR). The asymmetric stretching Si-O band is intensified at $\sim 995 \text{ cm}^{-1}$ with hydration indicating the formation of C-S-H. The carbonate peaks at 2360, 1420 and 875 cm^{-1} were formed due to the reaction atmospheric CO₂ in the air. SEM images yield the formation of tiny ettringite minerals in the voids after 28 days of curing. Portlandite, C-S-H, and low calcium sulfoaluminate (CSAH) were confirmed, which fill the pore spaces in the specimens and results in

hardening the structure. These cementation materials can be detected in the cement stabilized soil, providing excellent mechanical properties; thus, the combination of kaolinite-gypsum and recycled marble sludge at given ratios is useful to synthesize calcium sulfoaluminate-blended cement as an alternative to Portland cement.

Satee (2003) carried out research on the effect of liquid sodium silicate on the stress-strain behavior of a laterite soil classified as a silty gravel with high plasticity. Sodium silicate stabilization contents of 0.6M, 0.7M, and 0.8M were assessed as part of this study. Compacted UCS specimens at the Standard Proctor optimum water content and maximum dry density were cured for 0, 1, 14, and 28 days, and then subjected to UCS testing. The study concluded that the highest improvement in strength achieved for all of the curing periods was the 0.6M content. The soil gained strength proportional to the curing day, with all samples reaching their maximum strength at 28 days of curing.

Alan et al. (2003) performed sodium silicate stabilization of a Texas clay, which was composed of kaolinite, illite, and montmorillonite, with a high sulfate content. The soil was stabilized by the addition of liquid sodium silicate at the ratio of 10 and 50% by dry soil weight. Atterberg limits, Proctor tests, undrained triaxial compression tests, and one-dimensional swell tests were considered to examine the behavior of the stabilized soil. Although engineering properties were consistently improved at the given stabilizer ratios, there was not enough strength gain observed at the given additive ratios to be as useful in the field for stabilization applications (relative to other stabilization alternatives). The authors also reported that curing time plays a significant role in

developing the strength of cement compounds such as NAS and CAS during sodium silicate stabilization.

Guo et al. (2010) prepared geopolymers from a class C fly ash that was mixed with a combination of sodium hydroxide and sodium silicate, and cured up to 28 days in an air-conditioned room at 23 °C. Unconfined compressive strength tests and microstructural characterization of geopolymers were performed. The maximum improvement in strength was obtained at a 10% admixture ratio after 28 curing days. Also, further strength development was no longer evident beyond a 10% stabilizer admixture content. These findings highlighted that the increase in the ratio of the alkaline solution might augment compressive strength because the aluminosilicate presented in the raw material is dissolved quickly. Amorphous gels including calcium silicate hydrate (C-S-H) appear from 20 to 40° (2θ) as a broad and amorphous halo shape in the diffraction pattern. The geopolymeric reaction and the hydration reaction start at the same time within the gel system. Additionally, a new peak of zeolites, gismondine, appeared in the XRD pattern. FTIR spectroscopy weakly shows the main absorption bands of amorphous gels at 1036 and 1400 cm⁻¹ indicating cementation products such as CSH, C(N)ASH.

Suganya and Sivapullaiah (2016) investigate the role of sodium silicate as an additive in cement-treated organic soft clay soil cured for 28 days after stabilization. The UCS test was applied to evaluate the effect of additive dosage on the strength. The mineralogical and microstructural investigation was completed using XRD, SEM and pH measurements. Stabilized soil strength increased following increases in the quantity

of cement and sodium silicate in the tested specimens. However, there is no proposed optimum additive content in this research since the strength reduces relative to other tested specimens as the increase of sodium silicate content in the admixture continues to increase. Air-dried powder of the treated soil was used to identify the reaction products using XRD. Calcium silicate hydrate, (CSH), sodium calcium silicate hydrate, (N(C)SH), and sodium calcium aluminum silicate hydrate, (N(C)A-S-H) were detected at various intensities in the XRD testing that was performed. Peaks corresponding to CSH exhibited a higher intensity when the ratio of sodium silicate increased in the matrix. The pH changes of stabilized soil depend on the curing time. At any curing time, samples treated with sodium silicate have a higher pH than cement-treated soil. The pH of the admixture increased with the content of sodium silicate. A highly alkaline environment can dissolve reactive silica and alumina from the clay lattice into the pore solution, and accelerate the formation of hydration compounds that contribute to the overall strength improvement of the treated soil.

Latifi et al. (2013) considered the effect of non-traditional stabilizers on the geotechnical properties of tropical laterite soil treated with liquid sodium silicate stabilizer. A standard compaction test, the UCS, X-ray diffraction, SEM and FTIR tests were employed to determine mineralogic and microstructure properties of the natural and stabilized soils with different amount of stabilizer. Adding stabilizers into soil led to a decrease in the dry unit weight and a slight increase in the optimum moisture content. The main strength developments were achieved after 7 days of curing, with slight increases beyond this point. Also, higher contents of the stabilizing additive

beyond the optimum value (9%) reduced the compressive strength. In the XRD testing, a few peaks related to quartz and kaolinite diminished and reorganized due to the effect of chemical reactions, but no new peaks owing to the amorphous (gel-form) structure were detected. FTIR spectrum analysis shows a reasonable change in the Si-O bonding groups of soil particles. That is because of the chemical reaction of the stabilizer and the clay minerals. Based on the result of SEM, the newly formed gel compound of sodium aluminate silica hydrate (N-A-S-H) was believed to be the main reason for strength gain that was detected.

Pavithira et al. (2016) researched the effect of sodium silicate (Na_2SiO_3)/sodium hydroxide (NaOH) ratios on the synthesis of fly ash based geopolymer. Solution ratios of 1, 1.5, 2, and 2.5 were examined to investigate the improvement in strength and the elemental composition of the geopolymer. It was concluded that the compressive strength of the resulting geopolymer mixture by itself initially increased with ratios of 1 and 1.5; beyond 1.5 (2 and 2.5) the strength of the geopolymer was smaller. Similar increases and decreases in strength behavior were observed for geopolymer stabilization of a soft clay soil, which was also assessed (but not as the focal point) in the current study. It was noted that soluble silica can improve the strength, yet the presence of unreacted sodium silicate inhibits the polymerization process, which results in decreasing the strength. Energy dispersive X-ray (EDAX) reveals elemental compositions of samples. The finding from the test is that compressive strength increased until the ratio of Si/Al was approximately 3, which might be related to the formation of the three-dimensional cross-linked rigid network. For additional increases

in the ratio of Si/Al beyond 3, the compressive strength decreased, behavior which could be due to enhanced development of a two-dimensional network of linearly linked polymeric structures.

Hoy et al. (2016) investigated the strength development of recycled asphalt payment-Fly ash geopolymer treated with a combination of sodium hydroxide (NaOH) and sodium silicate, (Na_2SiO_3) solutions as an activator at four different contents (100:0, 90:10, 60:40, and 50:50). Specimens were cured at both 25 and 40 °C for 7 and 28 days. The unconfined compressive test was utilized to determine the strength development of stabilized specimens. The strength improvements were analyzed using SEM and XRD testing. Test results indicated that the highest development in strength was achieved at an early stage of geopolymerization (7 days) with Na_2SiO_3 , whereas the UCS values are lower without Na_2SiO_3 . That implies that additional of Na_2SiO_3 enhances the short-term strength development of recycled asphalt-fly ash geopolymers. Additionally, without Na_2SiO_3 , the geopolymerization is slower at 25 °C than 40 °C. Curing conditions and admixture composition affect the improvement in strength. The XRD pattern shows new silica and alumina rich products such as amorphous calcium silicate hydrates (C-S-H) and calcium aluminate hydrates (C-A-H), including crystalline phases of gypsum, labradorite, margarite, and mullite. At longer curing times, sodium aluminum silicate hydrate (N-A-S-H) was formed due to the high solubility of the silica present in the sodium silicate. Geopolymer samples of NaOH/ Na_2SiO_3 (50%:50%) yield amorphous cementation phases associated with strength enhancement, since C-S-H and C-A-H are co-existing products of the polymerization process. The high content of Na_2SiO_3

accelerates the geopolymerization due to highly soluble silicate being readily available in the solution.

Reig et al. (2014) investigated the effect of sodium silicate and sodium hydroxide on the compressive strength and microstructure of a stabilizing binder produced from porcelain waste. The pH value was higher than 11.6 for all treatment phases, but it decreased with increases in curing time. The decrease in pH is related to the formation of reaction products during the activation process. The compressive strength linearly increased with increases in the ratio of sodium once the ratio of silicate (SiO₂) was kept constant. The maximum improvement in strength was obtained after 7-days of curing at 65 °C. After activation process, the hump characterized by amorphous gels and calcium silicate hydrate (C(A)SH) gel was detected in the XRD at diffraction angles between 20 to 40° (2θ). As reported by Guo et al. (2010), these humps represent manufactured geopolymers. Zeolite crystalline such as gismondine, sodalite, Na-Herschelite, or hydroxysodalite were detected as secondary reaction products, in agreement with the findings reported by Dombrowski et al. (2007) and Duxon et al. (2007). During SEM measurements, a minor quantity of nitrite (sodium-calcium carbonate) and calcite were also identified in the treated samples as the amount of sodium increased. According to Criado et al. (2007), the main band associated with the amorphous gel is ~1071 cm⁻¹. After the alkali activation process, the band shifted to lower frequencies (1020 and 1013 cm⁻¹), behavior which is attributed to a newly formed NASH gel yielding improved material strength behavior.

Yi et al. (2010) studied the treatment efficiency of alkali-activated ground-granulated blast furnace slag (GGBS) for the stabilization of a soft marine clay, relative to stabilization of the same clay with Portland cement (PC). The influence of additives including carbide slag (CS), Na_2CO_3 , NaOH, Na_2SO_4 , NaOH-CS, Na_2SO_4 -CS and Na_2CO_3 -CS on the stabilization efficiency was examined for up to 180 days of curing. The results indicate that Na_2CO_3 -GGBS has no noticeable effectiveness in the strength development at any curing age. The admixture of NaOH-GGBS yielded the highest strength gains at 7, 28 and 90 days, although the UCS was reduced beyond the 90 day point due to microcracking on the samples. PC stabilized clay had lower strength values than that those clays which were stabilized with CS-GGBS sample. The strength value of NaOH-CS-GGBS and Na_2CO_3 -CS-GGBS stabilized clays decreased after 90 days. The most efficient binder combination was Na_2SO_4 -CS-GGBS for this kind of marine clay, which yielded strengths that were at least two times higher than PC stabilized clays at any curing stage. Regardless of additive type, CSH were detected in all of the treated marine clays as the main hydrated products. CAH and hydrocalumite belonging to the family of hydrated calcium aluminates were observed in the sample stabilized with NaOH-GGBS and CS-GGBS. Additionally, considerable ettringite was detected in the Na_2SO_4 -CS-GGBS stabilized clay, which provides strength enhancement. However, the formation of CAH disappeared after adding Na_2SO_4 into the mixture, and the crystalline phase of ettringite minerals increased due to increasing sulfate ions in the binder.

Sukmak et al. (2013) examined the factors that influence strength improvement in a clay-fly ash (FA) geopolymer consisting of fine aggregates. Liquid alkaline

activators sodium silicate (Na_2SiO_3), and sodium hydroxide (NaOH), abbreviated as L, were used in various combinations. In the study, the influence of $\text{Na}_2\text{SiO}_3/\text{NaOH}$ ratio, L/FA ratio, and curing conditions were investigated. The ratios of $\text{Na}_2\text{SiO}_3/\text{NaOH}$ examined in this study were 0.4, 0.7, 1.5, and 2.3, while the L/FA ratios examined in this study were 0.4, 0.5, 0.6, and 0.7 by dry mass. The UCS samples were prepared using a hand-operated hydraulic jack at the selected optimum water content to achieve the maximum dry unit weight. All specimens were stored at room temperature for 24h before being cured in the oven at 75°C for 48 h. The results indicated that the most effective strength development occurred at optimum values of $\text{Na}_2\text{SiO}_3/\text{NaOH}$ and L/FA of 0.7 and 0.6 respectively. An extreme reduction in strength for the clay-FA polymer with excessive alkali activator ($\text{L/FA} > 0.6$) was attributed to the precipitation of dissolved Si and Al at an early stage before the initial fabrication process; this process yielded the formation of cracks on the FA particles.

Ridtirud et al. (2011) reported that the optimum ratio of $\text{Na}_2\text{SiO}_3/\text{NaOH}$ for fly-ash based geopolymer was 1.5, in order to achieve the maximum unconfined compressive strength for a stabilized sand. The strength linearly increased with a high content of Na^+ ions in the mixture where Na^+ is significant for the formation of geopolymers by creating charge balancing ions. However, unreacted sodium silicate in the mixture tended to reduce the compressive strength of mixed soil as the higher presence of sodium silicate blocked evaporation of water, which was then distributed to three-dimensional networks of aluminosilicate geopolymers.

Jun and Oh (2015) discussed the strength reduction during the curing process of fly-ash, and gypsum geopolymer stabilized with sodium silicate and sodium hydroxide solution. The Fly-ash activated strength was reduced due to microcracks in the matrix that formed due to excessive amounts of Na and Ca ions at an early stage in the polymerization process. Also, the strength of the samples continually decreased with increases in curing time. Noncrystalline zeolite phases may also cause micro-cracks to develop due to their fast-growing process that can demolish a hardened matrix. Unreacted soluble silicate accelerates the growth rate of crystalline zeolites beyond 28 days curing time, yet they are too small to be detected by the XRD. The gypsum addition, 2 to 6%, into the admixture resulted in regaining the strength at 28 curing days; yet, over 6% gypsum content, the overall strength tended to get lowered markedly. Additional gypsum promoted growing a new NaSO_4 mineral, thenardite, in the matrix, which can reserve a considerable portion of Na^+ ions at the early age of polymerization. Low concentration of Na^+ assists in preventing reduction of strength due to slowing down the growth rate of zeolitic minerals. Optimum gypsum content might prevent possible strength deterioration by reserving Na^+ and delaying the process of silicate dissolution during geopolymer formation.

Boonserm et al. (2012) investigated the influence of fuel gas desulfurization using a gypsum (FGDG), bottom ash (BA) and fly-ash (FA) based geopolymer, which they examined utilizing FTIR and FESEM techniques. The FGDG was mixed at dry weight ratios of 0%, 5%, 10%, and 15%, and the ratios of BA/FA examined were 100:0, 75:25, 50:50, and 25:75. Sodium silicate and NaOH were selected as alkaline stabilizer

agent to activate both BA and FA geopolymers and were cured at 40 °C for 48h, and then kept curing for an additional 7 days at 25 °C. UCS tests were conducted to determine the effects of stabilizers on the mechanical properties of the fly ash based geopolymer. Microstructural tests, XRD and SEM, characterize new cementation phases developing during geopolymerization. Increased FA content in the binder considerably increases that overall strength compared to only FGDG treated specimens. This is due to glassy phase and high reactivity of FA in comparison to BA. Additional FGDG (5-10%) significantly increases high content FA geopolymer mortars since a high concentration of sulfate ions in the system promotes the dissolution of aluminum ions in BA and leads to enhance stronger polymers. The microstructural analysis confirms this process. New crystalline zeolites containing sulfate ions were detected in both XRD and FESEM images, including vishnevite, thenardite, and gel formations of CSH. It is believed that the strength improvement is due to the presence of some of those crystalline and gel phase materials. FTIR analysis is also performed in the range of 4000-500 cm^{-1} . Broad bands at 3700-2200 cm^{-1} and 1700-1600 cm^{-1} were observed for all geopolymer pastes were assigned to O-H stretching and H-O-H bending due to the absorbed water on the surface or porose structures of manufactured polymers. The wave numbers of 1200 and 636 cm^{-1} represents SO bonding that shows chemical reactions occurring between the SO_4 ions and the alkaline solution.

Arrifin et al. (2013) prepared a geopolymer concrete using blended ash polymer (BAP) concrete based on pulverized fuel ash (PFA) and palm oil fuel ash (POFA) activated with the ratio of $\text{Na}_2\text{SiO}_3/\text{NaOH}$ (2.5) solutions. Ordinary Portland cement

(OPC) was prepared to compare results as a control procedure. Specimens were cured in water for 28 days at 28 °C. Afterwards, specimens were exposed to 2% (H₂SO₄) sulfuric acid for 1, 3, 6, 12 and 18 months to determine the effect of sulfuric acid on strength development. The results were characterized using unconfined compressive strength tests, XRD, SEM and FTIR analysis. The initial strength gradually decreased for both both the BAP and OPC concrete specimens during the exposure time. In alkali-activated concrete (BAP), the X-ray diffraction patterns revealed amorphous and semi-crystalline phase of NASH. Moreover, another phase of geopolymerization exhibited as nanostructure of zeolites such as gemelinite and sodalite, though OPC concrete resulted in CSH products. FTIR stretching bands of O-H and H-O-H and carbonate were detected at 3700 to 2200 cm⁻¹, 1645 cm⁻¹, and 1425 cm⁻¹ respectively. The primary binder gel of OPC, the asymmetric stretching mode of C(A)SH, was observed at 1010 cm⁻¹ whereas NASH gel fabricated in the binder system was located at 1040 cm⁻¹. The presence of untreated gypsum led to shifted water component and chemically water molecules from 3435 cm⁻¹ to 3405-3555 cm⁻¹ and 1625-1690 cm⁻¹ respectively. Meanwhile, the existence of calcite in the binder system transferred to CSH gel from 1010 to 1145 cm⁻¹, which states decomposition of the main binder in OPC. After exposure to sulfuric acid, there were no differences regarding cementation products between the unexposed and exposed in the BAP specimens, whereas the reaction products, CSH, and OH phases, were decomposed as a result of acid exposure in the OPC. The results indicate that sulfuric acid attack presented little or no effect on the microstructure of BAP concrete compared with OPC concrete.

Nath and Kumar (2013) analyzed two types of iron making slags named Granulated Corex Slag (GCS) and Granulated Blast Furnace Slag (GBFS) as replacement of fly ash from 10 to 50% in blended geopolymers. The strength, FTIR, XRD, and SEM test were conducted and compared to both the geopolymer samples. The strength developed with the increase in the slag content for both cases due to the enrichment of C-S-H gels suited Puertas and Fernández-Jiménez (2003); Kumar et al. (2010). FTIR study states that GCS based geopolymer has more dense peak intensity because of more glassy and heterogeneous characteristics (Rees et al. 2007). The XRD patterns of samples revealed new crystalline phases and showed the decrease in the peak with increase in the slag content. The microstructure analysis confirms a fully reacted dense matrix including aluminum silicate hydrate and CSH for GCS based geopolymer.

2.3.1 An Overview of Recycled Gypsum and Sodium Silicate Stabilization

Gypsum greatly improves both the physical and chemical properties of soil (Arakelyan, 1986). Nevertheless, the favorable effects of gypsum on the engineering properties of soil relies on numerous factors such as the type of the soil, its mineralogical composition, the size and shape of soil particles, and the moisture content of the soil. Furthermore, the development of new cementing agents for soil stabilization using alkali-activated cementing agents known as “geopolymers” has become popular over the past several decades due to their high performance (high strength and durability). Geopolymers offer an environmentally friendly alternative to stabilization of soil via traditional ordinary Portland cement approaches (Davidovits, 1991). Geopolymer

stabilization results in improving soil properties by binding a variety of silica-rich materials such as kaolinite, bentonite, silt, and waste products such as fly ash, bottom ash with liquid alkaline activators like sodium silicate and sodium hydroxide. The hardening process of geopolymers depends on the type of stabilizers that are used to make the liquid alkaline solutions, and also the nature of the aluminum silicate sources such as clay particles (of varying mineralogy), silt particles (of varying mineralogy), other additives such as furnace slag, and environmental factors such as curing temperature.

The existing literature indicates that recycled gypsum can be utilized as a sustainable stabilization agent. The development of soil properties depends on the type of soil, stabilization conditions, and presence of additional stabilizers such as fly ash, furnace slag, lime, and cement. However, it is also reported that gypsum can reduce improvements in the stabilized soil strength as curing time increases since the presence of sulfate ions causes highly expansive crystalline minerals to grow; one example is thaumasite, which is found in lime-gypsum stabilization, and which has been referred to as “Manmade Expansive Soil” (Hunter 1988; Dermatas, 1995). It should be noted that gypsum is one of the most highly soluble salts found in nature, and the use of gypsum alone for soil stabilization may cause catastrophic damage to earth structures, subgrade soils, and buildings. This reason is why gypsum (or recycled gypsum) is often combined with other produced materials such as fly ash, marble waste powders, and ordinary Portland cement, and mixed with a wide range of clay soils, bentonite, kaolinite, marine clays, silts, silty-sands, and laterite soils. It is observed that the

utilization of gypsum in combination with other additives improves soil properties as much as other more traditional stabilization techniques.

Meanwhile, the usage of geopolymers has been shown to be potentially effective for various ground improvement projects, based on the current literature. Various soil types, including clays, silts, and aluminosilicate based waste products such as fly ash, bottom ash, and furnace slag have utilized to develop environmentally friendly cementing compounds without using traditional chemical stabilization agents. These geopolymer products have reportedly produced higher compressive strengths, have a greater resistance against sulfate than cement based products, low permeability, and the ability to immobilize some common heavy metal ions in their geopolymer structures (which is beneficial for stabilization of mine tailings and tailing dams' structures). Moreover, high temperatures are not required to prepare geopolymers; thus, energy consumption and the emission of CO₂ is relatively low compared to the production of traditional soil stabilizers such as ordinary Portland cement. Some geopolymer production processes also utilize waste stream materials, which provides additional environmental benefits (Gao et al., 2014; Hoy et al. 2016).

Consequently, several researchers have presented their findings regarding the effect of various gypsum compounds and geopolymers for stabilization of different soil types, while utilizing a diverse array of additives. Table 2.1 summarizes the results from a number of previous gypsum and alkaline activated stabilization research studies, which have been utilized to improve unfavorable engineering properties of different types of soils and waste materials.

Table 2.1 Effect of recycled gypsum and alkaline activation on the engineering properties of various soil types

References	Properties	Materials	Observations
Yilmaz and Civelekoglu, (2009)	Atterberg's limits, strength, swell behavior	Na-Bentonite Clay, Gypsum	Strength improves with increase of curing times. The liquid limit, plasticity index and swelling percentage reduce
Jha and Sivipullaiah, (2014)	Microstructural analysis, pH, Compaction, Compressive Strength	Montmorillonite soil, Gypsum	The acidity reduces with the increase of curing times. Strength decreases with the increase of gypsum content. The dry unit weight of stabilized soil gradually decreases while the OMC increases with the increase of gypsum content. Particles are coated with sulfate.
Ahmed et al., (2011, 2012)	Compaction, Compressive and tensile strength	Sandy Soil, recycled gypsum (5, 10, 15, 20%), plastic tray waste (0.25, 0.5, 1, and 2%)	The OMC and dry unit weight of soil significantly increase with the increase in recycled gypsum content in the soil. Compressive strength significantly improves than tensile strength. This could be due to flocculation of soil particles presence of calcium ions in gypsum, and hydration process of gypsum.
Gulleria and Dutta, (2012)	Compaction, The UCS, and FESEM	Gypsum, 0.9% Fly-ash, lime, 8% and wet/dry tire chips 5-15%. Reference mix prepared and cured 7, 28, 90 and 180 days	The OMC and dry unit weight of specimens do not affect the small portion of gypsum content. The UCS increases with the increase of curing periods. Dry, wet tire chips yield higher strength values compared to dry tire chips. Adding fly-ash to mixture considerably increases the strength, and accelerates to develop new cementation phases in a wet environment. New cementation compounds, ettringite detected.
Sato et al., (2012), Kuttah and Sato (2015)	Compressive strength test	Fine grain Decomposed granite soil, and dewatering cake containing organic materials bassanite and cement	The compressive strength of decomposed granite is higher than dewatering cake specimens. Organic content exhibits the improvement in the strength. The UCS slightly increases with the increase of curing ages regardless of soil type. Cement increase long-term strength values decomposed granite soil. Adding only basanite is not effective for strength development.
Latifi et al., (2013)	Compaction, UCS, microstructural analysis (XRD, SEM, FTIR)	Laterite soil (kaolinite), liquid sodium silicate	The OMC slightly increases while the dry unit weight decreases. First 7 days are significant for improvement in strength. The intensity of quartz and kaolinite gradually reduces, but no new peaks are depicted. SEM images and FTIR confirm NASH products.

Table 2.1 Continued

References	Properties	Materials	Observations
Kobayashi et al., (2013)	Compaction, compressive strength, effect of curing time	Fine sand, silty soil, recycled gypsum, cement	The OMC and dry unit weight of both soils increase with increasing gypsum content. A high percent of gypsum is significant for both soils. Most of the strength gain in 7-days. Thereafter, it is insignificant.
Sivipullaiah and Jha (2014)	Microstructural analysis, pH, Compaction, Compressive Strength, up to 90 days curing time	Expansive soil, Gypsum, fly-ash lime mixture	The OMC increases while the dry density decreases. The initial pH of bassatine-fly ash-lime significantly decreases compared to specimens without bassanite. Gypsum improves early stage strength of soil. New cementation compounds emerge CSH, CSAH.
Kilic et al., (2015)	Compressive and swell behavior	Highly plastic clay, gypsum, and lime at ratio 1:1 up to 15%	The mixture of gypsum and lime yields results in between those of only lime and only gypsum treatments in terms of the strength gain, swell pressure and percent. Strength weakens in between 7 and 28 days of curing. Optimum additive content was not proposed for the only gypsum treatment. 6% lime significantly decreased swell percent and swell pressure.
Ahmed, (2015)	Compressive strength, and mineralogical composition	Soft clay, bassanite, cement, and lime (1:1, 1:2, 1:3), curing 3, 7 and 28 days	Bassanite-cement gradually improves strength in all curing ages. The increase of bassanite-cement mixture content decreases the strength in comparison to the mixture of bassanite-lime content. Calcining, and formation of CASH
Jha and Sivapullaiah, (2015)	Atterberg's Limits, pH, compaction, compressive strength test, mineralogical analysis, cured up to 365 days	High degree expansive clay (CH), Gypsum-lime mixture (0,2, 4, 6%)	LL decreases while PL increases with increasing lime-gypsum content. γ_{dmax} decreases while OMC increases with increasing lime-gypsum content. Strength reduces between 14-90 days and regains beyond 90 days. Increasing gypsum ratios beyond the optimum stabilizer level result in reducing the strength. Formation of CSH, C(S)AH, emerge in all specimens, and depend on additive content and curing age.
Ahmed and El Naggar, (2016)	Compaction, Compressive strength, mineralogical analysis (XRD, FESEM, and pH	Bentonite, recycled bassanite, and mixture of cement and lime at 2:1 ratio	Compressive strength and dry unit weight increase with additional stabilizing additive, while the OMC decreases. The intensity of clay minerals decreases due to dewatering and flocculation during the various curing ages in XRD. Cementation compounds do not emerge in any samples.

Table 2.1 Continued

References	Properties	Materials	Observations
Kamei et al., (2013)	Compaction, compressive strength, FESEM analysis, cured 1, 3, 7 and 28 days	Kaolinite, admixture of recycled gypsum-coal ash (0 and 20%)	The OMC and dry unit weight of stabilized kaolinite decreased with increasing gypsum-coal ash admixture content. Early curing, 1-7 days, is more significant than later ages. The usage of only coal ash is not recommended due to lower strengths. Combination ratios impact Ettringite development during the curing intervals.
El-Alfi and Gado, (2016)	Microstructural analysis (XRD, SEM, FTIR), cured at 1150, 1200, and 1250 °C	Kaolinite (25%), Gypsum (20%), marble sludge (55%) (Sulfoaluminate cement)	New cementation compounds, CSH, ettringite, CASH, are confirmed by XRD, SEM images, and FTIR spectrometry after a long time curing age, which is portlandite and ettringite. The combination of materials successfully results in fabricated cementation materials yielding excellent mechanical properties.
Satee J., (2003)	Compressive strength, cured at different content, and up to 28 days (0, 14 and 28)	Highly plastic laterite soil, silty-gravel, liquid sodium silicate by 0.6M, 0.7M, and 0.8M	All specimens gradually achieve maximum strength within 28 days of curing at 0.6M additive content. The strength and additive concentration is relatively in proportion.
Alen F. et al., (2003)	Compressive strength, and effect of curing time at the ratios of 10 and 50%	Clay soil (kaolinite, illite, montmorillonite and sulfate ions), liquid sodium silicate	Sodium silicate is a primary chemical agent for aggregate materials without altering clay lattice. Curing is a significant factor in strength development. The improvement in engineering properties is inconsistent at given additive ratios.
Guo et al., (2015)	Compressive strength, mineralogical analysis (XRD, FTIR), cured up to 28 days at room temperature	Geopolymer from fly-ash mixed with NaOH and sodium silicate	Maximum strength displays within 28 days of curing by 10% stabilizer. The additional stabilizer is ineffective for strength development at any curing period. A broad halo was observed in the XRD pattern, which characterizes an amorphous phase of the geopolymer. A weak peak display in FTIR wavelengths represents the geopolymer materials.
Suganya and Sivapullaiah, (2016)	The UCS, microstructural analysis (XRD, SEM, FTIR), pH, 28 days of curing	Soft organic clay, sodium silicate (SS), cement	The strength increases with the increase of SS content. No optimum admixture ratio was proposed due to fluctuation of observed strength measurements. SEM images and XRD patterns confirm CSH, N(C)SH and N(C)ASH compounds resulting in improving soil properties. The initial value of pH increases with the increase of additive content during the curing ages.

Table 2.1 Continued

References	Properties	Materials	Observations
Pavithira et al., (2016)	UCS, microstructural analysis, (SEM), Cured 1, 7 and 14 days in 70 °C	Soft clay soil, Na ₂ SiO ₃ / NaOH (ratio of 1, 1.5, 2 and 2.5), and fly-ash based geopolymer	The compressive strength initially increased with the increase in the additive ratio, up to 1.5 Na ₂ SiO ₃ / NaOH. Beyond an additive ratio of 1.5, the strength of the specimens tended to decrease. This is due to an excess of untreated sodium silicate inhibiting polymerization. Unreacted fly ash particles were observed for high content ratio stabilized samples in the SEM.
Hoy, (2016)	The UCS, Microstructural analysis (XRD, SEM), curing at 25 and 40 °C, 7 and 28 days	Recycled asphalt payment-fly ash geopolymer using mixture of NaOH /Na ₂ SiO ₃ , (100:10, 90:10, 60:40)	The strength of stabilized specimens gradually increases with the increase in curing time. The high content of Na ₂ SiO ₃ improves short-term strength (at 7-days). A specimen without Na ₂ SiO ₃ yields lower strength values. High temperature improves the strength. New compounds, CSH, CAH, and NASH, emerge in the XRD pattern and SEM images at both short- or long-term curing ages. High Na ₂ SiO ₃ content accelerates the production of geopolymer materials.
Criado et al., (2007); Dombrowski et al., (2007); Duxon et al., (2007); Reig et al., (2014)	Compressive strength, pH, cured 65 °C, mineralogical analysis (XRD, SEM, FTIR)	Geopolymer using porcelain waste, sodium silicate, and sodium hydroxide	The UCS gradually increases up to 7 days. The amorphous and crystalline phase of new compounds present in the XRD pattern, such as CASH and NASH, sodalite, and gismondine. SEM images confirm the formation of sodium calcium carbonate. FTIR wavelength shifted to lower frequencies indicating geopolymer formation.
Yi et al., (2010)	Compressive strength, XRD, SEM, cured 7, 28, and 180 curing days, at room temperature	Marine Clay soil, blast furnace slag, cement. Combination of Carbide slag, NaOH, Na ₂ SiO ₃ , Na ₂ CO ₃ , and Na ₂ SO ₃	The additive combination is carbide slag, Na ₂ SO ₃ , and blast furnace slag with NaOH. Regardless of admixture type, CSH is a main product appearing in all specimen XRD and SEM scans. Ettringite and CAH emerge in samples treated using NaOH, CAH disappears after adding Na ₂ SO ₃ . Curing days are ineffective indicator of relative crystalline phase geopolymer products.
Sukmak et al., (2013)	Compressive strength, additive ratios, cured at 75 °C, 48h in oven, 24h at room temperature	Geopolymer from clay- fine fly ash aggregates. Bound with liquid NaOH, Na ₂ SiO ₃	Clay-fly ash-NaOH polymer binder tends to give lower strength values than NaOH/ Na ₂ SiO ₃ activated specimens. Additive ratios are bigger than 0.6 and 0.7, which causes an extreme reduction in the strength due to crack formations occurring through the hardening process of sodium silicate solution, resulting in lower strengths.

Table 2.1 Continued

References	Properties	Materials	Observations
Jun and Oh, (2015)	UCS, XRD, FESEM	sodium silicate, Sodium hydroxide, fly-ash, gypsum based geopolymer (2, 4 and 6%), cured at 60 °C, and 1, 7 and 28 days	Fly ash treated specimens rejected due to microcracks occurring during the fast-growing process of polymerization in early curing age. Optimum gypsum ratio is 4%. Additional stabilizers decrease overall strength since Na ions are captured by sulfate from gypsum, developing NaSO ₄ resulting in decreasing Na concentration. Thus, growth of zeolites delayed due to insufficient amount of Na ions. Tiny CSH formations detected in the XRD scan. Unreacted silicate detected up to 28 days of curing.
Boonserm et al., (2012)	FTIR, UCS Cured at 40 °C for 2 days and then cured at 40 °C for 7 days	Gypsum (0, 5, 10, and 15%) bottom ash, fly ash (100:0, 75:25, 50:50, 25:75) geopolymer. Stabilization agents as NaOH, Na ₂ SiO ₃	The soil treated using 15% gypsum yielded strengths that were generally lower than the strengths measured for the 0, 5, and 10% gypsum levels. Increasing fly ash content in bottom ash-fly ash mixtures greatly improves the strength. Strength improves due to the glassy phase of cement compounds developing in binder mortar. Cracks detected over gel and crystalline phases, which decreases the strength. Zeolites (vishevite, and thenardite) including sulfate and gel phase (CSH) cementation materials were indicated in the binder mortar
Arrifin et al., (2013)	The UCS, FTIR, XRD, SEM, Cured for 28 days at 28 °C, exposed 2% H ₂ SO ₄ (1, 3, 6, 12, and 18 months)	Geopolymer from binder ashes (Palm oil ash and fuel ash) concrete alkaline activated using combination of Na ₂ SiO ₃ / NaOH (2.5), compared with ordinary Portland cement concrete	The initial strength gradually decreases after the H ₂ SO ₄ exposition. The amorphous and semi-crystalline phase of new cementation products appears such as NASH gel as well as zeolites natrolite and sodalite. The existence of calcite minerals are evident in CSH phases indicating modification of binders. FTIR spectrum confirms the development of NASH, zeolites, and CSH. There are no distinct differences between H ₂ SO ₄ exposed and unexposed specimens in the geopolymer binder. However, H ₂ SO ₄ decomposed the cement products over time.
Nath and Kumar, (2013)	Compressive strength, up to 180 curing days, at room temperature, As replacement of fly-ash polymer	Marine Clay, blast furnace slag, Corex Slag, and cement. Combination of Carbide slag, NaOH, Na ₂ SiO ₃ , Na ₂ CO ₃ , and Na ₂ SO ₄	The most efficient additive combination is carbide slag, Na ₂ SO ₄ , and blast furnace slag with NaOH in this research. Na ₂ CO ₃ shows no effect on strength improvement. Regardless of admixture type, CSH appears in all specimen X-ray diffraction tests. Ettringite and CAH emerge in samples treated by NaOH.

As shown in Table 2.1, chemically altering the microstructure and mineralogy of different types of soils (e.g., clay, silt, and sand) using various chemical additives, waste materials (e.g., fly ash, carbide slag, palm oil ash, recycled bassanite, gypsum, pavement asphalt) as well as liquid polymers such as sodium silicate and/or sodium hydroxide can improve poor soil engineering properties. These improvements can occur when some additives are used alone; in other cases, some additives are shown to work better when used together. In general, geopolymer stabilization may allow for reduction in the utilization of ordinary Portland cement in geotechnical engineering projects, since strong and durable cementation products similar to cement stabilization can be produced, in some cases with beneficial reuse of waste stream materials from other sources.

The use of waste materials for making alternative cementation products can improve the engineering properties of different types of soils, and reduce the production of ordinary Portland cement, effectively reducing the large amounts of CO₂ that are produced worldwide due to the production of cement. The use of geopolymers, which are alkali-activated aluminosilicate cementation products, shows significant promise for the process of soil stabilization. The utilization of waste products and geopolymers for soil stabilization projects has become favorable around the world due to their environmental and engineering benefits. Hence, the current study examines the effectiveness of recycled gypsum and sodium silicate are selected as soil stabilizers to investigate the effect of their combinations on kaolinite and bentonite clays, respectively.

Chapter 3

EXPERIMENTAL APPROACH

3.1 Soils and Stabilizers

3.1.1 Soils

Clays, in particular soft clays, often lead to problems for various geotechnical engineering structures, such as slope stability, bearing capacity, excessive settlement, lateral squeeze, etc. (e.g., Chinkulkijniwat et al., 2015; Horpibulsuk et al., 2009, 2010). As such, they are commonly considered to be a good candidate for soil stabilization. The behavior of two types of stabilized clays was examined in this research, a kaolinite and a bentonite. The kaolinite (White Kaolinite) was purchased from Albion Kaolinite Company, located in Georgia, in the USA. The bentonite (Volclay, 200 mesh) was obtained from American Colloid Company, located in Illinois, in the USA. These two relatively pure clay minerals were chosen to be representative of low-plasticity and high-plasticity clay behavior.

3.1.1.1 Stabilizer Liquid Sodium Silicate

An alkali stabilizer, liquid Sodium Silicate, S, 99.9% purity, was purchased from Eisen-Golden Laboratories in the USA. This stabilizer was created by dissolving Sodium Silicate ($\text{Na}_2\text{SiO}_4 \cdot \text{H}_2\text{O}$) in water with the ratio of 41% Sodium Silicate and 59% distilled water

3.1.1.2 Recycled Gypsum

Recycled gypsum was obtained from a local supplier, USA Gypsum Drywall Recycling Service Company, in the USA. Recycled gypsum ($\text{CaSO}_4 \cdot 2\text{H}_2\text{O}$) contains 21.77% Calcium, 0.39% Magnesium, 16.39% Sulfate and 61.45% water (H_2O).

3.2 Macrostructural Soil Characterization

3.2.1 Moisture Content

The water content of the base material that is being stabilized is important for soil stabilization research, as it plays a critical role in cementation and geopolymer formation (Hamzah et al., 2015). Consequently, oven-dried moisture contents (ASTM-D2216-10) were utilized to determine the moisture/water content of the soil and admixture. During the laboratory testing that was performed, representative samples were selected from the entire amount of materials and weighed with a 0.1% accuracy balance. During the oven drying process, the specimens were dried at 110 ± 5 °C for 24 hours in a thermostatically controlled oven.

3.2.2 Particle Size Distribution

Grain size analyses were performed using hydrometer testing (ASTM-D421-85), in order to determine the particle size distribution of the kaolinite and bentonite clays. Following the ASTM procedure, representative samples were prepared by weighing approximately 50 grams of each clay powder. The selected soil was then soaked in distilled water containing a dispersing agent (sodium hexametaphosphate) for

18 hours. The hydrometer test was then performed to assess the amount of silt and clay particle sizes. After the final hydrometer reading, the suspension of clays was transferred to a No. 200 (75- μm) sieve and washed with tap water until the wash water was clear. The retained material on the sieve was transferred to a suitable container, and dried in the oven at 110 ± 5 °C to determine the quantity of sand particles in each of the specimens (ASTM-D422-63).

3.2.3 Liquid Limit, Plastic Limit, and Plasticity Index

Atterberg limits of both clays were determined following the procedures outlined in ASTM-D4318-17, using representative specimens for each soil that were prepared by passing them through a No.40 (475- μm) sieve. The liquid limit device was then used to obtain the liquid limit of each clay. To determine the plastic limit of the clays, representative soils were rolled to a 3.2-mm thread diameter on a glass plate until the thread broke/crumbled under the applied rolling pressure. As a final step, the water content of the liquid limit test and plastic limit test clays was measured following the methodology outlined in ASTM D2216-17. The plasticity index of the materials was determined for each soil based on the difference between the plasticity and liquid limit index properties.

3.2.4 Classification of Soils for Engineering Purpose

Soil classification of the tested specimens was performed using the Unified Soil Classification System (ASTM-D2487-11). As part of this process, information from the

particle size characterization and liquid limit and plastic limit index testing was utilized to determine the resulting soil classifications.

3.2.5 Specific Gravity

The specific gravity of clays passing the 4.75-mm (No. 4) sieve can be determined by means of a water pycnometer test, following the procedures outlined in ASTM-D854-14. The procedure of oven-dried specimens, Method B, was utilized in the current study, and distilled water was used in the test. The specific gravity of each clay was measured by determining the weight of clays and water slurry in the pycnometer, compared to the weight of a pycnometer only filled with water.

3.2.6 Acidity/ Alkalinity (pH) Testing

The value of pH for untreated and stabilized soils was determined using the procedure of pH in distilled water in accordance with ASTM D4972-13. (OAKTON Ph 450). Following this approach, approximately 10 g of material was tested at a time. For testing, the soil was mixed with distilled water at the ratio of 1:5 by mass, and disturbed every 10 minutes for 1.5 hours before determining a pH value (Miller and Azad, 2000). The pH meter was calibrated in accordance with ASTM-D4972-13. This measurement indicates the degree of alkalinity or acidity in the treated soil, which plays a significant role during either polymerization or cementation.

3.2.7 Laboratory Compaction Testing

Standard Proctor compaction testing was performed to assess the relationship between compacted soil dry unit weights and the molding water content of soils (ASTM-D698-12e2), for both untreated and stabilized soils. Following this test procedure, the tested clays were compacted in a 101.6-mm (4-in) diameter mold using a Proctor hammer dropped from a height of 305 mm (12-in).

For stabilized soil compaction testing, approximately 1800 grams of air dried clay was mixed with various quantities of recycled gypsum and sodium silicate, to achieve the targeted test ratios of stabilizer(s) to base soil. The resulting mixture was stirred and mixed further by hand to ensure consistency throughout the prepared test specimen. Various quantities of distilled water were then sprayed on each of the various compaction specimen mixtures, to achieve the desired moisture content for each of the compaction test points. This procedure was performed for at least five different points in order to determine the compaction curve, which is the relationship between the maximum dry unit weight (kN/m^3) and the optimum moisture content of the treated soils, for a given level of compaction effort.

3.2.8 The Unconfined Compressive Strength Test

The unconfined compressive strength of untreated and stabilized soil was determined using a strain-controlled application of axial load, following the procedures outlined in ASTM D2166-16. The rate of application of axial strain that was utilized in the current study was one percent per minute. All measurements were collected using

an automatic data acquisition system. Each sample was loaded until maximum peak stress was reached, over a total range of axial strain application of 15%. The cross-sectional area of each test specimen was measured before testing.

3.3 Microstructural Soil Characterization

3.3.1 X-Ray Fluorescence (XRF)

X-ray fluorescence analysis is widely used to obtain elemental composition of all kinds of solid or liquid materials (Uo et al., 2015). Wavelength dispersive X-ray fluorescence spectrometry (WDXRF) is chosen due to its reliability and unrivaled accuracy of results (Geiman, 2005). It is a powerful technique that has been used successfully to investigate various types of cement, polymers, mining, and industrial materials (e.g., Arulrajah et al., 2015). The XRF was employed to determine the elemental composition of both unstabilized clays in this research. Approximately 10g of both untreated soils were scanned to determine their elemental compositions in this research.

3.3.2 X-Ray Diffraction, (XRD)

X-Ray diffraction analysis is one of the most significant tools to identify, categorize and quantify minerals (Latifi et al., 2004; Komnitsas and Zaharaki, 2007; Waseda et al., 2011). It has been extensively utilized to examine crystalline materials and cementation products (e.g., Yilmaz and Civelekoglu, 2009; Guo et al., 2010; Bignozzi et al., 2014; Jha and Sivapullaiah, 2016; Latifi et al., 2016). The basic principle

of XRD relies on diffraction of X-rays through the unique structures of crystalline materials, as shown in Figure 3.2 (e.g., Lanford and Louer, 1996).

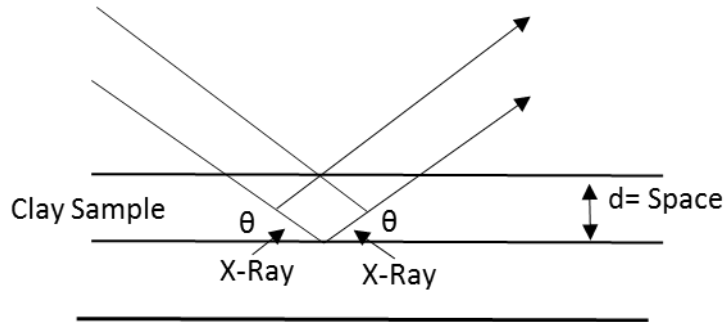


Figure 3.1 Reflection of X-ray from the plane in a solid.

Using XRD, the path differences between two waves can be obtained as follows:

$$2\lambda = 2d \sin(\theta) \quad (1)$$

For the interface between these waves, the Bragg's equation is derived from the path differences number of wavelength:

$$n\lambda = 2d \sin(\theta) \quad (2)$$

where n is an integer of the constructive interface, λ is the X-ray length, d is the spacing between lattice planes, and θ is the reflection angle. The d -spacing values for different minerals are determined by measuring the reflection of X-rays that have been directed at the tested materials.

X-ray diffraction of the untreated and treated specimens was performed using a Bruker D8 ADVANCED X-ray diffractometer. In this device, X-Ray radiation is emitted by copper, $\text{CuK}\alpha$ radiation ($\lambda = 1.5418 \text{ \AA}$) at 40 mA and 40kV in the range of 5°

- 80° in 2θ , with 0.05° per second scanning steps. The scanning step was integrated at the rate of the 1s interval. To prepare test specimens, approximately 1-2 g of untreated or stabilized materials were crushed with an agate mortar and placed in a sample holder. The detected peaks were identified using the standard line patterns from the Powder Diffraction File database supplied by International Center for Diffraction Data (ICDD) and compared with the available XRD data in the current literature (e.g., Bignozzi et al., 2014; Jha and Sivapullaiah, 2016; Guo et al., 2010; Latifi et al., 2016; Yilmaz and Civelekoglu, 2009).

3.3.3 FTIR-ATR Spectroscopy

Fourier transform infrared (FTIR) spectroscopy can be utilized to characterize the presence of geopolymers that are formed as an amorphous material, as the geopolymers may not be detected by XRD due to their lack of crystalline structure (Worasit et al., 2011). In the current study, the group of chemical structures existing in untreated and stabilized soil was explored using an ATR-FTIR approach, in which ATR stands for attenuated total reflectance. The Bruker Tensor 27 shown was utilized to classify the functional chemical groups in untreated and stabilized soils based on vibrational and rotational energies of different molecular bonds in materials. For the tested soils in the current study, approximately 0.5g of treated soil powders were scanned for each test. All scanning spectra of tested specimens were employed using 4 cm^{-1} resolutions at 64 scans per spectrum between 500 cm^{-1} and 4000 cm^{-1} .

3.3.4 FESEM/EDAX Analysis

Field Emission Scanning Electron Microscopy (SEM) with Energy-Dispersive Spectrometry (EDAX) was utilized in the current study to detect the complex chemical synthesized polymers. For this testing, a Zeiss Augira 60 CrossBeam FIB-FE-SEM was used. This device is a high vacuum SEM, which was chosen since under a high vacuum fewer electrons can be dispersed, allowing for higher-resolution images. Samples were pulverized and gently dried in a temperature controlled oven (at approximately 60 °C) for 24 hours before being coated by a sputtering process on a carbon fiber covered steel sample holder. The operational voltage in the SEM device was set to 15kV to take images. The magnification during the imaging process was set to 5000-20000Kx to capture the stabilization reaction products that were formed on the clay lattice.

During the sputtering process, both untreated and stabilized specimens were coated using a gold/palladium sputtering coater for approximately 90 seconds (DETON VACUUM DESK IV); the purpose of this sputtering is to increase the electron conductivity of samples, allowing for higher resolution SEM images and EDAX analysis.

3.3.5 N₂-BET Surface Area Analysis

The determination of the surface area of the solid particles in the soil matrix provides useful information about the chemical and physical properties of the soil samples since cementation/polymerization forms on the surface of the soil particles (e.g., Michell and Soga, 2005). The nitrogen-based Brunauer-Emmett-Teller (N₂-BET)

surface area test was utilized to assess change in surface area and the associated pore structure for selected stabilized specimens at various curing periods. These tests were performed using a Micrometric ASAP 2002. This device uses the multipoint BET surface area technique based on complex gas absorption on the soil surface (Brunauer et al. 1938). The absorption data can be linearly plotted by comparing the absorbed volume against the relative pressure (P/P_0), where P is the initial gas pressure and P_0 is the vapor pressure. The test was conducted at a temperature of 77.35 K (-198.5 °C), the 1 atm boiling point of liquid N₂, and the measurement time was set to 15 seconds. In the current work, the tested specimens had a mass between 1.5-2g.

3.4 Methods for Preparing and Testing Specimens

Two types of base soils were selected for stabilization in this research, a bentonite clay and a kaolinite clay. Both soils were sieved using a No. 40 (0.420-mm) mesh to remove and discard any larger particles that were present. Approximately 1000 g of air-dried soil was used to produce batches of three different specimens for strength testing. Distilled water was used to adjust the moisture content of the prepared specimens to the optimum moisture that had been determined for that particular mix design from prior Standard Proctor laboratory compaction testing.

With respect to the introduction of the stabilizing additives, recycled gypsum was combined with both clays by soil mass, prior to the addition of liquid to the soil/stabilizer mixture. The liquid sodium silicate was blended with the distilled water before being sprinkled onto the soil mixture at the desired ratio (by mass). For this

research, sodium silicate was not directly applied to the soil mixture as it can cause the stabilized soil to harden immediately, which makes further mixing challenging and the resulting mixture non-uniform (e.g., Geiman, 2005). Distilled water was sprayed on the soil/stabilizer mixture by hand (as shown in Figure 3.7) and then further hand mixing for three to five minutes was utilized to achieve a more uniform moisture distribution at the desired moisture content.

3.4.1 Process of Mixing Soil and Stabilizer

3.4.1.1 Soil and Stabilizer Mix Design

In this research, four different admixture contents were prepared for each of the three soil stabilizing approach that was explored. Specimen preparation was performed in three separate ways (for the three separate stabilizing approaches) for each of the four different additive contents. For the first type of stabilization (“gypsum only”), recycled gypsum was blended in a dry state with Bentonite (to form “BG”) and Kaolinite (to form “KG”) at the desired admixture ratio, and then distilled water was added to the mixture to bring it to the desired moisture content. Gypsum only specimens were prepared at 3%, 6%, 9% and 12% gypsum by dry soil mass. For the second type of stabilization (“sodium silicate only”), an alkali activation agent, Sodium Silicate, was added into a measured volume of distilled water, and the resulting solution was mixed with the tested soils (to form “BS” and “KS”). Sodium silicate only specimens were prepared at 3%, 6%, 9% and 12% sodium silicate levels, by preparing sodium silicate

solutions at the appropriate concentration (g/cm^3) to achieve both the target additive level (by dry mass of sodium silicate) and the desired moisture content in the prepared specimen. For the third type of stabilization (“gypsum and sodium silicate”), recycled gypsum was mixed with the soils, and then sodium silicate was added to the distilled water, and the solid and water mixtures were then combined. Gypsum and sodium silicate specimens were prepared at 3%, 6%, 9% and 12% stabilizer levels, with a 50%/50% ratio being utilized between the gypsum and sodium silicate. A dry mass combination approach was used for combining the gypsum with the base clay soil, and the sodium silicate solutions were prepared at the appropriate concentration (g/cm^3) to achieve both the target additive level (by dry mass of sodium silicate) and the desired moisture content in the prepared specimen. The name of the resulting stabilizer mixtures that were prepared using this approach is Bentonite-Gypsum-Sodium Silicate (BGS) and Kaolinite-Gypsum-Sodium Silicate (KGS).

3.4.2 Curing Conditions

3.4.2.1 Curing Temperature and Humidity

Specimens were prepared at a relatively constant room temperature 21 ± 2 °C. Additionally, to prevent moisture loss during the curing period, specimens were placed in a clear polyethylene plastic jar and then sealed with a plastic cling film, and then placed in a clear polyethylene plastic bag. To prevent moisture loss during the curing period, samples were sealed with a plastic cling film and then placed in a clear

polyethylene plastic jar and bag. All specimens were cured in a sealed container with a high level of relative humidity (maintained via a water bath) throughout the curing periods, as shown in Figure 3.2.

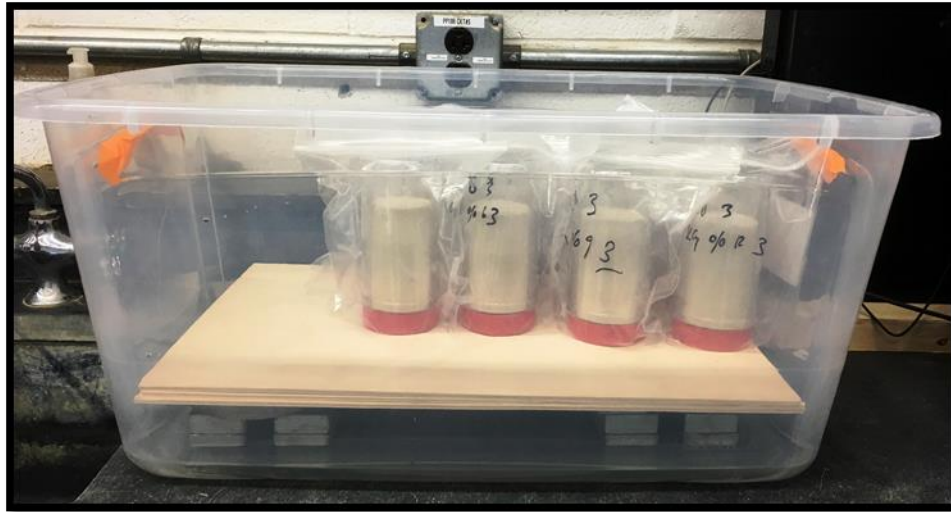


Figure 3.2 Curing bath utilized to achieve proper humidity condition.

3.4.2.2 Curing Time

The effect of various curing times was assessed as part of this research, with 0, 3, 7, 14, 28 and 56 days curing periods all being examined. Three samples were prepared and tested for each curing time period to help provide a more accurate test results.

3.4.3 Sample Preparation and Extraction Procedure for the Strength Testing

The tested soils were mixed with the desired content of the admixture and a quantity of distilled water sufficient to reach the optimum water content using a palette

knife for moisture uniformity; the optimum water content for each mixture had been determined previously using a series of Proctor tests. A cylindrical steel mold with an internal diameter of 50mm and height of 100mm (Figure 3.3) was fabricated to produce unconfined compressive strength (UCS) test specimens. Unconfined compression strength tests were performed in accordance with the recommendations made in ASTM D2166-16; following the recommendations made in the standard, the target height to diameter ratio that was utilized for specimen preparation was 2.

After mixing the stabilized soil mixture to ensure a more uniform moisture content, one-third of the resulting mixture was placed into the mold using a spoon and then compacted using a hydraulic jack. This process was repeated two times more (e.g., each specimen was prepared in three equal compressed soil layers), to prepare a fairly uniform specimen at the desired unit weight. The specimens were then capped, placed in the sealed containers, and cured for the desired curing period. Upon completion of curing, the caps placed at the top and bottom of a given specimen were removed, and then the compacted specimen was extracted from the mold using a steel plunger pushed by a hydraulic jack. (Ahmet and Naggar, 2016; Latifi et al. 2016).

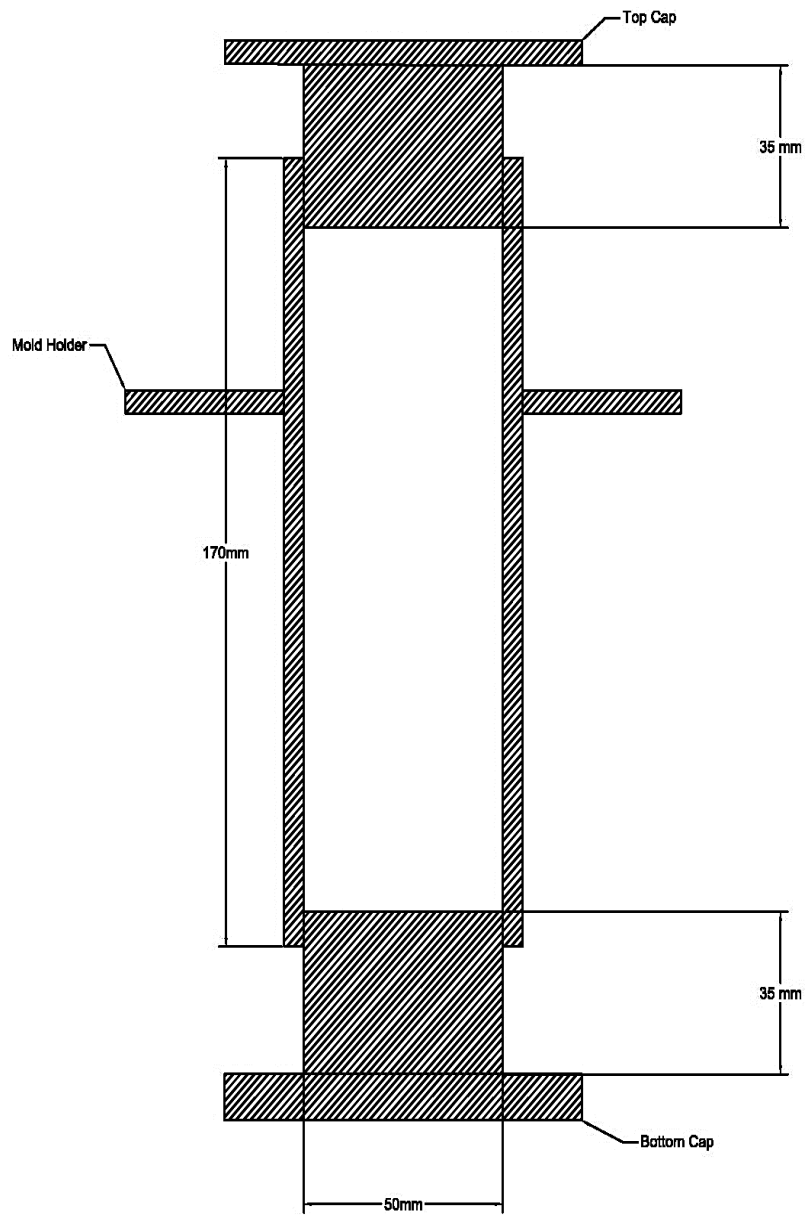


Figure 3.3 Dimensions of manufactured mold for preparation of the UCS test specimens.

The UCS specimens shown in Figure. 3.3 were placed into the plastic polyethylene jar and covered using plastic cling film to prevent moisture loss during the curing process. All specimens were cured in the moist box shown in Figure 3.2, providing 100% relative humidity for 3, 7, 14, 28 and 56 days of curing in a temperature controlled room at 21 ± 2 °C, as suggested by Yilmaz & Civelekoglu (2009).

After sufficient curing time, specimens were removed from their polyethylene jars and measured and recorded their diameter, height, and weight before testing. Afterwards, stabilized specimens were subjected to UCS testing immediately, in accordance with ASTM D2166-16, at a constant loading rate of 1%/min until the maximum strength peak was obtained or until the accumulated axial strain reached 15%. After that, tested specimens were placed into the oven to evaluate their final moisture content. The initial compressive strength was assessed as the average of the strengths of three similarly cured specimens following the recommendations of Ahmed and El Nagggar (2016).

Chapter 4

TEST RESULTS AND DISCUSSIONS

In the following chapter, the results of laboratory tests performed for two types of soils that have generally poor geotechnical engineering properties are presented. In the first section of the chapter, the results from general soil characterization and material tests are provided. In the second portion of this chapter, the results from the soil stabilization tests that were performed are presented and discussed, along with the results from the microstructural characterization testing that was performed for the stabilized soil specimens.

4.1 Material Characterizations

This study was conducted on natural, pure untreated Bentonite and Kaolinite clay powders, which were obtained from American Colloid Company and Albion Kaolinite Company located in the USA, respectively. Recycled gypsum was derived from a local supplier, USA Gypsum Drywall Recycling Service Company. Liquid sodium silicate was purchased from Eisen-Golden Laboratories.

4.1.1 Soil Descriptions

The Bentonite and Kaolinite clay minerals used for the test were air-dried under laboratory conditions in the University of Delaware geotechnical engineering laboratory. Visual inspection of the air-dried soils shows that the color of Kaolinite is yellowish-white, whereas the Bentonite has a dark grey color.

Particle size analysis of these clays was performed using hydrometer and sieve testing, in accordance with ASTM-D421-85. The resulting particle size distribution curves for representative samples are shown in Figure 4.1. As shown, approximately 99.5% of both clays passes through the No. 200 sieve (0.075 mm). Therefore, both soils are classified as fine-grained soil. The bentonite soil has a clay fraction (0.002 mm) of 30%, and the kaolinite soil has a clay fraction of 40% (Figure 4.1), meaning that for both soils the predominant particle size is clay. As shown, the kaolinite soil has a much greater percentage of silt-sized specimens than the bentonite.

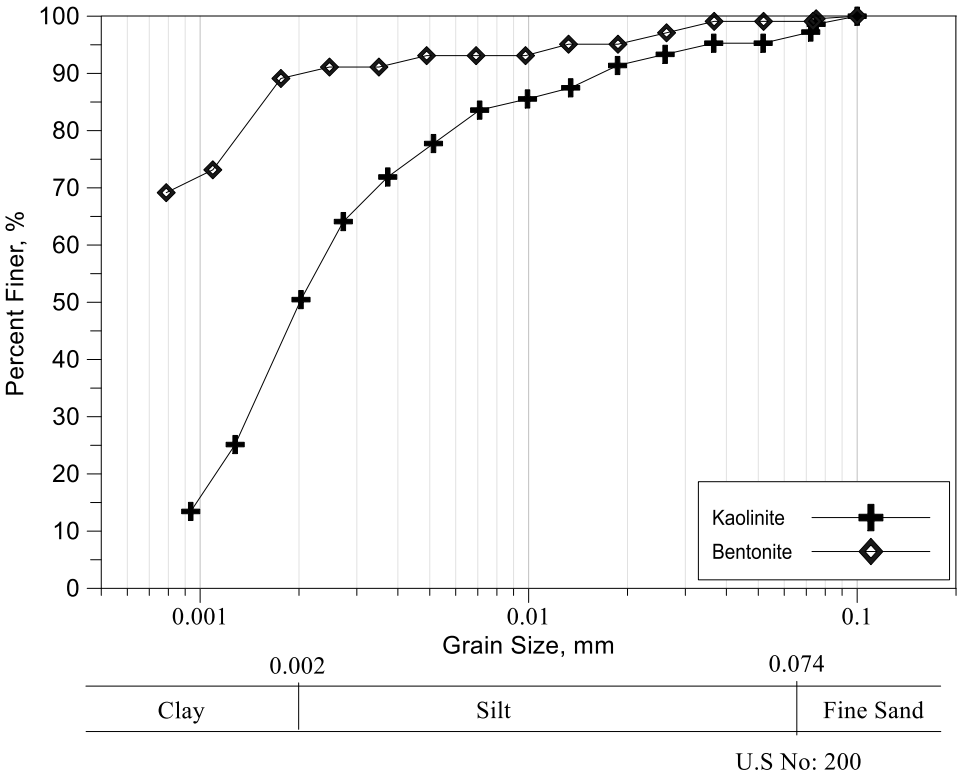


Figure 4.1 The grain size distribution of tested bentonite and kaolinite clays.

Atterberg limit testing was performed for both clay soils on particles passing through the 475 μm (No. 40) sieve, following ASTM D 4318-17. The results from tests on representative specimens of both clay minerals are shown in Table 4.1. Soil classification of both clays was then performed following the USCS standard, ASTM D 2487-11 (Table 4.1).

Following the USCS, the tested Bentonite classified as a highly plastic fat clay (CH). The results from Standard Proctor testing (ASTM D698-12e2) indicated that the maximum dry unit weight of the Bentonite was 11.26 kN/m³, at an optimum moisture content of 27.53 percent.

The tested Kaolinite classified as an elastic silt (MH) following the USCS. The maximum dry unit weight determined by standard Proctor testing was 13.77 kN/m³, at an optimum moisture content of 27.97 percent.

Soil pH values were measured in 1:5 soil/water suspensions using an electronic pH meter, in accordance with the recommendations made in ASTM D4972-13. The values of pH for bentonite, kaolinite, recycled gypsum and the sodium silicate solution are 7.80, 4.4, 6.4, and 13.20 respectively. Additional geotechnical engineering properties of the natural soils are summarized in Table 4.1, which were determined using specific gravity testing (ASTM D854-14), unconfined compressive strength testing (ASTM D2166-16), and N₂-BET testing (ASTM D D3663-03-15).

Table 4.1 Geotechnical engineering characteristics of Bentonite and Kaolinite

Engineering and physical properties	Values	
	Bentonite	Kaolinite
pH (L/S=5)	7.80	4.40
Specific gravity	2.64	2.67
Surface area (m ² g ⁻¹)	19.92	16.96
Liquid Limit (LL) (%)	370.64	60.80
Plastic limit (PL) (%)	92.09	34.16
Plasticity index (PI) (%)	278.55	26.64
ASTM classification	CH	MH
Maximum dry density (kN/m ³)	11.26	13.77
Optimum moisture content (%)	27.53	27.97
The unconfined compressive test (kPa)	61.8	66.05

Table 4.2 provides the chemical composition of the tested clay soils, as determined by X-ray fluorescence (XRF) (ASTM D5381-93). As shown, both clays have a very small amount of calcium ions in their chemical compositions. Before testing specimens were prepared, air-dried recycled gypsum was screened to remove any solid particles or contaminating materials such as papers, paints, woods, and fiber. The chemical composition of the recycled gypsum and sodium silicate solution used in this research is presented in Table 4.3, based on the results from additional XRF testing.

Table 4.2 Chemical composition of tested clays

Chemical compositions, (%)									
	Al ₂ O ₃	SiO ₂	Na ₂ O	MgO	K ₂ O	CaO	Fe ₂ O ₃	SrO	ZrO ₂
Bentonite	24.592	59.184	8.0741	4.481	0.315	0.826	2.006	0.018	0.014
	Al ₂ O ₃	SiO ₂	P ₂ O ₅	MgO	K ₂ O	CaO	TiO ₂	Fe ₂ O ₃	ZrO ₂
Kaolinite	52.325	45.954	0.1112	0.278	0.185	0.012	0.827	0.289	0.021

Table 4.3 Chemical composition of additives

Chemical compositions (oxides), (%)					
Additives	CaO	MgO	SO ₄	Na ₂ SiO ₄	H ₂ O
Recycled Gypsum	27.77	0.39	16.39	-	55.45
Sodium Silicate	-	-	-	41	59

4.2 The pH Test Results of Stabilized Soils

As noted previously, pure bentonite and kaolinite were mixed with 3%, 6%, 9%, and 12% additive content levels (using three different stabilizing approaches), and cured at different curing intervals of 0, 3, 7, 28, and 56 days. The change in the pH over the curing periods was measured after 1.5 h of mixing for both of the prepared clays that had been stabilized. It is noted that samples selected to take pH measurement were collected from the same soil admixture that was used to prepare the UCS test specimens. As shown in Table 4.1, the kaolinite clay forms a more acidic environment ($\text{pH} < 7$) once water has introduced the system, whereas bentonite clay results in a more alkaline environment ($\text{pH} > 7$). The level of acidity or alkalinity plays a significant role in the development of cementation/ geopolymerization products.

4.2.1 Bentonite Clay

4.2.1.1 Mixture of Recycled Gypsum and Bentonite

The initial values of pH for the stabilized samples at the various content of additives were measured corresponding to the curing times and additive content of bentonite-recycled gypsum mixture and presented in Figure 4.2.

The changes in pH confirm that the recycled gypsum increases the acidity of pure bentonite at 0 days of curing, a change which is the most pronounced from 0 to 3%, and which shows further acidification in a diminishing fashion between 3 and 12% gypsum. However, as curing of the specimen progresses, specimen at all additive concentrations exhibit an increase in pH into the alkaline environment range. More pronounced changes of the specimens from acidic to alkaline occur at the higher additive concentration levels. These changes in acidity are a result of chemical processes and reactions that are occurring within the stabilized soil specimens. These changes in acidity can also affect the rate of the various chemical reactions that are occurring during the curing process. The increase of the pH with curing time can possibly be attributed to the exchange of monovalent ions of bentonite by calcium ions of the recycled gypsum (e.g., Jha and Sivapullaiah, 2014).

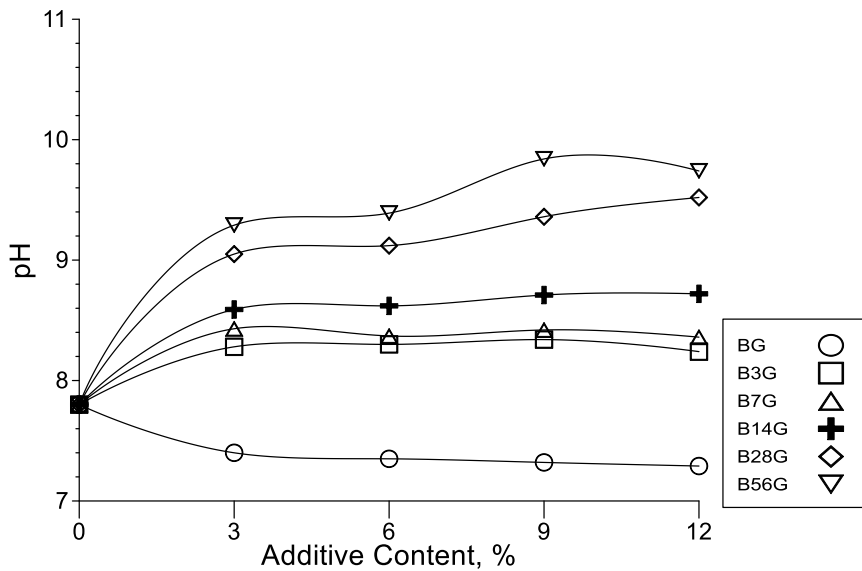


Figure 4.2 pH values of bentonite-recycled gypsum mixture (BG) at various additive contents and curing time intervals.

4.2.1.2 Mixture of Sodium Silicate solution and Bentonite

The initial values of the pH taken over the curing periods of alkaline activated (Na_2SiO_3) bentonite are present in Figure 4.3. The level of alkalinity increases with the increase of the curing ages and additive content. However, the pH approximately remains steady with additional curing periods up to 14-days of curing at low content, 3%, and 6%, of the sodium silicate. After that, a sudden pH increment occurred with 9 and 12% additive content between 28 and 56-days of curing. The high content of alkaline solution resulted in increasing the level of pH during the curing interval due to nature of the sodium silicate, which the maximum value of pH reached approximately 11.85 out of 14.0.

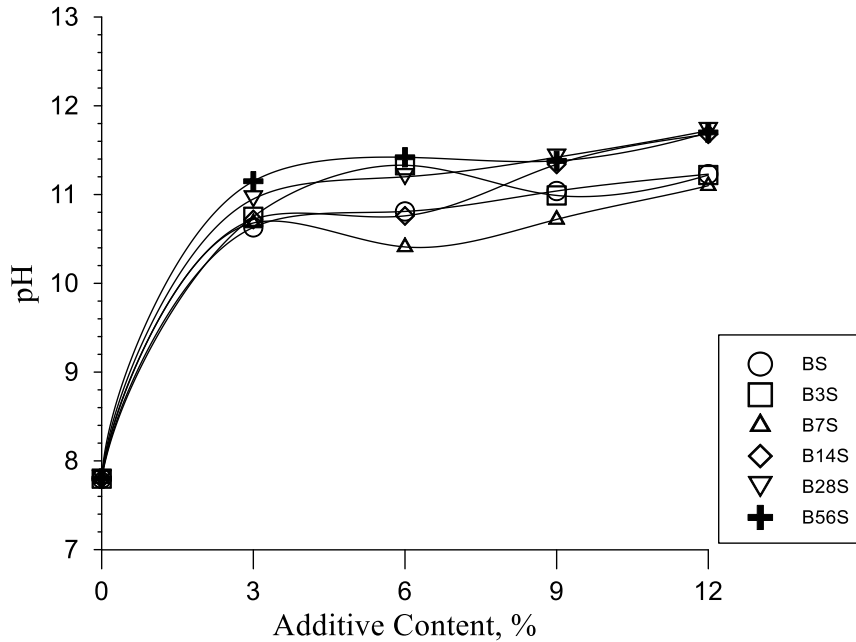


Figure 4.3 pH values of bentonite-sodium silicate solution admixture, (BS), at various additive contents, and curing time intervals.

For sodium silicate stabilization, which is an alkali activation reaction, at a higher value of pH, dissolution of the clay alumina and silicate dramatically accelerates, which plays a significant role in continuing the chemical reactions such as pozzolanic cation exchange in the stabilized soil (e.g., Kamei et al., 2013). Hydrated silica and alumina react with mobilized sodium and calcium ions dissolved during hydration to manufacture secondary cementation materials, but this pozzolanic activity may require an extended curing period (Petry and Little, 2002). It is believed that the hydrated cementitious compounds that are formed participate in the long and short-term strength development.

4.2.1.3 Mixture of Recycled Gypsum, Sodium Silicate Solution, and Bentonite

The initial values of pH recorded at various curing periods for recycled gypsum and sodium silicate stabilized bentonite are shown in Figure 4.4. As shown, the level of pH increased with increasing additive content for all of the admixture contents that were assessed. Interestingly, for all admixture concentrations, the pH increases from 0-3 days of curing, then decreases from 3-7 days of curing, and then increases again from 7 to 56 days of curing. The most acidic environment was observed at the 7-day curing mark, which is different than what was observed for the gypsum only and sodium silicate only stabilized specimens. This could be due to the reaction conditions in the soil matrix, such as what would occur if the dissolution of the stabilizers and the stabilization reaction occurred slowly (e.g., Little and Nair, 2009). Delayed availability of the monovalent ions such as calcium from the recycled gypsum and sodium from the sodium silicate solution postpones the reaction between source material and monovalent ions into the polymerization system. The highest value of pH was obtained at a 12% additive ratio at 56-days of curing.

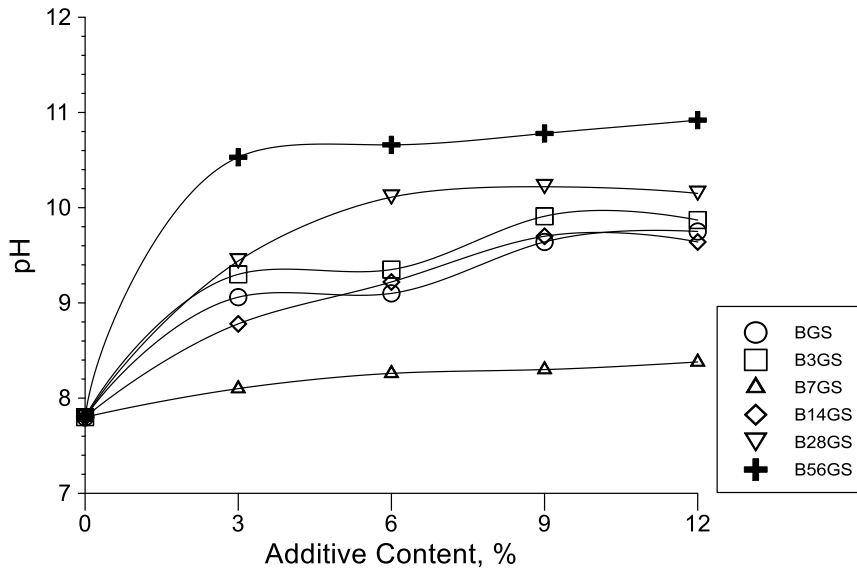


Figure 4.4 pH values of gypsum, recycled gypsum, and sodium silicate mixtures (BGS), at various additive contents and curing time intervals.

4.2.2 Kaolinite Clay

4.2.2.1 Mixture of Recycled Gypsum and Kaolinite

The pH values of kaolinite clay treated with various recycled gypsum contents and subjected to various curing intervals are shown in Figure 4.5. As shown, at 0-days of curing, the alkalinity increased with increases in additive content, with a significant jump from 0-3% additive content, and only moderate and relatively constant changes from 3% to 12% additive content. With additional curing time, the stabilized soil generally becomes more alkaline (i.e., the pH increases), though all pH measurements of stabilized kaolinite indicated an acidic environment overall (i.e., $\text{pH} < 7$). This behavior is attributed to the release of calcium ions from the recycled gypsum into the

pore water, where they can react with aluminum and silicate from the kaolinite via cation exchange (e.g., Jiang et al., 2009; Jha and Sivapullaiah, 2014).

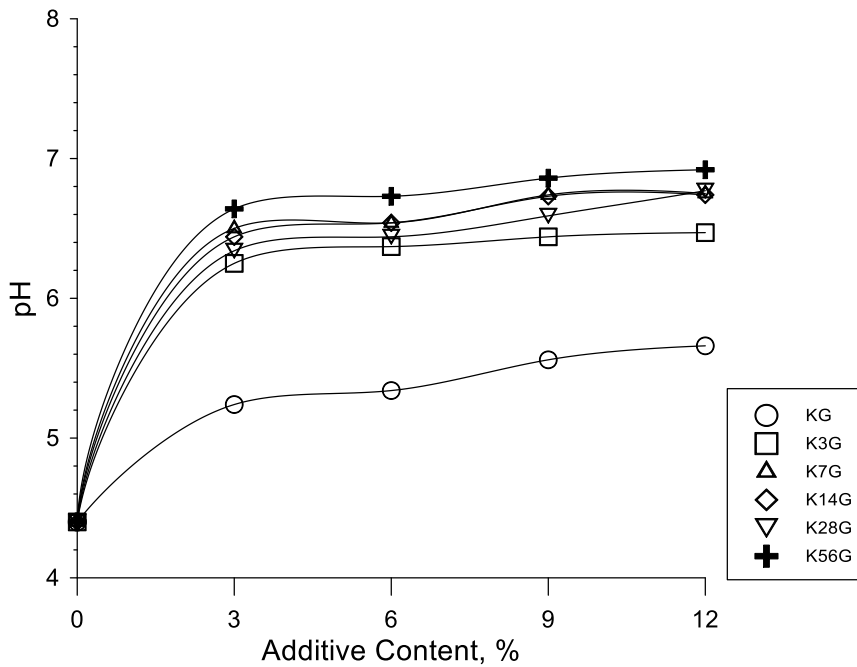


Figure 4.5 initial pH values of recycled gypsum-kaolinite mixture, (KG), at various content and curing time intervals.

4.2.2.2 Mixture of Sodium Silicate Solution and Kaolinite

As shown in Figure 4.6, the initial level of pH of the untreated kaolinite is considerably increased once the alkaline solution was introduced into the clay matrix (i.e., a big jump from 0-3% additive content). The pH then remains relatively constant from 3%-12% additive content. In other words, the increase of the additive contents into soil admixture beyond the 3% level does not affect the acidity levels of treated soils

significantly. Some general increases in pH were observed with increasing curing time; this behavior is attributed to dissolution of stabilizer and clay over time, which allows free cations to replace monovalent ions of soil in the soil matrix. This reaction process decreases the level of acidity in the soil environment, allowing new cementation compounds to be formed as a result of a highly alkaline environmental condition and readily available cations such as sodium and calcium in the contact solution (Nath and Kumar, 2013).

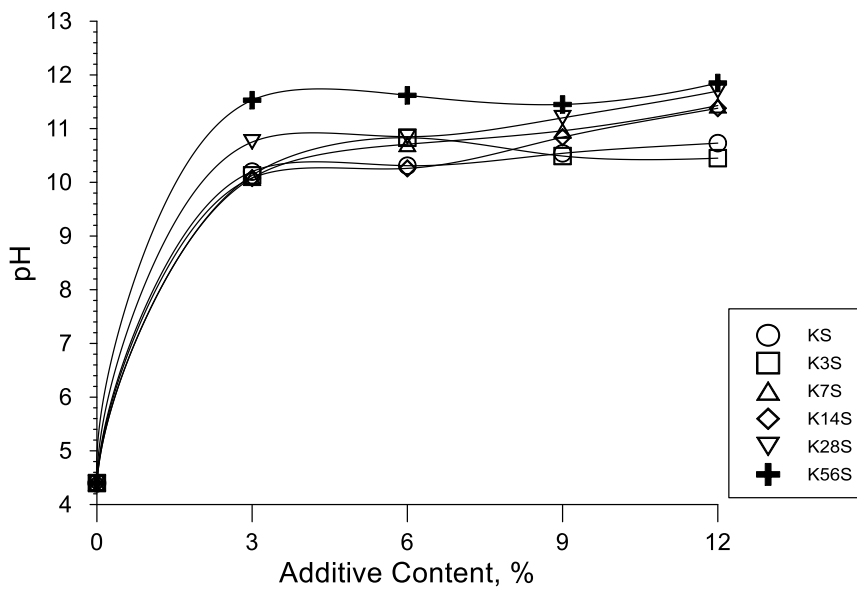


Figure 4.6 pH values of kaolinite- sodium silicate-mixture (KS), at various additive content and curing time intervals.

4.2.2.3 Mixture of Kaolinite, Recycled Gypsum and Sodium Silicate Solution

The pH values of specimens with additive contents of 3, 6, 9, and 12%, for kaolinite clay stabilized with recycled gypsum and sodium silicate, are shown in Figure 4.7.

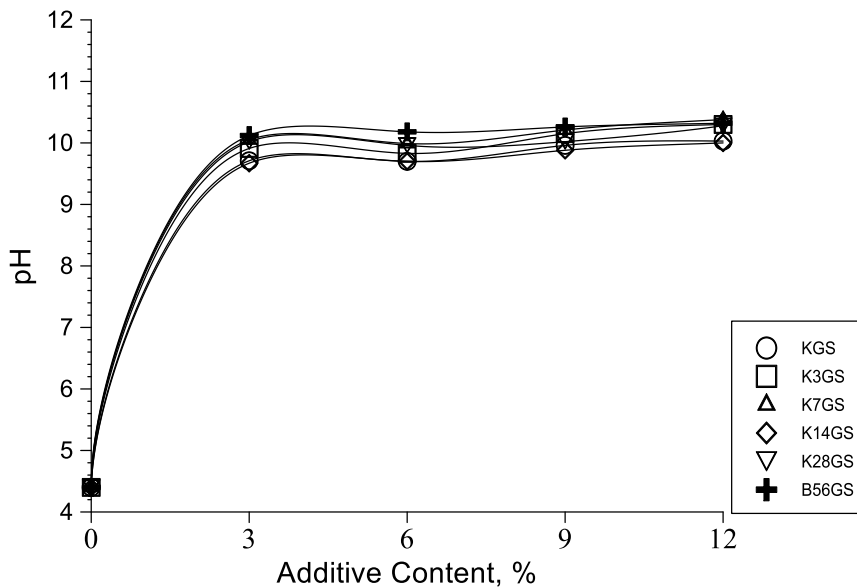


Figure 4.7 pH values of kaolinite, gypsum, sodium silicate, (KGS), 50%:50%, at various additive contents, and curing intervals.

In a similar fashion as the kaolinite stabilized with sodium silicate only, a significant increase in pH occurred as the stabilizer content was increased from 0% to 3%, with only very minor changes being observed as the stabilizer percentage was increased from 3% to 12%. It is also observed that the initial pH values of treated samples tend to increase with the increase of the curing periods, albeit relatively slightly

in contrast to the changes that happen when the stabilizer content is increased from 0% to 3%. This behavior indicates that the chemical reaction may occur slowly between the soil and admixture additives in the soil matrix. The observed reduction of pH values may be due to the replacement of monovalent ions of soil by the calcium ion of recycled gypsum (e.g., Jha and Sivapullaiah, 2014).

4.2.3 Effect of Additives on Standard Compaction Results of Bentonite

The values of optimum moisture content and maximum dry unit weight for untreated and treated bentonite test specimens were determined using Standard Proctor compaction (ASTM D698-12e2 and the associated results are presented in Figure 4.8 (a, b, and c). Bentonite, (BUNT), was mixed with recycled gypsum (BG), liquid sodium silicate (BS), and a combination of recycled gypsum and sodium silicate (BGS) at various stabilizer contents (0%, 3%, 6%, 9%, and 12%).

As shown in Figure 4.8, an increase in the presence of recycled gypsum is associated with an increase in the optimum moisture content and a slight increase in the dry unit weight. The increase in unit weight is likely associated with dewatering and flocculation, which reduce volume and therefore result in an increase of unit weight with increasing admixture ratios. The presence of calcium components in the recycled gypsum encourages the soil particles to flocculate in the matrix, which can cause an increase in the dry unit weight (Jha and Sivapullialah, 2016). Once the recycled gypsum ratio by mass is over 9%, the maximum dry unit weight noticeably decreases with an apparent increase in optimum moisture content from 27.16% to 31.44%. The increase

in the optimum moisture content when the recycled gypsum is mixed with the soil can be explained as follows: First, more water is required in a proper compaction to achieve the maximum dry density when the fine materials such as recycled gypsum are added to the soil (Holtz& Kovac, 1981). Second, the loss of compaction energy may reduce the maximum dry density while breaking the cementitious bonds which can occur between clay and recycled gypsum (Kuttah and Sato, 2015).

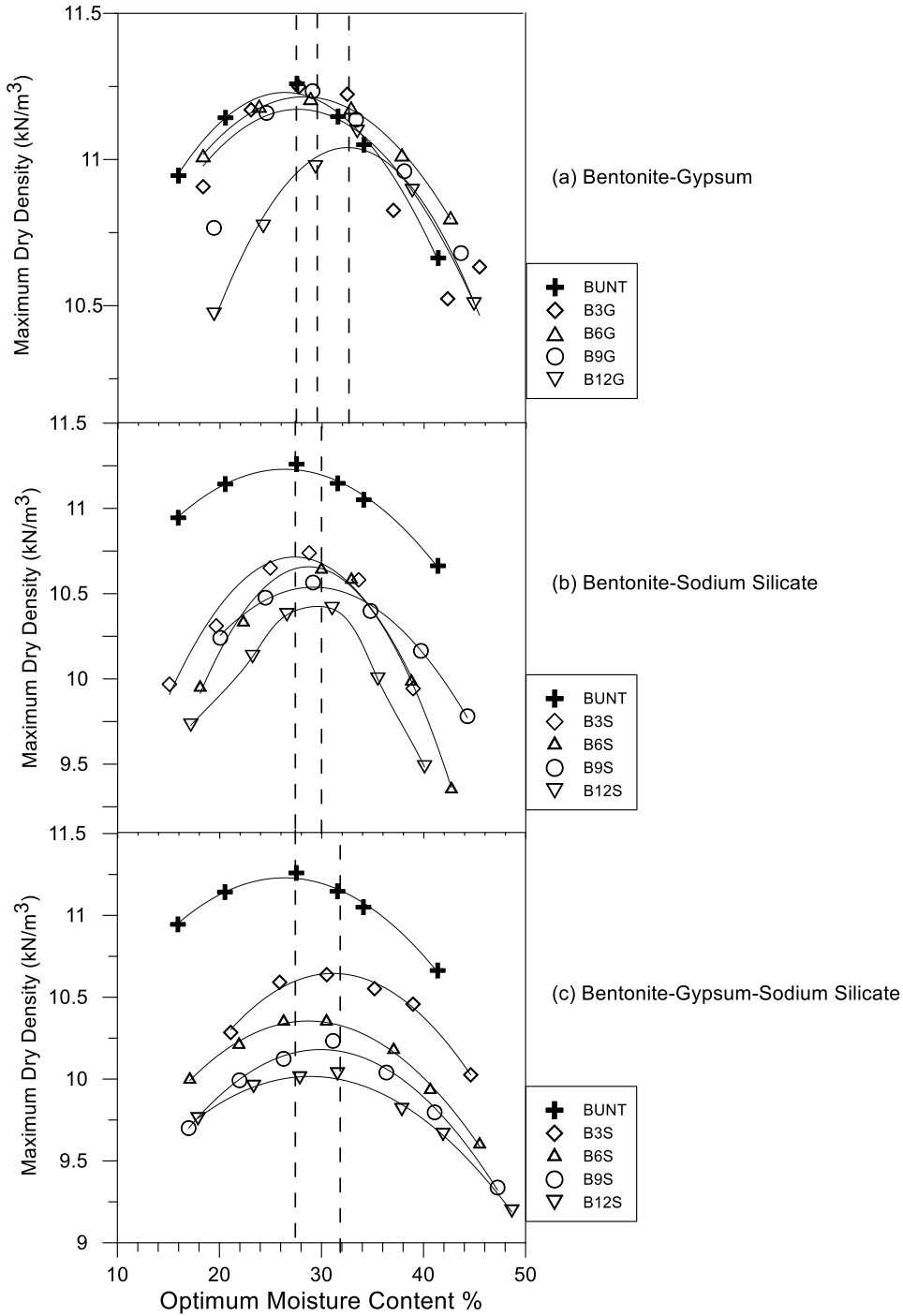


Figure 4.8 Compaction tests for untreated and stabilized Bentonite: (a) Bentonite-Gypsum (BG), (b) Bentonite-Sodium Silicate (BS), and (c) Bentonite-Gypsum-Sodium Silicate (BGS).

Figure 4.8b shows the relationships between dry unit weight and optimum moisture content of the compacted bentonite and sodium silicate (BS), at various stabilizer ratios, 0%, 3%, 6%, 9%, and 12% by mass. As shown, the maximum dry unit weight, (γ_{dmax}), tends to decrease significantly when the sodium silicate content is increased from 0% to 3%, and then decreasing at a smaller, more steady rate as the stabilizer content is increased from 3% to 12%. As the stabilizer content is changed from 0% to 12%, there is a slight increase in the optimum moisture content (i.e., from 27.16% to 30%). The decrease in dry unit weight is rather small among the stabilized soils, which results in a balance between sodium ions and the negative ions on the clay surface (e.g., Türköz et al. 2014; Latifi et al. 2015). The reduction of the dry density can be attributed to particle flocculation and agglomeration developed by the rapid cation exchange in the soil and stabilizer mixture (e.g., Jha and Sivapullaiah, 2014). The increase of the optimum moisture content is attributed to relatively quick exothermic reactions between the soil and additives that cause a loss of water (Latifi et al., 2014). This compaction data is in general agreement with the results of Susmak et al., (2003), who investigated the stabilizing effects of sodium silicate solution, sodium hydroxide, and fly ash on a silty clay.

Figure 4.8c shows the relationships between dry unit weight and optimum moisture content of the compacted bentonite, recycled gypsum, and sodium silicate (BGS), at various stabilizer ratios, 0%, 3%, 6%, 9%, and 12% by mass. Figure 4.8c shows that the dry unit weight of stabilized bentonite significantly decreases with increases in moisture content beyond the optimum moisture content. As the additive

ratio in the soil is increased, the dry unit weight is decreased, with the biggest change in unit weight being observed when the stabilizer content is increased from 0 to 3%. The OMC of treated specimens stays relatively the same for different stabilizer levels, generally near 30.8%, (± 1). The reduction in the maximum dry unit weight with changing stabilizer concentration can be attributed to particle flocculation and agglomeration caused by cation exchange processes between the soil and the admixture of sodium silicate solution and recycled gypsum (e.g., Salonki and Zaman, 2002; Geigman, 2005; Nigussie, 2011; Kamei et al., 2013).

4.2.4 Effect of Additives on Standard Compaction Results of Kaolinite

The values of optimum moisture content and maximum dry unit weight for untreated and treated kaolinite test specimens were determined using Standard Proctor compaction (ASTM D698-12e2), and the associated results are presented in Figure 4.9 (a, b, and c). As shown in Figure 4.9a, adding recycled gypsum to the kaolinite (KG) soil had only a very minor effect on the dry unit weight and OMC at various stabilizer percentages. The maximum dry unit weight of untreated kaolinite was 13.77 kN/m³, and the maximum density of stabilized kaolinite at 3%, 6%, 9% and 12% recycled gypsum ratios was 13.79, 13.73, 13.68 kN/m³, well within the margin of error for this type of test. Similarly, the OMC of untreated kaolinite was measured as 26.92%, whereas the OMC of treated kaolinite (KG) at 3%, 6%, 9% and 12% recycled gypsum ratios was measured as 29.25%, 30%, 30.5% and 30.7%, respectively (essentially no change within the margin of error of the test). This behavior is similar to what was observed for the

standard Proctor compaction of the bentonite stabilized with recycled gypsum (Section 4.2.1), but without the significant changes that were observed for the 12% gypsum/bentonite mixture.

Figure 4.9b shows that mixing soil with a sodium silicate solution (KS) causes the maximum dry unit weight to decrease significantly as the stabilizer content is increased from 0-3%, after which point it remains relatively constant (i.e., from 3% to 12% stabilizer levels). The maximum dry unit weight of the treated kaolinite is 13.07, 12.99, 12.95, and 13.01 kN/m³ for increasing stabilizer percentages, respectively. The optimum moisture content increases from 27.3% to 31.1%, again with most of that change happening from a 0% to 3% stabilizer change. The optimum moisture content of K3S and K6S was 30.0%, and K9S and K12S was 31.1%, respectively.

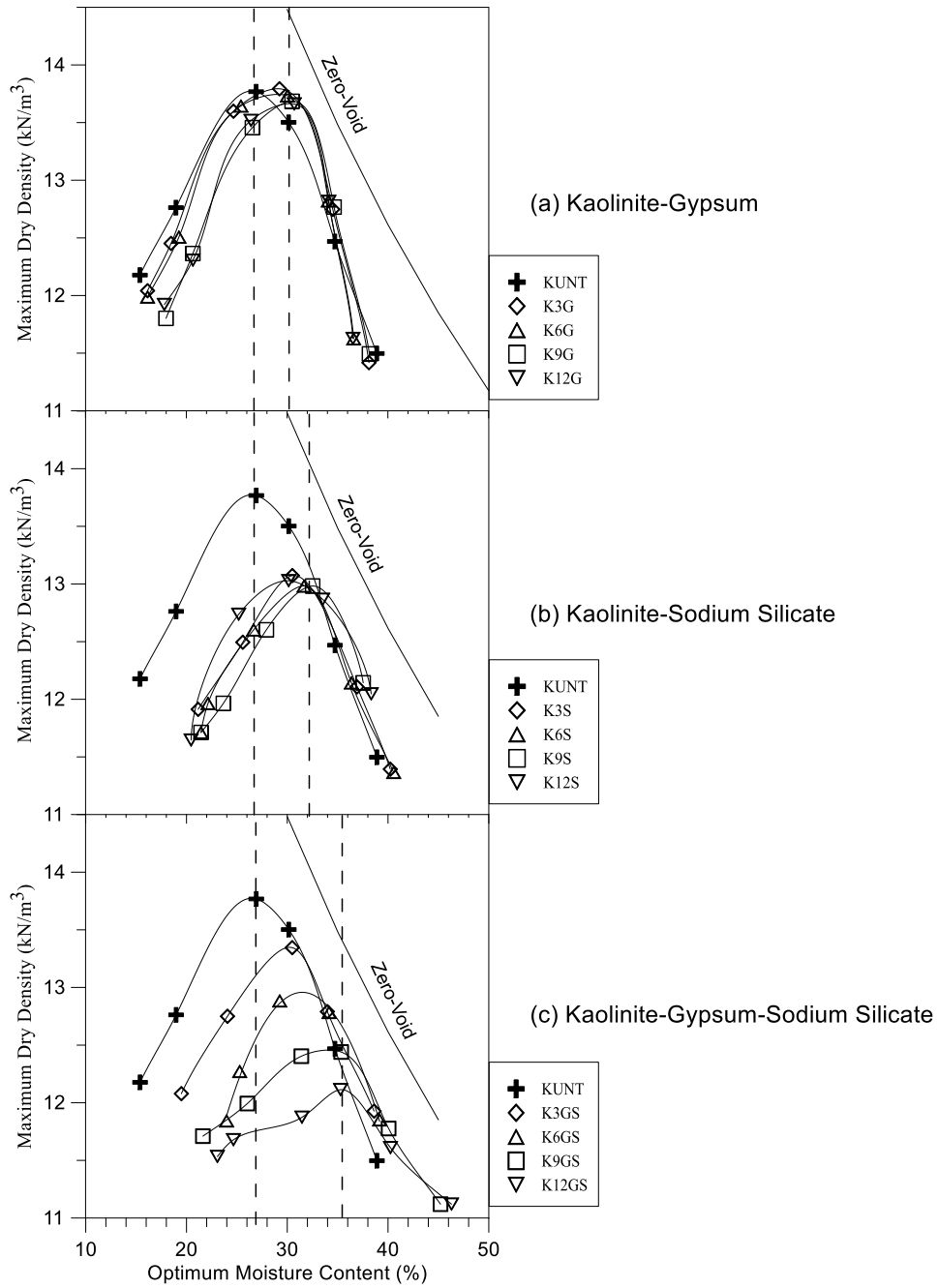


Figure 4.9 Compaction test results for untreated and stabilized Kaolinite: a) Kaolinite-Gypsum (KG), b) Kaolinite-Sodium Silicate (KS), and c) Kaolinite-Gypsum-Sodium Silicate (KGS).

Interestingly, the observed compaction results for the kaolinite-gypsum-sodium silicate (KGS) mixtures is different from either the KG or the KS mixtures. In particular, a more gradual and consistent trend in behavior was observed, with dry unit weights decreasing and optimum moisture contents increasing as the additive content was increased (Figure 4.9c). The measured dry unit weight values were 13.77, 13.34, 12.88, 12.40, and 11.87 kN/m³ for the untreated and increasing additive content specimens, respectively. The OMC increases consistently from 27.3% to 34.7%. Reduction in the unit weight with increasing the moisture content is related to the replacement of monovalent ions of soil with calcium and sodium, altering the clay particles to manufacture new cementitious compounds such as CAH and NASH (Kuttah and Sato, 2015). Also, it is attributed to the lower specific gravity of recycled gypsum and alkaline solution (Na₂SiO₃) compared with soil. Similar results were obtained by Jha and Sivapullaiah, (2014) for gypsum stabilized soil.

4.3 Unconfined Compressive Strength Test Results of Stabilized Soils-

Stabilized soil (kaolinite and bentonite) mixtures were prepared at the optimum moisture content and compressed to their respective maximum dry unit weight in order to prepare UCS test specimens. UCS specimens were prepared using various additive combinations (recycled gypsum, sodium silicate, and a 50:50 mixture of recycled gypsum and sodium silicate) and various additive concentrations (3%, 6%, 9%, and 12%). Prepared specimens were then cured in the temperature controlled room (21 ±1 °C) and in a moisture box for time intervals of 0, 3, 7, 14, 28, and 56 days. Results from

the UCS testing on untreated kaolinite and bentonite as well as treated kaolinite and bentonite specimens are provided in the following sections.

4.3.1 Effect of Recycled Gypsum on Soils

The results presented herein are only for the admixture of bentonite-recycled gypsum, (BG) and kaolinite-recycled gypsum, (KG) at the same additive content, but different curing ages.

4.3.1.1 Bentonite Clay

Figure 4.10 provides UCS test results for BG mixtures at different curing ages. As shown, in general, the addition of recycled gypsum improves the strength of natural bentonite significantly, even without any curing time being allowed for the specimen. Also, the increase in compressive strength that was observed is not strongly correlated with the admixture percentage; i.e., at a curing time of 0 days, a 3% stabilizer showed the biggest gain in strength, but at 28 days a 12% stabilizer showed the biggest gain in strength.

Interestingly, this significant initial increase in compressive strength is diminished significantly at longer curing periods for all admixture ratios. Most specimens exhibited a decrease in strength from 0-3 days of curing, followed by an increase in strength from 3-14 days of curing, followed again by a decrease in strength from 14-56 days of curing. Overall, the strength of bentonite-recycled gypsum specimens decreased from 0-56 days of curing, going from strengths that were

approximately 8 times greater than unstabilized specimens to a little more than 2 times greater than unstabilized specimens. Importantly, final compressive strengths even after 56 days of curing are still more than twice as high as the untreated specimen strengths for all admixture concentrations, showing the beneficial effect of this stabilizer overall for unconfined compressive strength gain.

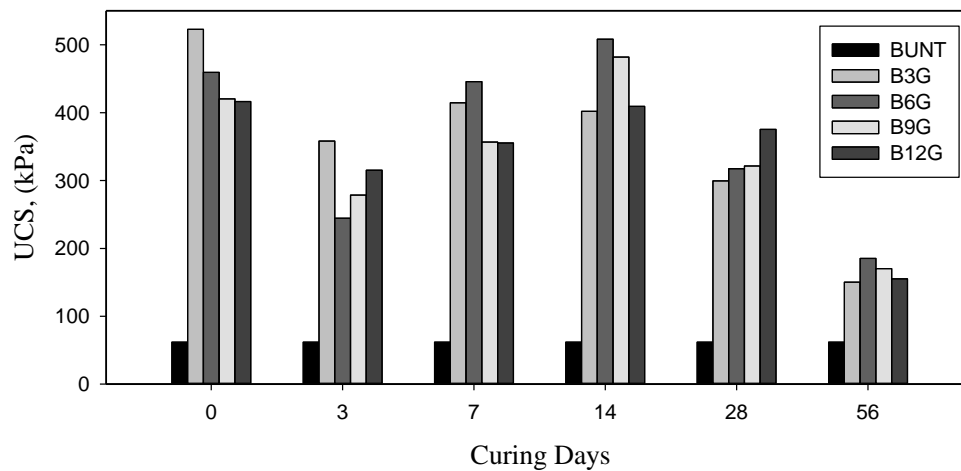


Figure 4.10 The effect of curing time on the unconfined compressive strength of bentonite-recycled gypsum mixtures (BG) at different additive contents.

On average, mixtures with 9% or 12% stabilizer showed relatively equal or smaller strength gains than mixtures with 3% or 6% stabilizer, with the results being somewhat variable in this regard at different curing stages.

Overall, it is believed that the presence of recycled gypsum in the soil matrix improves the strength of pure bentonite efficiently up to about a 6% stabilizer level;

beyond this amount tends to have a negative effect on strength development. These results agree in principle with the findings of Yilmaz and Civelekoglu (2009) and Jha and Sivapullaiah (2014).

The strength decreases immediately after 3-days of curing. It is believed that the immediate reduction in strength is associated with the decrease in pH (increase in acidity), which can decrease the diffuse double layer spacing in the clay and change subsequent cementation reaction processes (Jha and Sivapulliah, 2016).

The hardening process in the short-term curing period is most likely relevant to the exchange of calcium ions of the recycled gypsum by positive charges in the clay lattice (Jha and Sivapulliah, 2016). The reduction in acidity with curing period leads to strength gain for short-term strength development. Therefore, the clay minerals encounter flocculation forming stronger blocks of clay that prevent water from distributing within the soil matrix. Meanwhile, a chemical reaction occurring among calcium, aluminum, and silicon ions already existing in the treated clay develops complex aluminate and silicate products that result in enhancing the strength of the soil at a generally slow rate for long-term curing ages. The presence of fabricated complex aluminate-silicate compounds will be discussed in future sections of this chapter. It should be noted that the selection of the optimum additive content for bentonite is challenging due to the deterioration of strength during the curing intervals, which is in agreement with Jha and Sivapulliah (2016). Consequently, since seems it seems to work almost as well as any of the other stabilizer percentages that were assessed, an additive ratio of 3% was selected for further microstructural analysis.

4.3.1.2 Kaolinite Clay

Similarly, the effect of recycled gypsum on the UCS of stabilized kaolinite clay was investigated at different additive contents (3%, 6%, 9%, and 12%) and curing intervals (0, 3, 7, 14, 28, and 56 days), and the associated results are presented in Figure 4.11.

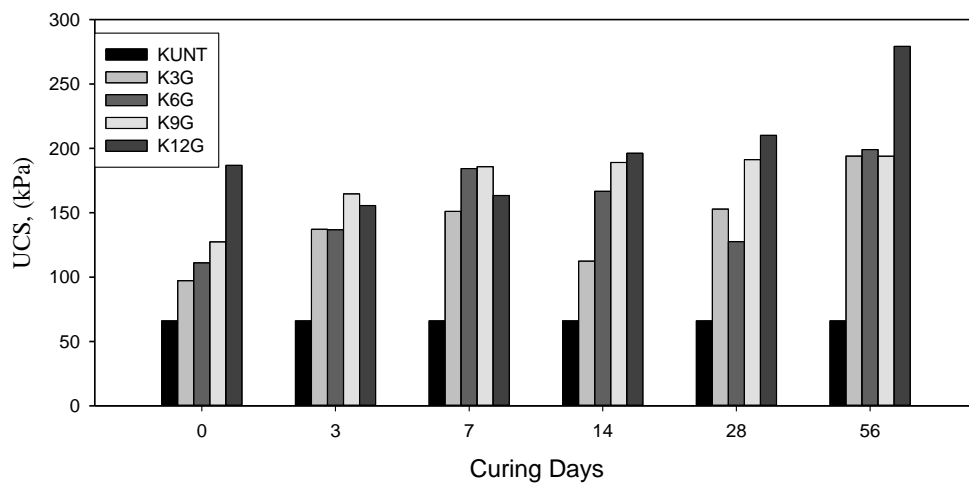


Figure 4.11 The effect of curing time on the unconfined compressive strength of kaolinite-recycled gypsum mixtures (KG) at different additive contents.

All stabilized specimens showed an initial increase in UCS over untreated specimens, though not as large of a jump as what was seen for the stabilized bentonite specimens. Measured strengths tended to increase gradually and consistently with curing time for most stabilized specimens, with the highest strengths being observed at the longest curing times. This points to a time-dependent cementation reaction as being a significant contributor for at least some of the long-term gains in strength that were

observed. Generally, 9 and 12% of the selected additives showed greater increases in UCS than the 3% and 6% additive levels.

The most significant strength development was observed at the end of 56 days of curing; this behavior is attributed to the low reactivity of kaolinite minerals requiring more time to react with stabilizers (Miranda-Trevino and Coles, 2003). Also, the low value of pH might be delaying solubility of the aluminate-silicate source which chemically reacts with calcium ions in the pore water, as shown in Figure 4.5. The 0-day UCS gain of the 12%-additive treated specimens was 186 kPa, which is almost 3 times greater than the untreated kaolinite (66 kPa). For the 12% stabilized specimen, the increment of strength after 3 and 7-days of curing decreases, which is then followed by a consistent improvement in strength. Exhibiting somewhat different behavior, the 9% stabilized specimens saw a gradual and consistent increase in strength from 66 kPa (untreated) to 125 kPa (stabilized, 0-day strength) to 196 kPa (stabilized, 56-day strength), an approximate strength gain of a factor of 3. It can be observed that further strength development is relatively minimal after 7-days of curing.

In most cases, the improvement in strength over time in calcium-based chemically stabilized soils depends on the textural changes, including the exchange of free stabilizer ions dissolved in the pore water and free alumino-silicate minerals in the clay lattice, which associate to form cementitious products that bind soil particles and fill the pore space between particles (Latifi et al., 2016). It is well-known that a high pH environment substantially increases the solubility of aluminate-silicate minerals (e.g., Tingle and Santoni, 2003). The pozzolanic reaction will continue to fabricate

cementation products such as zeolites or hydrated aluminosilicates in the presence of free calcium ions, aluminum, and silicate.

As compared with bentonite stabilized by recycled gypsum, the KG gives more consistent results than BG. The maximum strength development achieved through bentonite samples at 3 and 14 days of curing occurred at 3 and 6% of stabilizer contents, respectively, while KG reached its highest strengths at 9 and 12% additive levels after 28 and 56 days of curing – much more systematic and predictable results. This behavior may be due to the relative reactivity of the aluminum silicate sources in the base materials that are being stabilized, and the related chemical reactions that occur with extended curing conditions for various water contents of the stabilized specimens. Also, a higher recycled gypsum content (12%) achieves more effective stabilization of kaolinite clays relative to the bentonite clay additive content (3%) in this research. This could be the fact that kaolinite clay is less reactive with the stabilizer relative to the bentonite soils which contain a large amount of montmorillonite. Moreover, a longer time may be necessary to develop new cementation products for KG samples owing to their lower rate of chemical reaction.

4.3.2 Effect of Sodium Silicate on Soils

Results from UCS testing on untreated bentonite and kaolinite clays (BUNT and KUNT) and the same clays stabilized using a sodium silicate solution (BS and KS), at various additive contents and curing ages are presented in Figures 4.12 and 4.13, in the following sections.

4.3.2.1 Bentonite Clay

It is evident in Figure 4.12 that all of the UCS values for sodium silicate stabilized bentonite are significantly higher than the untreated bentonite. The largest gains in strength at the end of the curing period (56 days) were observed for the 12% and 9% additive mixtures; however, higher strength values for these mixtures were actually observed at intermediate curing periods (i.e., the 3, 7, 14, and 28 day strengths were all higher than the 56 day strength for these mixtures, with the strength increasing to its peak from the 0 to 3 day mark and tending to decrease from there). Specimens stabilized with 6% sodium silicate followed a similar trend in behavior, but tended to peak at the 7 days point, and specimens with only 3% stabilizer exhibited their largest gain in strength immediately after stabilization, before any curing had happened. This can be explained due to a fast reaction occurring between the stabilizer and soil. Concurrent testing for pH indicates an immediate increase in this value to over 10.5 after the introduction of the sodium silicate (an “alkali activator”) to the soil. The process of geopolymerization is believed to start immediately by the dissolution of alumina silicate from the base clay material that is being stabilized (Khale and Chaundary, 2007). The strength of the resulting geopolymers is associated with the nature of the reactions that occur between silica and alumina in the existence of alkali ions; the evolution of these reactions is indicated by the level of acidity throughout the curing period (Phummiphan et al. 2016).

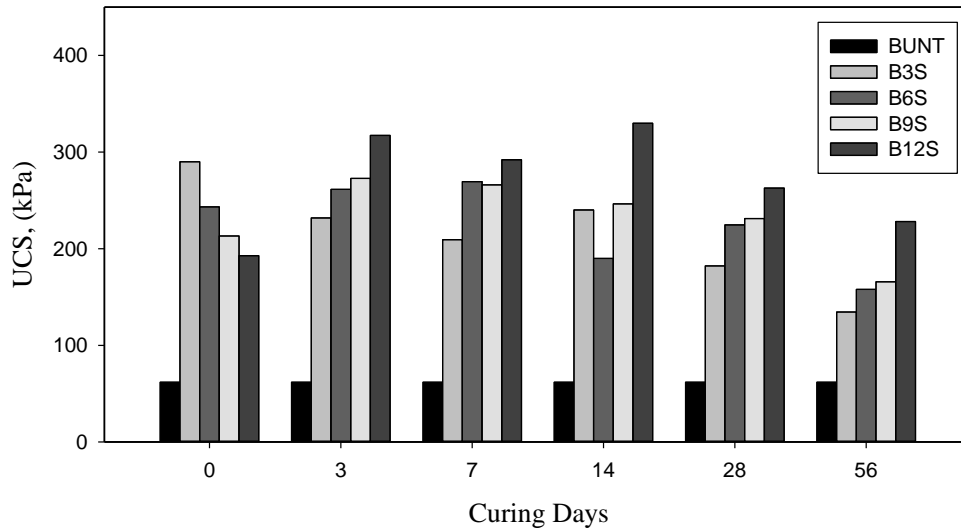


Figure 4.12 The effect of curing times on the unconfined compressive strength of bentonite-sodium silicate (BS) at different additive contents.

For this soil stabilization process, the addition of sodium silicate (an alkali activator, Na_2SiO_3), acts as a binder to manufacture amorphous geopolymer or zeolites (Xu and Van Deventer, 2000). Note that the pH presented in Figure 4.3 increases significantly from 0-3% stabilizer, and much more gradually from 3-12% stabilizer. It is believed that this significant change in pH encourages the dissolution of aluminate silicate from the clay particles, allowing stabilization reactions to then occur between the soil and alkaline solution (Miranda-Trevino and Coles, 2003). However, it is observed that the strength reduces after 14 days of curing although the value of pH is still convenient for polymerization to occur in the binder system.

Higher compressive strengths were achieved for the specimens treated with 12 and 9% sodium silicate content between 3 and 14-days of curing. The specimens

stabilized with 12% sodium silicate resulted in higher strength than those stabilized with 9% sodium silicate at all curing ages, despite the higher strength that was observed for the 9% sodium silicate at a 0-day curing time. Nonetheless, it was observed that the UCS tends to decrease after 14-days of curing. This behavior can possibly be attributed to excessive positive surcharge due to an abundance of positive ions at a given location, which make it difficult for cementation products to form (Tingle et al. 1989; ; Katz et al. 2001; Rauch et al. 2002; Tingle and Santoni, 2003). The observed results are consistent with those that have been observed by other researchers (e.g., Cheng et al. 2003; Heah et al. 2012; Bignozzi et al., 2014; Gao et al. 2014; Pavithra et al. 2016) who have reported that the presence of excess alkaline solution in a stabilizing mixture can decrease the strength once fly-ash based geopolymers were synthesized. As shown in Figure 4.12, the stabilized bentonite specimens with 12% sodium silicate solution reveal the maximum strength development at 3, 7 and 14-days of curing, with later decreases in strength; these results are therefore consistent with what has been reported in earlier studies (e.g., Bignozzi et al., 2014; Gao et al. 2014); it should be noted that not all researchers have observed the same findings in this area, indicating the complexity of the reactions that are involved (e.g., Vali Vakili et al., 2016). Besides, 3% admixture exhibits a significant improvement in strength nearly instantly, which could be due to the quick reaction between soil and alkaline solution in the soil mixture.

4.3.2.2 Kaolinite Clay

The UCS strength of kaolinite stabilized with sodium silicate is shown in Figure 4.13. As shown, all stabilized specimens exhibit strengths that are at least 1.5 to 2 times greater than those measured for untreated specimens. The higher concentrations of the alkaline activator appear to play a role in diminishing the gains in compressive strength that were observed at both the short- and long-term curing periods. It is believed that the high content of unreacted aluminum silica source with the increase of sodium silicate content in the specimens acts as weakness site, reducing the overall strength of the stabilized specimens (e.g., Gao et al., 2014). Also, a high content of alkaline solution causes the binding agents to become sticky due to the vicious structure of sodium silicate in the soil matrix. Large amounts of the sodium silicate may discourage the cementation or geopolymerization process over the various curing periods (e.g., Heah et al., 2012). Gao et al. (2014) observed a lower compressive strength development for metakaolinite stabilized with a high content of sodium silicate in the early curing ages.

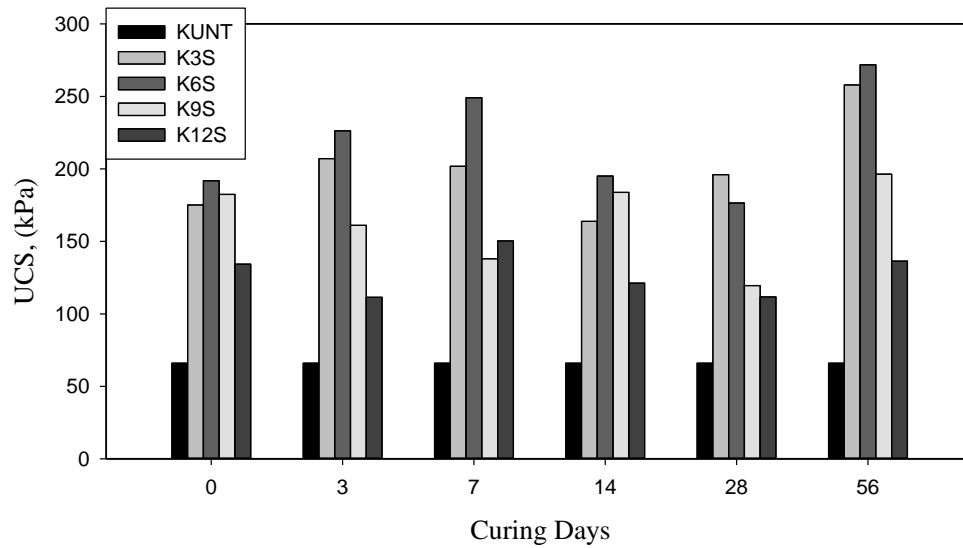


Figure 4.13 The effect of curing times on the unconfined compressive strength of kaolinite-sodium silicate mixtures (KS) at different additive contents.

Generally larger strength gains were observed for kaolinite stabilized with 3 and 6% sodium silicate. The significant improvement in strength was observed with the addition of 6% alkali activator to the soil mix. The strength of KS mixture with 6% sodium silicate, K6S, is increased by factors of 2.9, 3.4, 3.8, 3.0, 2.7 and 4.1 after the various curing periods, respectively. Likewise, the strength of K3S is increased by factors of 2.7, 3.1, 2.5, 3.0 and 3.9 after the various curing periods, respectively. This confirms that 3% and 6% stabilizer contents provide sufficient amounts of sodium silicate to dissolve silicate and alumina that are present in the soil matrix at higher alkaline environment ($\text{Ph} > 10$, as shown in in Figure 4.16), allowing for subsequent formation of cementitious compounds with additional curing (e.g., Sivapullaiah and Jha, 2014). The reduction of strength for specimens treated with over 6% sodium silicate is

likely due to the presence of unreacted stabilizer in the soil matrix, which interferes with the formation of cementitious bonds during the geopolymerization process (e.g., Sukmak et al. 2013). It is also related to the presence of undissolved Al-Si particles, the nature of amorphous gel that is formed, and any surface reactions between the gel and Al-Si source materials (e.g., Komnitsas and Zaharaki, 2007).

When comparing the UCS results for BS and KS, it can be observed that both pure soils were improved by the addition of the sodium silicate, for all additive contents and curing periods that were examined. Much of the strength gain that was observed happened immediately for both of the stabilized soils. Some additional strength gain was observed for various additive mixtures in the 3-7 day range for both the kaolinite and bentonite, with some of the bentonite specimens continuing to gain strength out to 14 days. The untreated kaolinite seemed to exhibit greater strength gains when stabilized with 3-6% of sodium silicate, while the untreated bentonite responded with greater strength gains to the 9% and 12% stabilizer levels. The largest gains in strength were observed for kaolinite after 56 days of curing, while the largest gains in strength for bentonite were observed in the 3-14 day range of curing, with longer curing times beyond this point tending to result in a decrease in soil strength from the peak recorded values.

The optimum sodium silicate content in this study was determined to be 3 and 6% for kaolinite, and 9 and 12% for bentonite, respectively. Thus, it is obvious that the type of soil plays a significant role regarding the strength development based on the admixture content in the soil. The following specimens consisting of 6% and 12%

sodium silicate were selected for a detailed microstructural investigation that will provide better understanding into the mechanisms of kaolinite and bentonite stabilization: K6S3, K6S14, and K6S56; B3S12, B7S12, and B14S12, respectively.

4.3.3 Effect of the Admixture of Recycled Gypsum and Liquid Sodium Silicate on Soils

The UCS of the untreated bentonite soil and bentonite soil stabilized with various quantities of a combined (50:50) recycled gypsum and sodium silicate mixture (BGS) at various additive contents and curing periods are presented in Figures 4.14 and 4.15, in the following sections.

4.3.3.1 Bentonite Clay

It is observed that after the addition of the recycled gypsum and sodium silicate solution, the development in strength generally increases by more than a factor of two (Figure 4.14). Most of this strength gain happens immediately for all of the stabilizer ratios that were assessed. From the 0 to 7 day curing mark, the stabilized specimens tended to decrease somewhat in strength, which was then followed by a strength gaining trend from 7 days to 56 days of curing. Overall, little change in strength to a slight increase in strength was observed from 0 to 56 days of curing.

The “slump” in strength at intermediate curing times may be associated with development of an undesirable cementation environment, (i.e., $\text{pH} < 10$, as shown in Figure 4.4), which discourages pozzolanic reactions between the stabilizers and soil

(e.g., Hunter, 1988). The small enhancements in strengths that are observed with curing times up to 56-days can be attributed to greater cementation occurring as the pH value increases (Figure 4.4). The small gains in strength that are observed over time imply that the reaction between stabilizers and soil is generally limited in nature.

In general, the observed behavior may be related to the low pH values, which are unfavorable for the dissolution of calcium and sodium ions from the additives. In other words, the soil will be more easily dissolved at higher pH values, (i.e., $\text{pH} > 10$), allowing for more reactions with available calcium and sodium ions to produce pozzolanic compounds contributing to the strength development. Thus, the dissolution of aluminum-silicate minerals is a slow process in the low pH conditions that are shown in Figure 4.4 – as a result, the long-term stabilization reactions that occur tend to happen at a slower rate to the medium level pH values that were observed for the tested specimens (i.e., in the 8-10 range).

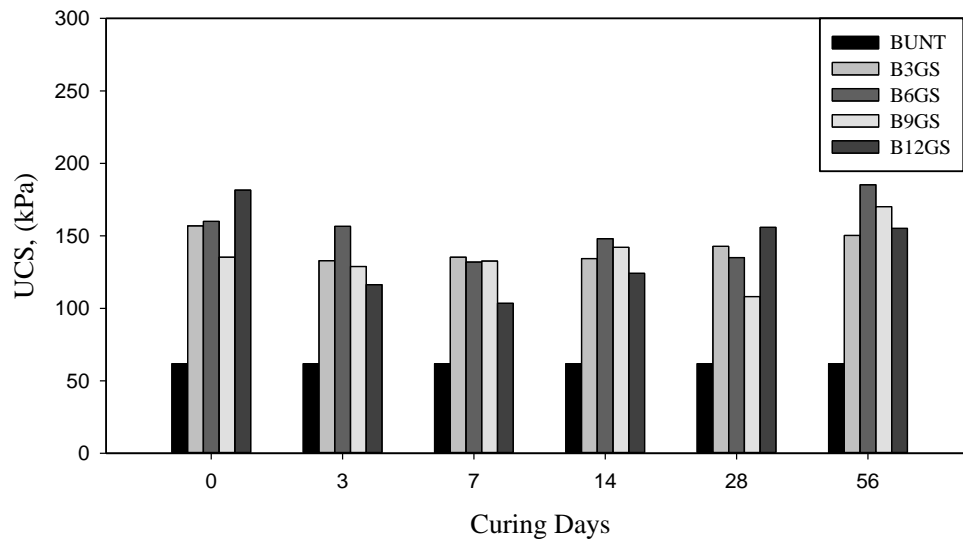


Figure 4.14 The effect of curing time on the unconfined compressive strength of bentonite-recycled gypsum-sodium silicate mixtures (BGS) at different additive contents.

Comparing the strength of the treated BGS specimens in Figure 4.14, it can be observed that the largest gains in strength at 56 days occur for the 6% additive content. The strength increase ratios of 6% additive stabilized versus untreated specimens are 2.6, 2.5, 2.1, 2.4, 2.3, and 3.0 for the various curing times that were assessed, clearly showing the aforementioned “slump” in strength that occurs at intermediate curing times. For 0 days of curing, that largest increase in strength was observed for the 12% recycled gypsum-sodium silicate mixture. This may be due to the high content of stabilizers realizing monovalent ions quickly into the pore water (Jha and Sivipullaiah, 2016). The rapid availability of calcium and sodium silicate may accelerate immediate

improvement in the strength through various pozzolanic reaction and cation exchange processes between the soil and admixture at the early stage of curing.

4.3.3.2 Kaolinite Clay

In a similar fashion, kaolinite was combined with a 50:50 mixture of recycled gypsum and sodium silicate (KGS) at various stabilizer ratios, as an alkali activator to produce a geopolymer. After specific curing periods, UCS tests were conducted to measure the changes in strength that occurred with curing time for the various stabilizer mix ratios that were assessed. The results from the associated UCS testing are presented in Figure 4.15.

As shown in Figure 4.15, the UCS values for all of the additive mix ratios that were assessed showed a significant increase in strength relative to the untreated kaolinite values. Moreover, the UCS tended to increase gradually at a fairly consistent rate for the entire 56 days curing period, for all of the stabilized specimens that were tested. Interestingly, specimens with 3% stabilizer exhibited results that were consistently higher than those with 9% stabilizer, and specimens with 6% stabilizer exhibited results that were consistently higher than those with 12% stabilizer. There was also a significant drop in strength when the mix ratio was changed from 6% to 9% stabilizer. This behavior is attributed to an excessive amount of unreacted stabilizers, particularly sodium silicate, which may cause a reduction in compressive strength over the curing times (e.g., Heah et al. 2012; Bignozzi et al.; 2014; Gao et al. 2014; Pavithra et al. 2016). Thus, the optimum recycled gypsum and sodium silicate content could be either

3 or 6% of admixture (50%:50%) in this study; 6% yields larger gains in strength, but only by a modest amount for the additional volume of stabilizer that is utilized (i.e., a 3% stabilizer level represents the most efficient use of the additive from a cost/sustainability standpoint.

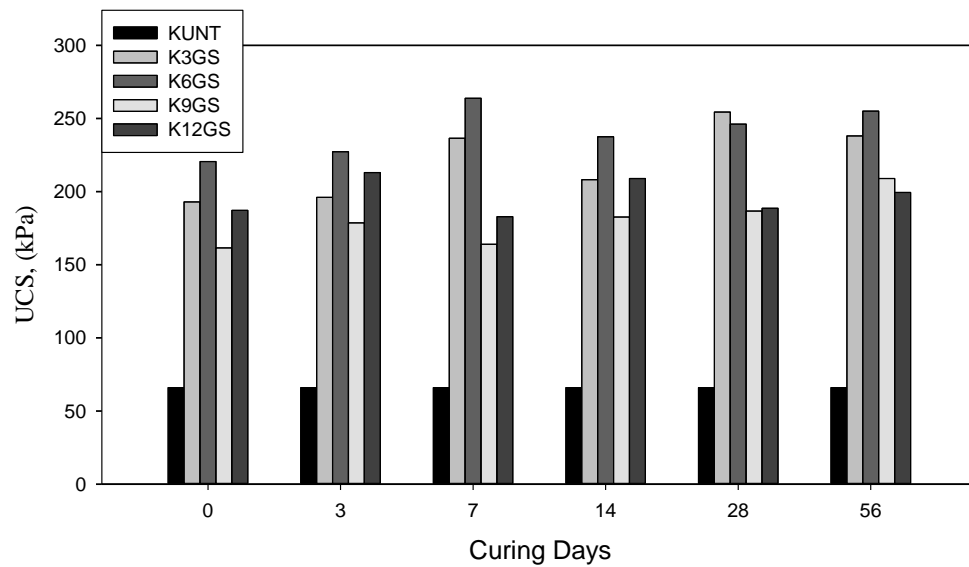


Figure 4.15 The effect of curing time on the unconfined compressive strength of kaolinite-recycled gypsum-sodium silicate mixtures (KGS) at different additive contents.

The ratios of strength gain for 3% admixture stabilized soil relative to untreated soil are 2.92, 2.97, 3.58, 3.18, 3.85, and 3.60 for the various curing ages that were assessed, respectively. The maximum strength gains for 3% stabilized soil occurred at 28-days of curing, however the maximum strength gain for 6% stabilized soil occurred at 7-days of curing. In general, most of the strength gain that occurs for the 3% and 6%

stabilized specimens appears to happen within the first 7 days of curing; this indicates that the majority of the cementation that occurs tends to happen at relatively early curing times.

Similarly, the strength gain ratios of treated kaolinite with a 6% admixture content were 3.34, 3.44, 4.0, 3.60, 3.73, and 3.86 for the various curing times that were assessed, respectively. From 0-7 days of curing, the strength of the stabilized specimens gradually increases and attains the maximum value of the strength. The samples cured for 14 days lose approximately 10% of their overall strength, and then the specimens regain their strength moderately. The enhancement in the strength, thereafter, follows a consistent rising pattern up to 56-days of curing.

By comparing Figure 4.14 (BGS) and Figure 4.15 (KGS), at the same content of additives and curing periods, both soils efficiently augment the strength over the curing time at various additive contents, relative to the untreated soil strength. The type of base soil that is stabilized yields a different pattern of strength gain even though for both soils the enhancement of the soil strength is successful overall. The alkali-activated mixture of kaolinite and recycled gypsum specimens revealed a more consistent, predictable, and sustainable pattern of strength development than the alkali-activated mixture of bentonite and recycled gypsum. The combination of additives allows for relatively small additive usage overall, yielding fairly impressive gains in strength for both of the stabilized soils. Also, both the stabilized bentonite and kaolinite tended to show decreases in measured strength once the amount of stabilizer present in the soil mixture

exceeded a certain level. The reduction in the strength is associated with unreacted additives in the soil matrix, in a similar fashion as what was postulated for BS.

For the recycled gypsum-sodium silicate stabilized soils, development of UCS relies upon the geopolymerization process, which is controlled by the reaction between a primary Al-Si source, an alkali activator, and heat conditions. If these materials are available, cementing materials such as geopolymers and hydrated gels can form via geopolymerization and pozzolanic reactions, as well as cation exchange activities during the curing time. The activities of the chemical reactions can generate new cementation compounds such as hydrated aluminosilicates and zeolites decreasing the soil porosity while filling the voids between the clay particles. Thus, this phenomenon increases the strength of the soil (Hoy et al. 2016).

In this regard, the UCS results indicate that a 6% additive content is an optimum value for both bentonite and kaolinite clays for further investigation using microstructural analysis techniques; however, somewhat different strength gain values were observed for the different curing times that were assessed at this stabilizer level. Kaolinite exhibits its peak strengths at 7, 28 and 56 days of curing, while bentonite exhibits its peak strengths at 3, 14 and 56 days of curing (for a 6% additive content, neglecting the 0 day strength gain).

To confirm this phenomenon, microstructural analysis has been performed on tested UCS specimens using X-ray diffraction (for detection of new cementitious crystals), Field emission scanning electron microscopy, (for assessment of morphological structure), Fourier transforms infrared spectroscopy, (for assessment of

material bonding), and N₂-BET surface area testing (for overall surface area assessment). The results from these tests are discussed in more detail in the following sections.

4.4 X-Ray Diffraction Results of Stabilized Soils

X-ray diffraction (XRD) is a fundamental technique that can be used to characterize the crystalline materials that are present in a soil matrix. XRD tests conducted on both untreated and stabilized soils can show changes in crystalline mineralogy that occur as a result of the stabilization process. Tests were performed on both bentonite and kaolinite soils that had been stabilized with recycled gypsum, sodium silicate, and a 50:50 mixture of recycled gypsum and sodium silicate, at various stabilizer concentrations and curing time intervals. Note that new cementation compounds can also be generated with an amorphous phase, which will not be detected in the XRD diffraction patterns; the FESEM/EDAX testing that is described later in this chapter can be used to investigate the phase and chemical composition of the amorphous binders that are formed by the stabilization process.

XRD results for the untreated kaolinite and bentonite clay that were examined in this testing program are provided in Figure 4.16. As shown in Figure 4.16a, the kaolinite clay is mainly dominated by kaolinite (K), with large-scale mineral peaks at 2θ angles of: 12.15°, 20.5°, 36°, 45.3°, 49°, and 61.8° (PDF# 00-001-0527, JCPDS, 1995). Quartz (Q) is at 21°, 39.3°, and 51.7° (PDF# 01-077-8628, JCPDS, 1995), halloysite (H) is at 35.7° and 38-39° (PDF# 00-060-1517 & 00-060-0342, JCPDS,

1995), and illite (I) is at 19.7°, 22.6°, and 41.6° JCPDS (1995). Kaolinite and halloysite have a similar chemical composition except that halloysite incorporates excessive water molecules in the crystal case system in which internal water molecules can migrate readily (e.g., Hillier and Ryan, 2002). Illite is a common impurity in kaolinite group minerals, which is seen in clear quantities in the clay matrix. Thus, some of the kaolinite, halloysite, and illite peaks are not identical in the diffraction pattern, since these peaks can overlap with each other (e.g., Hillier and Ryan, 2002). Also, weak peaks corresponding to the primary reflection from goethite were detected so that those peaks may be assigned as minor impurities, but the absence of peaks related to the reflection of goethite (47.7°) prevents a positive identification. The diffraction peaks for kaolinite are in agreement with the results presented by Worasith et al. (2001) and JCPDS (1995).

Untreated Bentonite consists of montmorillonite (M), quartz (Q), cristobalite (C), illite (I), mullite (Mu), anorthite (A), and as trace minerals, hematite (H), and rutile (R), which are present in the XRD spectra shown in Figure 4.16b. The dominant clay minerals present in the untreated bentonite sample are montmorillonite ($2\theta = 8.4^\circ, 19.4^\circ, 21.5^\circ, 28^\circ, 38^\circ, 54.6^\circ$ and 62° , PDF#00-029-1499, JCPDS, 1995), and illite ($2\theta = 18.3^\circ, 34.4^\circ, 42^\circ, 68^\circ, \text{ and } 73^\circ$, PDF#00-002-0050, JCPDS, 1995). Other mineral reflections were observed at approximately $21^\circ, 27.3^\circ, \text{ and } 50.6^\circ$ for quartz, and 29.3° for cristobalite (PDF# 01-074-1811, and 01-073-9378, JCPDS, 1995). Anorthite is also detected in the diffraction spectra located at about $27.6^\circ, 31.1^\circ, \text{ and } 41.5^\circ$ (PDF#01-070-0287, JCPDS, 1995). The main reflection peaks from rutile (TiO_2) were observed at approximately $40.1^\circ, 22.3^\circ$ (PDF# 00-03-0619, JCPDS, 1995).

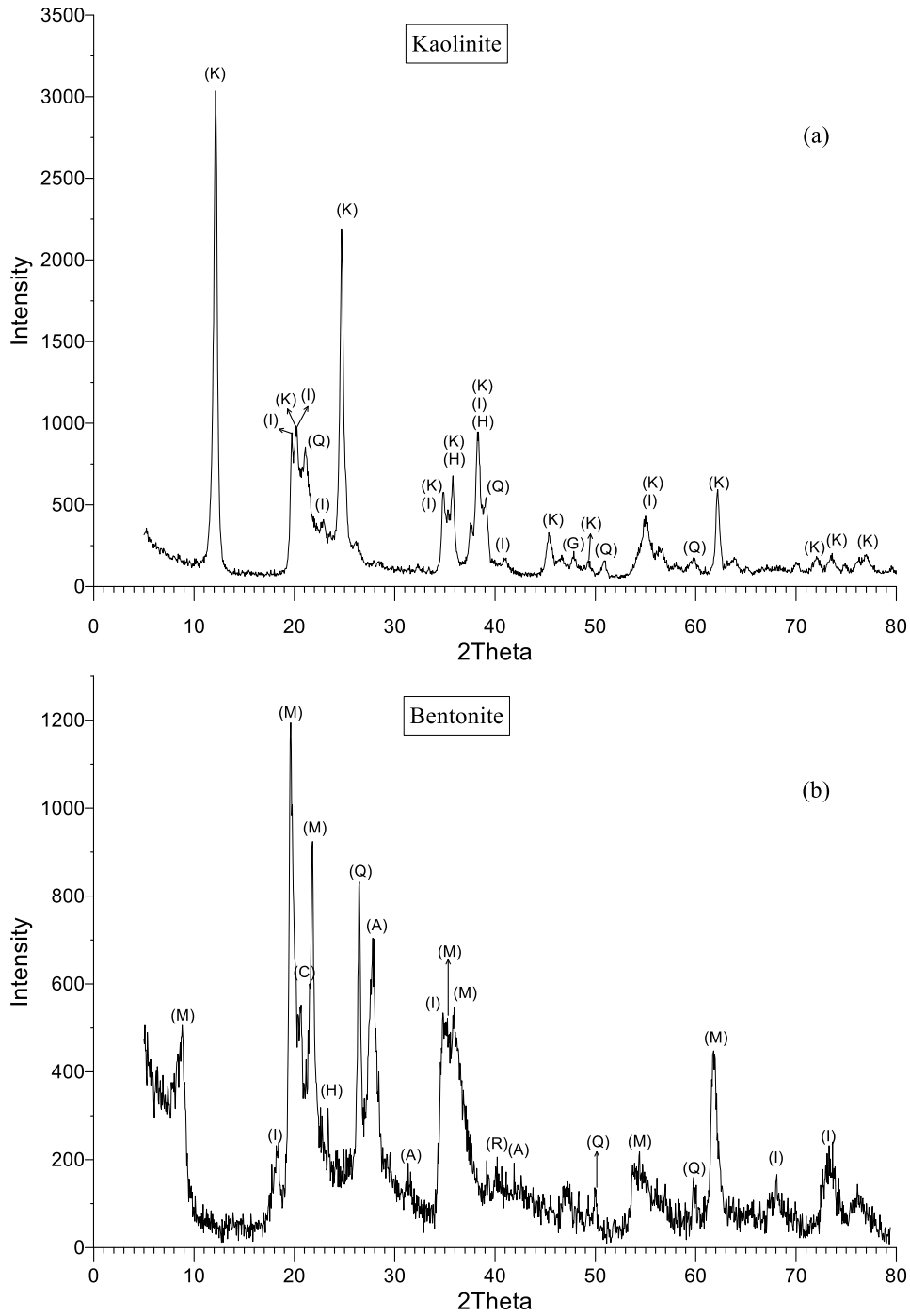


Figure 4.16 X-ray diffraction patterns for untreated, (a) Kaolinite, and (b) Bentonite.

4.4.1 Effect of Recycled Gypsum on Soils

X-ray diffraction was utilized to characterize the crystalline reaction products that were formed once recycled gypsum was introduced into the pure bentonite and kaolinite mixtures. The effect of different curing intervals was explored, and the results are presented in the following sections.

4.4.1.1 Bentonite and Recycled Gypsum

Figure 4.17a, b, and c reveals X-ray diffraction results of bentonite treated by 3% recycled gypsum at 3, 14 and 28-days of curing. Noticeable changes in the X-ray diffraction results of treated bentonite samples can be observed in comparison to the untreated bentonite. After treatment, the reflection intensities of montmorillonite and quartz decrease with increases in curing time. That means montmorillonite minerals chemically weathered as the interaction of the stabilizer on the soil matrix, which forms new calcium-based aluminum silicate phases as well as sodium-calcium phases (e.g., Yoobanpot et al., 2017).

It is believed that CAS, CSH, and (N)CASH play an essential role for increasing the engineering properties of soil by strong chemical bonding and mechanical contact, and their void-filling tendency (e.g., James et al. 2008). Furthermore, new reflections were detected for the treated specimens at 3, 14, and 28 days, due to the formation of cementation crystalline materials at two-theta angles of 31.2° and 33.5° , which are associated with the formation of calcium silicate hydrate (CSH) JCPDS (1995). After 3 days of curing, sodium calcium aluminum silicate hydrate ((N)-CASH, PDF# 00-013-

0129, JCPDS, 1995) also exhibited a very small peak at 33.2° , which was indistinguishable as the curing time was increased

Another new reflection peak corresponding to calcium aluminum silicate hydrate (CASH, PDF#00-015-0179, JCPDS, 1995) phases was observed at about 51.3° in stabilized bentonite in 14 and 28 days of curing. The reflection peak at $\sim 30.7^\circ$ for specimens cured for 3 days is attributed to the formation of calcium aluminum hydrate (CAH, PDF# 00-072-1868) JCPDS, (1995) other specimens also have weak reflection peaks at roughly the same angle.

Additional weak reflection peaks indicating the possible presence of calcium sodium silicate hydrates containing sulfate ions (CNSH, PDF#01-089-8618, JCPDS, 1995) were observed at $2\theta = 42.1^\circ$ and 49.7° in the specimen that was cured for 3 days. With additional increases in curing time, the observed $2\theta = 42.1^\circ$ peak disappears, and the $2\theta = 49.9^\circ$ diffraction peak is weakened.

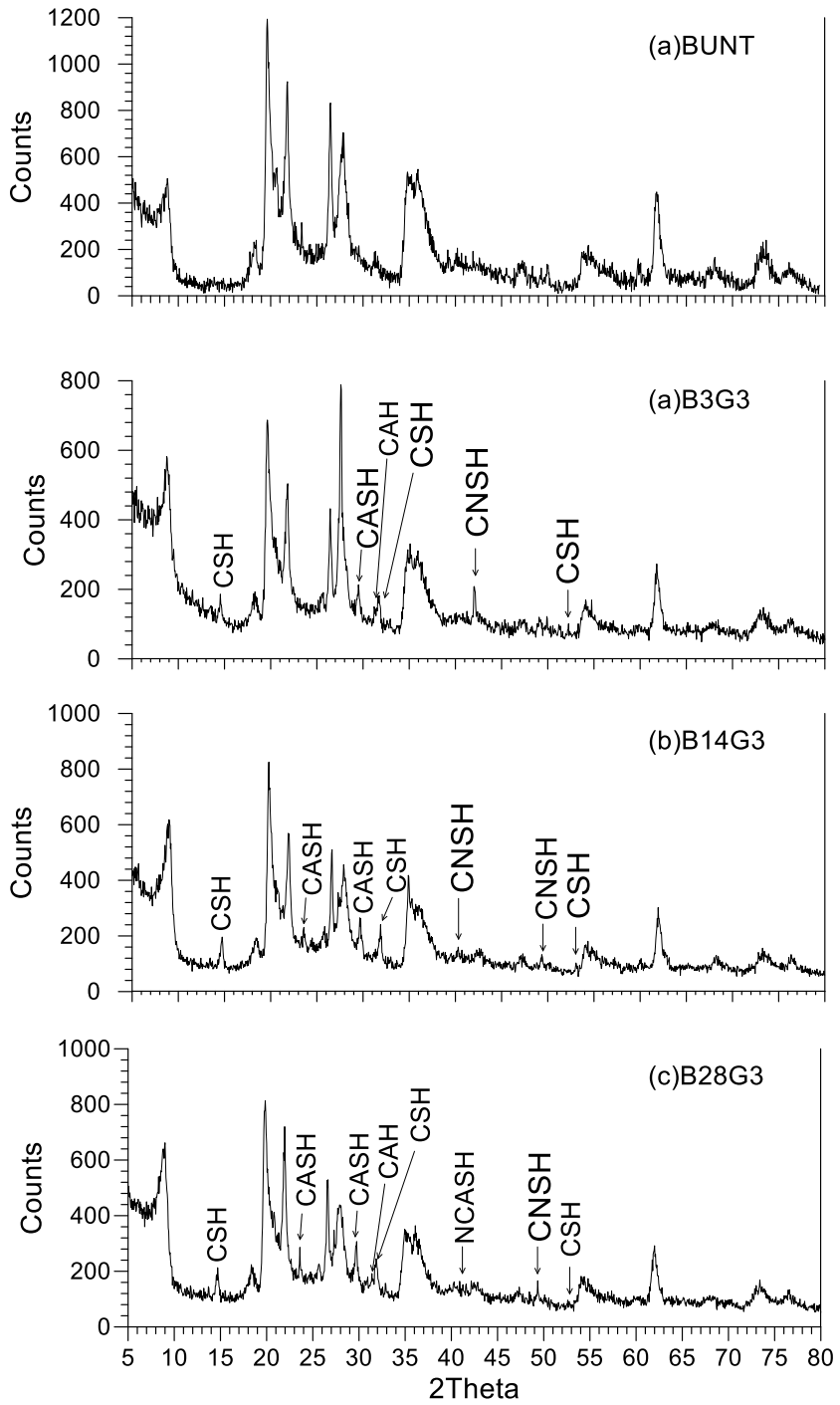


Figure 4.17 X-ray diffraction patterns for bentonite stabilized with recycled gypsum (BG) at the same additive content and different curing times.

4.4.1.2 Kaolinite and Recycled Gypsum

X-ray diffraction results for kaolinite stabilized with 12% recycled gypsum at 14, 28, and 56 days of curing are presented in Figures 4.18a, b, and c, respectively. As shown, the X-ray diffraction pattern for stabilized kaolinite experienced a reduction in some of its mineral peaks (particularly kaolinite). This observed change can be associated with the effect of the stabilizer, which likely induces chemical weathering of the clay minerals (Latifi et al., 2016). Quartz mineral was also detected in the stabilized specimens, and it has been consumed slowly over the curing intervals, as shown in the figure since their intensities have been reduced (Zhang et al., 2012).

The examination of the X-ray diffraction results for stabilized kaolinite demonstrates that mineral composition of the soil solids changes as a result of stabilization. New cementation products are fabricated, including calcium silicate hydrates (CSH), calcium aluminate hydrates (CAS), calcium aluminate silicate hydrates (CASH), and calcium silicate hydrate minerals consisting of carbonate (CO_3). The evidence of these fabricated cementation products is as follows: New observed reflections at $2\theta = 14.5^\circ$ are attributed to the formation of calcium aluminum silicate hydrates with carbonate (CO_3) (CASH- CO_3 , PDF#00-036-0378 called “Partheite”, JCPDS, 1995). In the lower diffraction region, at $2\theta = 8.1^\circ$, new peaks imply the formation of calcium aluminate silicate (CAS PDF#00-029-0329, JCPDS, 1995), but the intensity is weak, so distinguishing the peaks is difficult. A high reflection peak centered at $2\theta = 24.6^\circ$ indicates more significant formation of calcium aluminum hydrate (CAH, PDF#00-025-0181, JCPDS, 1995). However, this sharp observed peak

dissipates for the specimens tested at longer curing periods (28 and 56 days). Calcium aluminate silicate (CAS) peaks are more strongly evident at $2\theta = 29.5^\circ$ and 32.0° , and more weakly evident at 39.5° (PDF# 01-072-1868, JCPDS, 1995). Moreover, the specimen cured for 56 days reveals a gel diffraction hump at $2\theta \approx$ between 8° and 10° . Other researchers have observed that the gel phase of various cementation products can manifest itself as a hump shape in the diffraction patterns, rather than as a new sharp reflection peak (Garbev et al., 2007).

These new observed peaks in the XRD data indicate the formation of new cementation products, in a dynamic reaction environment that is continually evolving with curing time. It should be noted that the general reflection intensities of the aluminum silicate source materials tend to reduce with increases in curing period. However, the reader should also take into account the fact that there is likely some natural variation that occurs in measured XRD results from sample to sample (i.e., natural sample variation), and that all of the tested XRD specimens correspond to unique samples that are taken, so some variation is to be expected in the measured XRD results.

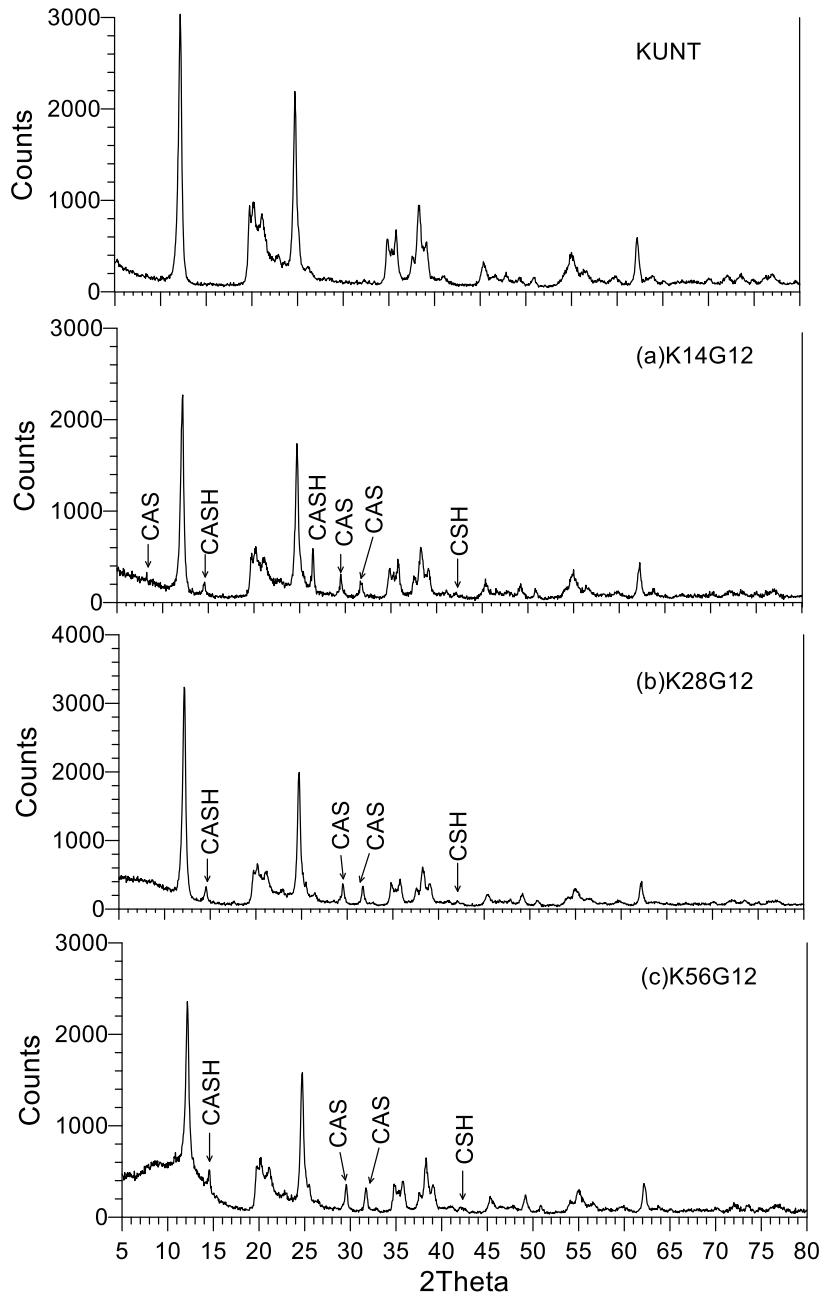


Figure 4.18 X-ray diffraction patterns for kaolinite stabilized with recycled gypsum (KG) at the same additive content and different curing times.

4.4.2 Effect of Sodium Silicate Solution on Soils

X-ray diffraction was utilized to characterize the crystalline reaction products that are formed once the sodium silicate solution was introduced into the pure bentonite and kaolinite mixtures. The effect of different curing intervals was explored, and the results are presented in the following sections.

4.4.2.1 Bentonite and Sodium Silicate Solution

Figures 4.19a, b, and c depict the XRD patterns of the stabilized bentonite by 12% additive after 3, 7 and 14 days of curing at room temperature, respectively. The primary diffraction intensity for montmorillonite and quartz is slightly decreased with the increase in the curing time after initial mixing. This observed behavior supports the hypothesized reaction between the soil and the alkaline solution. In Figure 4.16b, the anorthite mineral (calcium silicate) centered at $2\theta = 30.1^\circ$ disappears as the curing time increases. Some new peaks are shifted to a higher degree of diffraction angle as the curing period increases, which could indicate the formation of new cement compounds in the binder system (Yu et al., 1999).

The specimen cured for 3 days (Figure 4.19a) exhibited a weak diffraction peak at $2\theta = 13.5^\circ$ corresponding to calcium aluminate hydrate (CASH) (PDF#00-011-0589, also referred to as zeolite, JCPDS, 1995). Likewise, the same component (CASH) was observed in the B7S12 specimen, displaying as a weak diffraction peak at $2\theta = 13.5^\circ$. In the B7S12 specimen, a new sharp crystalline peak was observed at $2\theta = 50.5^\circ$, indicating the presence of sodium calcium aluminum silicate (NCASH) hydrates with

zircon elements (Zr) (PDF#01-075-9361, JCPDS, 1995). Additionally, other calcium aluminum silicate (CAS) products yielded a small sharp peak at $2\theta = 31.4^\circ$ (PDF#01-070-2314, JCPDS, 1995).

Figure 4.19b depicts the XRD diffraction pattern for the B7S12 specimen. Two new diffraction peaks were observed for this specimen: one at $2\theta = 23.7^\circ$ corresponding to sodium aluminum silicate (NAS), a type of zeolite (PDF#00-037-0411 JCPDS, 1995), and a second very small peak at $2\theta = 30.1^\circ$ likely corresponding to calcium aluminum silicate hydrate (NCASH) (PDF#00-047-0003, JCPDS, 1995).

No new peaks of significance were observed in the XRD pattern for the B14S12 samples. That indicates that after alkaline activation, neither crystalline cementation products nor zeolite type of reaction materials were formed under this research condition, for the small sample location that was assessed. Further investigation of this phenomenon will be performed using FESEM/EDAX test techniques since the XRD test is incapable of detecting gel formations of various cementing materials in the diffraction pattern.

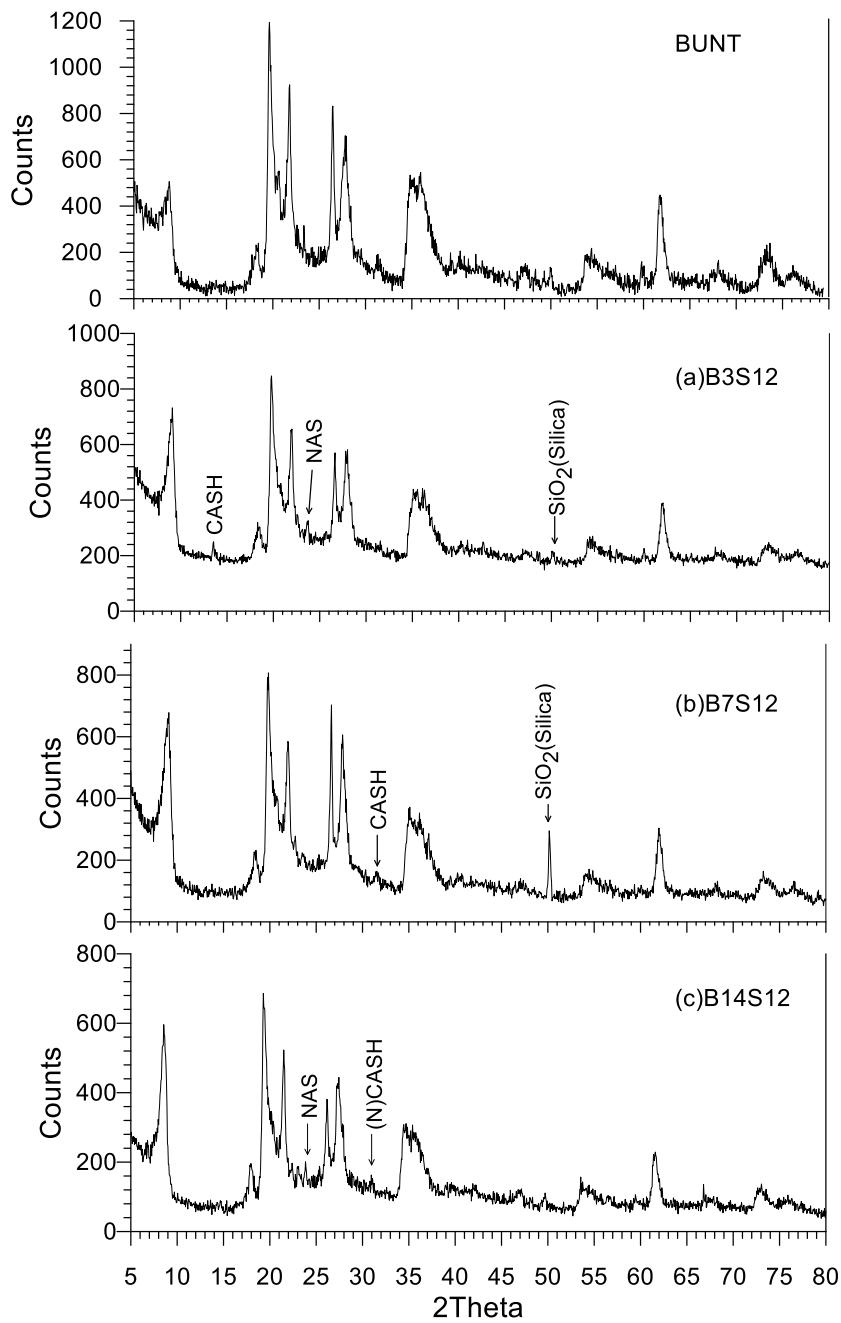


Figure 4.19 X-ray diffraction patterns for bentonite stabilized with sodium silicate (BS) at the same additive content and different curing times.

4.4.2.2 Kaolinite and Sodium Silicate solution

Figures 4.20a, b, and c depict the XRD patterns of the stabilized kaolinite by 6% additive after 3, 7 and 56 days of curing at room temperature, respectively. A change in the general reflection pattern of the treated kaolinite can be observed over the various curing time intervals. New clear diffraction peaks were observed at $2\theta = 42.2^\circ$, and 42.4° , corresponding to sodium aluminate silicate hydrate (NASH) reaction products containing magnesium and iron in the diffraction patterns for the samples that were cured for 3 and 56 days, respectively. Similarly, weak new diffraction peaks were detected at $2\theta = 16.3^\circ$ and 16.5° for both specimens that were cured for 3 and 56 days. According to the JCPDS (1995) database, these reflection peaks indicate the presence of sodium aluminate silicate hydrates (PDF#00-028-0779, JCPDS, 1995).

There is a very small diffraction peak appearing in the sample that was treated for 7-days at $2\theta = 28.1^\circ$, corresponding to a sodium aluminate silicate hydrate (NASH) zeolite-type of cementation product (PDF#00-037-0252, JCPDS, 1995). Other new peaks are notably not apparent in this specimen. Overall, the detection of newly formed cementation products is difficult in this binder system (i.e., treated by liquid sodium silicate additives) since the cementing product may not be able to form a crystalline phase during the stabilization process. Instead, it is expected that cementing compounds will be fabricated having amorphous (non-crystalline) characteristics. (e.g., Katz et al., 2001; Brough and Atkinson, 2002; Tingle et al., 2007; Fernandez et al., 2011).

Note that one of the highest compressive strengths measured for sodium silicate stabilization of kaolinite was achieved after 7 days of curing. However, the XRD test

shows little formation of new crystalline structures of significance in the diffraction pattern. This indicates that majority of the cementing compounds that are formed are likely amorphous in nature, and other characterization techniques, e.g., FESEM/EDAX and FTIR will be necessary for identifying the presence of these fabricated gel compounds in the binder matrix.

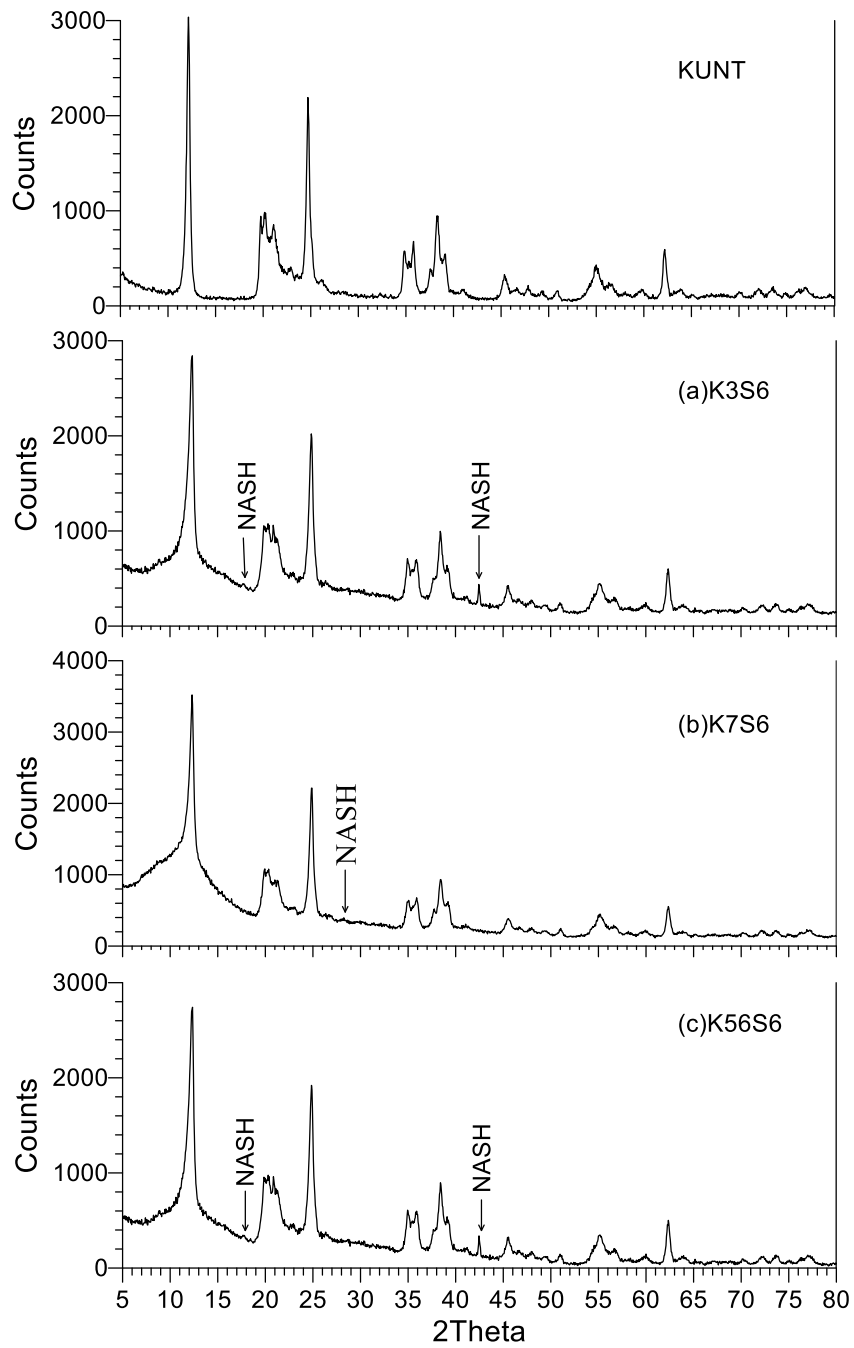


Figure 4.20 X-ray diffraction patterns for kaolinite stabilized with sodium silicate (KS) at the same additive content and different curing times.

4.4.3 Effect of the Admixture of Recycled Gypsum and Liquid Sodium Silicate on Soils

X-ray diffraction was utilized to characterize the crystalline reaction products that are formed once the pure bentonite and kaolinite clays were mixed with the combined recycled gypsum and sodium silicate stabilizer. The effect of different curing intervals are explored, and the results are presented in the following sections.

4.4.3.1 Bentonite and the Mixture of Recycled Gypsum and Sodium Silicate Solution

Figures 4.21a, b, and c depict the XRD patterns of the bentonite stabilized with a 6% mixture (50:50) of recycled gypsum and sodium silicate after 3, 7 and 56 days of curing at room temperature, respectively. A noticeable change in the diffraction pattern of the bentonite stabilized by 6% additive was observed. In all of the stabilized specimens, a number of the diffraction peaks are decreased slightly. This observed behavior is attributed to the effect of the additives and their inducement of a weathering process on the aluminate-silicate minerals such as montmorillonite in the clay matrix. A sharp peak at 50.1° implies some unreacted silica remains available in the clay matrix as the curing process progresses, similar to what was observed by El-Alfi and Gado (2016). It is also observed that the peak centered at 47° in the diffraction pattern of untreated and treated specimens has weakened with increases in curing time. This indicates that the illite minerals shown in Figure 4.16b have taken part in the chemical reactions that occur as curing progresses.

XRD results for stabilized bentonite after 3 curing days are presented in Figure 4.21a. The new reflection peak located at $2\theta = 14.2^\circ$ is a calcium silicate hydrate product (CSH) (PDF#00-003-0606, JCPDS, 1995). Two additional reaction products are indicated by reflections at $2\theta = 29.5^\circ$ and $2\theta = 31.2^\circ$, corresponding to calcium silicate hydrate (CSH) phases (PDF#00-003-0548; 00-009-0210, respectively, JCPDS, 1995). Additionally, a weak reflection peak is observed at $2\theta = 42.1^\circ$ referring to nepheline hydrate, a sodium aluminum silicate hydrate (NASH) (PDF#00-010-0459, JCPDS 1995).

Figure 4.21b depicts the diffraction patterns of treated bentonite after 14 days of curing. By comparing the 14-day cured specimen with the 3-day cured one, new reflection peaks with lower intensities can be observed at some locations. This could be due to slow chemical reaction processes occurring between stabilizers and clay particles, as the initial pH of the specimen cured for 14 days has a lower value than the specimen cured for 3 days. These observed peaks are identified as calcium aluminum silicate (CAS), and calcium aluminum silicate hydrate (CASH), like the cementation products that are presented in the previous section above. Additionally, sodium calcium aluminum silicate hydrate (NCASH, PDF#00-013-0129, JCPDS, 1995) gives a high peak located at $2\theta = 23.1^\circ$. Interestingly, this peak is undetectable in the diffraction patterns of other specimens. This may be due to low crystallinity and decomposition of aluminum silicate hydrate compounds as curing progresses.

The XRD pattern of treated bentonite after 56 days shown in Figure 4.21c exhibits new diffraction reflection peaks. Calcium silicate hydrate (CSH) (PDF#00-003-0606, JCPDS,1995) exhibits a strong diffraction peak at $2\theta = 14.3^\circ$, the same as what was observed for the other specimens. Sodium-calcium silicate hydrate (NCASH) is detected at $2\theta = 29.6^\circ$ (PDF#00-003-0269, JCPDS, 1995), and $2\theta = 29.1^\circ$ (PDF#00-013-0129, JCPDS, (1995)). The reflection peaks at $2\theta = 31.6^\circ$ and 31.9° indicate the formation of calcium silicate hydrates (CSH) (PDF#00-009-0210, JCPDS, 1995), and sodium aluminum silicate hydrate (NASH) (PDF#00-018-1198, JCPDS, 1995). The observed diffraction peak at $2\theta = 42.7^\circ$ corresponds to calcium aluminum silicate hydrate with carbonite (PDF#00-002-0061, JCPDS, 1995).

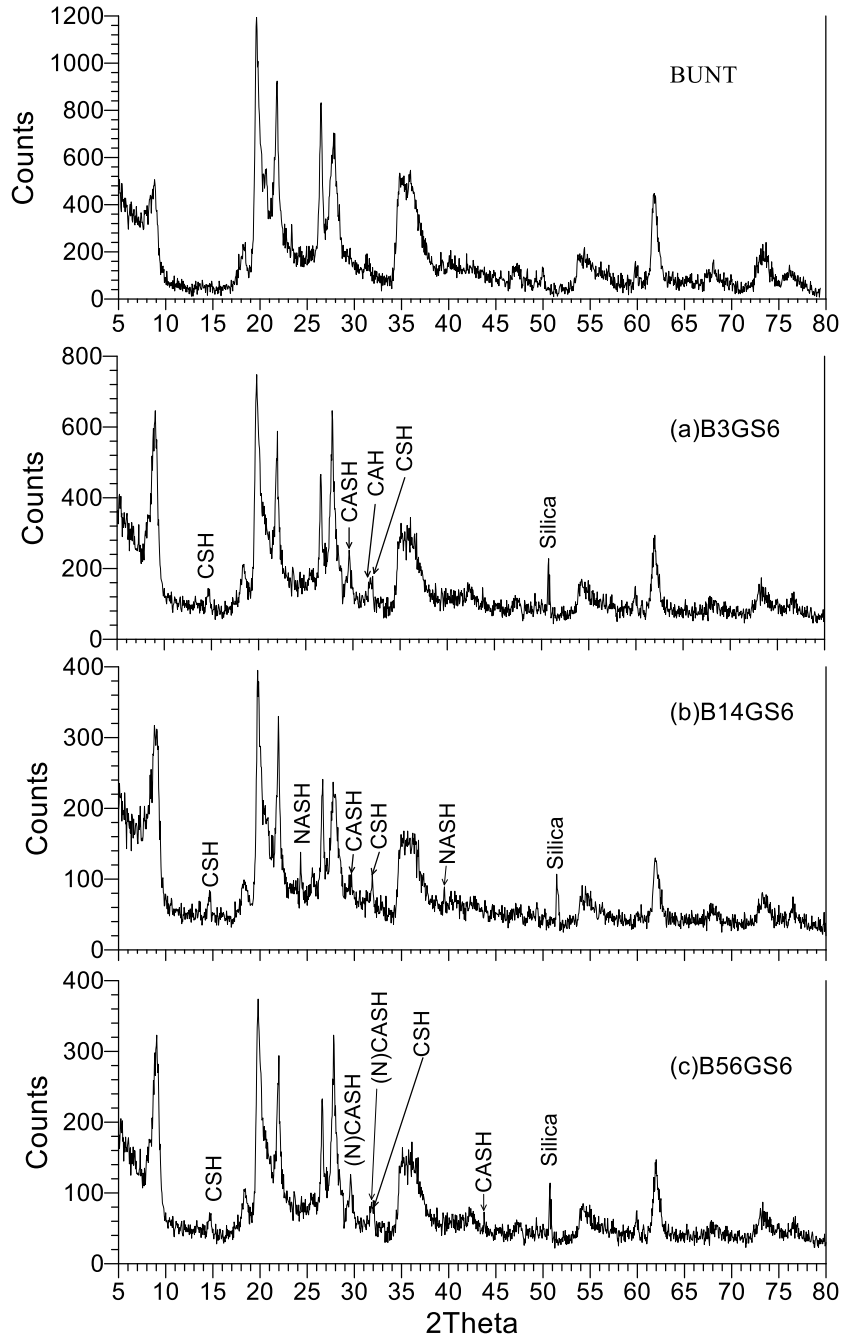


Figure 4.21 X-ray diffraction patterns for bentonite stabilized with recycled gypsum and sodium silicate (BGS) at the same additive content and different curing times.

4.4.3.2 Kaolinite and the Mixture of recycled Gypsum and Sodium Silicate Solution

Figures 4.22a, b, and c depict the XRD patterns of the stabilized kaolinite by a 6% mixture (50:50) of recycled gypsum and sodium silicate after 7, 28, and 56 days of curing at room temperature, respectively. As shown, the diffraction peaks of kaolinite are clearly evident (similar to the untreated specimen), but there are also some new smaller diffraction peaks that appear over the various curing times. This could be related to slow reactivity of kaolinite minerals having solid plate structures requiring more time to react with the stabilizers even though the level of alkalinity (pH ~ 10 for all curing intervals) is appropriate for alkaline activation of the soil (Komnitsas and Zaharaki, 2007). Due to the poor crystallinity of the fabricated cementitious compounds, only weak peaks emerge in the XRD reflection patterns with curing time; new amorphous compounds of NAS, NCASH, etc. may not be detected by the XRD test.

X-ray diffraction analysis results for a stabilized kaolinite specimen cured for 7 days is shown in Figure 4.22. As shown, a new diffraction peak at $2\theta = 8.2^\circ$ is identified, corresponding to calcium aluminum hydrate that includes sodium and magnesium ions (NCAH; PDF#00-05-1714, JCPDS, 1995). After that peak, two weak peaks appear at $2\theta = 14.3^\circ$ and 18.1° , indicating the formation of sodium aluminum silicate hydrates (NAS) (PDF#00-037-0411, JCPDS, 1995). There is also a new sharp peak observed at 20.2° , implying untreated silicon dioxide in the binder system (PDF#01-082-1554, JCPDS, 1995). Lastly, sodium calcium aluminum silicate hydrates (NCASH) are detected as weak peaks in the diffraction pattern at $2\theta = 29.7^\circ$, 31.1° and 31.7° , which

corresponds to one of the zeolite minerals “Stilbite-Ca” (PDF#00-024-0884, JCPDS, 1995).

XRD analyses of the kaolinite-stabilizer mixture cured for 28 days are presented in Figure 4.22b. As shown, calcium aluminum silicate was hydrated in comparison to early curing ages, and transformed into calcium aluminum silicate hydrate (CASH) centered at $2\theta = 8.8^\circ$ (PDF#00-002-0047, JCPDS, 1995). This could be related to the negative charges on the clay surface attracting pore water in the binder system, a phenomenon noted by Holtz and Kovacs (1981). Sodium aluminum silicate hydrates (NASH) were detected at $2\theta = 17.3^\circ$ and 31.8° (PDF#01-076-0862, JCPDS, 1995). The weak peak centered the angle of 29.7° is attributed to sodium aluminum silicate hydrate (NASH), a type of zeolite mineral (PDF#00-034-0524, JCPDS, 1995). A sharp diffraction peak at $2\theta = 20.2^\circ$ shows the presence of unreacted silicon dioxides in the binder system (PDF#01-082-1554, JCPDS, 1995).

XRD analyses of the kaolinite-stabilizer mixture cured for 56 days are presented in Figure 4.22c. The reflection intensities of kaolinite at various 2θ positions are slightly diminished relative to the untreated kaolinite results, which indicates chemical weathering of the kaolinite minerals. This weathering is associated with subsequent cementation reactions that occur between the weathered base materials compounds in solution and the binder, which leads to increased UCS strengths. New reflection peaks are observed in a similar fashion to previous specimen results. A weak reflection peak at $2\theta = 14.7^\circ$ corresponds to the formation of sodium aluminum silicate (NAS) compounds (PDF#00-035-0424, JCPDS, 1995). The reflection peak at 20.2° (unreacted

silicon dioxides) is no longer clearly apparent in the diffraction pattern, indicating that this compound may have been consumed during the long-term curing process. The observed peaks at $2\theta = 29.3^\circ$ and 31.9° correspond to sodium calcium aluminum silicate hydrate with iron and magnesium ions (NCASH, PDF#01-076-0862, JCPDS, 1995) a type of zeolite mineral. It can be observed that the reflection peak of sodium aluminum silica, which occurs approximately at $2\theta = 18^\circ$ is undetectable in the diffraction pattern, indicating that this crystalline compound may not be present in the specimen. The reflection of unreacted silica is also not detected at the 56 curing days point. In general, the new diffraction peaks that are observed tend to manifest themselves fairly weakened for the various curing time intervals, which could be due to the low crystallinity of cementation compounds or could be associated with the reaction speed between the admixture of stabilizers and kaolinite minerals. Detailed research regarding the development of new amorphous cement compounds will be investigated via FESEM/EDAX analysis.

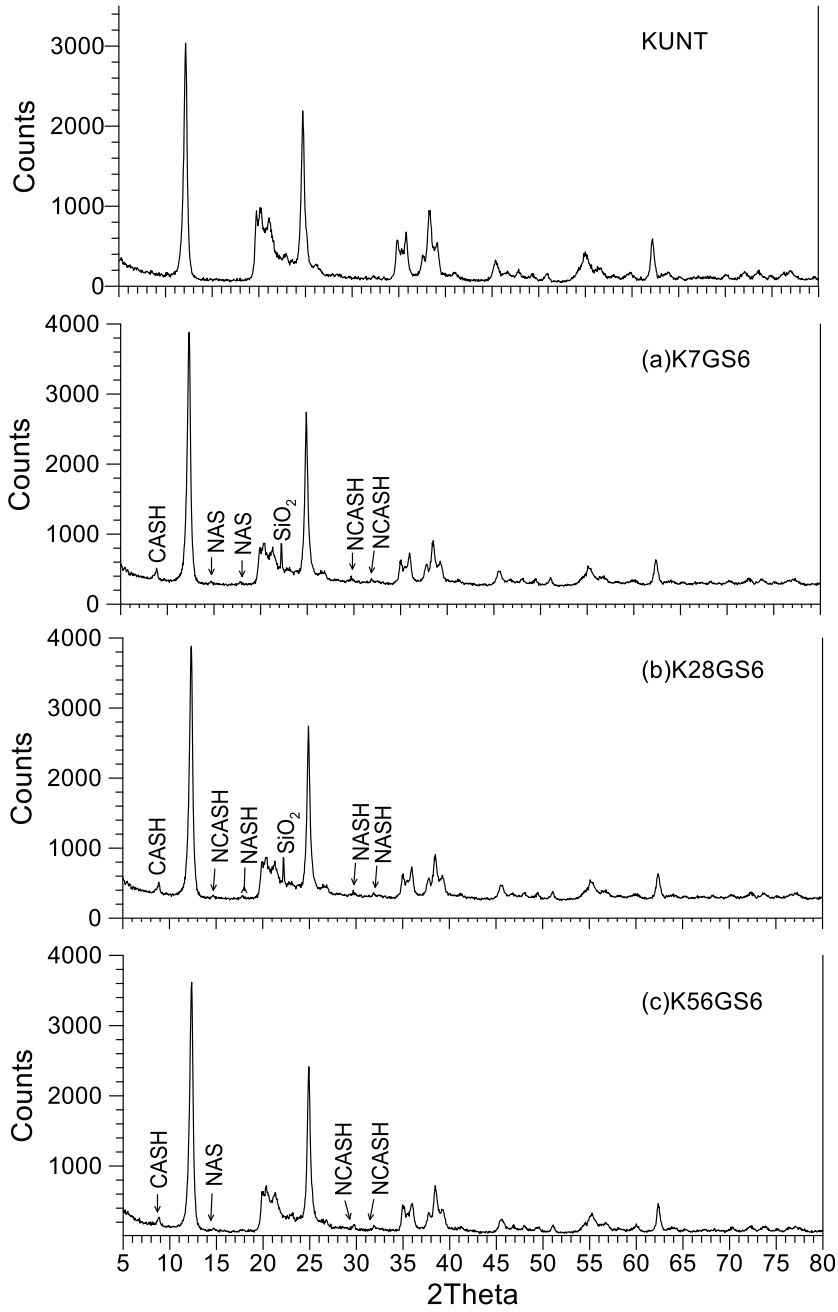


Figure 4.22 X-ray diffraction patterns for kaolinite stabilized with recycled gypsum and sodium silicate (KGS) at the same additive content and different curing times.

4.5 FESEM/EDAX Analysis of Stabilized Soils

Field emission scanning electron micrographs were carried out on soils blended with recycled gypsum only, sodium silicate only, and on a 50:50 mixture of recycled gypsum and sodium silicate, at different curing times. The selected specimens used in this technique are the same as those that were subjected to the X-ray diffraction analysis.

Figure 4.23a shows an FESEM image of the untreated bentonite clay including its EDAX spectrometry. The clay minerals have a smooth surface structure as well as non-crystalline shape around the surface. The chemical composition of untreated bentonite was shown to be made up of aluminum, silicon, sodium, and potassium.

Figure 4.23b shows an FESEM image of the untreated kaolinite clay including its EDAX spectrometry. Kaolinite minerals typically reveal “book-sheet” structures, and there is almost no void between the two layers. The chemical composition of untreated kaolinite minerals is also presented in the following figure. It primarily consists of silicon, aluminum, sodium, magnesium, and iron.

Note that the locations for both sets of EDAX spectrometry are randomly selected. The initial elemental composition of both soils is presented in Table 1. Other elements (such as titanium, calcium, iron, etc.) might be present at other imaging sites for both clays.

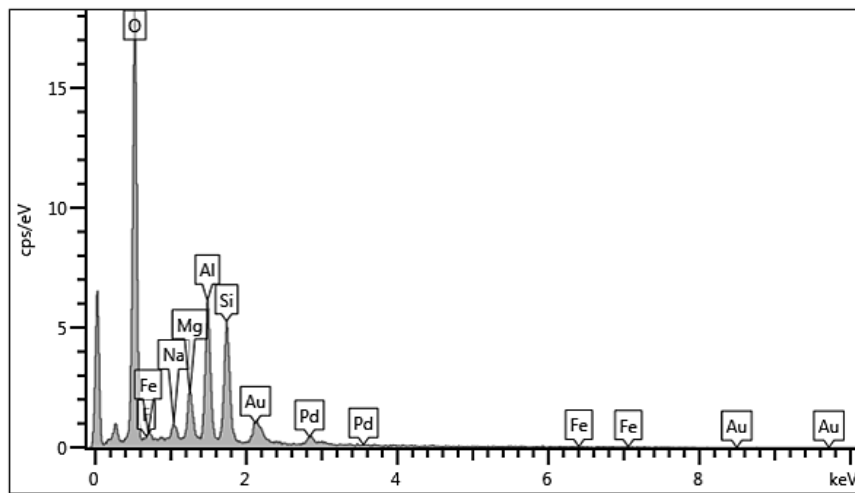
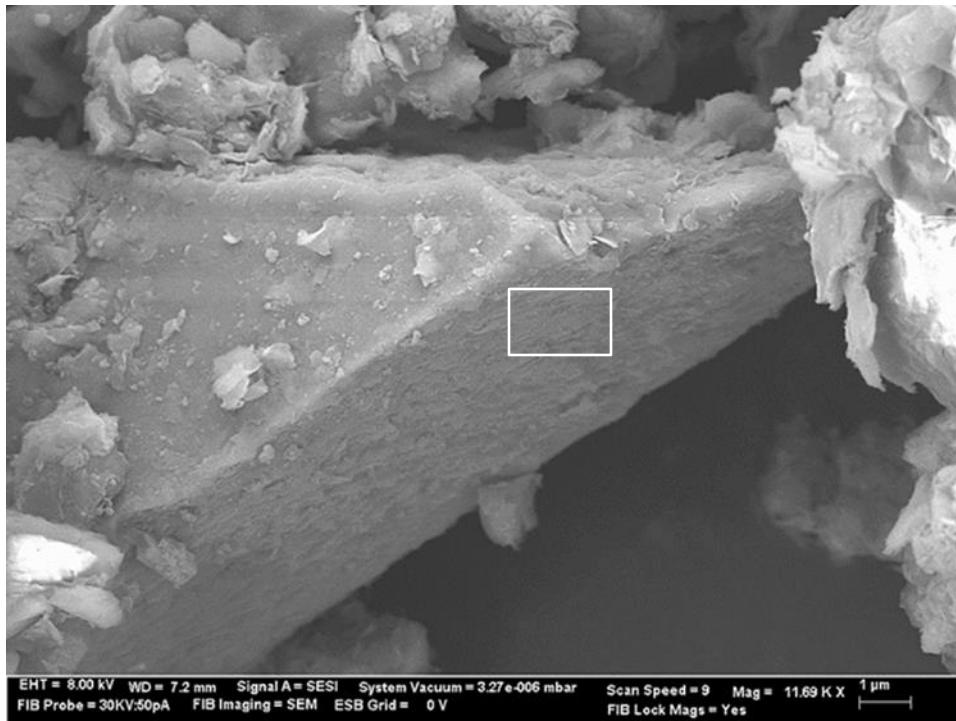


Figure 4.23a FESEM micrograph images and EDAX results of untreated bentonite. (ETH=8.00kV; WD= 7.2 mm, Mag=11.00KX). (Element legend: Na: Sodium, Si: Silicate, Al; Aluminum, Fe: Iron, Mg: Magnesium, Au: Gold, Pd: Palladium).

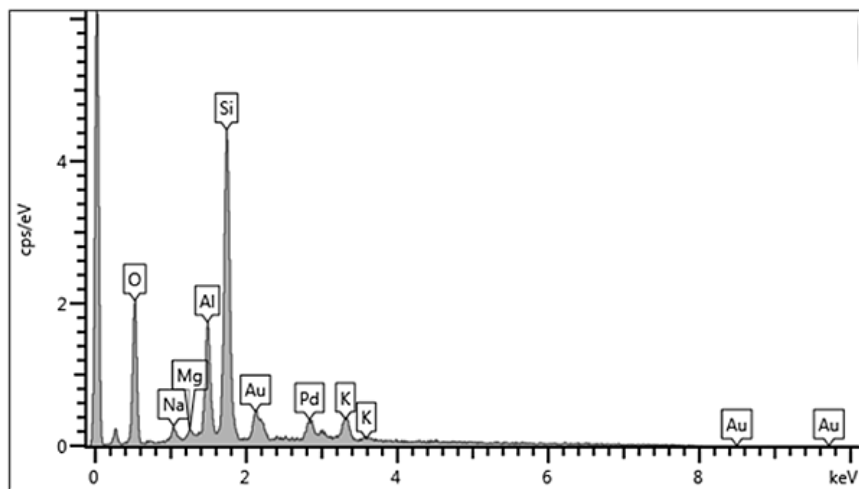
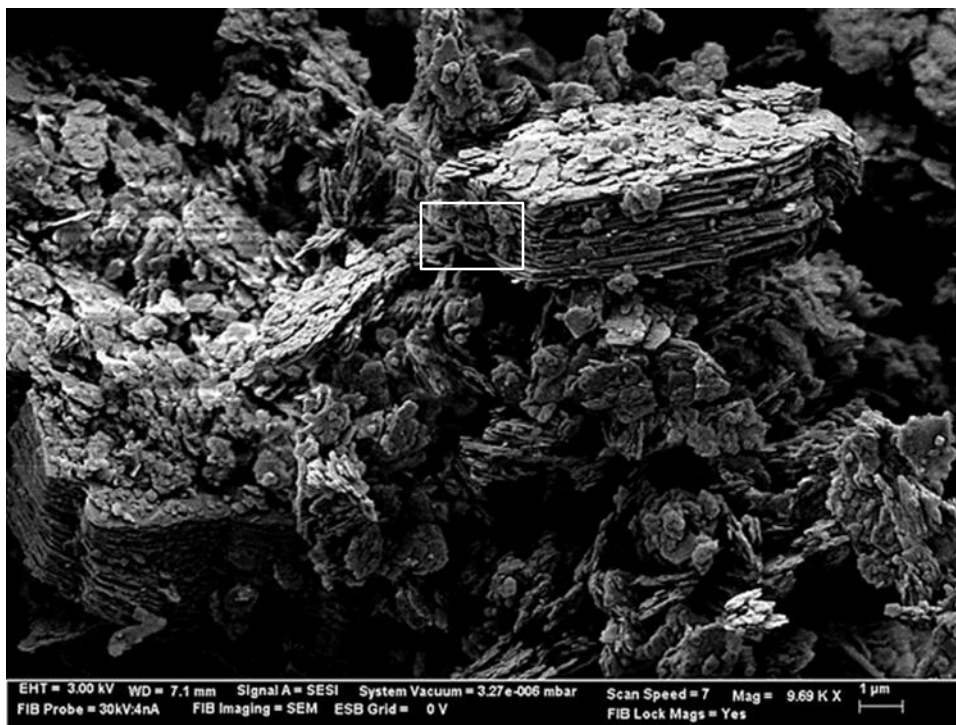


Figure 4.23b FESEM micrograph images and EDAX results of untreated kaolinite. (ETH=3.00kV; WD= 7.1 mm, Mag=9.69KX). (Element legend: Na: Sodium, Ca: Calcium, Si: Silicate, K: Potassium, Al: Aluminum, O: Oxygen, Mg: Magnesium, Au: Gold, Pd: Palladium).

4.5.1 Effect of Recycled Gypsum on Soils

4.5.1.1 Bentonite and Recycled Gypsum

Figures 4.24 to 4.29 depict the FESEM results for 3% additive treated bentonite after 3, 14 and 28 days of curing. As shown, the soil structure was modified from a porous structure to a flocculated structure due to chemical stabilization during the curing time. Modifications, dissolutions and cloud formations in the soil matrix with curing period are demonstrated by the FESEM images. The microstructure of the soil-recycled gypsum mixture shows that formation of new compounds in the matrix not only fill the voids but stick upon the clay particles as a cloudy formation.

Figures 4.24 to 4.29 reveal that more cement compounds in the form of white clumps are detected with longer over shorter curing intervals. Furthermore, some clay particles were covered in high content silica gel that has a wavy shape. Thus, the clay particles are bound firmly together by the new crystalline and noncrystalline products which are confirmed by the presence of cloudy formation, flaky particles in the soil-recycled gypsum matrix. In addition, the structure of the new matrix and network patterns due to stabilization of soil dissolution/modification can cause micro cracks with the increase of curing time, which may be the reason for sometimes measuring lower strengths in the UCS tests (Sukmak et al. 2013).

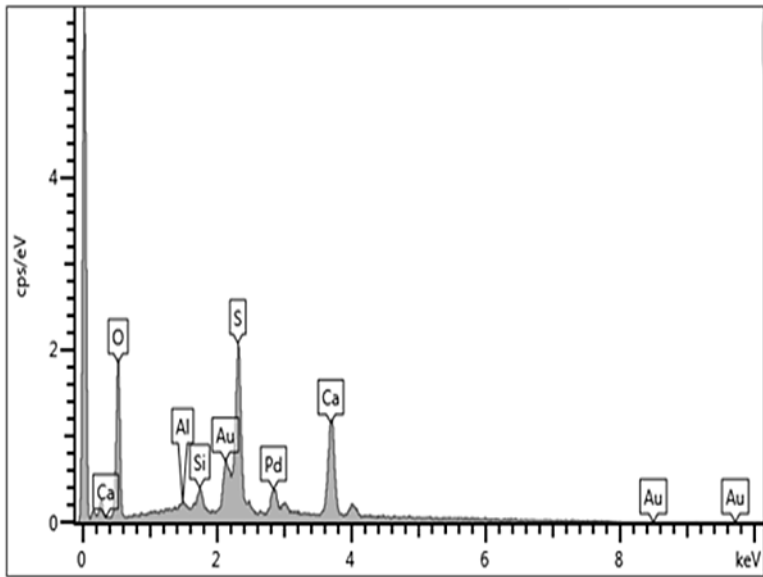
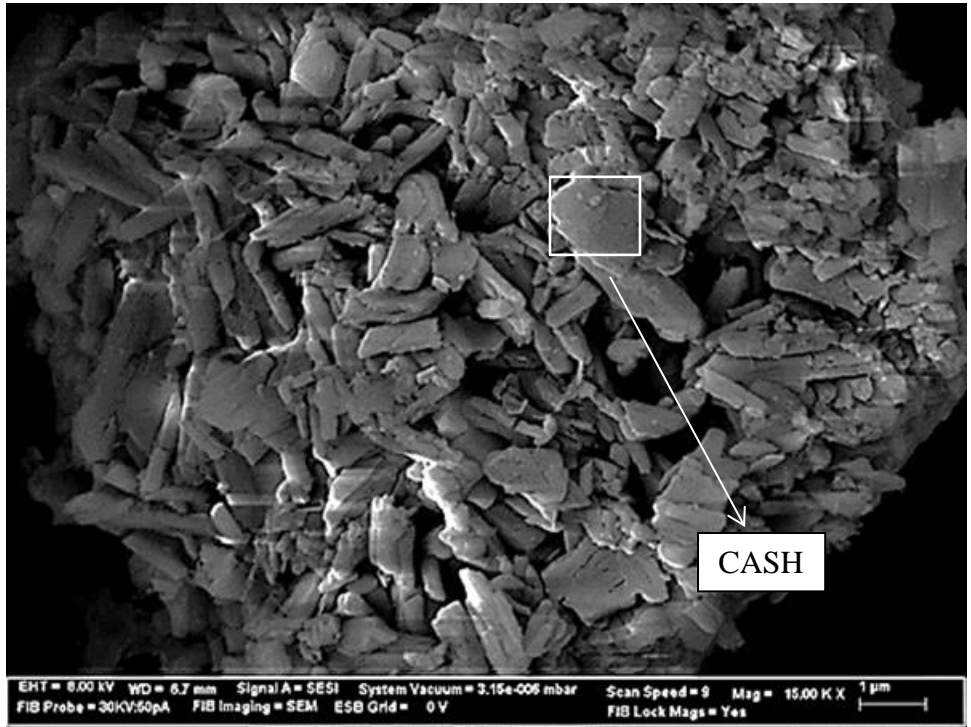


Figure 4.24 FESEM-EDAX image, B3G3. (ETH=8.00kV; WD= 6.7 mm, Mag=15.00 KX). (Element/compound legend, CASH = Calcium Sodium Aluminum Silicate Hydrate, Si:Silicate, Al:Aluminum, Ca: Calcium, S: Sulfate).

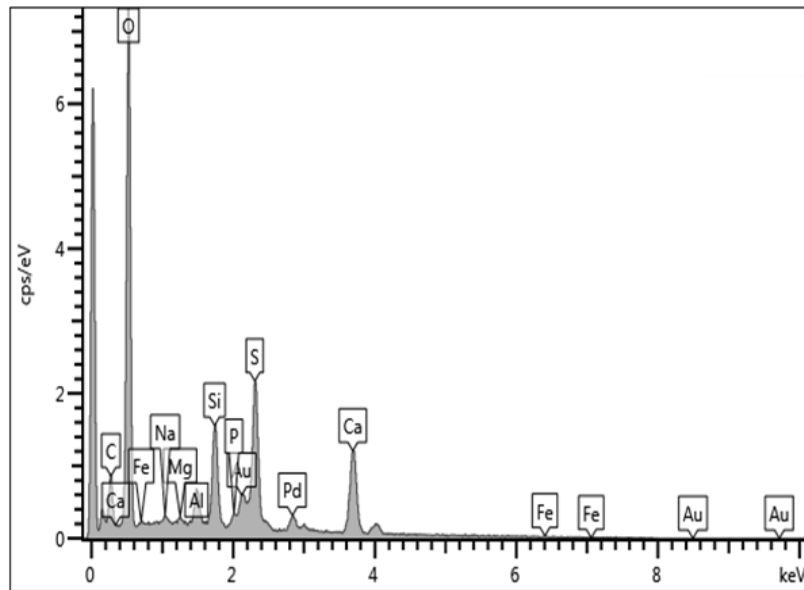
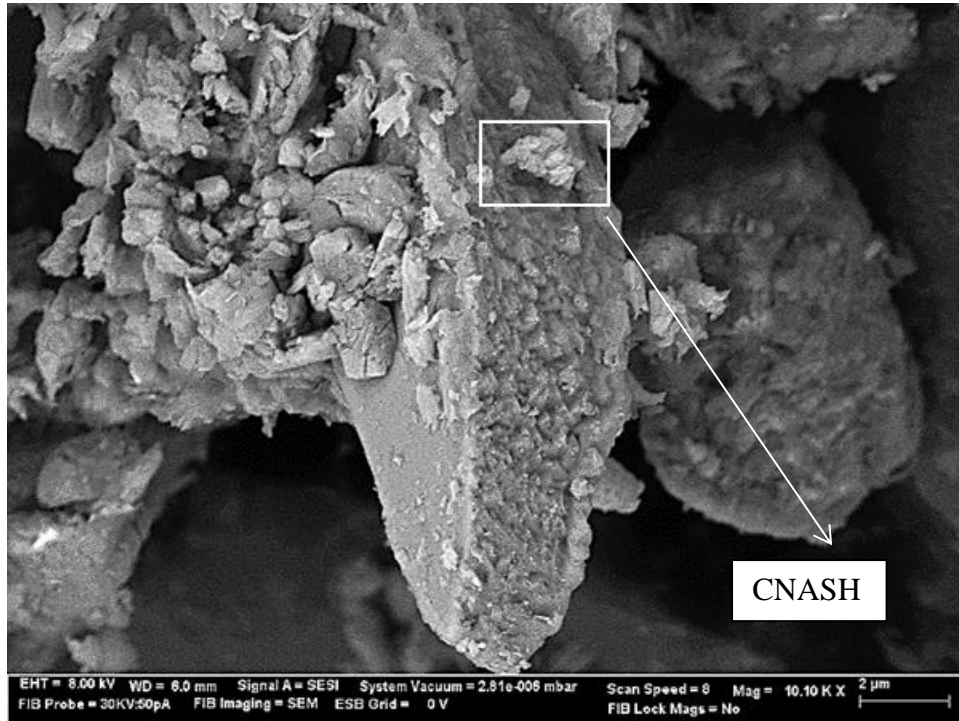


Figure 4.25 FESEM-EDAX image, B3G3. (ETH=8.00kV; WD= 6.0 mm, Mag=10.10 KX). (Element/compound legend: CNASH = Calcium Sodium Aluminum Silicate Hydrate, Si: Silicon, Al: Aluminum, Ca: Calcium, Na: Sodium, Fe: Iron, Mg: Magnesium, S: Sulfate).

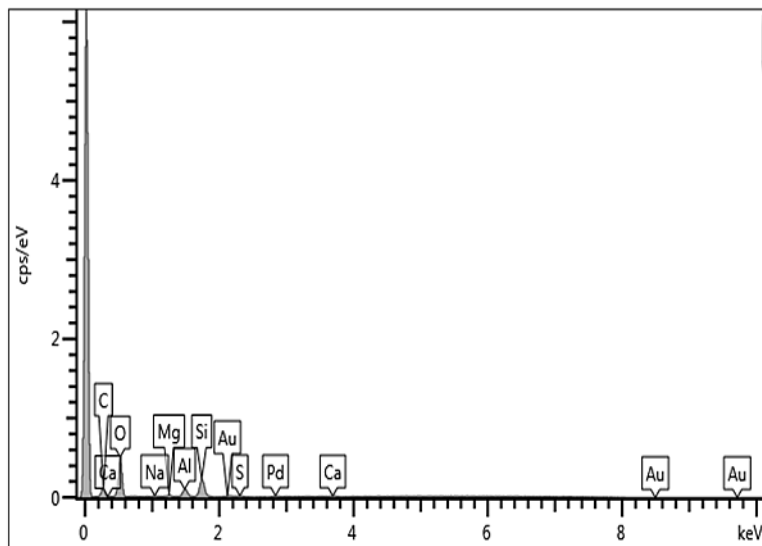


Figure 4.26 FESEM-EDAX image, B14G3. (ETH=8.00kV; WD= 6.8 mm, Mag=10.00 KX). (Element/compound legend: NASH = Sodium Aluminum Silicate Hydrate, Si:Silicon, Al:Aluminum, Ca: Calcium, Na: Sodium, Mg:Magnesium, S: Sulfate, Pd: Palladium, Au: Gold).

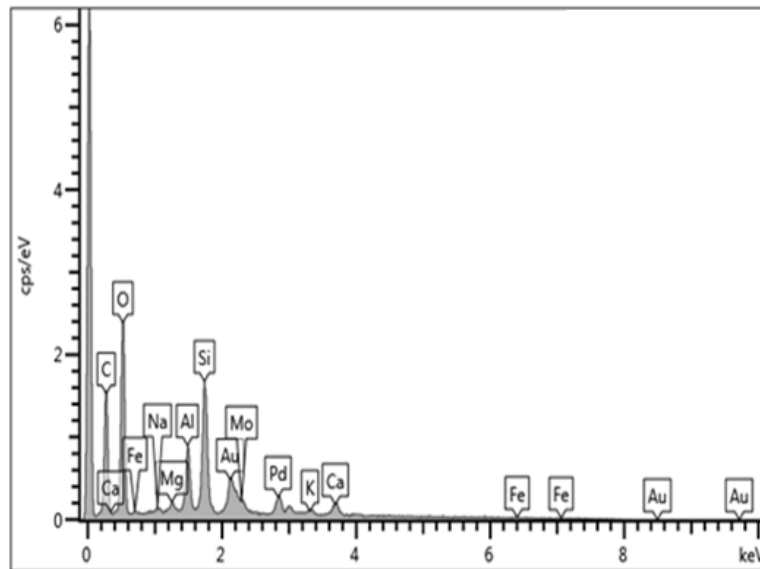
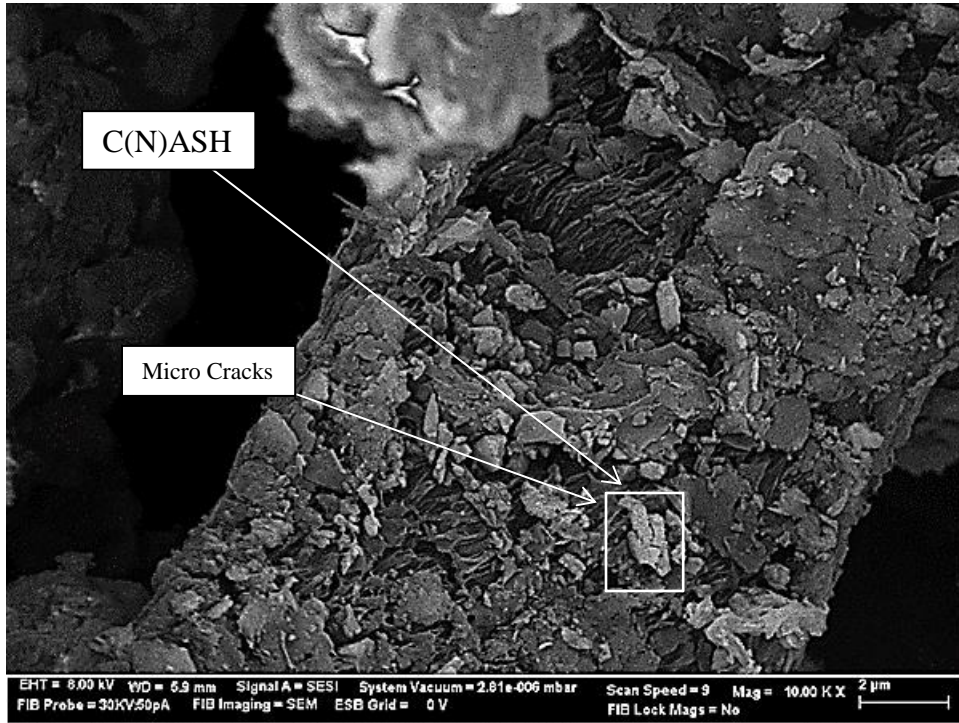


Figure 4.27 FESEM-EDAX image, B14G3. (ETH=8.00kV; WD= 6.8 mm, Mag=10.00 KX). (Element/compound legend: CASH= Calcium Aluminum Silicate Hydrates; Si: Silicon; Al: Aluminum; Ca: Calcium; Na: Sodium; Mg: Magnesium; K: Potassium; Fe: Iron; S: Sulfate; Pd: Palladium; Au: Gold).

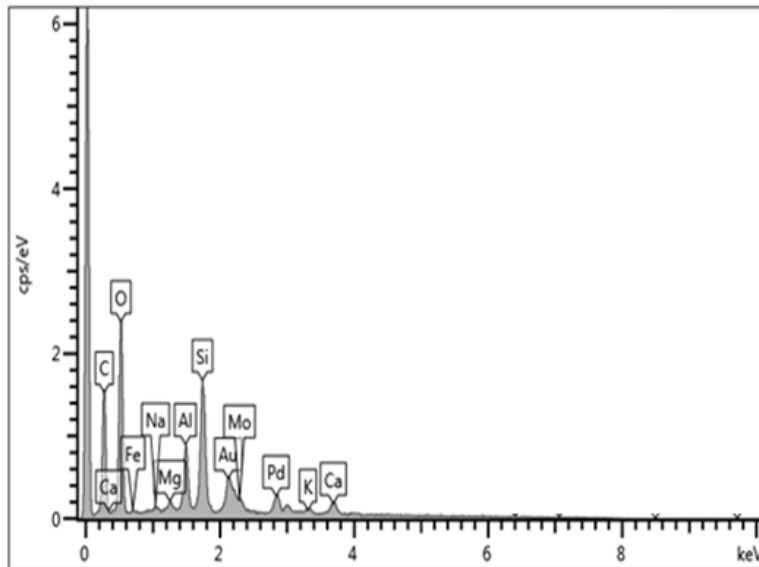
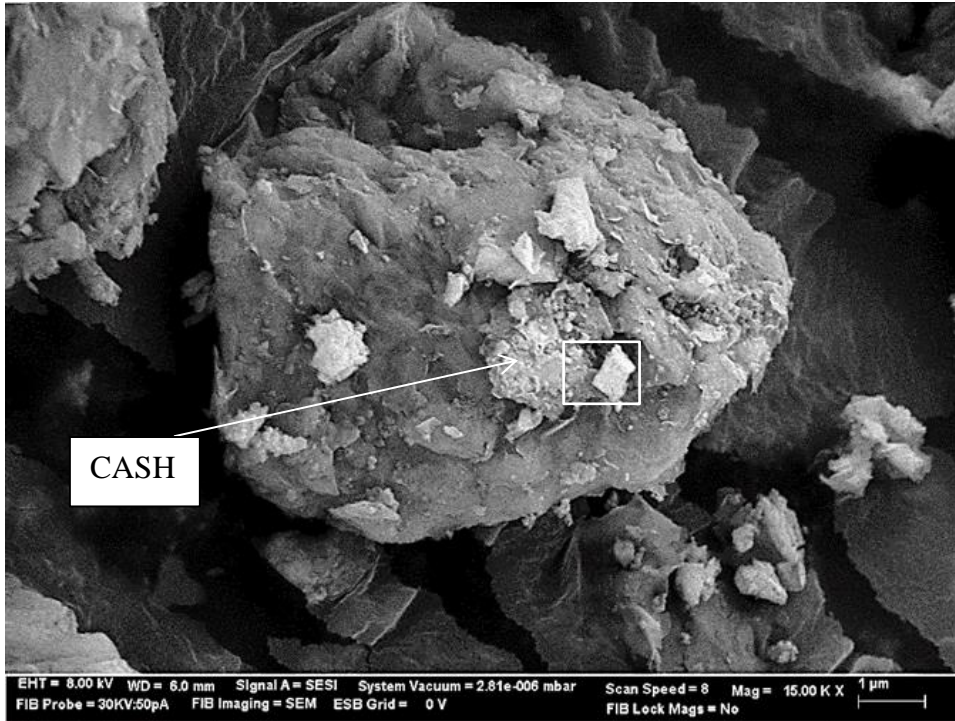


Figure 4.28 FESEM-EDAX image, B28G3. (ETH=8.00kV; WD= 6.0 mm, Mag=15.00 KX). (Element/compound legend: CASH= Calcium Aluminum Silicate Hydrate, Si:Silicon, Al:Aluminum;Ca: Calcium; Na: Sodium; Fe: Iron; Mg:Magnesium; S: Sulfate; Pd: Palladium; Au: Gold).

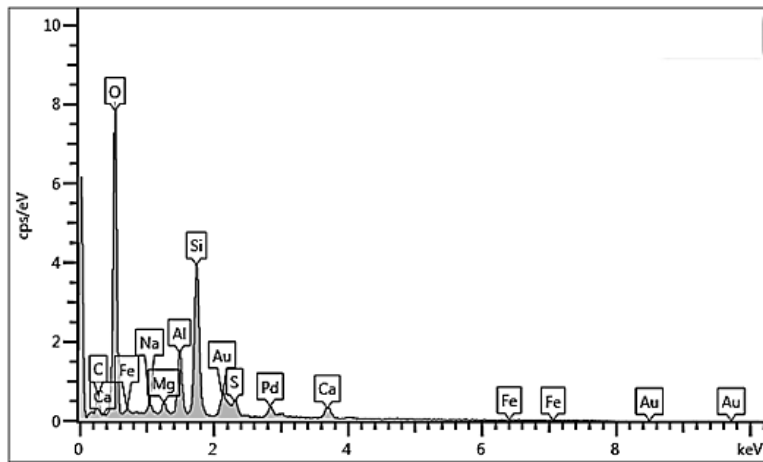
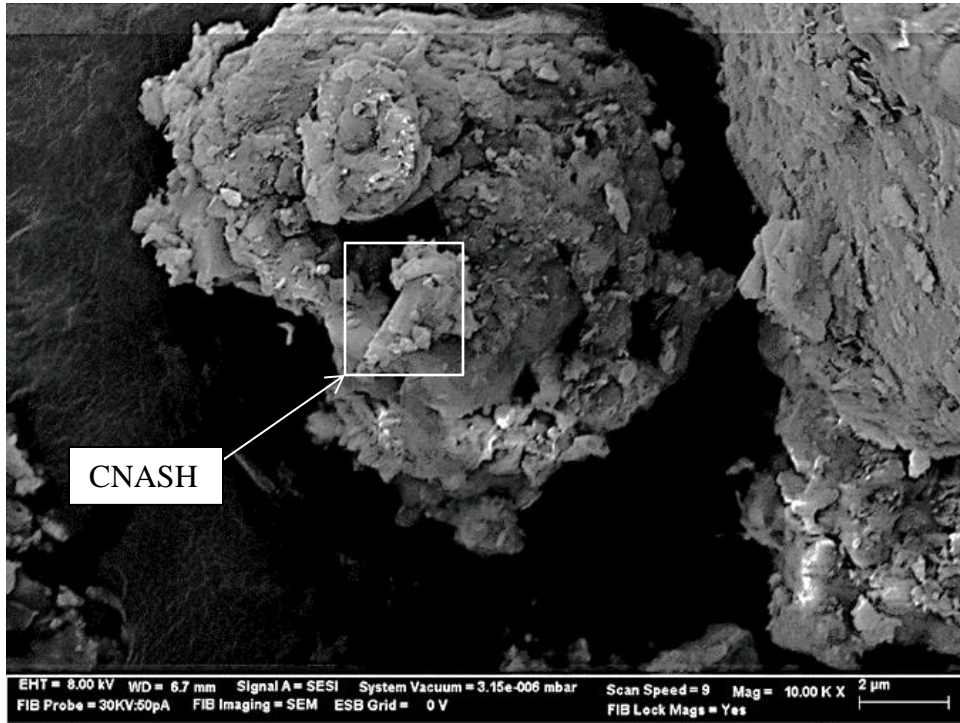


Figure 4.29 FESEM-EDAX image, B28G3. (ETH=8.00kV; WD= 6.7 mm, Mag=10.00 KX). (Element/compound legend: CNASH= Calcium (Sodium) Aluminum Silicate Hydrate; Si:Silicon; Al:Aluminum;Ca: Calcium; Na: Sodium; Fe: Iron; Mg: Magnesium; S: Sulfate; Pd: Palladium; Au: Gold).

The EDAX results in Figures 4.27 and 4.29 show that the cementation materials containing sulfate ions (SO_4) are formations of calcium silicate hydrate (CSH), calcium aluminate silicate hydrate (C(N)ASH), and calcium aluminate hydrate (CAH), (e.g., Peethamparan et al. 2008). These new products can also contain a low content of sodium, magnesium and iron ions that are evidence of dissolution of the source material that occurs in the presence of the selected additive, resulting in sodium-based aluminum silicate hydrate (NASH) compounds. Calcium ions from recycled gypsum are increased during the long-term curing periods since the presence of newly formed calcium compounds is evident on the EDAX spectrums presented in Figures 4.27 and 4.29.

Also, the clay particles were coated with sulfate particles released by recycled gypsum as a consequence of their transformation in the binder system. Figures 4.26, and 4.27-4.29 show new crystalline phases that were formed after soil stabilization. The formation of new compounds may be attributed to the formation of zeolites having three types of structure: chainlike, sheetlike, and framelike (Jha and Sivapullaiah, 2014). Zeolites are generally formed in a more alkaline environment, while this soil combined with recycled gypsum creates a more acidic environment; however, according to Ming and Boettlinger (2001), it is possible to manufacture some zeolite minerals such as analcime and mordenite in acidic soils, which tend to manifest as only small peaks in XRD testing. Any observed decreases in strength can be attributed to the formation of zeolitic minerals that are expansive in nature. The findings in this research are in agreement with those of Sivapullaiah and Manju (2006) and Jha and Sivapullah (2016).

The increase of the silica and aluminum content in the soil transforms the montmorillonite structure with curing time, which is confirmed by a decrease of its intensity in the XRD test. The results of FESEM and EDAX testing are consistent with the XRD test results.

4.5.1.2 Kaolinite and Recycled Gypsum

Figures 4.30 to 4.35 show the FESEM results of 12% additive stabilized kaolinite after 14, 28, and 56 days of curing. Kaolinite minerals exhibit characteristic microstructure for this mineral, such as a “book-like” and “flaky” (Latifi et al., 2016). In the current study, the observation of changes in the representative specimen is challenging due to significant disturbance to the characteristic mineralogical shape of the kaolinite minerals (e.g., Ahmed and El-Neggar, 2016). This behavior is likely associated with a slow reaction process between the kaolinite minerals and recycled gypsum after the immediate strength gain reaction has occurred. The formation of new cementation materials is also potentially delayed because the clay mineral reaction surface is relatively limited due to the book-like nature of kaolinite minerals at the micro-scale (Tingle et al., 2007). It is also noticed that clay particles are coated with sulfate ions, which is evidence that recycled gypsum has been dissolved and taken part in the chemical reaction process. As shown in Figure 4.31, the clay particles have transformed from solid structures to aggregated features, but there is no visible evidence of geopolymer gel on the clay surface. The formation of white colors on the surface of treated clay could be evidence of new cementation materials, which indicates the

deformation of clay surface (e.g., Latifi et al., 2016). Based on the EDAX spectrometry results, changes in the surface of the clay particles are apparent, with smaller aggregated compounds being visible in the clay matrix; thus, calcium alumino-silicate hydrated (C(A)SH) is possibly formed in K14G12, as shown in Figure 4.28. The second micrograph of the same specimens in Figure 4.31 reveals that undissolved kaolinite minerals are observed on the clay surface, whereas the dissolution of kaolinite is increased the quantity of silicon ion. Also, there are no traces of other ions such as calcium, magnesium or sulfate even though the EDAX spectrometer detects some sodium ions.

Microanalyses of stabilized soil specimens K28G12 and K56G12 are presented in Figures 4.32-33, and Figures 4.34-4.35, respectively. Similar observations with the previous specimen are obtained in the FESEM and EDAX analyses for gypsum stabilized kaolinite. Unreacted kaolinite minerals are still visible in the clay matrix; however, the structure of kaolinite minerals is disturbed by the addition of recycled gypsum, which changes the book-sheet structures into a more random clay sheet orientation. Also, the EDAX analysis is utilized to assess the chemical composition of a randomly selected location on the clay particle's surface. The results reveal that the level of calcium increases with curing time, and that the clay particles are surrounded by sulfate ions that are released from the recycled gypsum. The results of the EDAX testing therefore indicate the formation of calcium-based alumino-silicate hydrates (CASH), which is in agreement with what was observed in the XRD patterns.

Similarly, in the second FESEM sample, Figures 4.32 and 4.35, modification or transformation of the clay structure is clearly observed, but neither calcium nor sulfate ions are detected on or around the surface of the clay particles. The EDAX analyses show that scanned region consists of sodium aluminum silicate containing magnesium ions (N(M)ASH). N(M)ASH was also detected in the X-ray diffraction testing; thus, this could be evidence that different kinds of cementation products are being formed during the stabilization process.

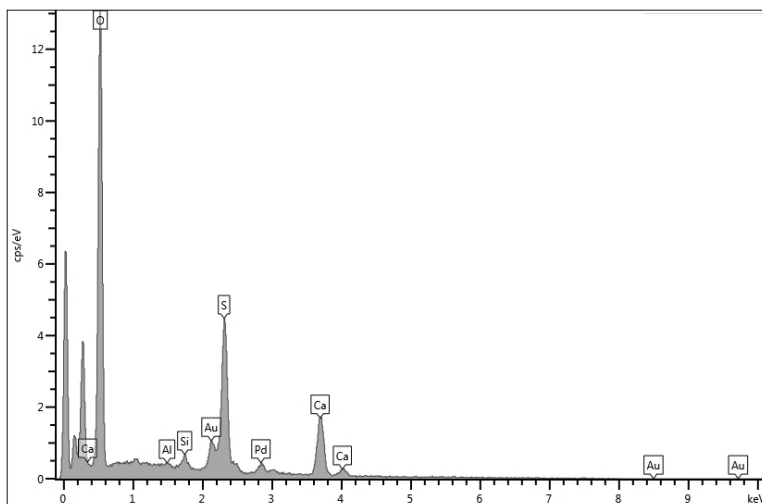
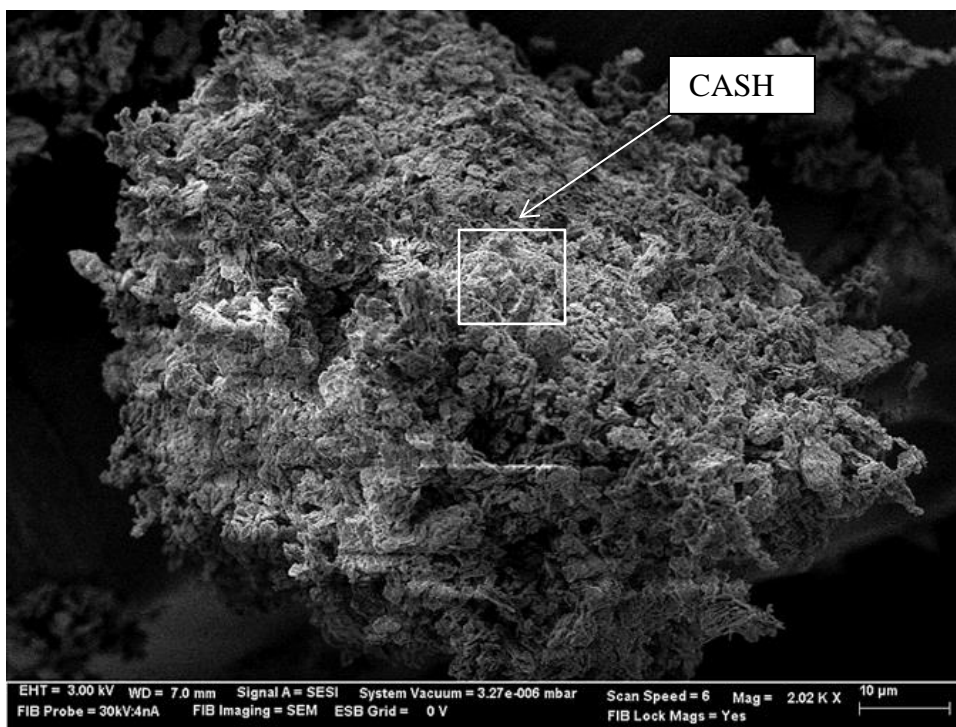


Figure 4.30 FESEM-EDAX image, K14G12. (ETH=8.00kV; WD= 7.0 mm, Mag=2.02 KX). (Element/compound legend: CASH = Calcium Aluminum Silicate Hydrate, Si:Silicon, Al: Aluminum, Ca: Calcium, S: Sulfate, Pd: Palladium, and Au: Gold).

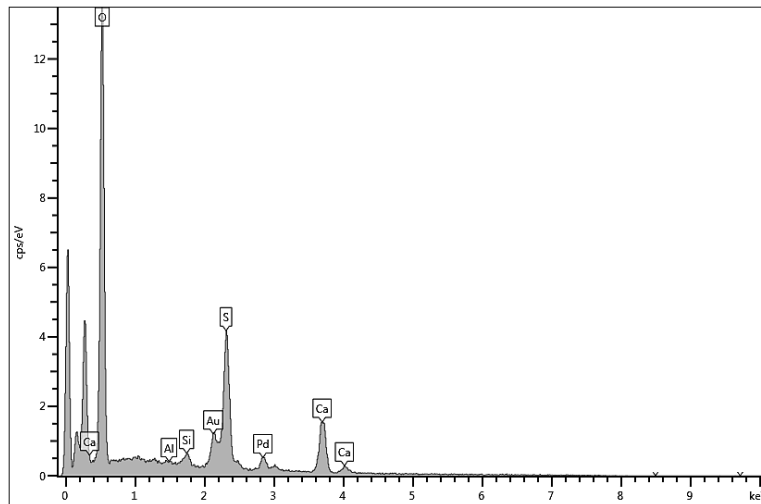
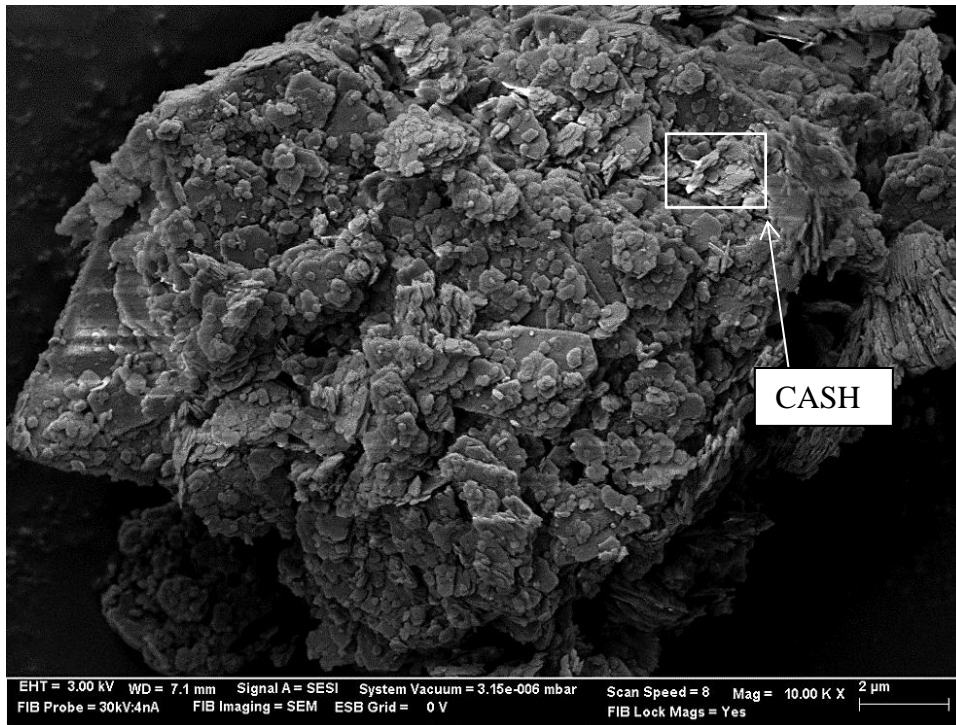


Figure 4.31 FESEM-EDAX image, K14G12. (ETH=8.00kV; WD= 6.7 mm, Mag=10.00 KX). (Element/compound legend: CASH = Calcium Aluminum Silicate Hydrate, Si:Silicon, Al: Aluminum, Ca: Calcium; S: Sulfate, Pd: Palladium, Au: Gold).

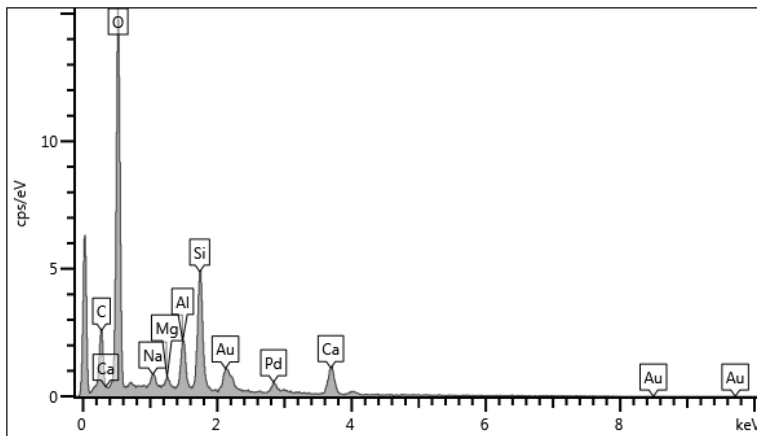
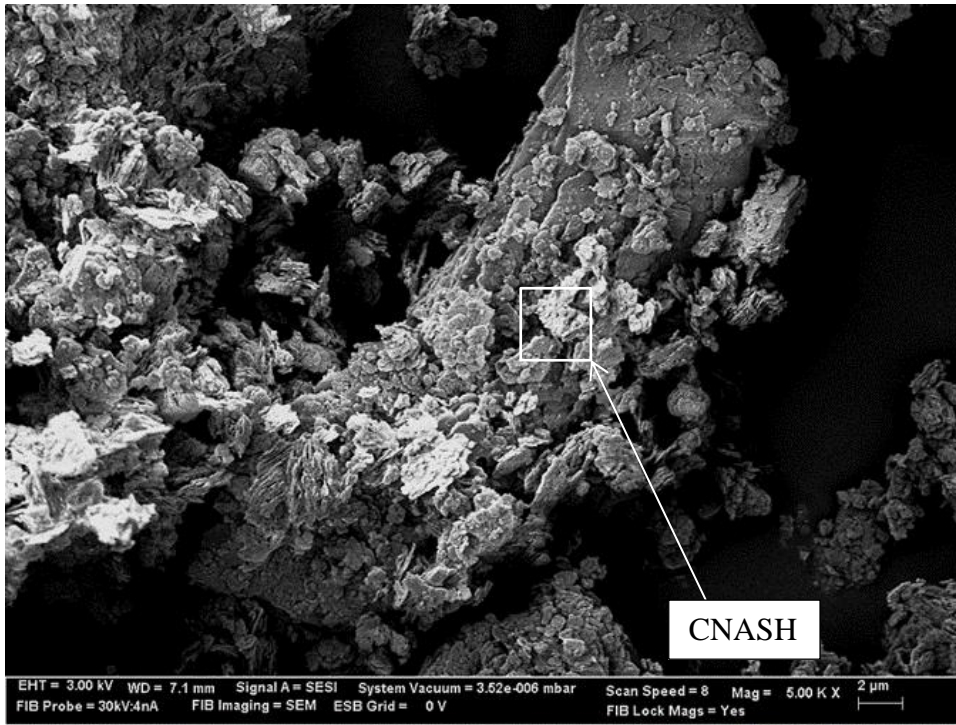


Figure 4.32 FESEM-EDAX image, K28G12. (ETH=8.00kV; WD= 7.1 mm, Mag=5.00 KX). (Element/compound legend: CNAS = Calcium Sodium Aluminum Silicate Hydrate, Si:Silicon, Al: Aluminum, Ca: Calcium, Na: Sodium, Mg:Magnesium, Pd: Palladium, Au: Gold).

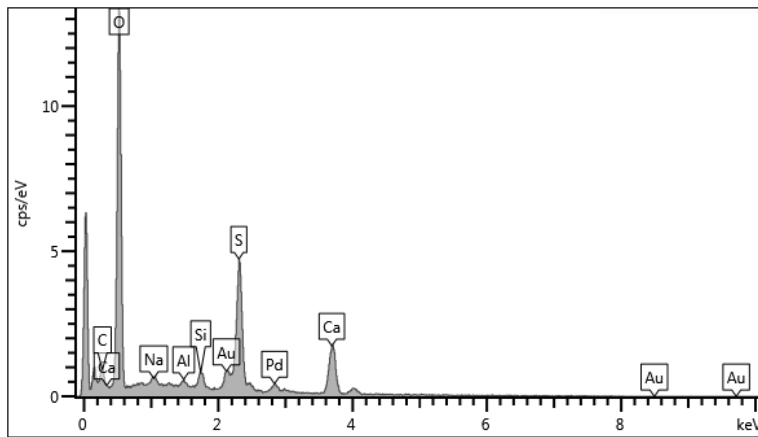
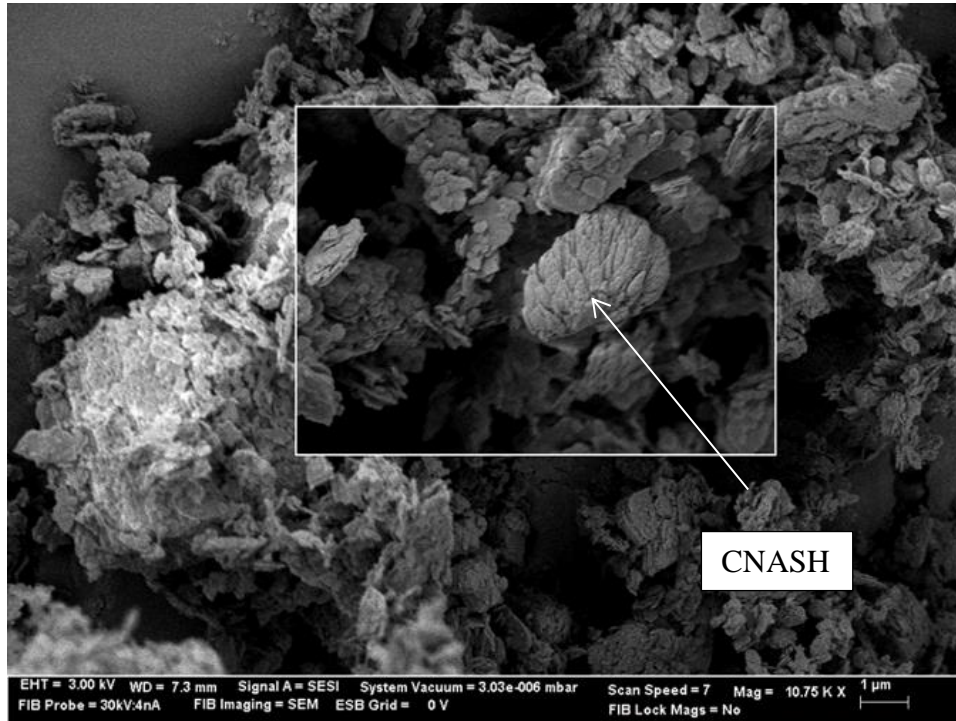


Figure 4.33 FESEM-EDAX image, K28G12. (ETH=3.00kV; WD= 7.3 mm, Mag=10.75 KX). (Element/compound legend: CNASH= Calcium Sodium Aluminum Silicate Hydrate, Si:Silicon, Al: Aluminum, Ca: Calcium, Na: Sodium, S: Sulfate, Pd: Palladium, Au: Gold).

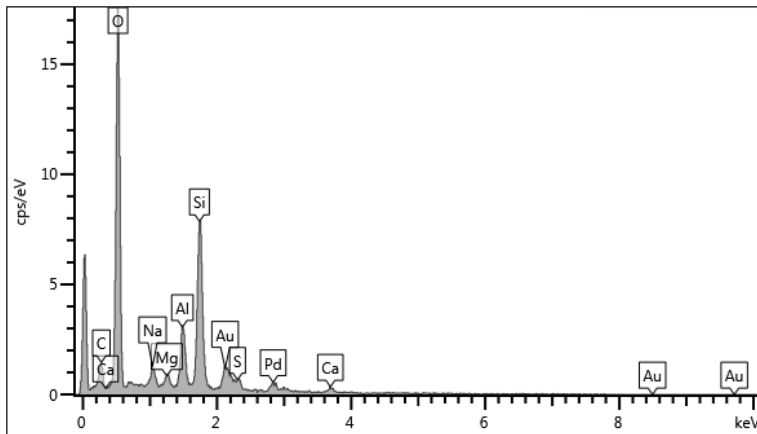
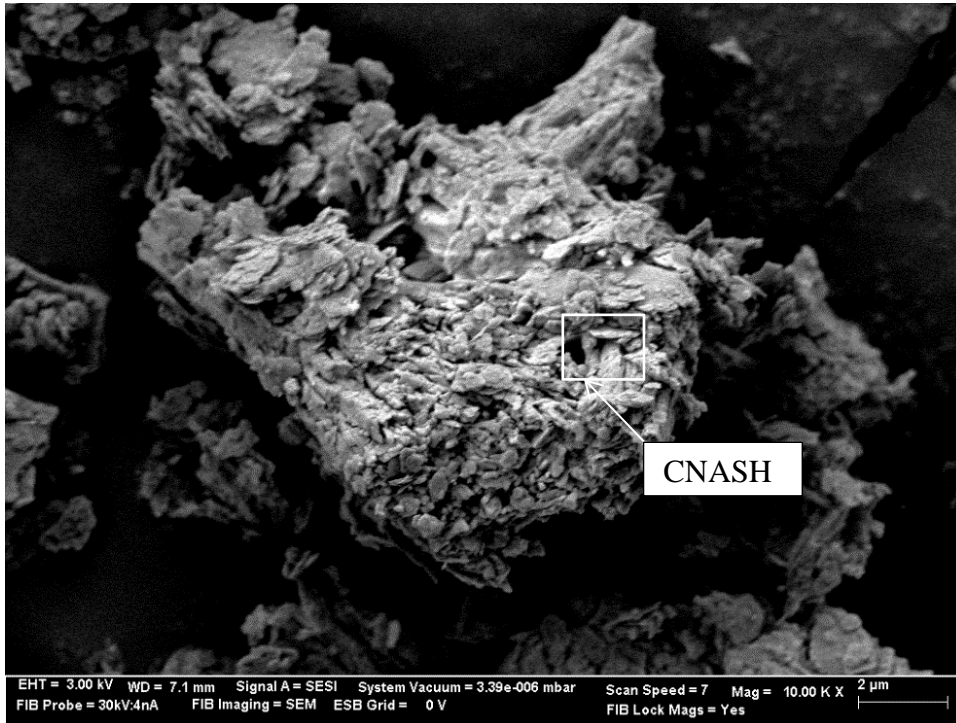


Figure 4.34 FESEM-EDAX images for K56G12. (ETH=8.00kV; WD= 7.1 mm, Mag=10.00 KX). (Element/compound legend: CNASH= Calcium (Sodium) Aluminum Silicate, Si:Silicon, Al: Aluminum; Ca: Calcium; Na: Sodium, S: Sulfate; Pd: Palladium; Au: Gold).

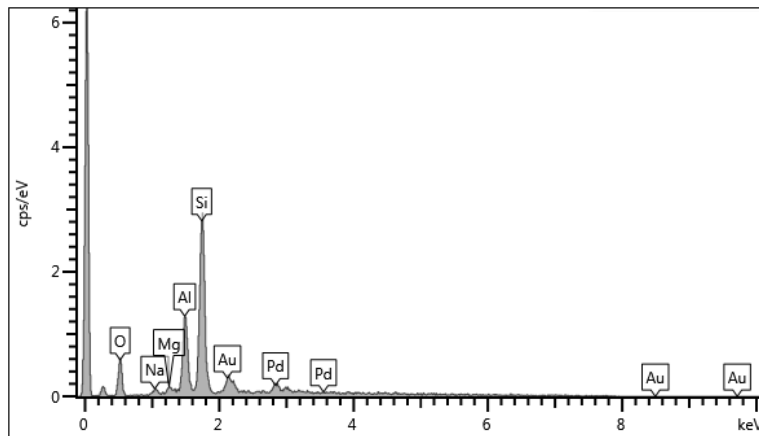
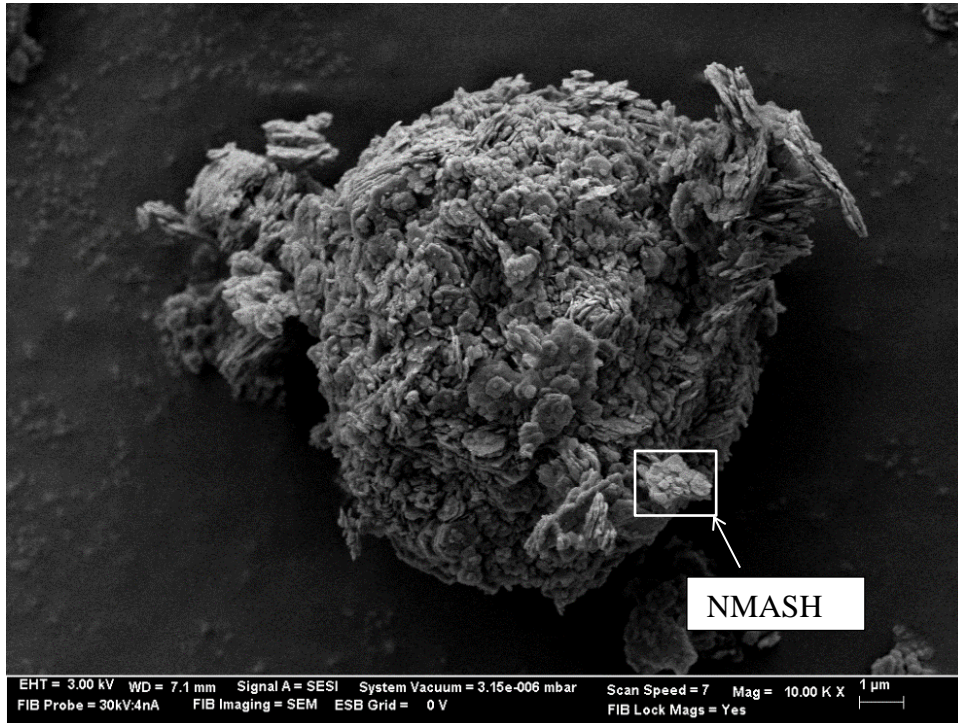


Figure 4.35 FESEM-EDAX images for K56G12. (ETH=8.00kV; WD= 7.1 mm, Mag=10.00 KX). (Element/compound legend: NMASH= Sodium Magnesium Aluminum Silicate Hydrate, Si:Silicate, Al: Aluminum, Ca: Calcium, Na: Sodium, Mg:Magnesium, S: Sulfate, Pd: Palladium, Au: Gold).

4.5.2 Effect of Sodium Silicate Solution on Soils

4.5.2.1 Bentonite and Sodium Silicate Solution

Bentonite stabilized only with sodium silicate was cured for up to 56 days of curing. Figures 4.36 to 4.41 present the FESEM results for 12% additive treated bentonite after 3, 7, and 14 days of curing. From those images, clay particles are activated by the alkaline solution to form new cement phases in the binder system. The chemical changes upon the clay surface can be observed by either the presence of agglomerates or individual lumps.

The EDAX results depict that the cementation products can contain different ions, such as iron, potassium, and magnesium, based on the chemical composition of the clay lattice where the alkaline solution and source material interact. This is evidence of the dissolution of the clay minerals (such as montmorillonite) releasing their ions into the pore fluid. The quantity of dissolved silicon ranges from day to day based on curing conditions at the same additive content. This could be attributed to the level of alkalinity which has increased over the curing time (Criado et al., 2005). Thus, the dissolution of source materials is expedited because of the highly alkaline environment (Rees et al., 2007).

Depending on the chemical composition of the binder, different binding phases can fabricate in the system. For example, Figure 4.37 reveals that only aluminum-silicate gel ($\text{SiO}_2 + \text{Al}_2\text{O}_3$) formed on the clay surface with a little interaction of sodium ions in the gel; thus, NASH (sodium aluminum silicate hydrates) were manufactured in

the soil-sodium silicate mixture. The primary product in the alkaline activated system herein is sodium aluminum silicate hydrates (NASH) and sodium-calcium aluminatesilicate N(C)AS since the Ca ions could participate in the reaction occurring between the soil and pore solution. Moreover, the presence of calcium and other ions such as iron (Fe) and magnesium (Mg) in the source material can engage in the binder phase, which can partially replace sodium ions with calcium ions to form (N(C)ASH). The role of cation replacement between calcium and sodium ions is unclear in N(C)ASH, whereas it has a positive effect on the mechanical properties of soil and binder.

New porous structures were detected in FESEM micrographs for all of the samples that were cured for different times. These structures can possibly be attributed to dissolution of the base material by the stabilizing additive; in some locations, these features are covered by new cementitious products, in other locations, they are still visible. The EDAX spectrum illustrates that the observed new compounds consist of (N)CASH (sodium calcium aluminum-silicate hydrates).

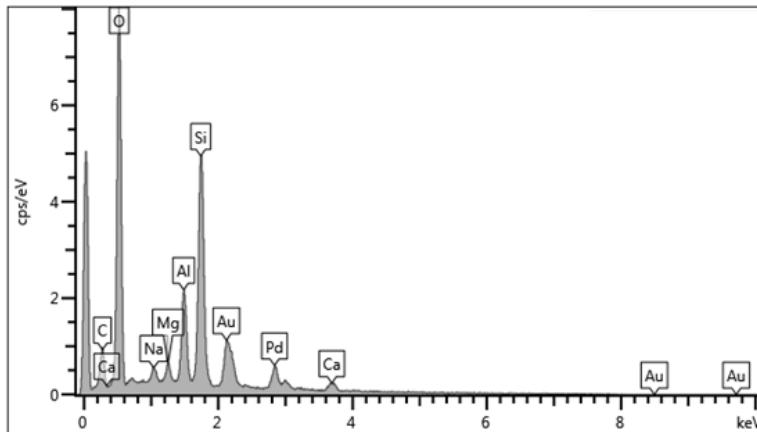
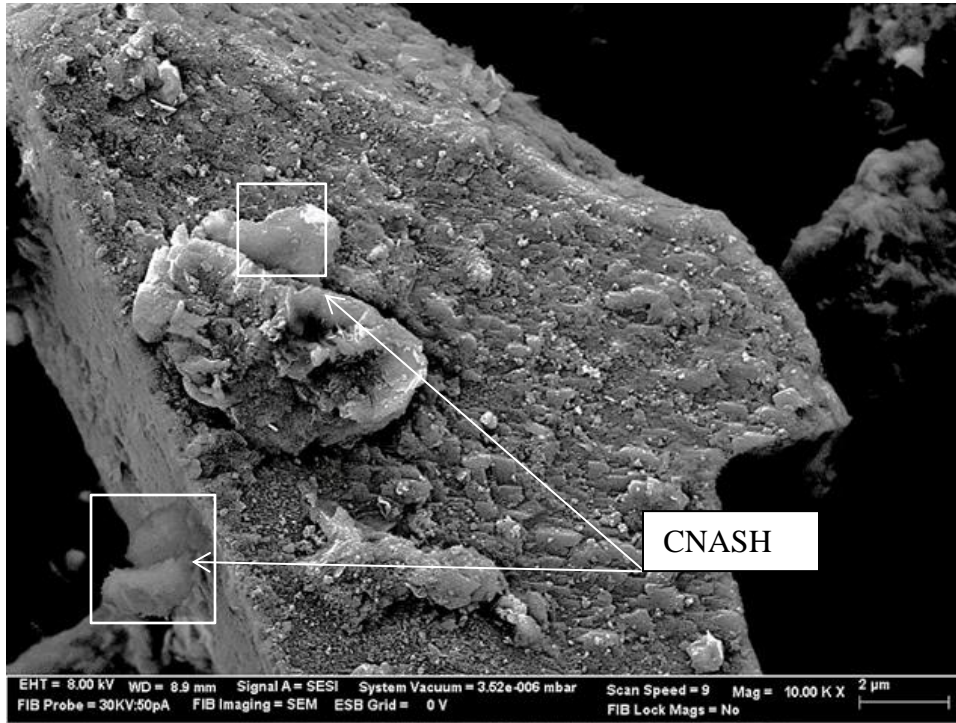


Figure 4.36 FESEM/EDAX image, B3S12. (ETH=8.00kV; WD= 6.9 mm, Mag=10.00 KX). (Element/compound legend: CNASH= Calcium Sodium Aluminum Silicate Hydrate, Na: Sodium, Al: Aluminum, Si: Silicate, O: Oxygen, Pd: Palladium, Au: Gold).

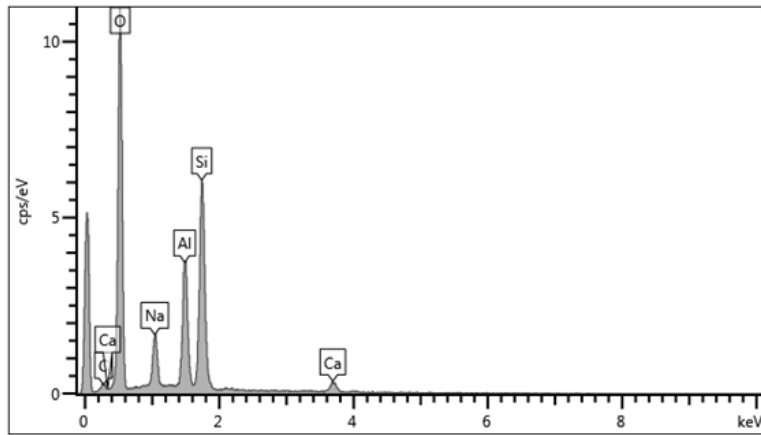
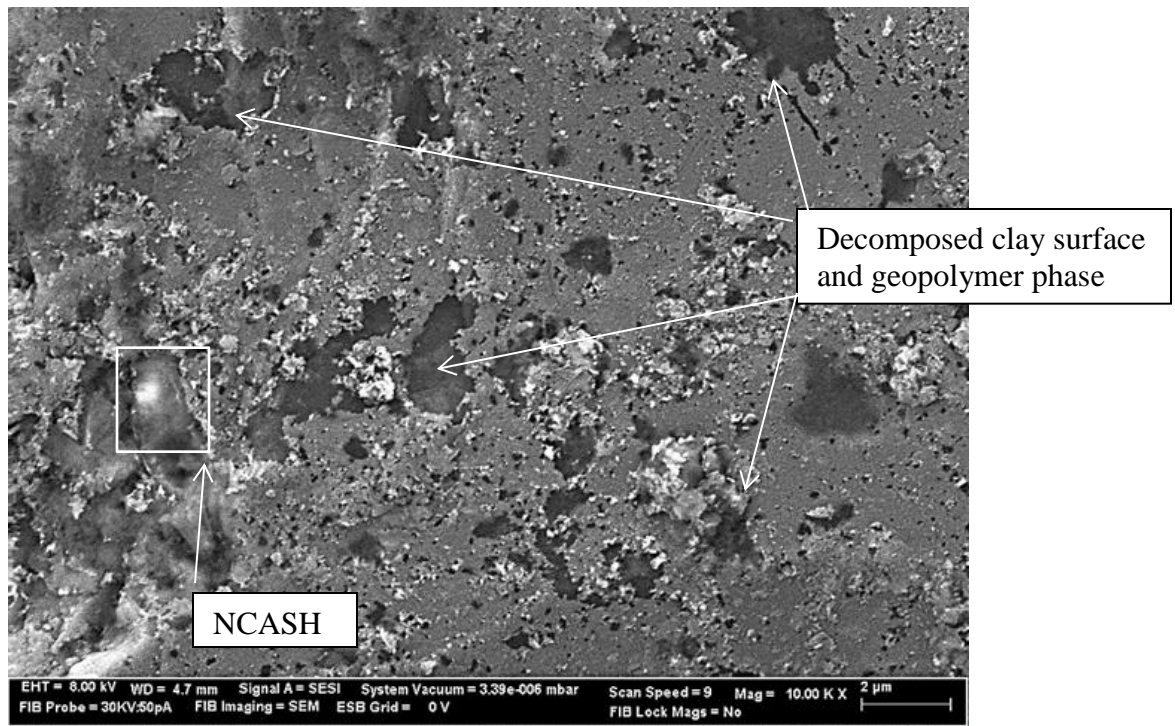


Figure 4.37 FESEM/EDAX image, B3S12. (ETH=8.00kV; WD= 4.7 mm, Mag=10.00 KX). (Element/compound legend: NCASH= Sodium Calcium Aluminum Silicate Hydrate, Na: Sodium, Al: Aluminum, Si: Silicate, O: Oxygen).

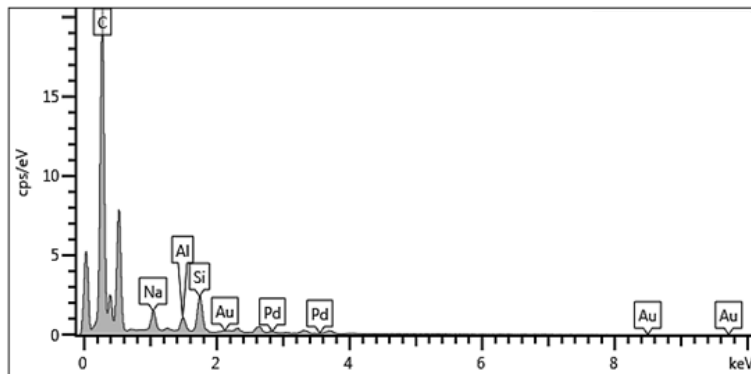
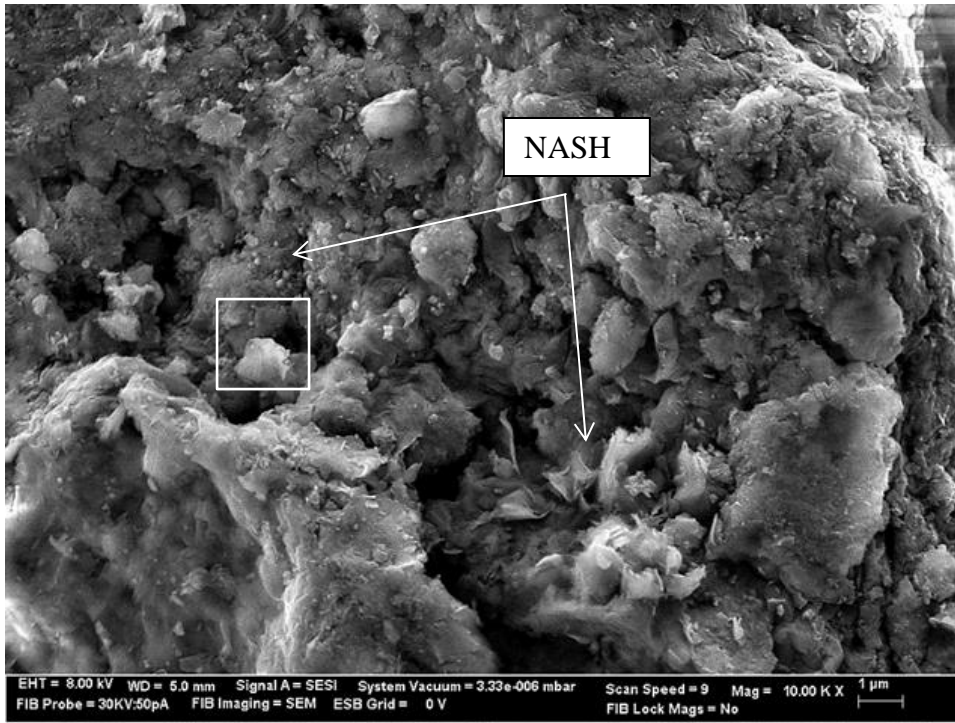


Figure 4.38 FESEM/EDAX image, B7S12. (ETH=8.00kV; WD= 4.7 mm, Mag=10.00 KX). (Element/compound legend: NASH= Sodium Aluminate Silicate Hydrate, Na: Sodium, Al: Aluminum, Si: Silicate, C: Carbon, Pd: Palladium, Au: Gold).

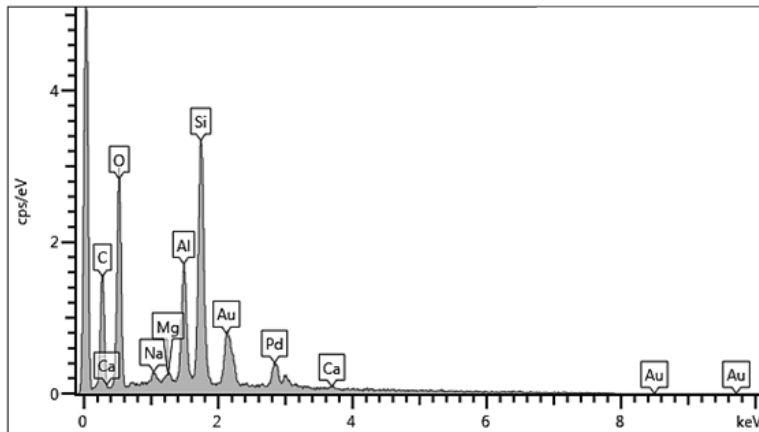
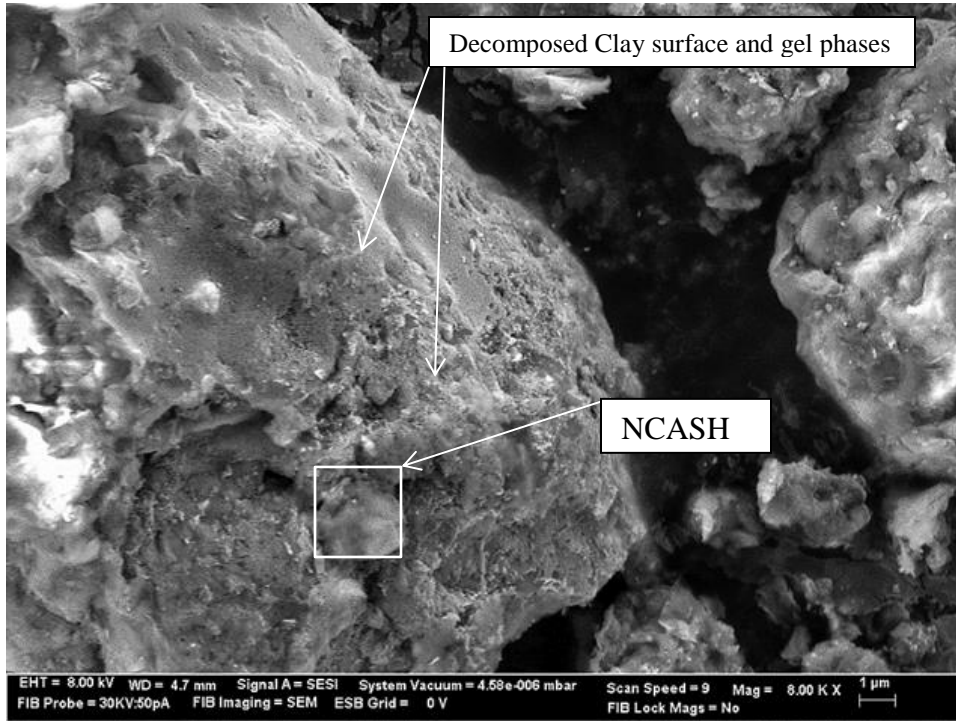


Figure 4.39 FESEM/EDAX image, B7S12. (ETH=8.00kV; WD= 4.7 mm, Mag=10.00 KX). (Element/compound legend: NCAS= Sodium Calcium Aluminum Silicate Hydrate, Na: Sodium, Al: Aluminum, Si: Silicate, C: Carbon, Pd: Palladium, Au: Gold).

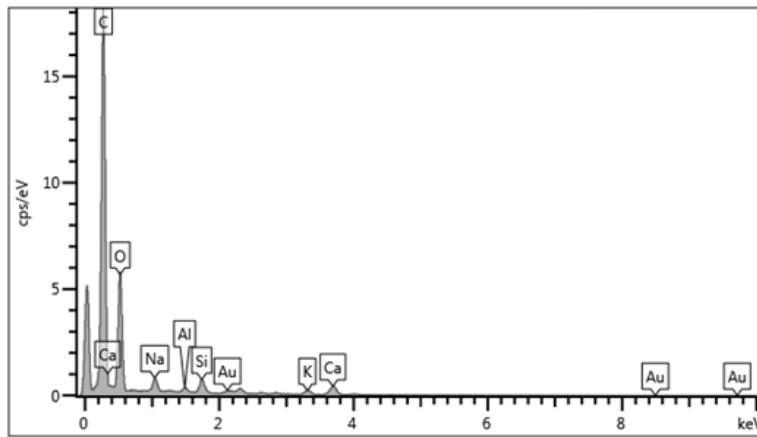
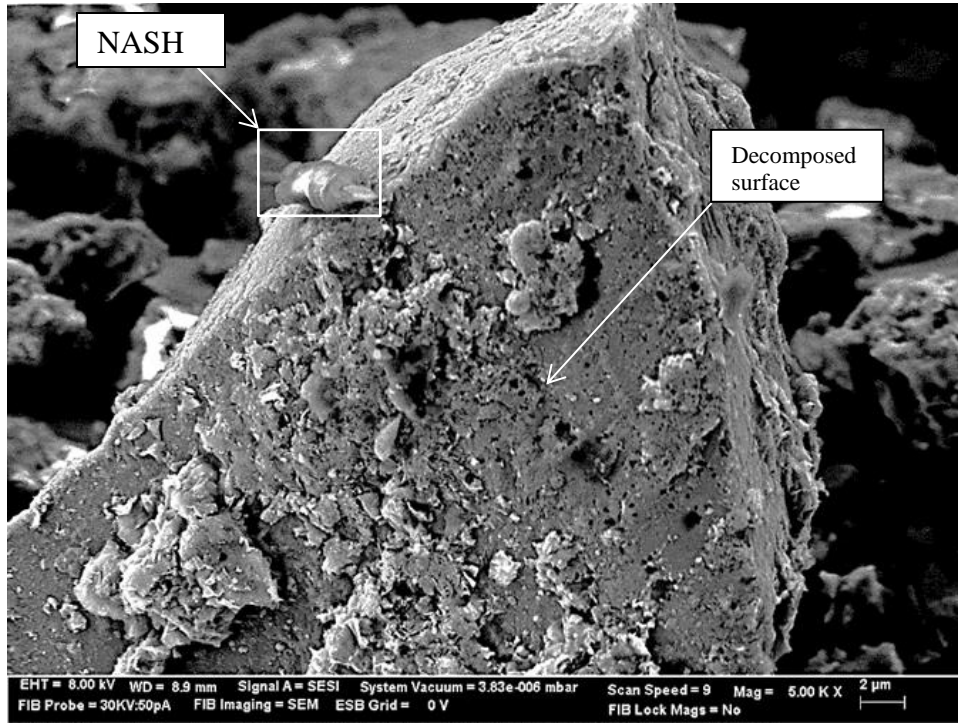


Figure 4.40 FESEM/EDAX image, B14S12. (ETH=8.00kV; WD= 6.9 mm, Mag= 5.00 KX). (Element/compound legend: NASH= Sodium Aluminate Silicate Hydrate, Na: Sodium, Al: Aluminum, Si: Silicate, Au: Gold, Pd: Palladium).

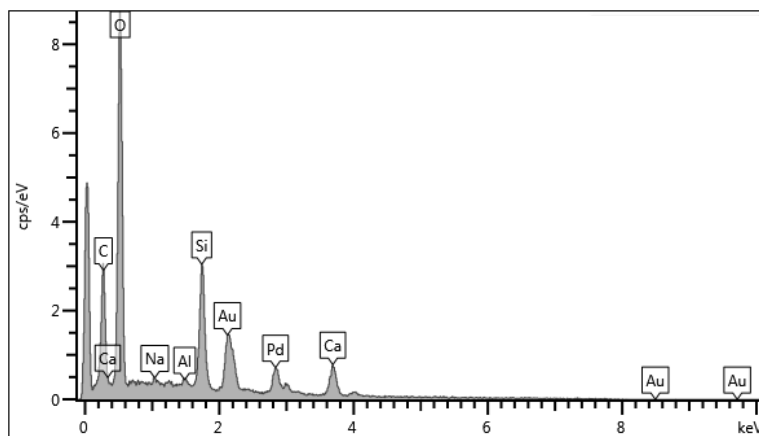
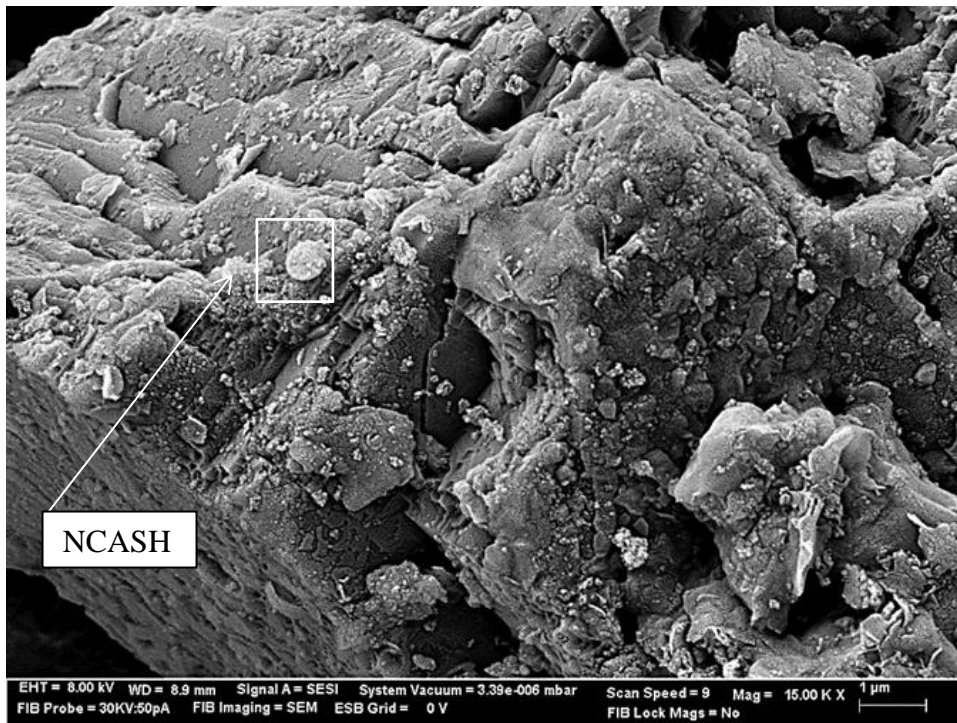


Figure 4.41 FESEM/EDAX image, B14S12. (ETH=8.00kV; WD= 6.9 mm, Mag= 15.00 KX). (Element/compound legend: NCAS= Sodium Calcium Aluminate Silicate Hydrate, Na: Sodium, Ca: Calcium, Al: Aluminum, Si: Silicate, Au: Gold, Pd: Palladium).

4.5.2.2 Kaolinite and Sodium Silicate Solution

The FESEM and EDX images of treated kaolinite by 6% sodium silicate for 3, 7 and 56 days of curing are presented in Figures 4.42-4.57. The transformation of microstructures in the three specimens is identified as partially reacted flaky/cloudy structures corresponding to the stabilization. This modification can be observed by examining how the specimen microstructures evolve from book-sheet structures to flaky aggregates.

The chemical activation of pure kaolinite increases the distance between the book-sheet layers (e.g., Latifi et al., 2016). This redesigns the mineral structures such that they manifest as more flaky aggregates. It is believed that the primary fabricated polymer material is formed by NAH (sodium aluminum silicate hydrates) during the stabilization progress (e.g., Figure 4.42 and 4.43). Decomposition/ transformation over the kaolinite particles was clearly observed in this stabilization study. Additionally, the dissolution of iron (Fe) and magnesium (Mg) is barely observed, which participate in the polymeric reaction chain. However, the transformation of aluminum (Al) and silicate (Si) increase significantly once the alkaline sodium silicate solution is introduced to the binder system, yet the reaction mechanism is believed to be somewhat slow after the 0-day strength gain has occurred due to low reactivity of the kaolinite minerals relative to bentonite (e.g., Das, 1994), and also possibly due to the lower pH of the kaolinite stabilization environment relative to bentonite. As shown in the XRD results in Figure 4.20, the intensity of the kaolinite minerals was reduced after the admixture was added into the system. This is evidence of the consumption of kaolinite

minerals by the stabilization reaction process. Besides, new sharp peaks emerge in the diffraction pattern in the K3S6 and K7S6 specimens, and as weak peaks that are exhibited in K5S6. It is known that cementation products can be formed as a crystalline phase resembling kaolinite minerals presenting hexagonal crystalline structures in the system (Xu and Van Deventer, 1994); thus, it is hard to distinguish both minerals in the FESEM micrographs, but the new flaky and cloudy structures are evidence that the transformation of pure kaolinite minerals has occurred in the stabilized kaolinite specimens.

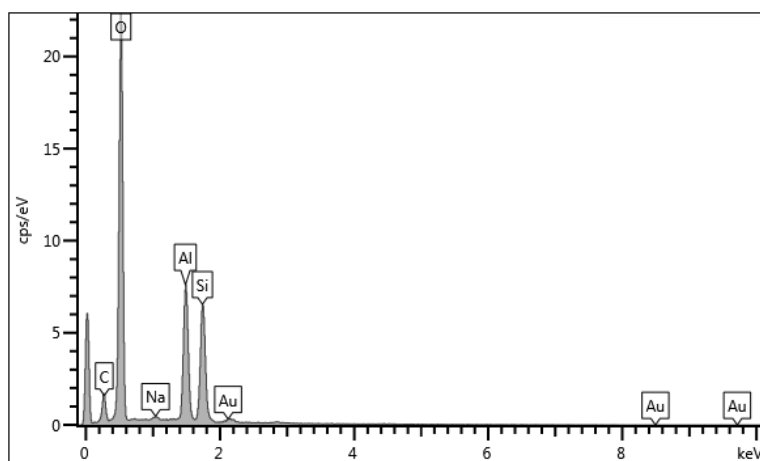
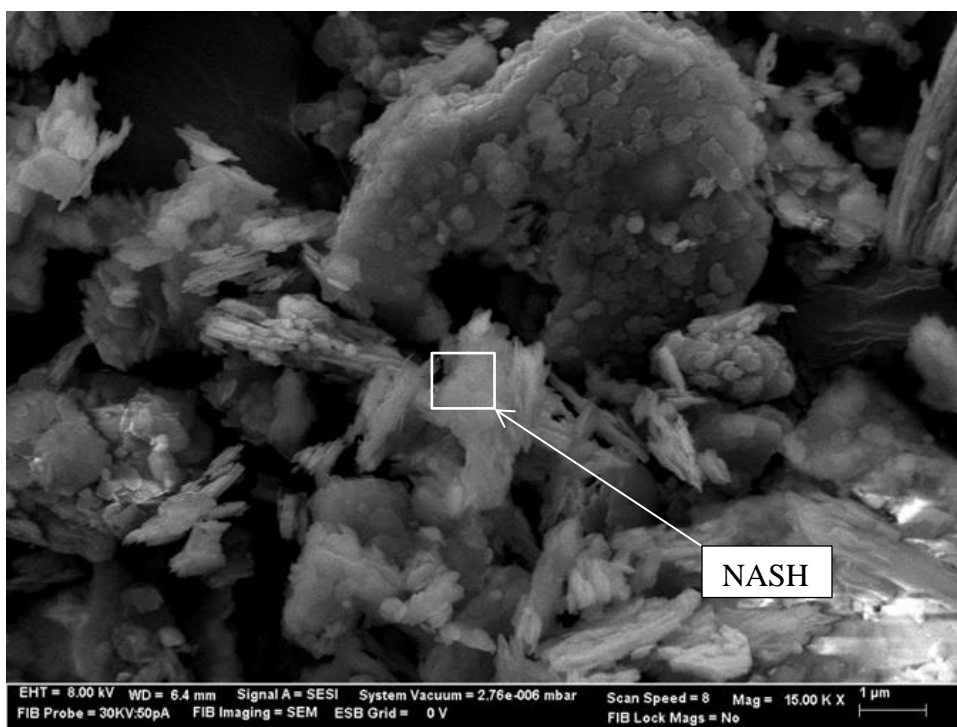


Figure 4.42 FESEM/EDAX images K3S6. (ETH=8.00kV; WD= 6.4 mm, Mag= 15.00 KX). (Element/compound legend: NASH= Sodium Aluminum Silicate Hydrates, Na: Sodium, Au: Gold, C: Carbon, O: Oxygen).

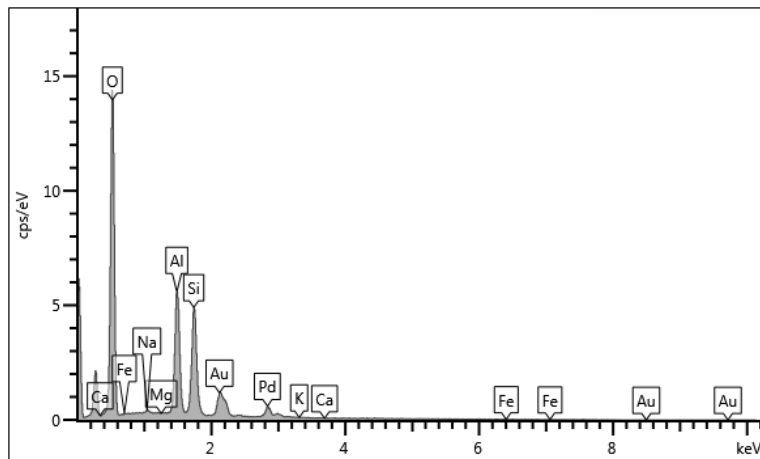
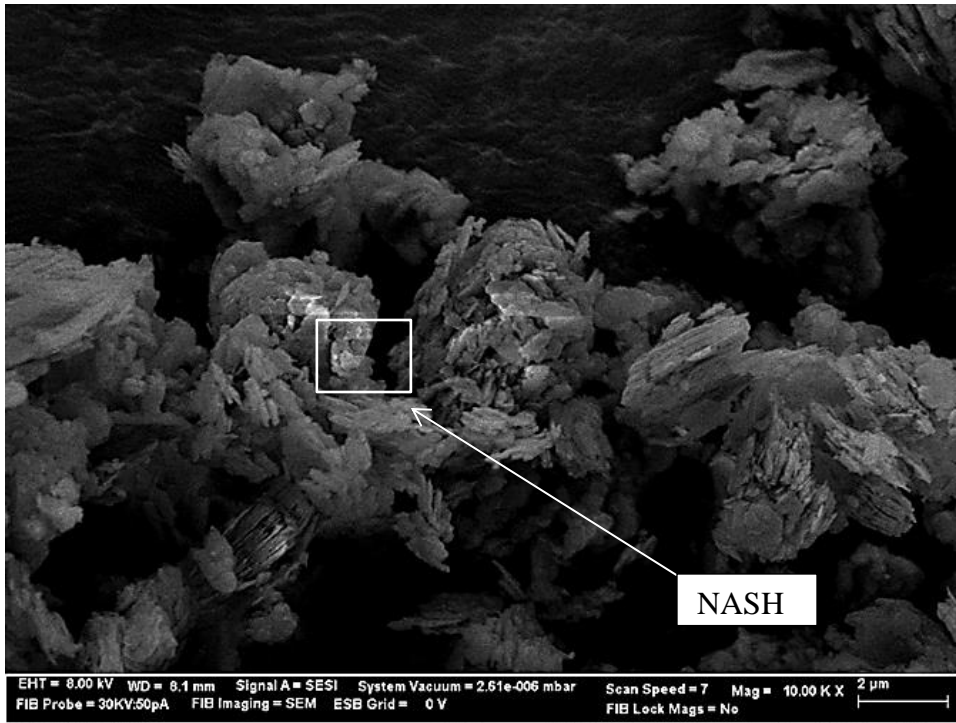


Figure 4.43 FESEM/EDAX image, K3S6. (ETH=8.00kV; WD= 6.4 mm, Mag= 15.00 KX). (Element/compound legend: NASH= Sodium Aluminum Silicate Hydrate, Mg: Magnesium, Fe: Iron, K: Potassium, Fe: Iron, Au: Gold, O: Oxygen).

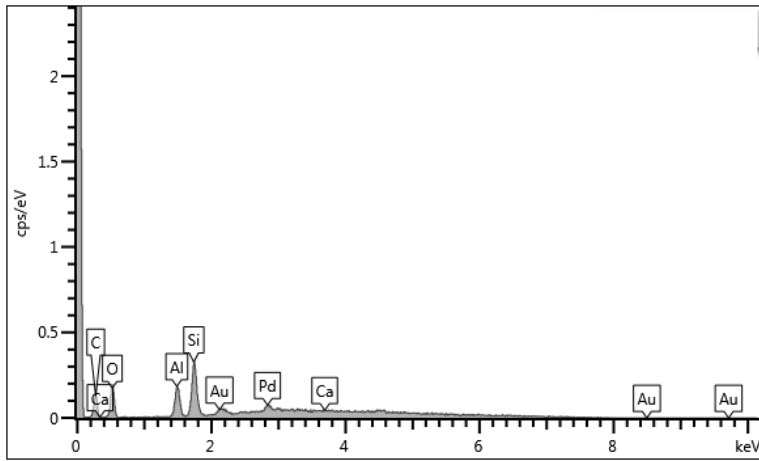
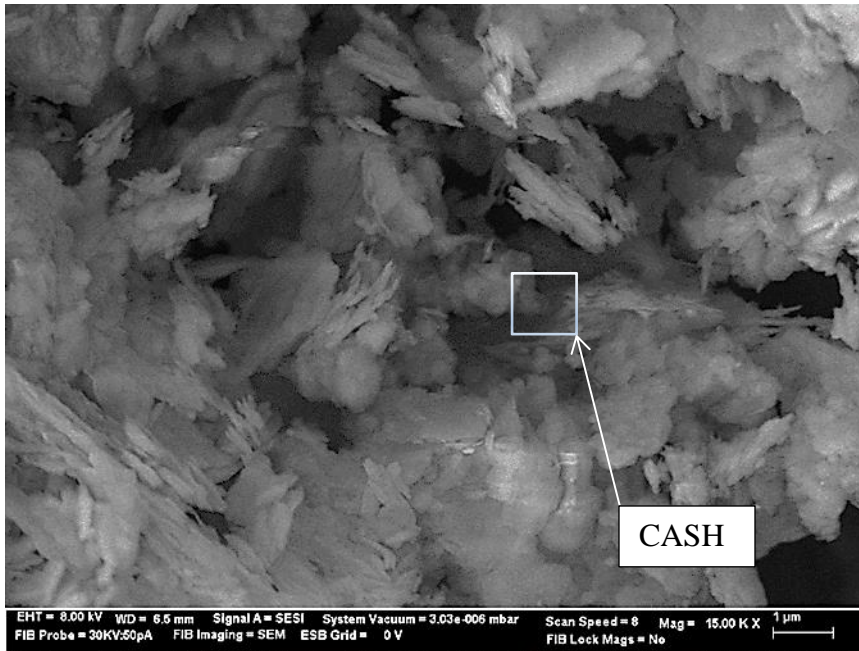


Figure 4.44 FESEM/EDAX image, K7S6. (ETH=8.00kV; WD= 6.5 mm, Mag= 15.00 KX). (Element/compound legend: CASH= Calcium Aluminum Silicate Hydrate, Ca: Calcium, Au: Gold, O: Oxygen, C: Carbon).

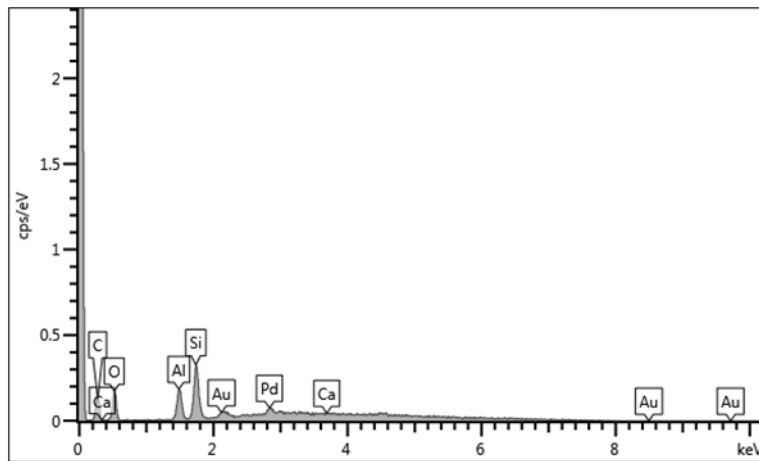
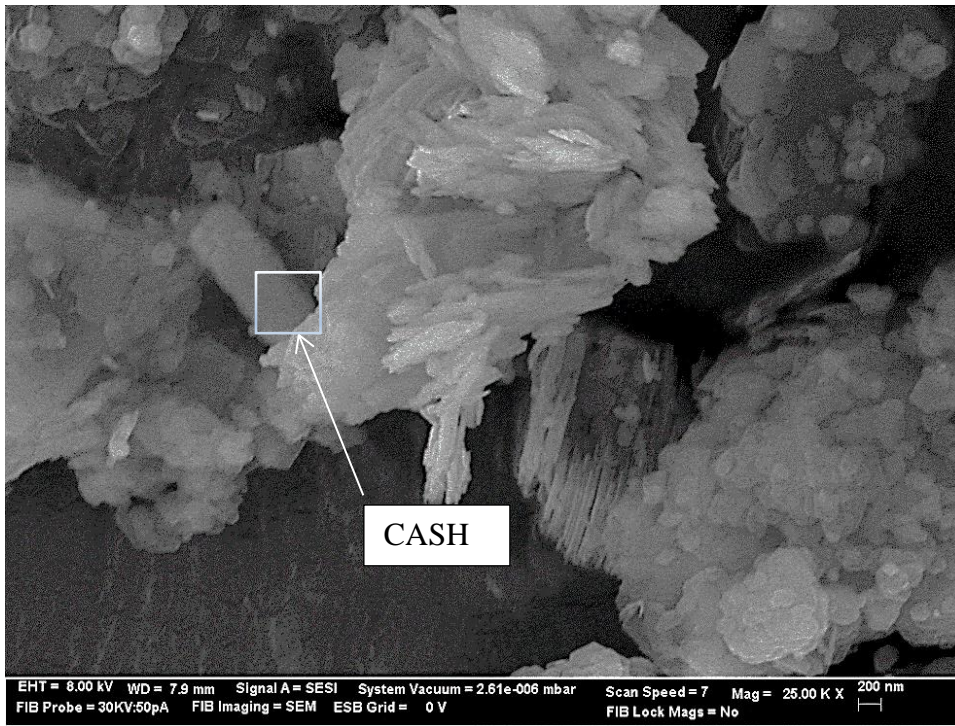


Figure 4.45 FESEM/EDAX image, K7S6. (ETH=8.00kV; WD= 7.9 mm, Mag= 25.00 KX). (Element/compound legend: CASH= Calcium Aluminum Silicate Hydrate, Al: Aluminum, Si: Silicate, Na: Sodium, Au: Gold, Pd: Palladium, O: Oxygen, C: Carbon).

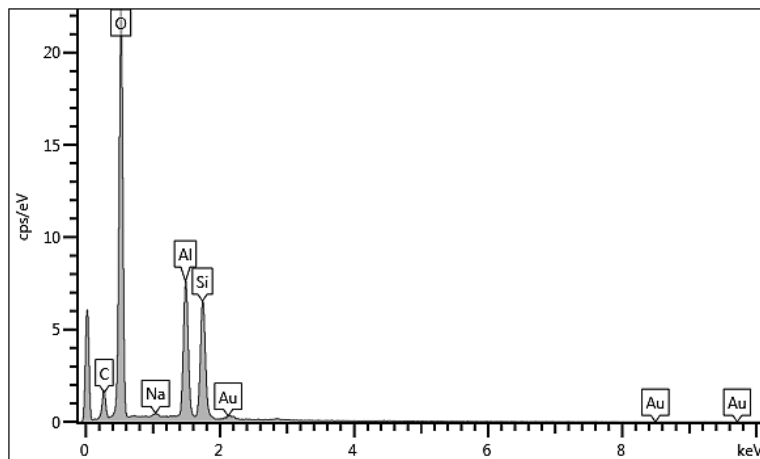
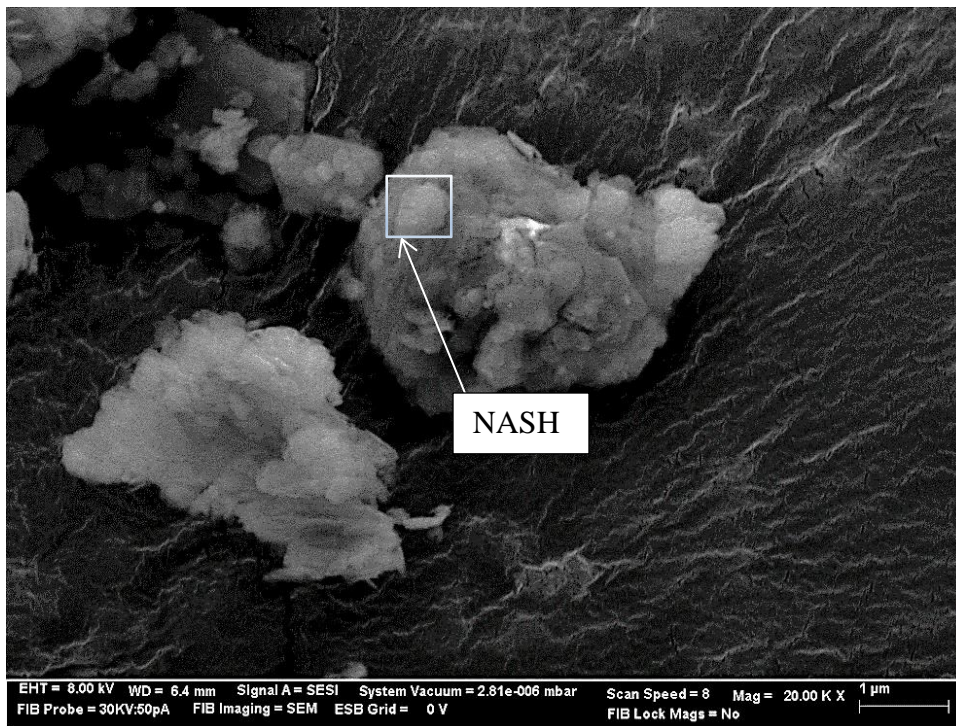


Figure 4.46 FESEM/EDAX images, K56S6. (ETH=8.00kV; WD= 6.4 mm, Mag= 20.00 KX).. (Element/compound legend: NASH= Sodium Aluminum Silicate Hydrate, Na: Sodium, Al: Aluminum, Si: Silicate, Au: Gold, Pd: Palladium, O: Oxygen; C: Carbon).

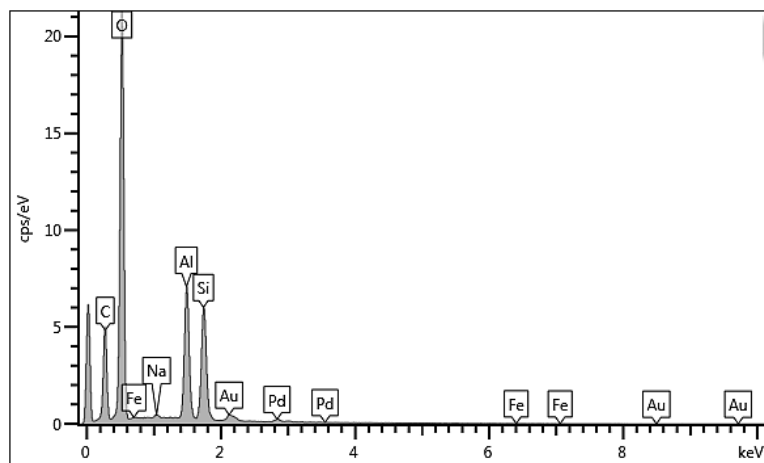
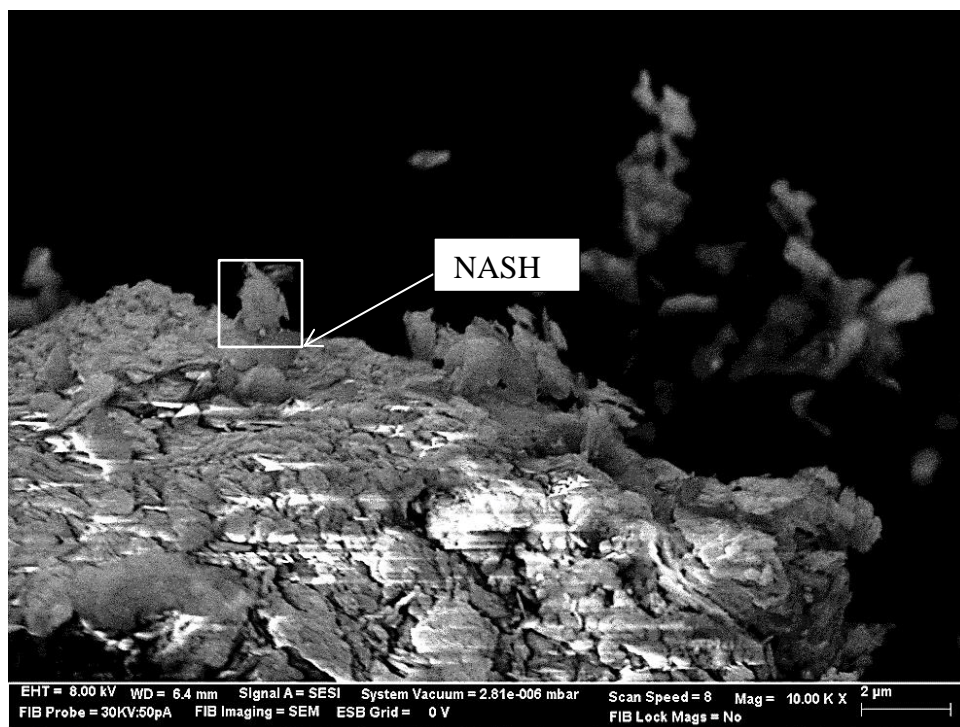


Figure 4.47 FESEM/EDAX image, K56S6. (ETH=8.00kV, WD= 5.4 mm, Mag= 10.00 KX). (Element/compound legend: NASH= Sodium Aluminum Silicate Hydrate, Al: Aluminum, Si: Silicate, Na: Sodium, Au: Gold, Pd: Palladium, O: Oxygen, C: Carbon).

4.5.3 Effect of Recycled Gypsum and Sodium Silicate Solution on Soils

4.5.3.1 Bentonite and Recycled Gypsum and Sodium Silicate Solution

The morphological features and transformation of the bentonite treated with a 6% admixture of recycled gypsum and sodium silicate solution (50%:50%) after 3, 14 and 56 days of curing are presented in Figures 4.48 to 4.53.

As shown, there is a growth of cementitious materials that contribute to the observed strength development that can be observed in all specimens at different curing intervals. Each of the new components exhibit different development structure such as gel phase ‘glassy content’, and circle type ‘shells’ on the surface of clay minerals.

Significant changes in the quantity of Al, Si, Na, and Ca ions were detected in the EDAX spectrum after the various curing periods. Calcium ions from recycled gypsum appear to be quickly consumed even at low concentrations, fabricating Ca phase products such as CS(A)H, with sodium ions (Na) that might contribute to the phases that are formed due to the alkali activation process. In this case, Only N(C)AS phases (sodium calcium aluminum silicate hydrate) could be fabricated at early curing ages (B3GS6), as shown in Figures 4.48 and 4.49 (which were also observed in the X-ray diffraction pattern). As shown, aggregated clay particles are coated with sulfate ions that have been released from the recycled gypsum.

By examining the specimen cured for 14 days, B14GS6, it is believed that the base clay particles are decomposed by the activator admixture, and then (concurrently) begin developing geopolymer structures. Figures 4.50 and 4.51 show that the clay

particles are remodified and in some cases partially consumed by the additives at several locations where new cementations gel formations accumulated. The observed fabricated material contains a high amount of Ca, Si, and Na ions based on the EDAX results. In this respect, the new cement products that are formed could be sodium calcium aluminum-silicate hydrates (N(C)AH), which are also detected in the XRD diffraction testing. Also, newly formed void spaces are observed on the clay lattice.

Another specimen (B14GS6) produced new gel phase cementation products sticking on the side wall of the clay particles. The observed gel, present in Figure 4.50, consists of high content of Ca, Si and Na ions; yet the quantity of Al ions is preferably less than others. This could be related to additive content increasing silicate concentration in the binder, which may delay the dissolution of Al ions in the source material (Suganya and Sivapullaiah, 2016). Additionally, some amount of potassium (K), iron (Fe), and manganese (Mn) elements are involved in the binder system, which indicate the dissolution of the source material. The clay surface appears to have been decomposed with time, leading to the formation of new porous structures all around the clay particles, some of which have been filled by the gel phase of cementation. This indicates that polymerization is uncompleted at the end of 14-days of curing. Thus, more time is needed to fill these voids. Otherwise, it negatively impacts on the improvement in strength.

B56GS6 depicts new cementation compounds resembling the shape of a sphere. It mainly contains Na, Ca ions as well as Mg (Magnesium) and hydrated aluminum silicates in Fig. 4.52, and 4.53. These observed compounds could be Na and Mg-rich

calcium aluminum silicate hydrated minerals that are fabricating with long-term curing, leading to a regain of strength after 28-days of curing (Latifi et al. 2016). Sulfate ions from the recycled gypsum are not detected around the observed materials. However, visible cracks are available around the clay particles. The cracking was probably due to the quick hardening properties of the silica-rich environment applying excessive pressure on the hardened matrix.

Decomposition can be observed around the clay particle in the specimen cured for 56 days (Figure 4.53). Na and Mg ions are not identical in the EDAX spectrum, but may participate in the chemical reaction chain at the time of polymerization. In addition to that observation, the clay particles it is highly coated by sulfate ions (S), which are believed to be formed by transformation of the recycled gypsum. The cement products have formed non-crystalline white cloud structures containing high Ca ions and low Al-Si ions in the binder system. This could be associated with the formation of CASH compounds including sulfate ions. Sulfate coated materials could impact the strength development progress according to Jun and Oh (2015), who reported that Na ions could be captured by sulfate ions; thus, the development of Na-rich compounds can be delayed during the polymerization process. The formation of aggregations of cementing compounds changes the surface appearance of the clay particles.

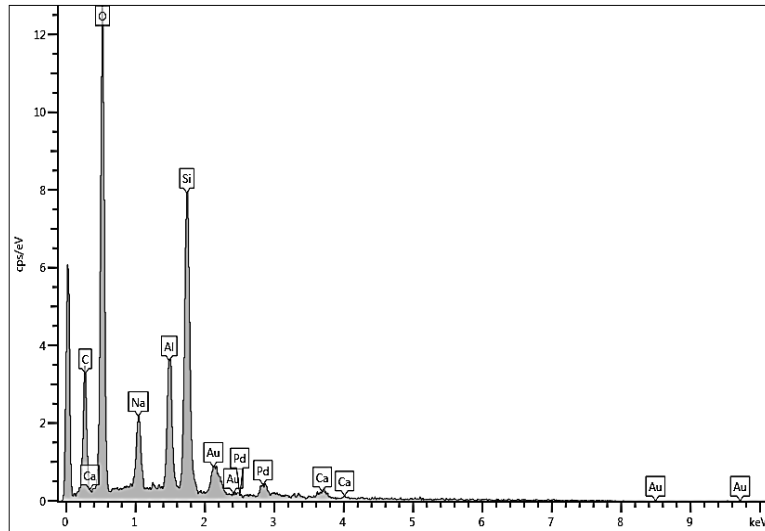


Figure 4.48 FESEM/EDAX images, B3GS6. (ETH=8.00kV, WD= 6.6 mm, Mag= 10.00 KX). (Element/compound legend: NCASH= Sodium Calcium Aluminate Silicate Hydrate, Na: Sodium, Al: Aluminum, Ca: Calcium, Au: Gold, Pd: Palladium).

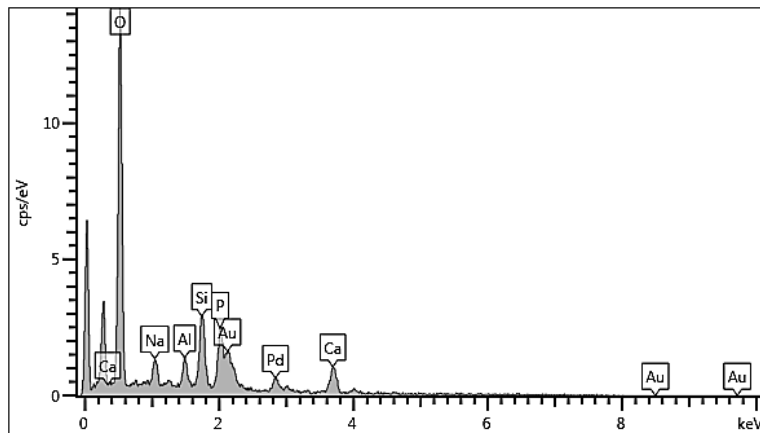
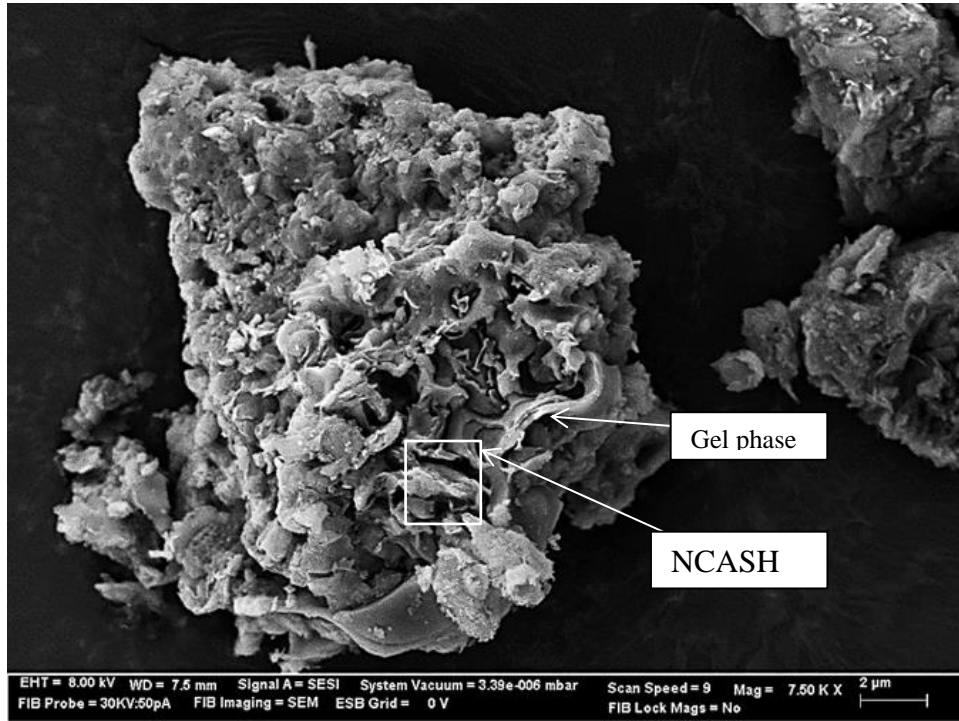


Figure 4.49 FESEM/EDAX images, B3GS6. (ETH=8.00kV, WD= 5.6 mm, Mag= 7.50 KX). (Element/compound legend: NCASH= Sodium Calcium aluminate Silicate Hydrate, Na: Sodium, Ca: Calcium, Al: Aluminum, Si: Silicate, P: Phosphorus, Au: Gold, Pd: Palladium).

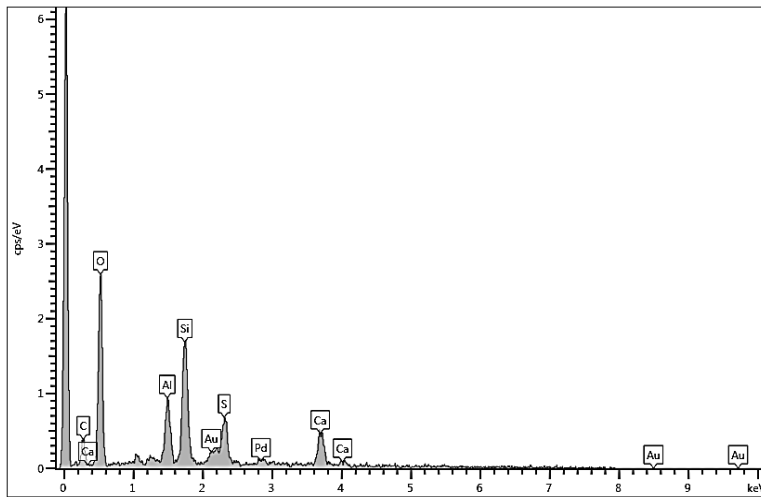
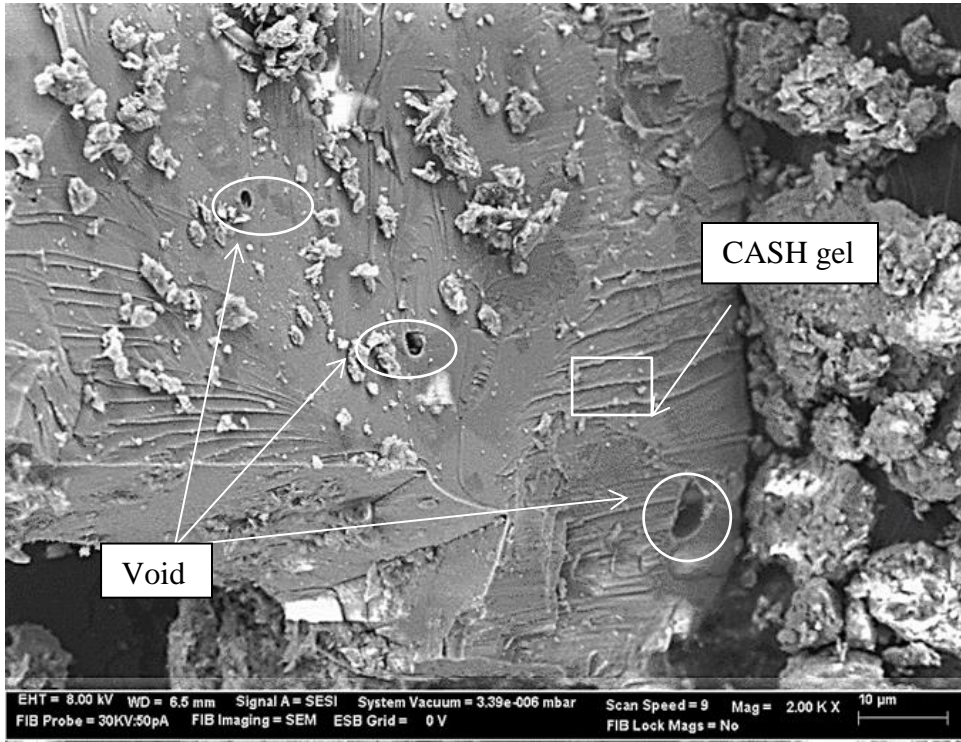


Figure 4.50 FESEM/EDAX images, B14GS6. (ETH=8.00kV, WD= 6.5 mm, Mag= 2.00 KX). (Element/compound legend: CASH= Calcium Aluminate Silicate Hydrate, Al: Aluminum, Si: Silicate, Ca: Calcium, S: Sulfate, Au: Gold, Pd: Palladium).

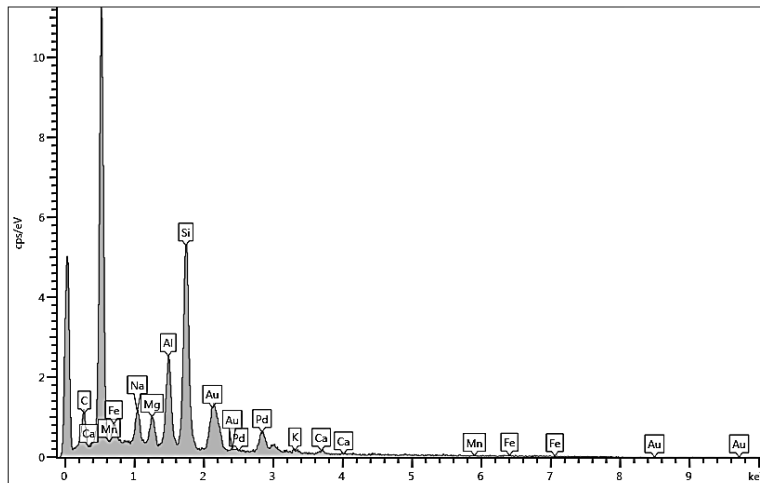
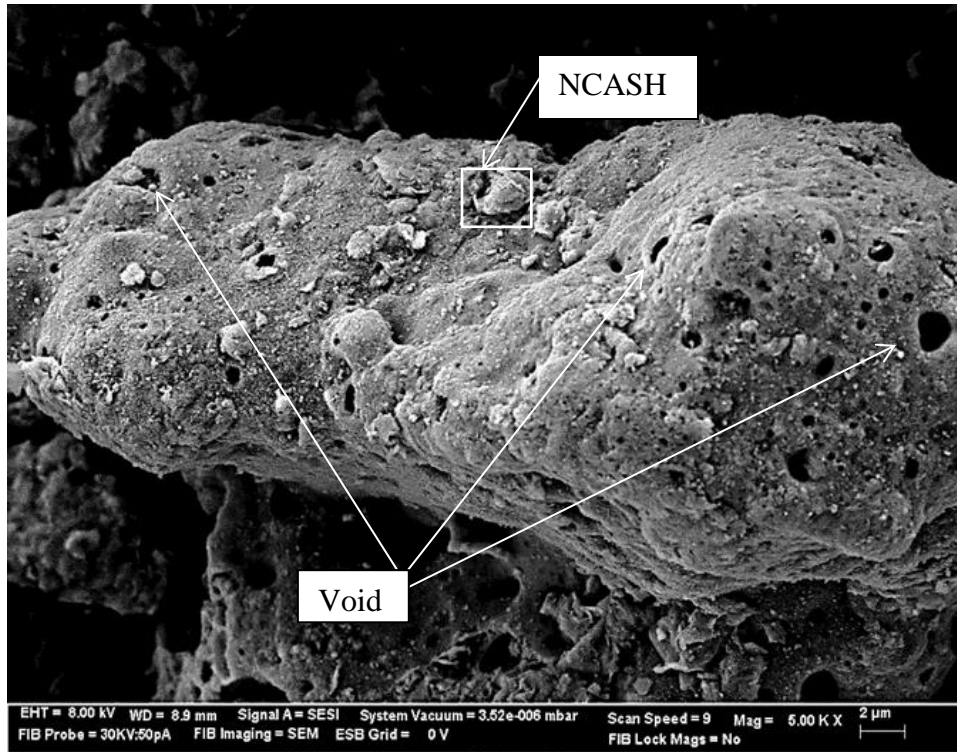


Figure 4.51 FESEM/EDAX images, B56GS6. (ETH=8.00kV, WD= 8.9 mm, Mag= 5.00 KX). (Element/compound legend: NMCAS= Sodium Magnesium Calcium Aluminate Silicate Hydrate, Na: Sodium, Ca: Calcium, Fe: Iron, Mg: Magnesium, K: Potassium, Mn: Manganese, Au: Gold, Pd: Palladium).

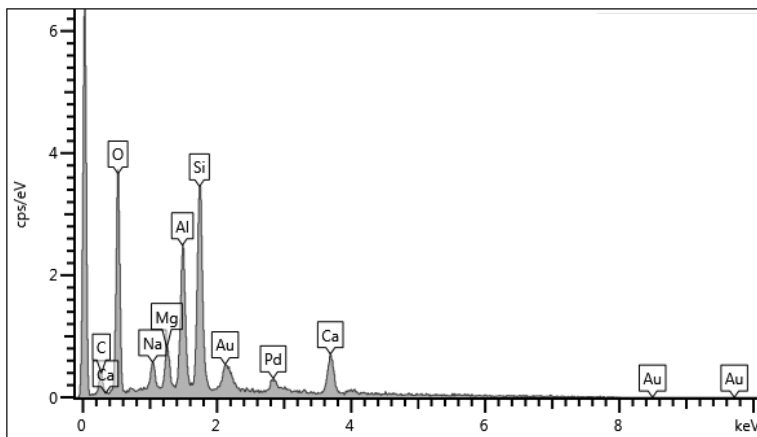


Figure 4.52 FESEM/EDAX images, B56GS6. (ETH=8.00kV, WD= 7.5 mm, Mag= 10.00 KX). (Element/compound legend: NCASH= Sodium-Magnesium-Calcium Aluminate Silicate Hydrate, Na: Sodium, Mg: Magnesium, Al: Aluminum, Ca: Calcium, Au: Gold, Pd: Palladium, C: Carbon).

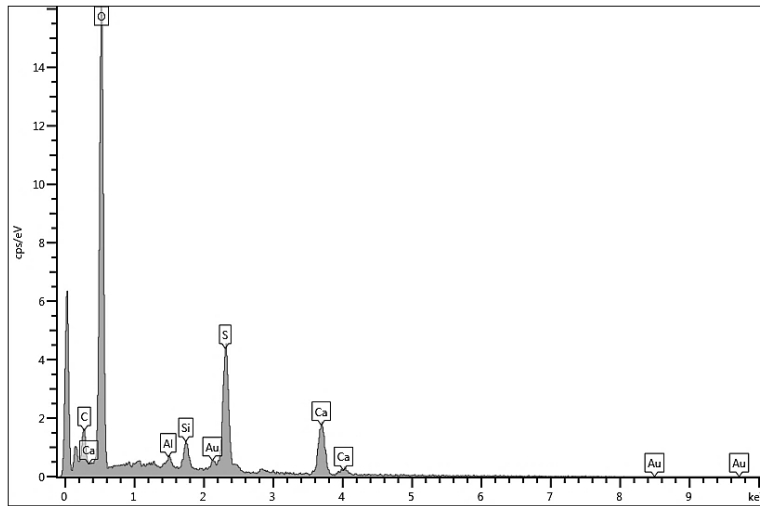
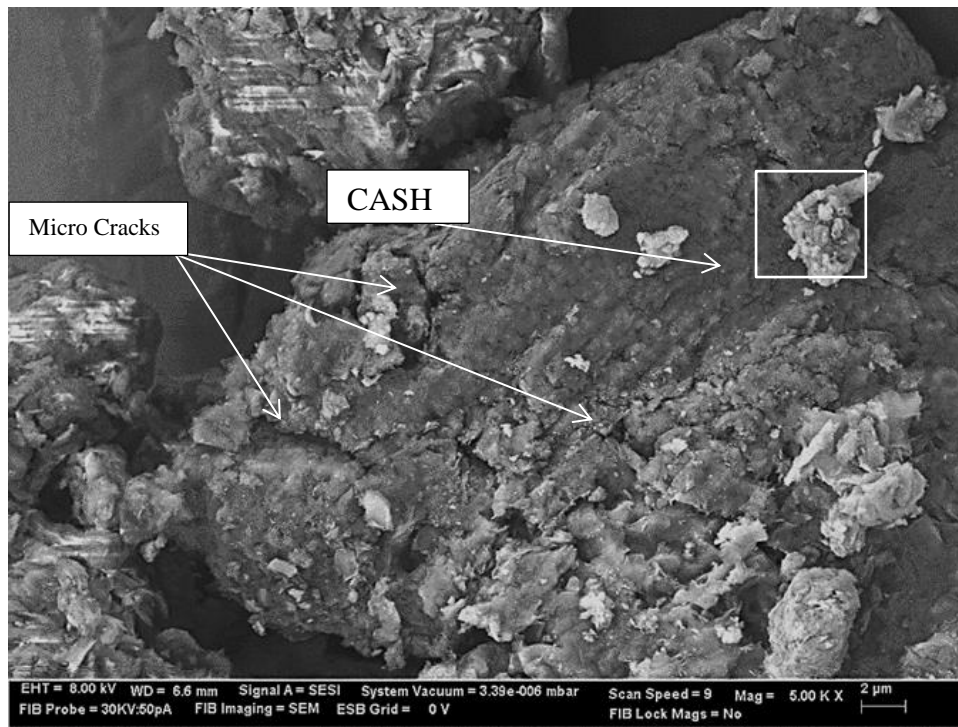


Figure 4.53 FESEM/EDAX images, B56GS6. (ETH=8.00kV, WD= 7.5 mm, Mag= 10.00 KX). (Element/compound legend: CASH= Calcium Aluminate Silicate Hydrate, Al: Aluminum, Si: Silicate, S: Sulfate, Ca: Calcium, Au: Gold, Pd: Palladium).

4.5.3.2 Kaolinite and Recycled Gypsum and Sodium Silicate Solution

Pure kaolinite was stabilized with a 6% mixture of recycled gypsum and sodium silicate solution (50%:50%). FESEM/EDAX techniques were utilized to investigate the effect of the stabilizing additives on changes in the soil microstructure after 3, 28, and 56 days of curing. The micrograph and EDAX spectrum results are presented in Figures 4.54-4.60.

In the early curing age, B3GS6, the modification of the clay surface can be observed, for example in Figure 4.54 and 4.55; however, the transformation of the source material is heterogeneous around the clay surface as the book-sheet structures are changed by the addition of the chemical stabilizers, as shown. The FESEM analysis reveals several cementation phases that co-exist in the matrix. The content of Si and Al varies in the binder system, and fabricated polymer gels are coated with sulfate ions in both specimens, which supports the idea that the stabilizers are interacting with the kaolinite minerals. This behavior can be associated with the level of alkalinity that is observed for the stabilized soil ($\text{pH} > 10$), which increase the solubility of aluminate silicate minerals. The observed modified products consist of small amounts of Na (sodium), Mg (magnesium), K (potassium), and Ca (calcium) ions. Another micrograph of the same specimen reveals a high quantity of Ca ion cementation products, implying the formation of CASH (calcium aluminosilicate hydrate), according to the EDAX spectrum; the formation of these cementation products is also supported by the observed X-ray diffraction pattern. The presence of sodium sulfate is also detected in the binder compounds that are formed. It is believed that free sodium ions in the pore solution react

with the sulfate ions, leading to an overall decrease in the quantities of free sodium ions in the system (Jun and Oh, 2015).

In the long term curing age, K28GS6, the FESEM observation of the selected specimens are shown in Figures 4.56 and 4.57. The results of images show residual clay particles surrounded by the glassy phase of geopolymers; it is these geopolymers to which the compressive strength increase is attributed. Sulfate ions are detected around the geopolymer assigned as a C(N)ASH, including some titanium ions (Ti, e.g., Figures 4.55, 4.56 and 4.58). Also, both cementation materials are covered by sulfate ions which are formed from the addition of recycled gypsum.

For K56GS, the FESEM micrographs (Figures 4.58 and 4.59) show that non-crystalline structures containing calcium and sodium ions are formed during the polymerization process. The observed geopolymer is believed to be calcium sodium aluminum silicate hydrate (CSAH), which appears to play an important role in the long-term strength gain process that occurs as a results of soil stabilization.

The second micrograph specimen is presented in Figure 4.59. This image shows kaolinite particles that are covered by the glassy phase of polymers containing sodium ions. Additionally, according to the EDAX spectrometry, dissolution of Al and Si elements from the source material is quite high compared to the previous specimens. The chemical composition of the gel phase indicates small amounts of sodium aluminosilicate hydrate (NASH).

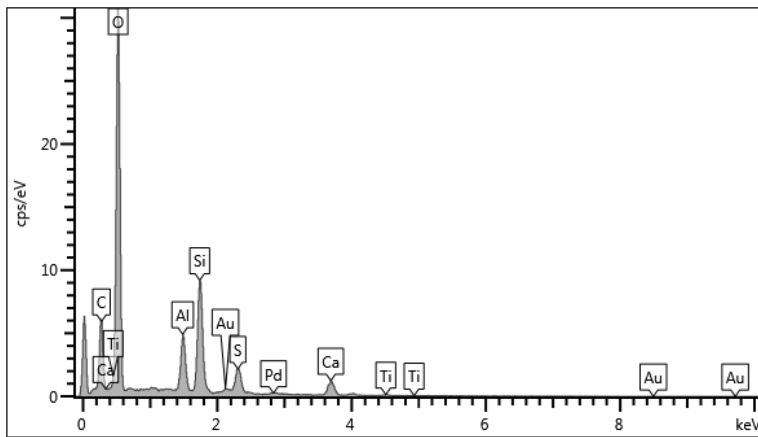
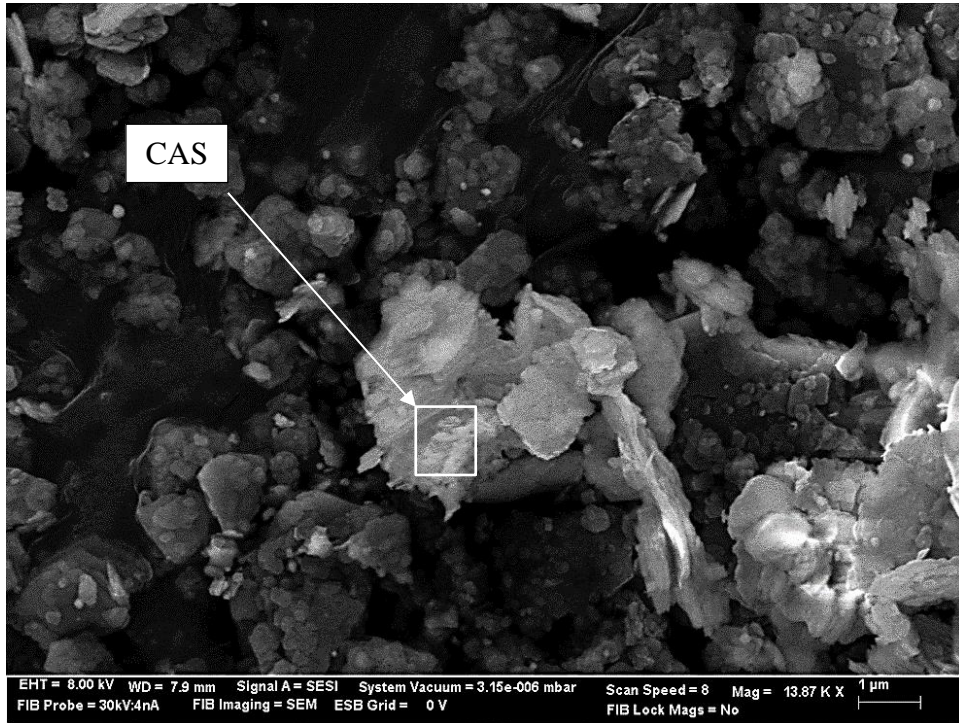


Figure 4.54 FESEM/EDAX images, K3GS6. (ETH=8.00kV, WD= 7.9 mm, Mag= 13.87 KX). (Element/compound legend= CAS Calcium Aluminate Silicate (Hydrates), Al: Aluminum, Si: Silicate, S: Sulfate, Ti: Titanium: Au Gold, Pd: Palladium).

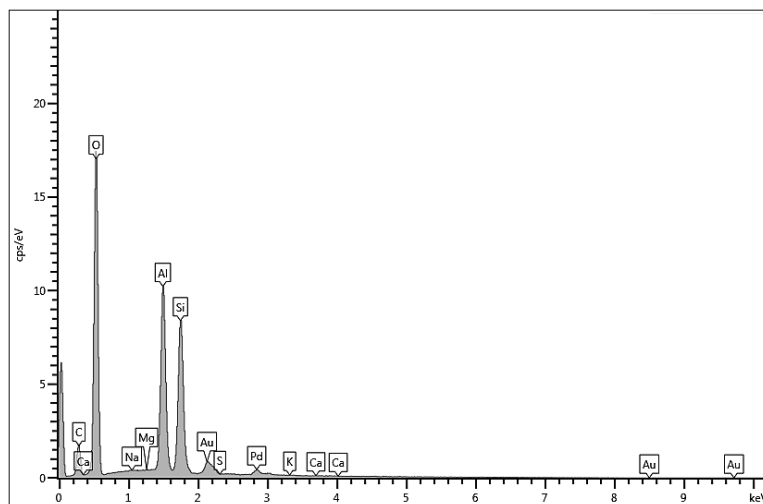
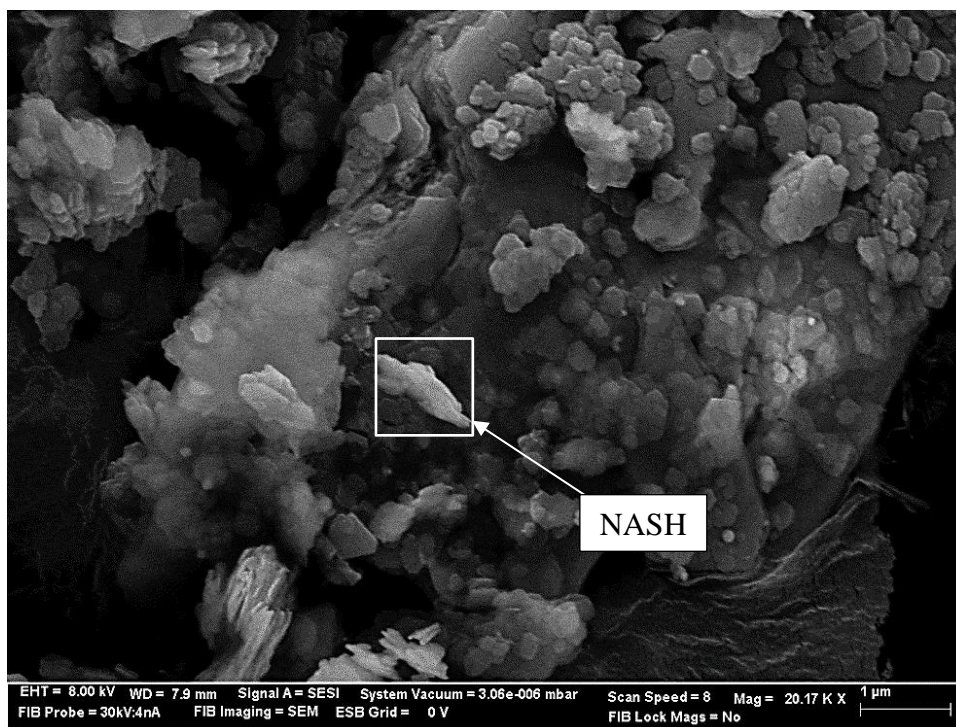


Figure 4.55 FESEM/EDAX images, K7GS6. (ETH=8.00kV, WD= 7.9 mm, Mag= 20.17 KX). (Element/compound legend: NASH= Sodium Aluminum Silicate Hydrates, Na: Sodium, Mg: Magnesium, Al: Aluminum, Si: Silicate, S: Sulfate, K: Potassium, Ca: Calcium, Au: Gold, Pd: Palladium).

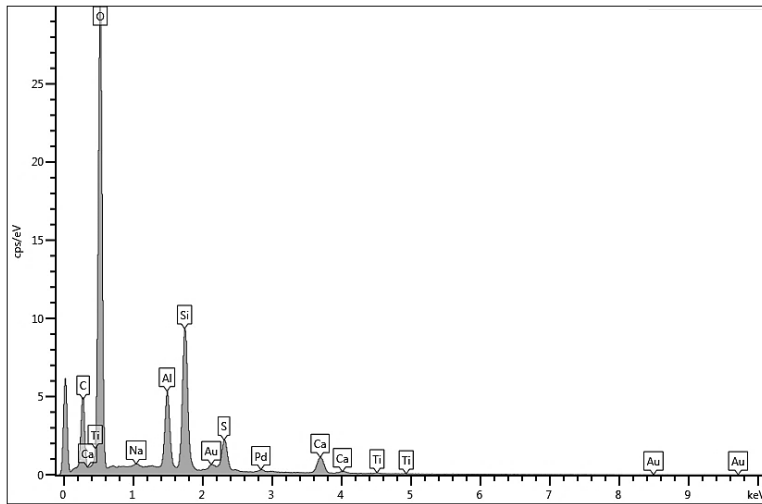
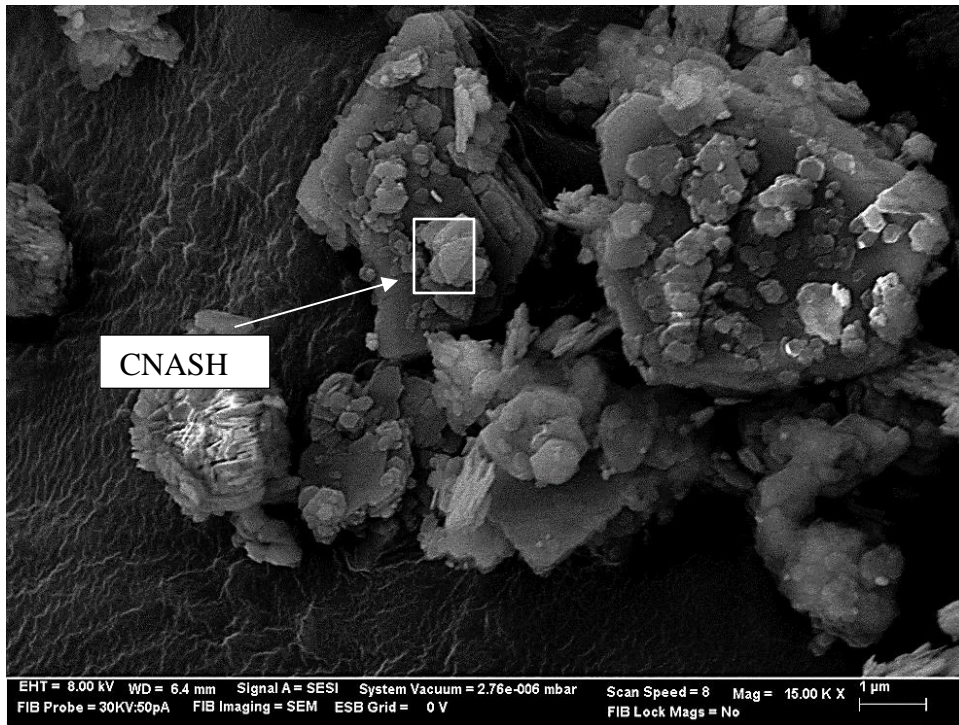


Figure 4.56 FESEM/EDAX images, K28GS6. (ETH=8.00kV, WD= 5.4 mm, Mag= 15.00 KX). (Element/compound legend: CNASH= Calcium (Sodium) Aluminate Silicate Hydrate, Na: Sodium, Al: Aluminum, Si: Silicate, Ca: Calcium. S: Sulfate, Au: Gold, Pd: Palladium).

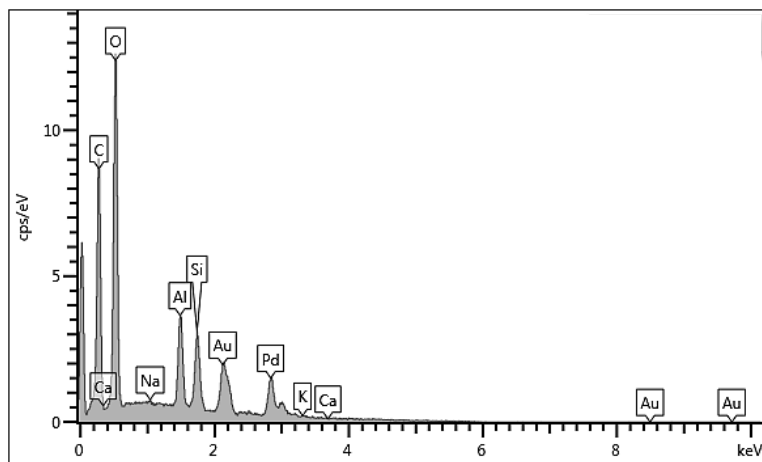
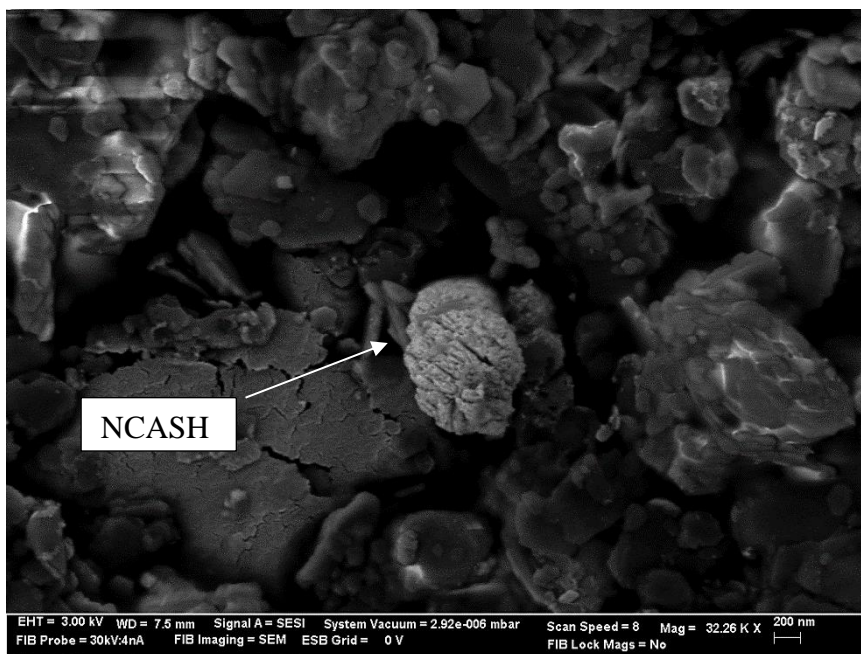


Figure 4.57 FESEM/EDAX images, K28GS6. (ETH=8.00kV, WD= 7.5 mm, Mag= 32.25 KX). (Element/compound legend: NCASH= Sodium Calcium Aluminate Silicate Hydrate, Na: Sodium, Ca: Calcium, K: Potassium, Au: Gold, Pd: Palladium).

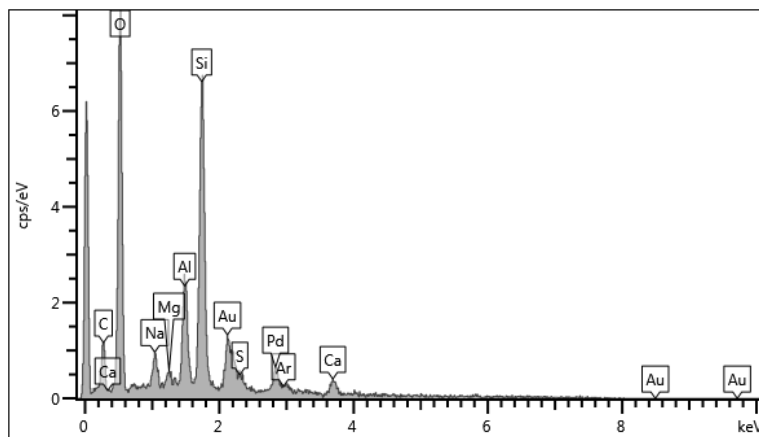
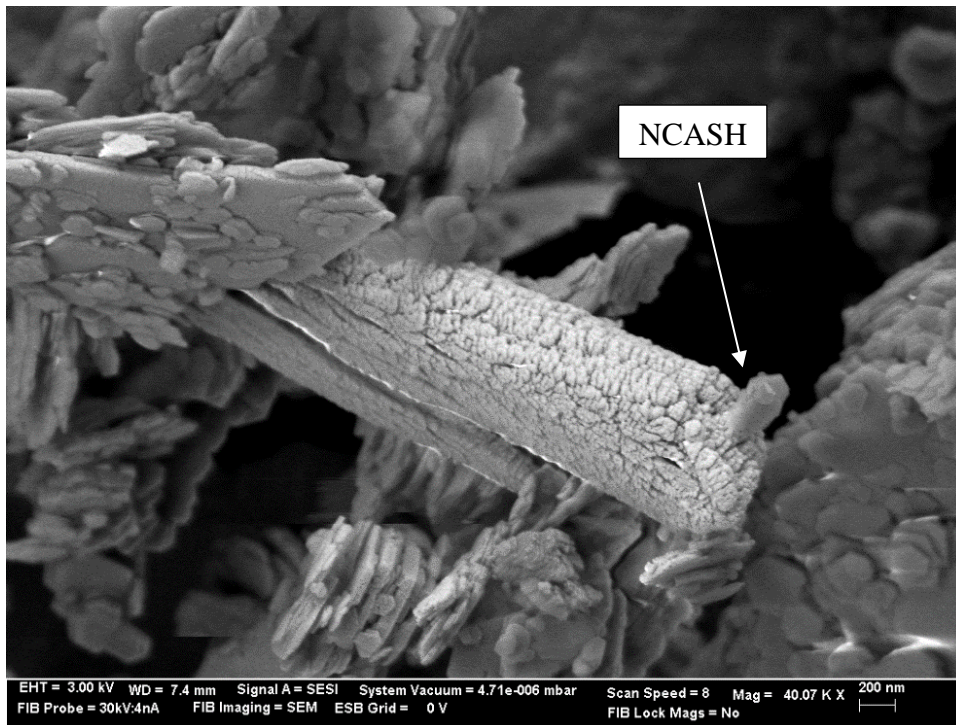


Figure 4.58 FESEM/EDAX images, K56GS6. (ETH=8.00kV, WD= 7.4 mm, Mag= 40.07 KX). (Element/compound legend: NCASH= Sodium Calcium Aluminate Silicate Hydrate, Na: Sodium, Mg: Magnesium, Al: Aluminum, Si: Silicate, S: Sulfate, Mg: Magnesium, Au: Gold, Pd: Palladium).

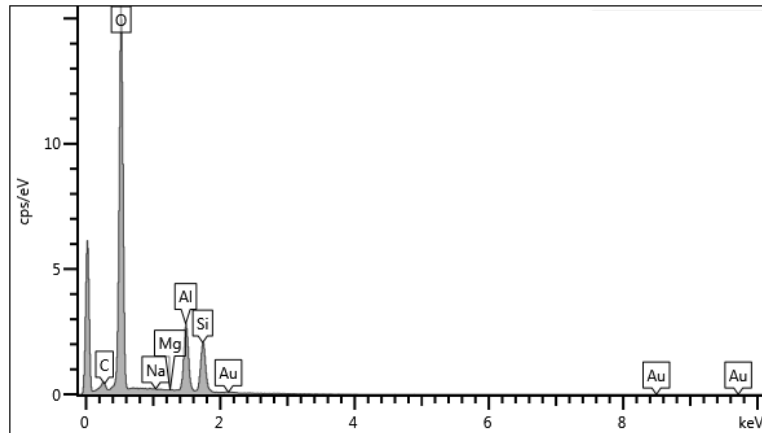
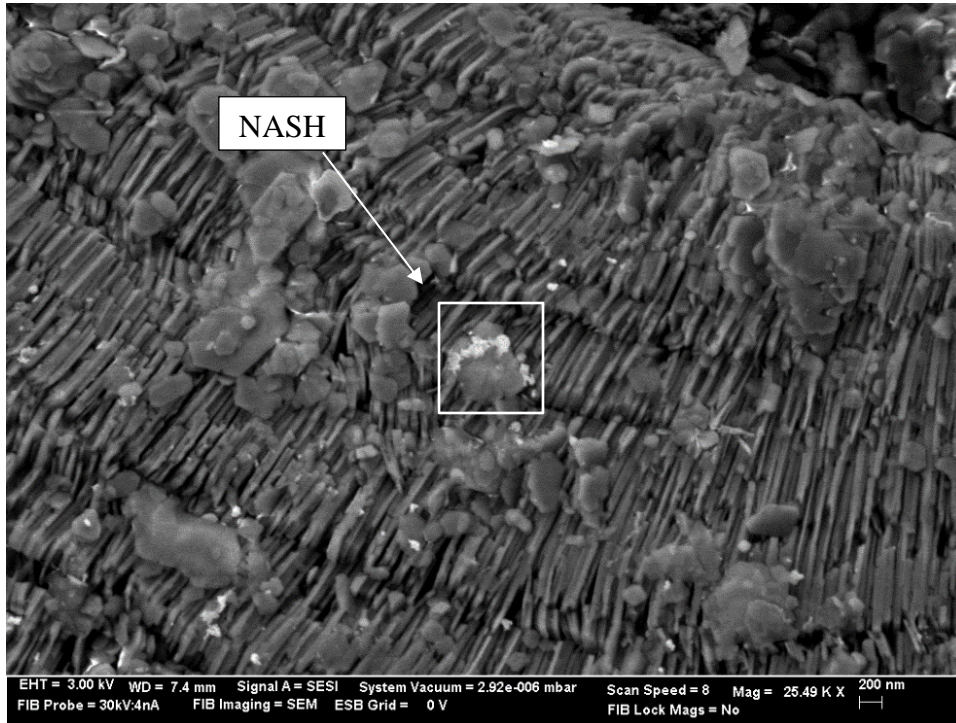


Figure 4.59 FESEM/EDAX images K56GS6. (ETH=8.00kV, WD= 7.4 mm, Mag= 25.49 KX). (Element/compound legend: NASH= Sodium Aluminate Silicate Hydrate, Na: Sodium, Mg: Magesium, Au: Gold).

4.6 FTIR Test Results of Stabilized

A series of FTIR tests were employed to determine the dominant functional groups of soil minerals for both untreated and stabilized soils in this study. The FTIR can measure the absorption bands at the characteristic wavelengths of bonds vibrating independently from one to another mineral present in the clay (Mu et al., 2014). In this study, an observed band ranging from 4000-500 cm^{-1} was examined using infrared spectroscopy.

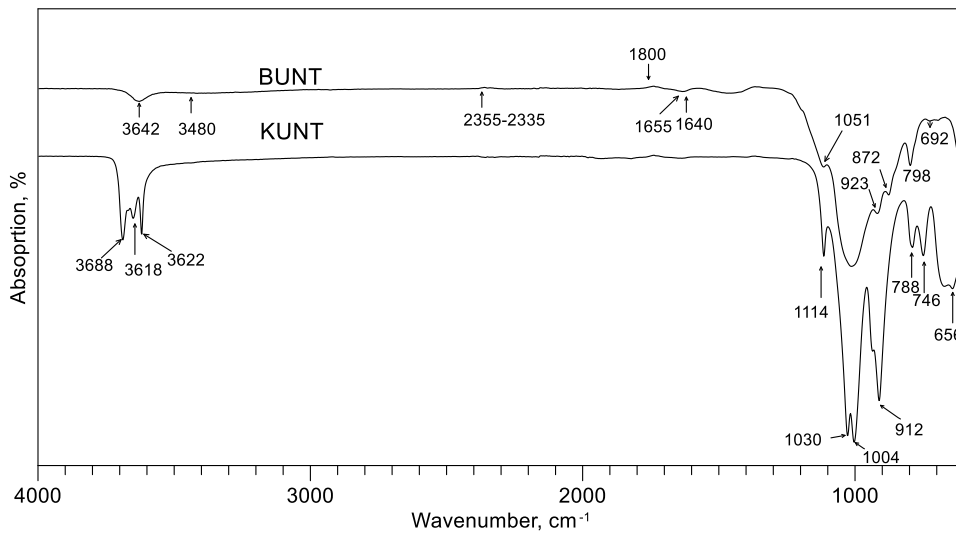


Figure 4.60 FTIR spectra of the primary absorption region in the untreated Kaolinite, (KUNT), and Bentonite (BUNT).

Figure 4.60 displays the absorption spectra of untreated bentonite (BUNT) and untreated kaolinite (KUNT). The spectrum curves of BUNT are characterized by montmorillonite with a single band at 3642 cm^{-1} that are followed by a broad weak band

between 3480-3450 cm^{-1} for OH stretching of structural hydroxyl groups and water (Madejova and Komadel, 2001). Two weak bands were detected at approximately 2335 and 2355 cm^{-1} for atmospheric CO_2 in the sample (Sahraoui et al., 2016; Pereira et al. 2017). The vibration peak in the 1640-1655 cm^{-1} range is considered to be the absorbed H-O-H mode of water (Latifi et al. 2016). For the lower wavelengths, montmorillonite shows a weak band at $\sim 1051 \text{ cm}^{-1}$ for the Si-O stretching vibration layer of silicate (Latifi et al. 2016). The FTIR peaks at 923 cm^{-1} and 872 cm^{-1} are associated with Al-OH-Al and Al-OH-Fe, respectively (Madejova and Komadel, 2001). Quartz peaks are also detected at 798 and 692 cm^{-1} , as the 400-800 cm^{-1} range is generally attributed to the Si-O bonds (Farmer, 1988).

The untreated kaolinite exhibited sharper bands than the untreated bentonite, as shown in Figure 4.60. The observed peaks at 3688 cm^{-1} , 3622 cm^{-1} , and 3618 cm^{-1} correspond to the IR spectra of the untreated kaolinite. The bands at 1114 cm^{-1} , 1030 cm^{-1} , and 1004 cm^{-1} are related to Si-O stretching vibrations in the kaolinite/halloysite, and the OH deformation of the hydroxyl groups displays at 912 cm^{-1} (Worasith et al., 2011). The existence of kaolinite is also endorsed by the Si-O vibrations at 788 cm^{-1} and 746 cm^{-1} (Madejova and Komadel, 2001; Worasith et al., 2011; Latifi et al., 2016). The band at 693 cm^{-1} is assigned to Si-O stretching vibrations corresponding to quartz, which is identified as an impurity in the XRD traces in both Worasith et al. (2011) and the present study. The presence of spectrum bands in the range of $\sim 1800\text{-}3480 \text{ cm}^{-1}$ is considered as octahedral O-H stretching vibrations.

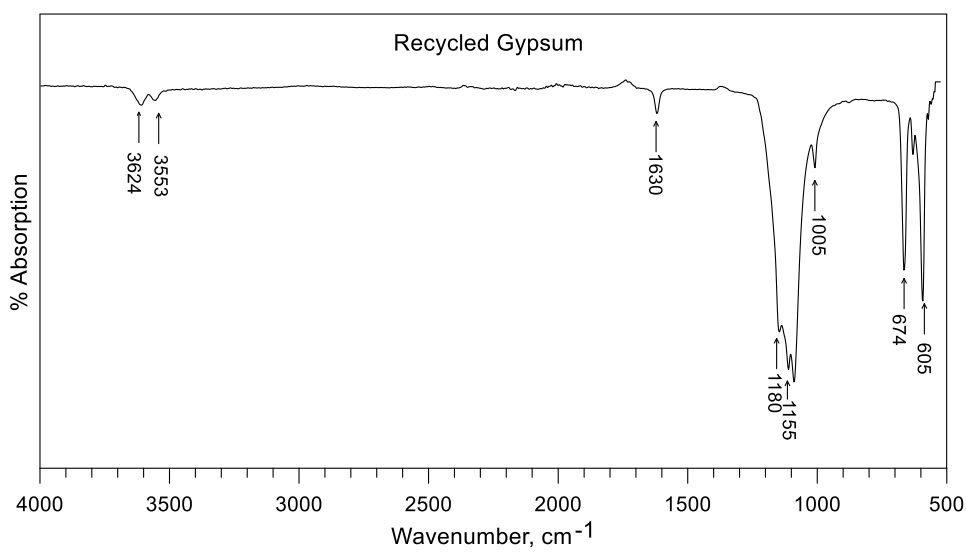


Figure 4.61 FTIR spectra of the primary absorption region in recycled gypsum.

Figure 4.61 shows the FTIR spectra of recycled gypsum between 500 and 4000 cm^{-1} wavelengths. The peaks at 3624 and 3553 cm^{-1} display H_2O stretching bonds in the recycled gypsum minerals (Bishop et al., 2014). The H_2O bending frequency appears at approximately 1630 cm^{-1} . The significant vibration band at 1000-1200 cm^{-1} is attributed to SO_4 from the recycled gypsum structure (Ca-Sulfates). Additionally, the vibration bands located at 674 and 605 cm^{-1} are assigned as the primary frequency of SO_4 in gypsum minerals at a lower wavelength (e.g., Salisbury et al., 1991; Prasad et al., 2005; Bishop et al., 2014).

4.6.1 Effect of Recycled Gypsum on Soils

4.6.1.1 Bentonite Clay and Recycled Gypsum

The FTIR spectra of the BUNT given in the previous chapter and 3% additive treated BUNT at different curing time periods, (B3G3, B3G14, and B3G28), are presented in Figure. 4.62.

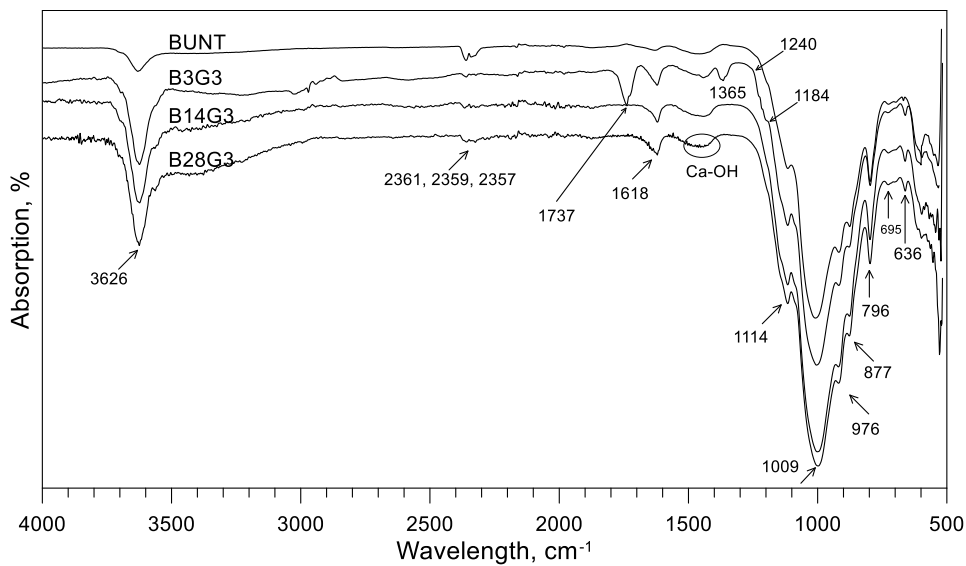


Figure 4.62 FTIR spectra of untreated (BUNT) and stabilized kaolinite with 3% recycled gypsum (BG3), at different curing times.

In the FTIR spectrum, the sequence of the spectra from montmorillonite shifts towards the higher wavelength from 3618 to 3626 cm^{-1} . Also, three bands were detected at approximately 2361, 2359 and 2357 cm^{-1} for atmospheric CO_2 in the samples, respectively (Sahraoui et al., 2016; Pereira et al., 2017). Also, there is a sharp peak located at 1737 cm^{-1} , which is the vibration frequency of carbon and oxygen according

to Hazarika et al., (2014). The wavelength of peaks at 1618, 1620, and 1630 cm^{-1} are assigned for the vibration wavelength of water (H_2O), from the recycled gypsum mixture (Bishop et al., 2014).

In B3G3, a significant new observation band was detected at around 1365 cm^{-1} that indicates that calcium ions from stabilizers bind with CO_3 to form CaCO_3 in the clay matrix (Garcia Lodeiro et al., 2008), whereas, in B14G3 and B28G3, the vibration bands at the same vibration region do not change significantly. Also, the bands of Ca-OH at 1391 and 1454 cm^{-1} are disturbed once the additive is introduced to the binder system.

Furthermore, there is a small distinction in the bands in the range of 1184-1240 cm^{-1} , associated with the vibration band of silica gel, Si-O-Si, which confirms that the aluminate silicate source materials dissolved over the curing ages. The observed band can be placed at $\sim 1114 \text{ cm}^{-1}$, corresponding to Si-O-T, (T = Si or Al), symmetrical stretching shifted lower frequencies, 1011, 1009, and 1111 cm^{-1} during the curing periods as a consequence of an alteration in the Si-O and Al-O bonds. This indicates that calcium ions may interact with the dissolved Si-Al to form CSH gels in the binder system. These results are in agreement with Andini et al. (2012) and Khater (2012).

The intensity of Al-Al-OH and Al-Fe-OH centered at 920-796 cm^{-1} was noticeably reduced with the increase of the curing time, as shown in Figure 4.62. This is due to weathering process of recycled gypsum in the clay lattice (Nacamoto, 1970). The peak at 678 cm^{-1} corresponding to Si-O stretching was transformed from a weak to intense peak as curing progressed, at the same additive content. This could be due to the

dissolution of silicate minerals, which would increase the quantity of silicon in the binder system. Moreover, the bands centered at 677 cm^{-1} for unstabilized soil shifted to a lower wavelength at 663 cm^{-1} for the 3% additive soil mixture. This spectrum region represents Si-O-Si bending bands, and is a typical band for CSH cementing products according to Garcia-Lodeiro et al., (2008).

4.6.1.2 Kaolinite Clay and Recycled Gypsum

The FTIR spectra of the KUNT and mixed with 12% additive at different curing ages, 14, 28, and 56 days are shown in Figure 4.63.

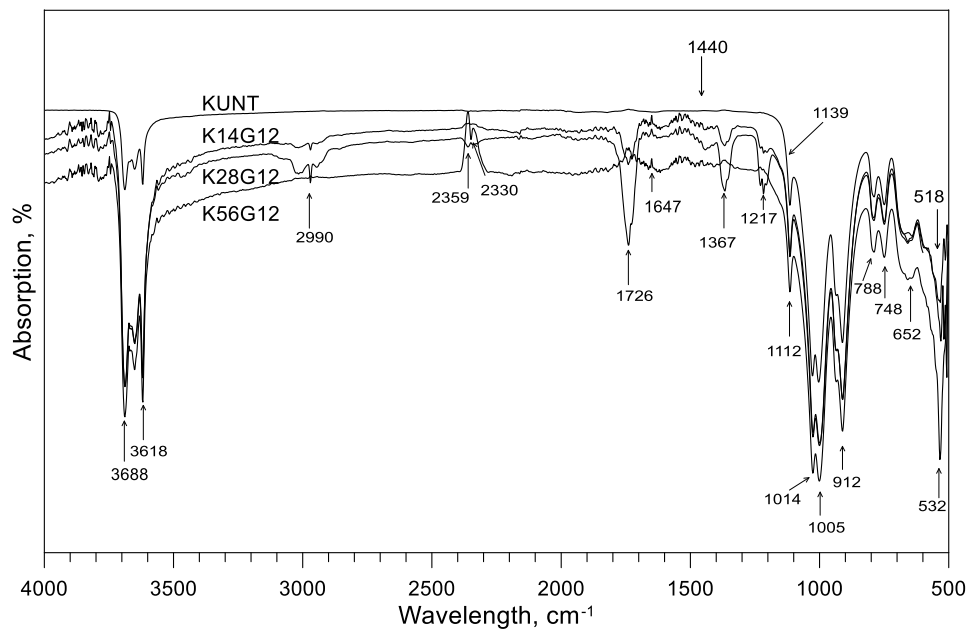


Figure 4.63 FTIR spectra of untreated (KUNT) and stabilized kaolinite with 12% recycled gypsum (KG12), at different curing times.

The bands between 3000 and 3688 cm^{-1} are assigned as the OH stretching from weak H_2O in the surface or cavities, with two sharp water vibration peaks appearing at $\sim 2990 \text{ cm}^{-1}$ after stabilization (Galan et al., 1996; Heah et al., 2012). The stabilization-induced peak at 1726 cm^{-1} is probably related to carbon-oxygen interaction in the soil matrix, and the band at $\sim 1112 \text{ cm}^{-1}$ is for the vibration of SO_4 from gypsum (Bishop et al. 2014; Hazarika et al. 2014). The vibration frequencies at 2359 cm^{-1} and 2330 cm^{-1} are possibly calcium carbonate (CaCO_3) and CO_2 , the former of which is created as a result of quick reactions between calcium ions and carbon dioxide from the air (Czuchajowski et al., 1976; Nayak and Singh, 2007; Martínez et al., 2014).

Some of the absorption bands become more intense as the curing period of treated specimens increases, due to the formation of cementation compounds. New peaks emerge between 1139 and 1440 cm^{-1} , exhibiting as either sharp or narrow shapes that can be observed at the various curing times. Two strong absorption peaks were observed at ~ 1367 and 1217 cm^{-1} , (Ca-OH vibrations), which indicate the formation of cementitious CA(S)H between the stabilizer and kaolinite (Khater, 2013; Martinez et al. 2014). The peak around 1005 cm^{-1} is associated with Si-O symmetrical stretching in tetrahedral in the gel structure, which becomes more intense after stabilization (Heah et al. 2012). This could be related to remodification of T-Si-O, where T = Al or Si, stretching band with calcium from recycled gypsum (Heah et al. 2012). Asymmetric tension groups of Si-O-Al and Al-O-Si intensively vibrating at ~ 927 and 912 cm^{-1} are shifted to a lower wavelength of about $910\text{-}902 \text{ cm}^{-1}$ as curing progresses as a result of chemical reactions between the stabilizer and additive.

Another band at 532 cm^{-1} representing Si-O-T, (where T = Al or Si) wavelengths gradually shifted to a higher vibration wavelength with the increase of curing periods at 3% additive content for B56G12. This could be due to the increase in dissolution of aluminum silicate ions, Si-O-Si/Al, in the binder, which have the $400\text{-}600\text{ cm}^{-1}$ range as as their bending vibration region; thus, CSH components are possibly manufactured. The band at 532 cm^{-1} is intensified from the $\sim 518\text{ cm}^{-1}$ wavelength that was observed in the untreated specimen due to hydrated aluminosilicate (CAS) (e.g., Garcia-Lodeiro et al., 2009 and 2011; Khater, 2013).

By increasing the curing time, the vibration bands tend to get stronger and move from a lower intensity to a higher intensity band. This behavior is due to the additives that form new cement components during the curing time, which corresponds to observed strength enhancement with increased curing time (Gao et al., 2014).

4.6.2 Effect of the Alkali Activator Liquid Sodium Silicate in Soils

4.6.2.1 Bentonite Clay and Sodium Silicate Solution

Figure 4.64 presents the FTIR spectra for untreated (BUNT) and 12% sodium silicate stabilized bentonite (BS) at 3, 7, and 14-days of curing. As shown, for the sodium silicate-stabilized bentonite, the O-H stretching vibration presents a well-defined peak at 3630 cm^{-1} that is increasingly more pronounced with curing time relative to untreated bentonite. Also, O-H stretching peaks weakly flank at around 3660 and 3620 cm^{-1} , and OH bending bands are generally in the range of $1630\text{-}1650\text{ cm}^{-1}$ (Heah

et al., 2012). Some additional activity detected at 2362 cm^{-1} indicates a reaction between calcium ions and CO_2 (potentially forming calcium carbonate), behavior which was also observed in FTIR tests on previous specimens such as KG. The vibration bands at 1442 , 1444 , and 1448 cm^{-1} became slightly more pronounced in comparison to untreated soil. This indicates that C-O, (CO_3), reacts with free calcium ions, dissolved by an alkaline activator, to form aragonite minerals (CaCO_3), indicated at 1444 cm^{-1} (e.g., García-Lodeiro et al., 2008).

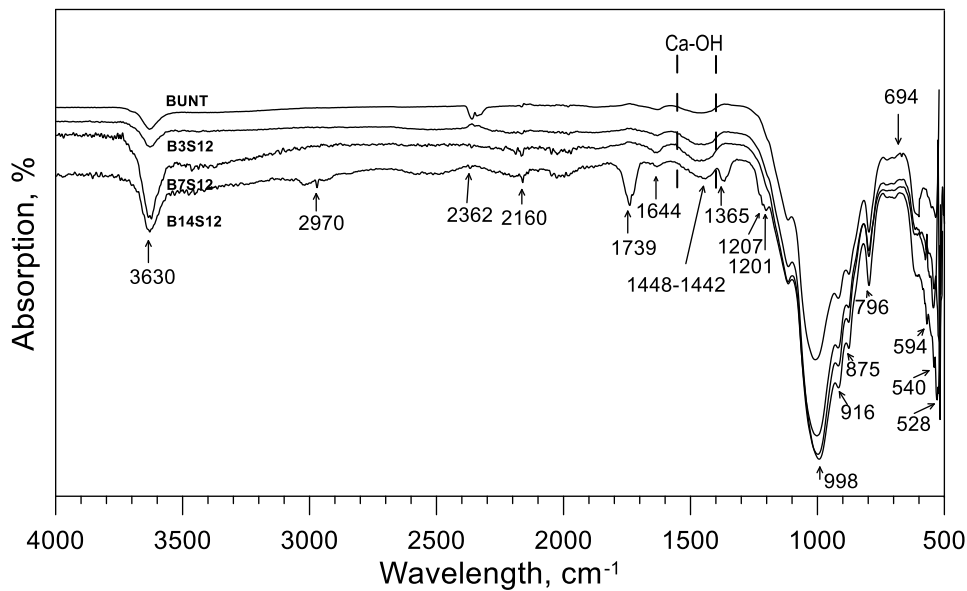


Figure 4.64 FTIR spectra of untreated (BUNT) and stabilized bentonite with 12% sodium silicate (BS12), at different curing times.

For B3S12, the observed peak at approximately 1644 cm^{-1} indicates the presence of water, O-H, bending vibrations on the aluminum silicate hydrates. It is noticed that the vibration bands become stronger as the curing time increases. New peaks appear at

$\sim 1232\text{-}1172\text{ cm}^{-1}$, the Si-enriched region making the bands more intense where NASH is possibility formed as result of alternating aluminum silicate via the presence of the alkaline solution, Na_2SiO_3 . Those new vibration bands are centered at 1201 and 1207 cm^{-1} and shifted to higher vibration frequencies compared with the untreated bentonite wavelength. The result of observed bands is generally consistent with the findings of Fernández-Jiménez and Palomo (2005) and García-Lodeiro et al., (2011); however, at the same vibration bands in B7S12 and B14S12, these wavelengths are nearly completely diminished.

The bands between 1300 and 850 cm^{-1} exhibit distinct vibration wavelengths corresponding to aluminosilicate structure of materials (Si-O-T, where T = Al or Si) (Sindhunata, 2006). With additional curing time, it appears that the vibration bands are shifted to a lower wavelength. This behaviour indicates that materials containing Al and Si are depolymerized by reacting with Ca and/or Na ions (e.g., Król et al., 2016; Kapeluszna et al., 2017). The bond at $\sim 991\text{ cm}^{-1}$ shows the alteration of the asymmetric bonds of Si-O-Si and Si-O-Al bending in the clay structure, montmorillonite, by being shifted to higher frequencies ranging from 991 to 1006 cm^{-1} over the curing periods, a phenomenon which has been confirmed by several researchers (e.g., Davidovits, 2008; Alonso and Palomo, 2001). The observed band at 904 and 906 cm^{-1} drifted higher wavelengths, 916 cm^{-1} respectively. It could be due to formation of new cementation materials. Moreover, weak absorption bands from 618-665 cm^{-1} indicate zeolites containing calcium ions (e.g., San Cristóbal et al., 2010). The band centered at 670 cm^{-1} can correspond to zeolite vibration frequencies, as reported by Chandrasekhar and

Pramada (1999), which are also indicated in the X-ray diffraction analyses by a weak peak; this appears logical, as the intensities of the observed bands are generally lower in the early curing days for the stabilized soils. It is believed that crystalline phases of geopolymers change into amorphous phases as the curing time increases.

4.6.2.2 Kaolinite Clay and Sodium Silicate Solution

Figure 4.65 presents the FTIR spectra for untreated (KUNT) and 6% sodium silicate stabilized kaolinite (KS) at 3, 7, and 56 days of curing. The FTIR spectra of the treated kaolinite characterized two major octahedral OH stretching vibration bands at 3684 and 3618 cm^{-1} . Stabilized soil reveals sharp vibration bands at 1026 and 999 cm^{-1} for Si-O-Si/Al stretching, and at ~ 925 and 912 cm^{-1} corresponding to OH deformation of hydroxly groups in the alkaline solution, which was shifted from 935 and 915 cm^{-1} . It is believed that modification of the band at 1026 cm^{-1} can be attributed to the formation of NASH, and modification of the bands at 999 and 915 cm^{-1} can be attributed to the formation of CSH. Garcia-Lodeiro et al. (2011) reported similar wavelengths for NASH and CSH via the use of an alkali activated aluminosilicate paste. The presence of kaolinite minerals are confirmed by the observed bands of Si-O at ~ 788 , 750, and 534 cm^{-1} .

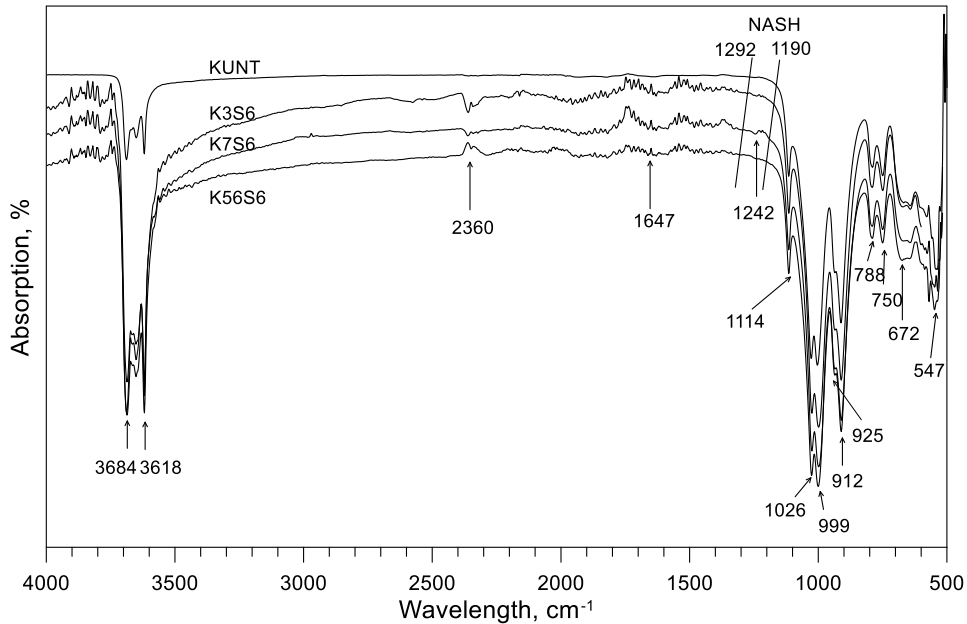


Figure 4.65 FTIR spectra of untreated (KUNT) and stabilized kaolinite with 6% sodium silicate (KS6), at different curing times.

New narrow observed bands from approximately 1292-1190 cm^{-1} in K7S6 indicate new polymerization compounds, NASH, formed over the curing ages as a result of the reaction between the source material and the sodium silicate solution, whereas other specimens reveal extremely weak vibration frequencies in the same region, which may be attributed to the degree of polymerization. It is also believed that the 989 to 1283 cm^{-1} region corresponds to Si-OH, as proposed by Uchino et al., (1991). However, the relative change of the intensities in this region is quite weak due to the low reactivity of kaolinite minerals, which means pure kaolinite resists reacting with the alkaline solution even though the band frequencies of Si-O-T, (T =Al or Si) are switched from higher values to lower ones through the polymerization process. In other words, an alkaline

solution, (Na_2SiO_3), slowly induces some modification of the pure kaolinite minerals. Therefore, due to relatively slow chemical reactions in the clay matrix, more curing time is required to develop new cementation materials.

There are also minor reductions in the intensities of the bonds at ~ 918 and 907 cm^{-1} , implying that the bending vibration of Si-O-T (where T = Al or Si) is being disturbed by the presence of the sodium silicate. The absorption bands of Si-O at $\sim 990 \text{ cm}^{-1}$ slightly shift to a lower wavenumber, $\sim 978 \text{ cm}^{-1}$, after the sodium silicate has been added into the system. This is attributed to the soluble sodium silicate content, which affects the Al or Si bonds in the source material that are dissolved by the sodium silicate solution. These bands may also be associated with the formation of a hydrated silica gel structure such as $\text{N}(\text{C})\text{AH}$, which is nondetectable in the X-ray diffraction pattern. Yu et al., (2006) and Fernández-Jiménez et al. (2011) have reported similar results with the current study. The bands at approximately 1190 cm^{-1} are also believed to be caused by the formation of different silicate gel phases in the stabilized soil matrix, but it is challenging to identify specific vibration bands in this region due to overlapping band interference and their fluctuating values.

The bands at 672 cm^{-1} complement the Si-O-Si stretching vibration of the SiO_4 tetrahedra in $\text{C}(\text{N})\text{SH}$. The reflection bands in this range ($675\text{-}600 \text{ cm}^{-1}$) change following the vibration of the Si-O-Si bonds, corresponding to reconstruction of the SiO_4 tetrahedra after specimens have been treated using Na_2SiO_3 . A similar vibration frequency of SiO_4 has been proposed by Garbev et al., (2007) and Paiste et al., (2016). The vibration band at 1647 cm^{-1} that is present in all of the specimens is attributed to O-

H bending vibrations that appear when water is present around calcium aluminate silicate hydrates (e.g., Yu et al., 1999).

4.6.3 Effect of Recycled Gypsum and Liquid Sodium Silicate in Soils

FTIR spectra analysis was used to assess different interactions between the stabilizers and clay materials at various curing ages. The stabilized soil was selected depending on the strength development process in Figures 4.66 and 4.67 for bentonite and kaolinite specimens, respectively. Both stabilized soils resulted in the improvement in strength at 3 and 6% admixture (50%:50%) of recycled gypsum and sodium silicate solution, (Na_2SiO_3).

4.6.3.1 Bentonite Clay with Recycled Gypsum and Sodium Silicate Solution

Stabilized bentonite specimens with 6% admixture were investigated using FTIR spectrometry analysis after 7, 14, and 56 days of curing, and the results are presented in Figure 4.66. As shown, the vibration band at $\sim 3624 \text{ cm}^{-1}$ corresponds to H-O-H stretching vibrations in clay, which reduces slightly from 3629 cm^{-1} as a result of the soil stabilization. There is a broad band reduction at $\sim 3500\text{-}2950 \text{ cm}^{-1}$ due to OH stretching as this region, which indicates the presence of water observed on the clay surface or captured in the pore space. Two absorption bands at ~ 2358 and 2328 cm^{-1} appear after stabilization, and are attributed to the reaction between CO_2 and calcium ions in the clay lattice during the test, behavior which has been observed over all specimens. H-O-H bending bands have been observed by other researchers from ~ 1590

to $\sim 1632 \text{ cm}^{-1}$ in untreated and stabilized systems (e.g., Khater, 2012; Bishop et al., 2014; El- Alfi, 2016).

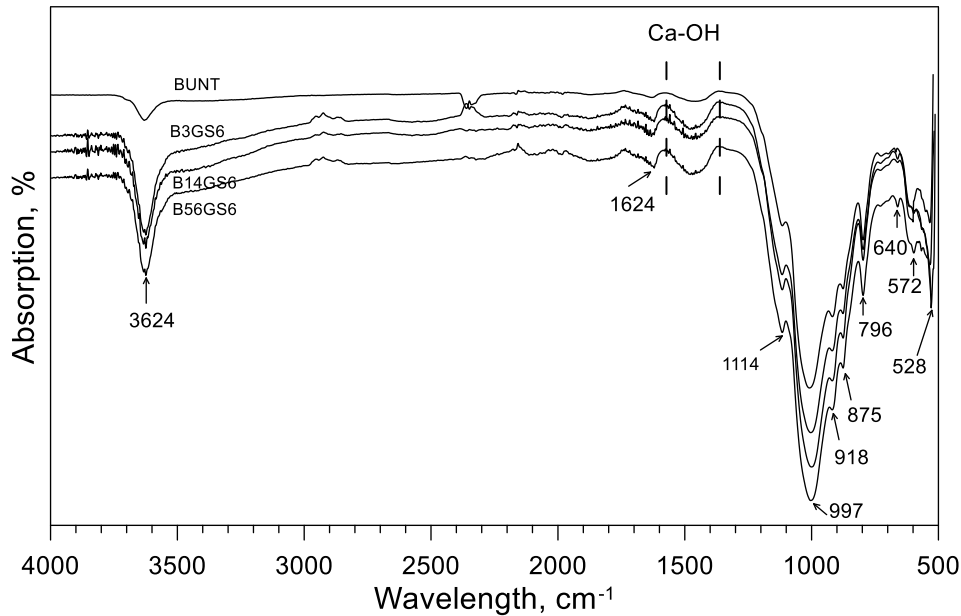


Figure 4.66 FTIR spectra of untreated (BUNT) and stabilized bentonite with 6% mixture (50:50) of recycled gypsum and sodium silicate (BGS6), at different curing times.

One of the significant changes in the FTIR spectra occurred between ~ 1267 and 1568 cm^{-1} . The bending band frequency located at $\sim 1462 \text{ cm}^{-1}$ indicates the vibration Ca-OH, as reported by Garcia-Lodeiro et al. (2009). Ca-OH reacts with the sodium silicate solution to accelerate the formation of amorphous or crystalline CSH or CASH; this in turn causes a water deficiency in the mixture and the level of the alkalinity to increase (Khater, 2012). The band around 920 cm^{-1} is attributed to the asymmetrical stretching vibration of Si-O-T (where T = Al or Si) bonds that exist in the aluminum

silicate sources, and the band placed at lower frequency, 918 cm^{-1} , is assigned as the deformation vibration frequency. This spectra is a characteristic spectra associated with the formation of C(A)SH gel structures in a calcium rich environment, according to Garcia-Lodeiro et al. (2011) and Fernández-Jiménez et al. (2011). For CSH types of geopolymer, two double tiny peaks are typically formed at around 657 cm^{-1} and 660 cm^{-1} (Garcia-Lodeiro et al. (2008) reported these peaks at 660 and 654 cm^{-1}). The wavelength of those bands slightly increases over the curing time relative to each other. Therefore, it is believed that the increased intensity of the band from 550 to 950 cm^{-1} could confirm the presence of fabricated polymeric gel structures, as indicated by the XRD and FESEM tests. Also, it is believed that the change of wavelength is proof of changes in the mineralogical structures of the clay (e.g., Worasit et al., 2011; Latifi et al., 2014).

4.6.3.2 Kaolinite Clay with Recycled Gypsum and Sodium Silicate solution

Stabilized kaolinite specimens with 6% admixture were investigated using FTIR spectrometry analysis after 7, 28, and 56 days of curing, and the results are presented in Figure 4.67. A broad band at 3572 and 1623 cm^{-1} in the spectrum of the stabilized kaolinite is attributed to water hydration in the clay lattice. Hydroxyl groups of OH bending bands in the treated kaolinite occur at ~ 3684 and 3618 cm^{-1} , and are observed to shift slightly as the curing process progresses. The bending bands at ~ 2359 and 2326 cm^{-1} correspond to the reaction products of calcium ions and free CO_2 in the air, as noted previously (e.g., Nayak and Singh, 2007; Martínez et al., 2014). Detection of a

possible CSH bending vibration peak at $1124\text{-}1205\text{ cm}^{-1}$ is indistinguishable owing to the weak vibration wavelength at this location, however the vibration band at $\sim 1645\text{ cm}^{-1}$ is believed to be H-O-H bonds in the hydrated compounds, possibly CASH, which are fabricated by the addition of sodium silicate and recycled gypsum. Similar behavior was observed by Susan et al. (2011), who performed studies on sodium silicate slag mortar.

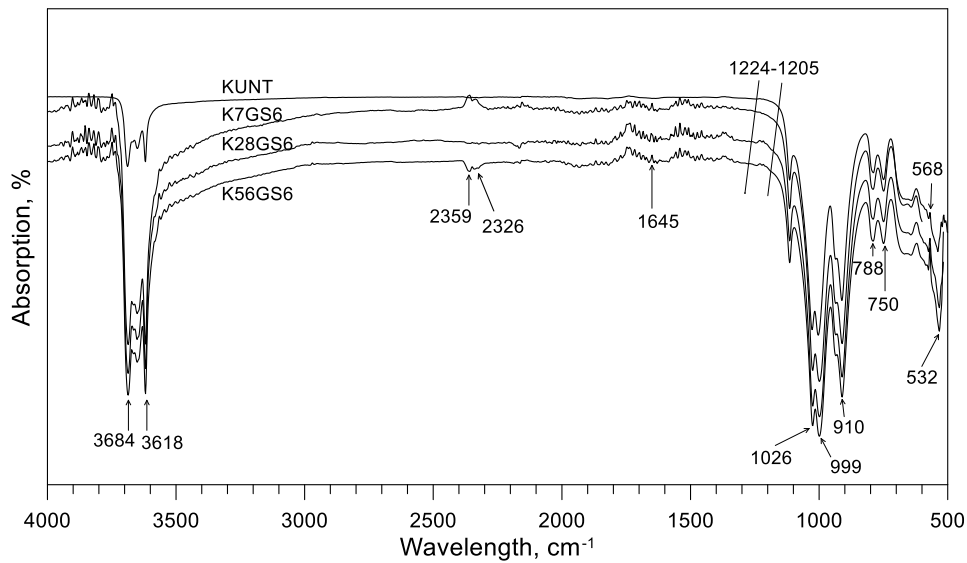


Figure 4.67 FTIR spectra of untreated (KUNT) and stabilized Kaolinite with 6% mixture (50:50) of recycled gypsum and sodium silicate (KGS6), at different curing times.

At lower wavelengths, changes in the stabilized kaolinite can be observed clearly during the curing ages. Other researchers have reported that the asymmetric stretching bands Si-O-T (where T is Al or Si within the CSH) generally appear around $900\text{-}1250\text{ cm}^{-1}$ (e.g., Karge, 1998; Khater, 2012). The band at $\sim 1114\text{ cm}^{-1}$ is

characterized by the asymmetric stretching wavelength of Si-O-Si, and the band at ~788 cm⁻¹ is attributed to symmetric stretching of the Si-O-Si (silica gels). The bands at 1028 and 1004 cm⁻¹ exhibited a shift in behavior to the higher frequency from ~ 1004 and 991 cm⁻¹, respectively. These band shifts indicate modification of Si-O-T (where T=Al or Si) stretching vibrations via the formation of silica gel, as a result of reactions between the stabilizing additives and base soil. The Si-O bands become stronger after the base soil is modified by the addition of the stabilizers. This behavior of the vibration band is more typical of the primary wavelength in N(C)ASH (Garcia-Lodeiro et al. 2011). The wavelength of 568 cm⁻¹ could be related to vibration of Al-O, possibly due to the presence of sodium silicate in the clay system; Tchakouté et al. (2016) proposed a similar vibration band at 573 cm⁻¹.

Note that the vibration bands of stabilized soil become more intense with increases in the curing time. A shift of certain bands towards higher vibration frequencies indicates formation of cementation materials in the system (Garcia-Lodeiro et al., 2007).

4.7 The Nitrogen-Based Brunauer-Emmett-Teller (N₂-BET) Surface Area Test Results of Stabilized Soils

In this research, the N₂-BET surface area test was conducted to assess changes in the surface area of untreated and stabilized soils, since the measurement of the specific surface area of treated soil is a significant property corresponding to the physical and chemical interactions that occur between soil particles and additives (e.g.,

Mitchell and Soga, 2005). The measured surface areas for BUNT and KUNT are 19.93 and 16.86 m²/g, respectively. N₂-BET test specimens were selected based on the maximum improvement in strength at various curing intervals. The selected N₂-BET specimens are consequently the same as those taken from the UCS test specimens for the XRD, FESEM/EDAX, and FTIR tests.

4.7.1 Effect of Recycled Gypsum on Soils

Surface area values of soils stabilized using recycled gypsum were measured for bentonite specimens B3G3, B14G3, and B28G3, and for kaolinite specimens K14G12, K28G12, and K56G12. The results of N₂-BET surface area for gypsum-stabilized bentonite and kaolinite are shown in the following two figures, respectively.

N₂-BET results for untreated and recycled gypsum stabilized bentonite after 3, 14 and 28 days of curing are presented in Figure 4.68. As shown, a significant reduction in the surface area of stabilized bentonite is evident within 3-days of curing. Based on the test results, the surface area of the stabilized samples slightly decreases with additional curing time beyond the 3-day mark. This behavior could be related to continuous chemical reactions occurring between the soil and additive, which cause the formation of cementation materials. The results of the N₂-BET analysis support the hypothesis that new cementation compounds tend to fill the void space between the clay particles. Hence, it can be concluded that one of the main reasons for the enhancement of the strength of soil is the cementation products that are formed in the clay void space.

Similar results of the N₂-BET analysis for untreated and recycled gypsum stabilized kaolinite for 14, 28 and 56 days of curing are depicted in Figure 4.69. As shown, a considerable reduction in the surface area of stabilized soil is observed after 14 days of curing. Additional curing beyond 14 days generally yielded no significant additional change in surface area. In other words, a time-dependent reduction in the surface area likely does not occur beyond the 14-day mark.

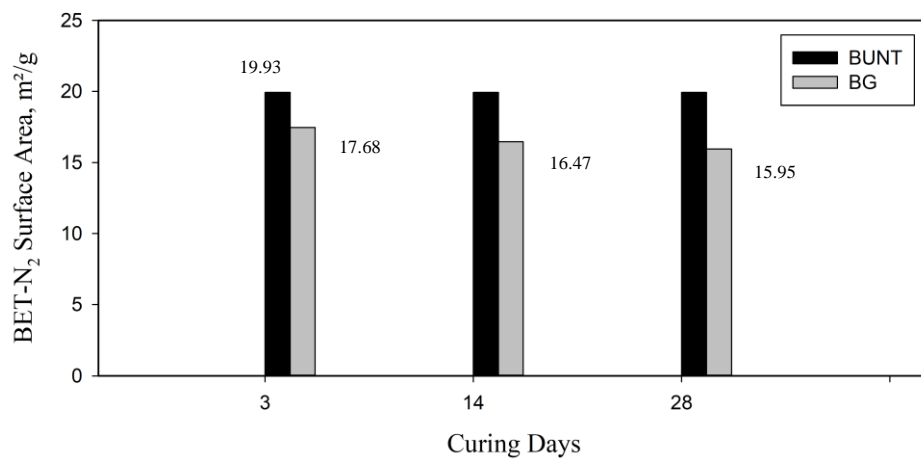


Figure 4.68 N₂-BET results for untreated (BUNT) and stabilized bentonite with 3% recycled gypsum (BG3), at different curing times.

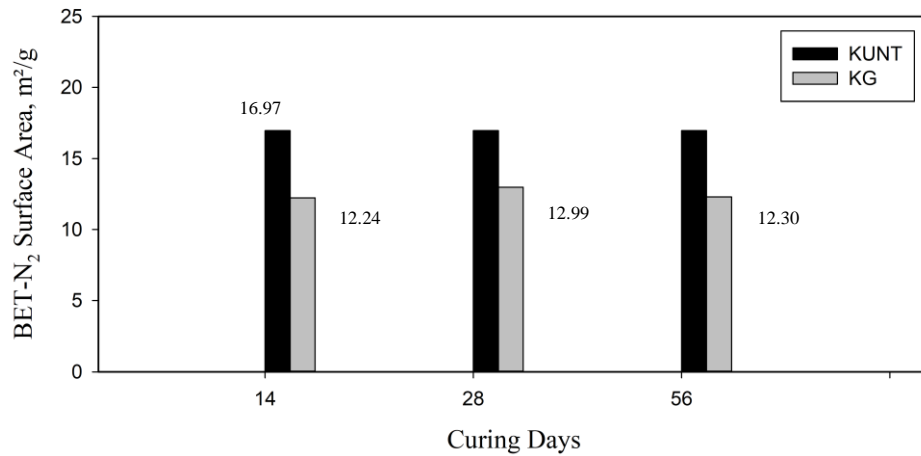


Figure 4.69 N₂-BET results for untreated (KUNT) and stabilized kaolinite with 12% recycled gypsum (KG12), at different curing times.

4.7.2 Effect of Sodium Silicate Solution on Soils

Changes in the surface area of sodium silicate stabilized bentonite and kaolinite are presented in Figure 4.70 and 4.71, respectively. The test specimens were selected based on the maximum improvement in strength. Tested specimens are B3S12, B7S12, and B14S12 for bentonite, and K6S3, K6S7, and K6S56 for kaolinite.

Figure 4.70 shows that the results of the N₂-BET analysis for untreated and 12% sodium silicate stabilized bentonite at 3, 7, and 14 days of curing. As shown, a substantial reduction in the external surface area was measured after 3-days of curing. Further curing from the 3 to 7 day mark led to a slight increase in the overall surface area of the stabilized soil. Additional curing from 7 to 14 days led to a slight decrease in the overall surface area, back to a level that was slightly less than what was observed at the 3 day mark. These findings imply that cementitious material filling of the void

space in the clay lattice does occur (and plays a role in enhancing the strength). However, the N₂-BET results imply that much of the pore space infilling that occurs happens within the first 3 days of curing. In general, these findings are consistent with the UCS test results.

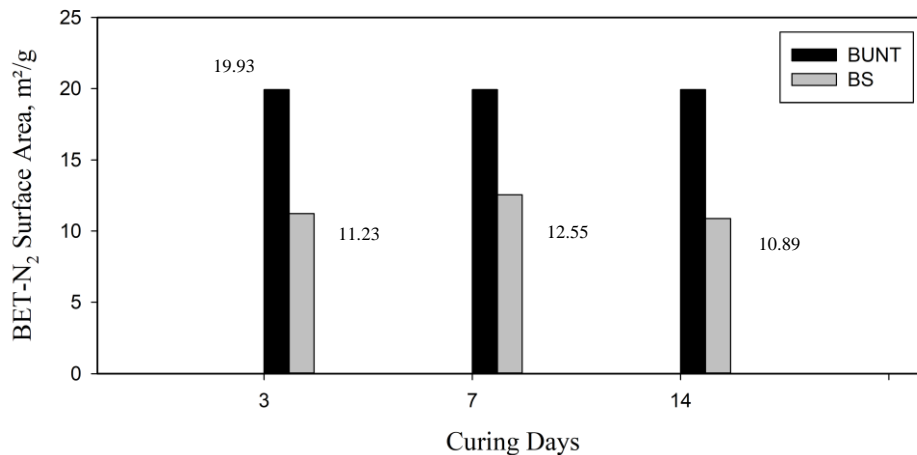


Figure 4.70 N₂-BET results for untreated (BUNT) and stabilized bentonite with 12% sodium silicate solution (BS12), at different curing times.

The N₂-BET test results for untreated and 6% sodium silicate stabilized kaolinite at 3, 7, and 56 days of curing are presented in Figure 4.71. As shown, a significant reduction in the surface area is observed after 3-days of curing. The surface area decreases slightly from 3 to 7 days of curing, and then remains stable from 7 to 56 days of curing. This data indicates that most of the pore-space infilling related reactions that occur happen between 0 and 3 days of curing, and that this reaction process is nearly completed by the 7-day curing point.

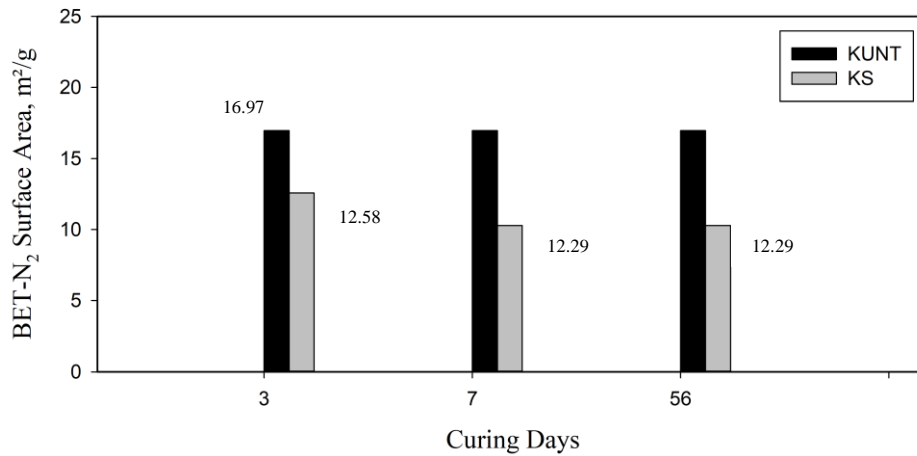


Figure 4.71 N₂-BET results for untreated and stabilized kaolinite with 6% sodium silicate solution samples (KS6), at different curing times.

4.7.3 Effect of Recycled Gypsum and Sodium Silicate Solution on Soils

The surface area of stabilized kaolinite and bentonite samples were assessed at 3, 14, and 56 days of curing intervals with a 6% admixture of recycled gypsum and sodium silicate solution (50%:50%) for bentonite, and at 7, 28 and 56 days of curing with a 6% admixture of recycled gypsum and sodium silicate solution (50%:50%) for kaolinite.

The results of surface area values are presented in Figure 4.72 for bentonite treated by a 6% content of admixture BGS at 3, 14 and 56 days of curing. The combination of recycled gypsum and sodium silicate solution tends to decrease the external surface area of the stabilized bentonite slightly after 3-days of curing. After 14 days of curing, stabilized specimens showed an increase in surface area, to a larger surface area than what was observed for the untreated specimens. After 56 days of

curing, the surface area decreased slightly again, to a level that was fairly close to the 3-day curing value. The increasing increment of the external surface area that was observed at 14 days of curing could be attributed to the decomposition of the clay surface during curing. There is sufficient time to weather the surface of clay particles, allowing new pore spaces to develop, though filling of these voids by cementation has not yet had sufficient time to occur. This hypothesized behavior is supported by the FESEM image analyses that were performed, as decomposition of clay particles is clearly indicated at 14-days of curing, as shown in Figures 4.50 and 4.51 (and also at earlier stages of curing, as shown in Figure 4.48). Time-dependent changes in soil microstructure are significant for bentonite treated by an admixture of recycled gypsum and sodium silicate. Consequently, for bentonite clay it is believed that longer curing times are beneficial for filling in the void space in the clay lattice by fabricated cement materials.

The results of the N₂-BET analysis for untreated and a 6% admixture of recycled gypsum and sodium silicate treated kaolinite (KGS) at 7, 28 and 56-days of curing are shown in Figure 4.73. As shown, the external surface area of the treated kaolinite reduces significantly from 0 to 7 days of curing, and then in slight additional increments from 7 to 28 and 28 to 56 days of curing. This could be due to low reactivity features of kaolinite minerals.

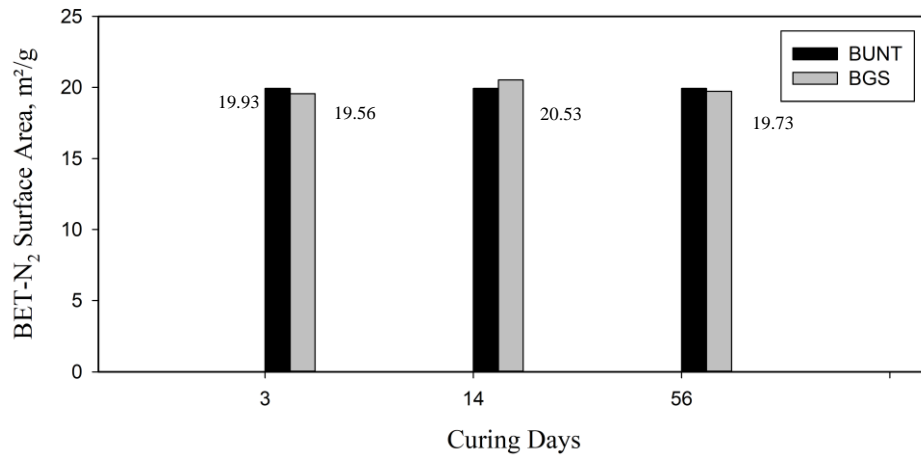


Figure 4.72 N₂-BET results for untreated (BUNT) and stabilized bentonite with a 6% admixture (50:50) of recycled gypsum and sodium silicate (BGS6), at different curing times.

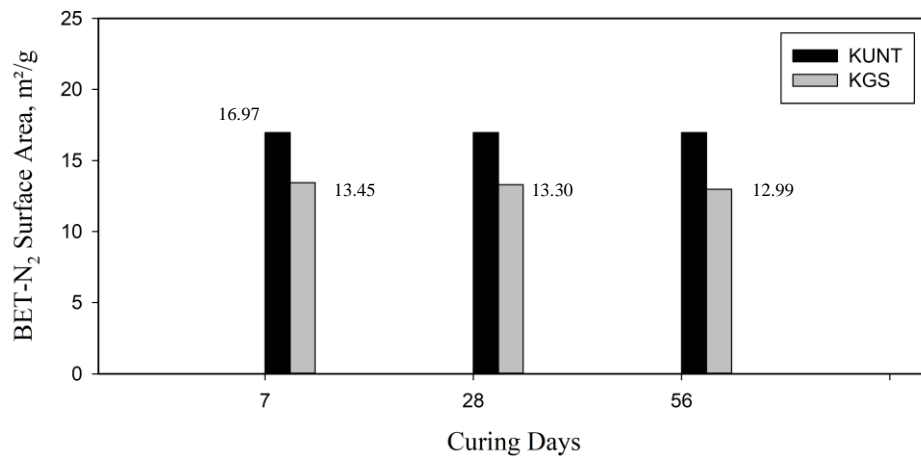


Figure 4.73 N₂-BET results for untreated (KUNT) and stabilized kaolinite with a 6% admixture (50:50) of recycled gypsum and sodium silicate (KGS6), at different curing times.

Chapter 5

SUMMARY AND CONCLUSIONS

In this research, a series of laboratory tests were performed to determine the strength development of bentonite and kaolinite clays blended with various quantities of: (1) 100% recycled gypsum, (2) 100% sodium silicate, in solution form, and (3) a 50%:50% combination of recycled gypsum and sodium silicate. These stabilizers were explored as sustainable “low carbon” additives that can be used to ensure significant strength gain in poor quality stabilized clay soils via geopolymer stabilization; it is envisioned that they can be used in place of traditional soil stabilizers such as lime and Portland cement. In this study, bentonite and kaolinite clays were stabilized with varying additive contents and cured in humidity controlled box and temperature-controlled room. Standard Proctor compaction tests were used to identify the ideal moisture content and density for treated specimen preparation. The enhancement of strength was analyzed utilizing UCS tests and supporting pH tests were utilized to look at the acidity/alkalinity during the stabilization reaction process. Additional microstructural test techniques including X-ray diffraction (XRD), FESEM/EDAX, FTIR, and N₂-BET surface area analysis were utilized to explore changes to soil microstructure that occurred during the post-stabilization curing process. General conclusions from this study are as follows:

Based on the initial pH values of untreated samples, the tested bentonite has an alkaline environment, and the tested kaolinite has an acidic environment. The bentonite soil immediately became more acidic once the recycled gypsum was added in the soil

(i.e., at the 0-day curing point), but the level of acidity was then decreased with curing time to levels that were significantly more alkaline than the initial value. The reduction in acidity of stabilized bentonite is attributed to the gradual exchange of the monovalent ions of soil and the calcium ions of the recycled gypsum. Somewhat different behavior has been observed as a result of mixing recycled gypsum and kaolinite clay, with the soil becoming more alkaline immediately (i.e., at the 0-day curing point), and then continuing to get more alkaline from there.

The effect of sodium silicate on the acidity level of both soils is significant since the acidity of the soils decreases considerably as soon as the stabilizer is added. Both soils immediately reach a similar level of pH regardless of curing time, after which the increase of the pH is noticeably limited. This phenomenon accelerates the dissolution/transformation of the aluminum silicate source (i.e., from the base clay material that is being stabilized) to form new cement compounds during the curing periods. It should be noted that the alkalinity level that was encountered with sodium silicate stabilization (i.e., $\text{pH} > 10$) was appropriate for the development of cementing compounds such as geopolymers, as an alkaline pH level increases geopolymer aggregation on the surface of the clay particles.

The admixture of recycled gypsum and sodium silicate solution has a different impact on the level of alkalinity of both soils. The pH of the kaolinite specimens is higher than the pH of bentonite specimens. Bentonite treated with the admixture increase the level of acidity until 7-days of curing; then it decreases importantly until 14 days of curing and reaches the lowest pH level, which could be related to slow

dissolution rates of calcium and sodium ions in the binder. Beyond 14-days of curing, the initial level of pH gradually increases for the varying additive contents. This is due to dissolution of the recycled gypsum, and sodium silicate is releasing more calcium and sodium ions which react with silicate ions in the binder. However, the change of pH level is not significant with varying admixture contents in the soil.

The level of alkalinity is immediately increased as a result of stabilization process and stayed almost at the same level over the curing times. However, the level of pH is slightly reduced after 14-days of curing. Additionally, the increment of the initial pH value is rather low after the admixture is introduced into the soil. This could be due to low reactivity of kaolinite minerals, which react slowly with the stabilizers.

The compaction behavior of treated bentonite and kaolinite clays at the different proportions of recycled gypsum and sodium silicate was assessed using a Standard Proctor compaction approach. The dry unit weight and optimum water content of stabilized bentonite and kaolinite act similarly in response to stabilization. The dry unit weight of the stabilized soils decreases slightly, and the optimum moisture content increases slightly with increasing amounts of recycled gypsum in the soil. This could be attributed to calcium ions from recycled gypsum altering granular particles in the soil. Additionally, recycled gypsum has a lower specific gravity compared with the soil. Therefore, the weight of pure soils reduces with the increase in the proportion of recycled gypsum.

Compaction tests on sodium silicate stabilized soils reveal noticeable effects of the stabilizer on the measured compaction behavior. The optimum moisture content of

bentonite-sodium silicate mixtures at different stabilizer contents increased, and roughly stays at the same level percentage for all admixture contents. The unit dry weight of the soil and stabilizer reduces significantly with the increase of sodium silicate content in the soil. However, the change in the dry density after addition of sodium silicate is rather small. Similarly, varying the ratio of sodium silicate in the soil leads to a reduction in the dry unit weight of kaolinite. The change in the dry unit weight of stabilized kaolinite is relatively small with additional increases of the stabilizing additive. Increases in sodium silicate increased the optimum moisture content of kaolinite for the same compaction effort. The observed changes between low and high content stabilizer ratios are rather small.

The admixture of recycled gypsum and sodium silicate decreased the unit weight of bentonite, significantly initially and then more gradually with increasing stabilizer quantities. Additionally, the optimum moisture content of stabilized bentonite increased and tended to stay steady with additional increases of the admixture content in the soil. Similarly, the kaolinite clay reveals a noticeable reduction in the dry density and increase in the optimum moisture content at different additive ratios under the same compaction effort. However, the pattern of decrease in the dry unit weight is similar to what was observed for bentonite stabilization, and the increment in the optimum moisture content also follows along in a similar fashion. Higher contents of stabilizers correspond to smaller change in water content and fairly uniform reduction in the dry unit weight. Overall, the reduction in the dry unit weight is attributed to the particles

possibly forming a more flocculated and aggregated structure due to rapid cation replacement in the binder mixture.

Based on the compressive test results, the strength development in this research depends on the type of soils which results in enhancing different strength values during the curing periods even though the strength of treated bentonite and kaolinite clays with a different ratio of recycled gypsum considerably improved. For the recycled gypsum (only) stabilized clays, high performance was obtained with a lower additive content (6%) for bentonite, whereas kaolinite needed a higher additive content (12%). Also, the effect of curing times for both soils are significant regarding strength gain perspective. Kaolinite-recycled gypsum mixture in high content, 12%, reveals sustainable strength improvements in short and long-term curing ages, though the lower content of recycled gypsum depicts maximum strength development in the early age of curing for bentonite clay. Moreover, the strength fluctuates during the curing intervals for the bentonite-recycled gypsum mixture. Thus, it is challenging to propose an optimum stabilization ratio for bentonite clay stabilized with recycled gypsum. For instance, the strength regained effectively in 28-days of curing by 6% additives, while in 3-days of curing, the maximum strength development was obtained by adding 3% additive in bentonite clay.

The use of a sodium silicate (only) solution augmented the performance of the tested bentonite and kaolinite. The most sustainable improvement in strength was obtained with a high content of sodium silicate, 12%, in the first 14-days of curing for bentonite stabilized sodium silicate solution. This could be due to the fast reaction between bentonite and the sodium silicate solution. It is noted that in zero-day curing,

the strength improved significantly at a low stabilizer content, which is significant for the quick strength development that is required for geotechnical engineering projects. Beyond 14 days, the strength development was diminished all of the proposed stabilizer (sodium silicate) ratios. This is probably related to the excess of liquid sodium silicate, which created gel formations that decreased effective contact between particles and/or caused microcrack formation in the stabilized soil system. Kaolinite, in contrast, needed a lower content (6%) of sodium silicate to develop the maximum strength compared with the bentonite-sodium silicate mixture. Curing time was also important up to 7 days (early curing ages); then the strength was lessened until 28-days of curing. After further curing ages (56 days), the strength was regained to the maximum strength that was developed among the tested kaolinite clay. It is noted that adding more sodium silicate into kaolinite clay inhibited the enhancement of strength, which could be due to the amount of unreacted sodium silicate inducing surface reactions between gel and clay particles in the soil matrix. It is evident that the type of soil plays an important role to develop strength since bentonite requires higher sodium silicate ratios (12%), but kaolinite sufficiently improves its strength at lower (6%) sodium silicate ratios.

The effect of the admixture of sodium silicate solution and recycled gypsum corresponding to strength development noticeably relies upon the type of the soils in this research. Kaolinite clay reveals more consistent results in comparison to stabilized bentonite specimens at the same additive content. Nevertheless, the maximum enhancement of the strength was obtained at a 6% additive ratio (50%:50%) by mass for both soil types. Higher contents of admixture (more than 6%) tended to decrease the

strength in any age of curing for the bentonite and kaolinite clays. This could be attributed to unreacted silica gel or an undesirable pH environment encouraging the dissolution of aluminate silicate source materials and fabrication of cementitious compounds in the binders since an excessive amount of sodium silicate gels prevents the other additives from effectively reacting and binding together. Both types of soils can be efficiently treated by adding up to 6% admixture for the long-term stabilization process.

The strength of the stabilized bentonite immediately increases until 3-days of curing. Further curing of specimens caused to reduce overall strength in 7-days of curing, but beginning from 14 days of curing strength was regained. This could be associated with low level of pH value, which starts rising (to $\text{pH} > 10$) after 14-days of curing; this accelerates the dissolution of aluminum clay sources. Thus, it is believed that by increasing the dissolution of the source material in highly alkaline environment new cementation compounds can be formed which augment the strength of bentonite. For kaolinite clay, the same content of admixture (6%) yields a sustainable improvement in the strength of the kaolinite at both short or long curing intervals compared with the stabilized bentonite specimens. Most of the significant strength gain occurred in first 7-days of curing. Afterwards, the improvement in strength is rather confined but continuously increased up to 56-days of curing.

The strength development and the initial pH values of the stabilized specimens yielded results that generally agreed with each other in this research.

The XRD diffraction patterns of stabilized bentonite and kaolinite confirm the formation of crystalline compounds such as CAS, CSH, NAS, and C(N)ASH. The formation of these types of cementitious compounds are believed to be the main reason behind the observed strength gain for the tested specimens. However, XRD testing is limited in that it cannot effectively detect the formation of amorphous gel structures that act as cementing agents in the diffraction pattern. In some cases, amorphous gels will appear as a slight hump in the XRD diffraction patterns, and in other cases they will be generally undetected, and other tests are warranted for their identification.

The result of XRD test shows that the reflection intensities of stabilized bentonite and kaolinite aluminum silicate minerals were slightly reduced after stabilization with recycled gypsum. This is evidence of a weathering action of the stabilizer on the clay lattice. Moreover, some new peaks emerge inside the reflection patterns of kaolinite and bentonite with increasing curing period. These peaks are characterized as CSH, (N)CASH, and CNSH for bentonite, and CASH, CAS, and CSH for kaolinite, at different locations in the reflection scan. Furthermore, after 56 days of curing the kaolinite-recycled gypsum mixture reveals a hump with a low reflection angle, which is believed to be the reflection pattern of a amorphous (gel) formation of a cementing compound.

The stabilized bentonite and kaolinite using only sodium silicate solutions exhibit new reflection peaks in the X-ray analysis. These peaks were identified as mainly NASH for the treated kaolinite at different curing times. However, reflection peaks in the lower values of 2θ angle were weakly observed. These could be associated

with the degree of crystallinity of cementation compounds (i.e., the formation of amorphous cementing agents). Moreover, new reflection peaks were not identical inside of the reflection pattern for the specimen cured for 7 days. On the other hand, the observed new reflection peaks for treated bentonite at different curing intervals and the same additive content indicated the formation of CASH, NAS, and NCASH compounds at various 2θ angles. Only the specimen cured for 7 days depicted a sharp reflection peak indicating a significant quantity of unreacted silicate in the clay lattice.

Bentonite and kaolinite clays cured with the admixture of recycled gypsum and sodium silicate (50%:50%) for different curing times revealed new reflection peaks in the diffraction patterns. The XRD analysis showed that the reflection intensities of minerals generally decreased due to a stabilizer-induced weathering process. Sharp peaks of unreacted silicate oxides were detected for all bentonite-additive admixtures at different curing times. This observation may be related to the decreasing strength pattern that was observed over a portion of the curing time in the UCS tests. The main reflection patterns of fabricated compounds are CSH, CASH and (N)CASH at several locations for the tested bentonite-stabilizer mixture. Likewise, kaolinite treated with the same content of admixture depicted new weak reflection peaks with the X-ray scans at different curing times. The unreacted silicon dioxide (SiO_2) showed a sharp reflection peak at 7 and 28 days of curing, which disappeared with further increases of curing time. The primary reflection peaks indicate the formation of CAS, NAS, NASH (including calcium ions), and CASH.

FESEM/EDAX tests was conducted in this research, in order to perform a more in-depth investigation regarding the fabricated cementation products. The results from these tests confirmed the existence of crystalline cementation products such as zeolites, and gel/polymer formations of amorphous products in the soil-stabilizer binders. Additionally, the clay surface of both types of soils was modified by stabilizers via erosion of the clay mineral surface, and the microstructural orientation of the clay particles also changed due to changes in the pore fluid chemistry which affected the diffuse double layer behavior. The transformation of clay particles and production of new cementation compounds are evident in the FESEM/EDAX test results, and these compounds are believed to augment the strength in both the short- and long-term soil stabilization process.

FESEM/EDAX test results were performed on bentonite clay treated with 3% recycled gypsum, and cured for 3, 14, and 28 days. The modification/polymerization that occurs on the surface of the clay particles was clearly observed in the FESEM/EDAX test results for the bentonite samples. Crystalline cement compounds consisting of CAS, and the gel phase of cementation products, C(N)AS were detected in the clay matrix at different curing intervals. The fabricated products may have in their chemical compositions other ions such as Fe and Mg. Moreover, some of the cementation materials were coated with sulfate ions dissolved from recycled gypsum, which displayed as having a “flaky and cloudy” appearance. This could explain the deterioration of strength that was observed with increasing curing time, behavior which

could be attributed to dissolution or transformation of recycled gypsum in the clay matrix.

Meanwhile, the kaolinite clay responded more favorably with curing time to the recycled gypsum treatment. The surface of kaolinite clays cured for 14 days exhibited a transformed structure on the clay surface, relative to untreated kaolinite minerals which had book-sheet structures in their matrix. A cementation reaction product was detected corresponding to magnesium aluminum silicate hydrate (MASH), which is believed to increase the strength of the soil, following the observations by Latifi et al. (2009). In general, the ratio of magnesium increases as a result of the dissolution of recycled gypsum and kaolinite minerals since recycled gypsum contains MgO in its chemical composition. Furthermore, by increasing curing times, the observed transformation is evident in the kaolinite-recycled binder system. Clay particles were similarly coated by sulfate ions, following the dissolution of recycled gypsum in the clay matrix.

The bentonite and kaolinite clays stabilized by 12 and 6% sodium silicate solutions, respectively, indicated clear changes in the clay structure for both types of soils. The surface of bentonite clay was consumed by the alkaline solution within 3 days of curing, which created new pockets and porous structures on the clay surface. After that, the formed voids began filling by gel formation of cementation products, such as N(C)ASH (including magnesium ions). Beyond 3 days of curing, more agglomeration and decomposition of clay surface were detected. Moreover, gel formation of new cement phases showed sodium aluminum silicate (NAS) as well as N(C)ASH (including magnesium ions). Longer curing (to 14 days) revealed cement products indicating the

crystalline phase of N(C)AS. Decomposed features on the clay particle surface were still observed, and a gel formation of new cement compounds adhered upon the side wall of clay particles consisting of sodium calcium aluminum silicate hydrates (NCASH).

The response of kaolinite minerals to alkaline solution treatment was also observed using FESEM/EDAX testing. After stabilization, the clay particles broke apart from each other, exhibited an increased occurrence of “flaky and cloudy” structures. New gel phase growths on the clay particles were also observed with increases in curing time. Additionally, the gel formation of NAS has been observed in all tested specimens; however, CAS gel was also observed in the specimen that was cured for 7 days.

The admixture of recycled gypsum and sodium silicate solution also modified both clay soil structures, as was observed in the FESEM/EDAX testing that was performed. Decomposition of existing clay mineral structures was observed in the clay lattice. New gel phases and spherical structures were also observed in the images. Infilling of the existing void structure was also observed as a result of chemical stabilization at different curing intervals, likely by gel (amorphous) formations.

The clay surface in bentonite was chemically eroded within 3 days of curing, and the formation of NCASH was also observed within that time. Also, the formation of gel was observed covering the clay particle surfaces, indicating sodium calcium aluminum silicate hydrate (NCASH) phases. After further curing time (14 days), the void space upon the clay particles increased noticeably. Additionally, a gel formation of cementation compounds was observed around the porous structures. Another image

was taken of a clay particle surface covered with CAS gel including sodium ions, yet there were still observed voids on the surface. With longer curing time, a new spherical phase of cementation products was observed on the surface, which included NCAH compounds. A fluctuating and undulating clay surface was observed, which included surface cracks and CASH compounds.

The kaolinite clay revealed new cementation phases in response to chemical stabilization using recycled gypsum and sodium silicate solution. The book-sheet structures of the kaolinite minerals were changed into flaky during the treatment periods. However, unreacted kaolinite minerals are still visible in the images even for samples cured for 56 days. However, the development of cementation products was clearly identified in the clay matrix. Crystalline, zeolite type, and gel phases of compounds indicate the formation of CAS and NAS in the clay lattice. It should be noted that the observed cementation materials exhibited some small cracks on their surface. This behavior could be due to the sample preparation technique, or possibly the heating process after the UCS test was conducted.

FTIR results of stabilized bentonite and kaolinite using additives depict the presence of new observation wavelengths with either a weak or strong intensity. These peaks emerged as a result of chemical reactions between the soil and additives, which lead to improvements in the weak engineering properties of soil.

The mixture of bentonite and recycled gypsum revealed new vibration peaks that are attributed to the formation of CAS. Also, the intensity of the Ca-OH bond of hydrated products slightly increased with the increase of curing times. CO₂ from the

atmosphere is believed to have participated in the chemical reaction process. The vibration wavelength of Si-Al-Si shifted to lower frequencies, indicating the weathering process that occurred on the additive and clay particles. Significant changes in the vibration bands between 1184 and 1240 cm^{-1} were observed at a relatively early curing age (e.g., 3 days). A new vibration peak that emerged at 663 cm^{-1} is evidence of the formation of CSH compounds.

The result of the kaolinite and recycled gypsum mixture revealed substantial changes in the vibration band. Similar to the bentonite gypsum scan pattern, CO_2 present in the air influenced the test analysis. The intense vibration bands centered at 1367 cm^{-1} and 1217 cm^{-1} indicated the formation of calcium-based hydrated silicate products (CASH), which weakened with the increase of curing times. O-H bending vibrations of hydrated materials were clearly observed at 1686 cm^{-1} . The vibration bands shifted to lower intensities at 789 and 761 cm^{-1} corresponded to the Si-O-Si stretching vibration wavelength that is commonly associated with the fabrication of CAS.

Sodium silicate stabilized bentonite and kaolinite clays presented major changes in their vibration wavelength. Bentonite blended with sodium silicate solution revealed the vibration bands of Ca-OH at 1444 cm^{-1} , a wavelength which increased with the increase of curing ages. The OH bending of hydrated products was weakly observed in all tested specimens. The bending vibration of NASH was strongly detected in the range of 1231-1172 cm^{-1} , at later curing ages (and not so much at early curing ages). The observed vibration bending bonds of Al-Si-T (where T = Al/Si) were slightly reduced due to chemical alterations of the aluminum-based materials that are present in the 1300-

850 cm^{-1} range, i.e., where the cementation compounds mostly developed. Zeolite minerals weakly vibrated at 618-685 cm^{-1} , yet the intensity of the peak was rather weak in the early curing ages.

The FTIR spectrometry of the kaolinite sodium silicate solution mixture showed significant changes in the vibration frequencies. The OH stretching vibration bond corresponding to CAH displayed at 1647 cm^{-1} like previous stabilized samples. Moreover, the observed vibration wavelength centered at 1242 cm^{-1} indicated the formation of NASH. The vibration band located 1444 cm^{-1} drifted to a somewhat lower frequency. This could be associated with the formation of N(C)AH.

The admixture of recycled gypsum and sodium silicate solution depicted less change in vibration patterns compared with other stabilized soil mixtures. Nonetheless, the change inside the vibration length could be clearly observed at several locations.

Bentonite stabilized with the combination of recycled gypsum and solution silicate presented major changes at bending vibration bands of Ca-OH, implying the formation of hydrated silicates. Also, the band that emerged at 1624 cm^{-1} was attributed to the presence of OH vibration in the hydrated silicate structures, possibility from the formation of CSH. The change in the vibration of the bond at 918 cm^{-1} is believed to correspond to the formation of CASH gel structures. New vibration peaks detected at a lower vibration wavelength of approximately 667-660 cm^{-1} are attributed to the formation of CSH.

Kaolinite stabilized with the same combination of recycled gypsum and sodium silicate showed a change in the wavelength of the FTIR spectra. The H-O bonds of

hydrated calcium silicate were observed at 1641 cm^{-1} in all of the tested samples. The change in the vibration bands at $900\text{-}1250\text{ cm}^{-1}$ weakly emerged where the compounds of NASH and CASH vibrated in response to the stretching bands of Si-O-Al/Si. The modification of Si-O-T (where T = Al-Si) bands at 1004 and 991 cm^{-1} were observed. This is evidence of a reaction between the aluminum silicate source materials and stabilizer mixture, which forms N(C)ASH. The vibration band of sodium silicate gel appeared at 568 cm^{-1} .

The results of the N_2 -BET surface area test showed the external surface area after stabilization of treated bentonite and kaolinite using recycled gypsum, sodium silicate solution, and their (50%:50%) combination. Observed results generally corresponded to the improvement in soil strength properties at different curing time intervals. However, the effect of additives varies based on the type of soil and curing period.

The admixture of bentonite and recycled gypsum N_2 -BET results showed that the external surface of bentonite treated with 3% additive noticeably decreased at an early point in the curing process. With increasing curing times, the surface area of the stabilized bentonite gradually decreased. Kaolinite stabilized with recycled gypsum (12%) also yielded a considerable initial reduction of surface area. However, after 28 days of curing, the surface area was generally the same as what had been observed initially (i.e., after the initial drop in surface area, things generally remained the same). This behavior could be the growth of new crystalline structures in the binder system. Beyond 28 days of curing, the surface area decreased to the same extent. Further curing

led to an additional reduction in the surface area of both clay soils. This is related to the continued chemical reaction between soils and stabilizer filling the porous structures in the clay matrix.

The result of stabilized bentonite and kaolinite using a 12 and 6% sodium silicate solution, respectively, revealed a significant reduction in the external surface area during the curing times. The external surface area of treated bentonite considerably reduced in the early curing time (3 days), and then it slightly increased with increases in curing age. The lowest surface area of treated bentonite was obtained within 14 days of curing, which is agreement with the UCS results. Similarly, a significant reduction in the surface area was observed in the samples of treated kaolinite in early ages of curing (i.e., 3 days). Additional curing decreased the external surface area of stabilized kaolinite further, yet the additional change in the area was rather small. Thus, the maximum reduction of the surface occurred within 7 days of curing.

N₂-BET tests were conducted on bentonite and kaolinite clays, which were both treated with a 6% admixture of recycled gypsum and sodium silicate solution (50%:50%). For the treated bentonite, the reduction of the external surface was almost nonexistent after 3 days of curing. Moreover, the surface area of bentonite treated for 14 days was observed to increase, marginally, over the untreated specimen value. This behavior could be due to the increase of voids on the clay surface as result of consumption of clay particles, or could just be natural specimen variation. With further curing (56 days), the surface area of the specimen again decreased slightly. This behavior is attributed to the slow filling of voids in the specimen with cementation

compounds. Thus, the time-dependent modification is more significant. It should be noted that the results of the N₂-BET surface area tests are in good agreement with the UCS and FESEM results.

A reduction of surface area was observed in kaolinite samples stabilized with a 6% admixture of recycled gypsum and sodium silicate solution (50%:50%). In early curing ages, the external surface was decreased, appreciably. With further curing times, an additional more gradual decrease in the surface area of the specimen continuously took place in the binder system. This is evidence that the stabilization of kaolinite clay using the admixture of recycled gypsum and sodium silicate solution is a time-dependent process. Thus, specimens that are cured for a longer time develop more cementation products filling the voids, leading to enhanced soil strength properties.

Overall, it was observed that both bentonite and kaolinite clay soils can be effectively improved by utilizing recycled gypsum and sodium silicate, respectively. Both the macro and microstructural analyses confirm the beneficial usage of either recycled gypsum and sodium silicate alone, or in combination, as low carbon non-traditional stabilizers. If used in combination, a 6% admixture of recycled gypsum and sodium silicate can be selected as an optimum additive content to improve the engineering properties of both soils tested in this study. Nevertheless, it is noticed that more time is required to improve the soil using the combination of recycled gypsum and sodium silicate solution in comparison to utilization of either of the additives by themselves for a soil stabilization research. It should be concluded that the development of cementation products (Geopolymers) and the associated improvement in the

stabilized soil strength rely on the type of clay and curing periods in this research. Further curing ages and additional detailed research regarding microstructural analysis should be investigated for a future research project including saturated macro and microstructural behavior of chemically treated soils using recycled gypsum and liquid sodium silicate as a low carbon alkaline activated geopolymer stabilization technique.

REFERENCES

- ASTM D4972-13 Standard Test Method for pH of Soils, West Conshohocken, PA, 2013, <https://doi.org/10.1520/D4972>
- ASTM D4318-17 Standard Test Methods for Liquid Limit, Plastic Limit, and Plasticity Index of Soils, West Conshohocken, PA, 2017, <https://doi.org/10.1520/D4318-17>
- ASTM D5521-5, (2006). Standard Practice for Classification of Soils for Engineering Purposes (Unified Soil Classification System). *ASTM Standard Guide*, 1–5. <http://doi.org/10.1520/D2487-11>.
- ASTM D2216-10 Standard Test Methods for Laboratory Determination of Water (Moisture) Content of Soil and Rock by Mass, West Conshohocken, PA, 2010, <https://doi.org/10.1520/D2216-10>
- ASTM D2166/D2166M-16 Standard Test Method for Unconfined Compressive Strength of Cohesive Soil, West Conshohocken, PA, 2016, https://doi.org/10.1520/D2166_D2166M-16
- ASTM D698-12e2 Standard Test Methods for Laboratory Compaction Characteristics of Soil Using Standard Effort (12 400 ft-lbf/ft³ (600 kN-m/m³)), ASTM International, West Conshohocken, PA, 2012, <https://doi.org/10.1520/D0698-12E02>
- ASTM D421–85., (2007). Standard Practice for Dry Preparation of Soil Samples for Particle-Size Analysis and Determination of Soil Constants. *ASTM Standards International*, 85(10), 1–2. <http://doi.org/10.1520/D0421-85R07.2>
- ASTM D422. (2007). Standard test method for particle-size analysis of soils: ASTM D 422. *ASTM International*, 63(Reapproved), 1–8. <http://doi.org/10.1520/D0422-63R07E02.2>
- ASTM D3663-03 (2015). Standard Test Method for Surface Area of Catalysts and Catalyst Carriers 1. *ASTM*, 92(October), 1–7. <http://doi.org/10.1520/D3663-03R15.2>
- Alan F. Rauch, Lynn E. Katz, and Howard N. Liljestrands, (2003). Evaluation of Nontraditional Soil and Aggregate Stabilizers. Project Summary Report 7-1993-s, Center for Transportation Research, University of Texas, Austin.

- Alonso, S., & Palomo, A. (2001). Calorimetric study of alkaline activation of calcium hydroxide-metakaolin solid mixtures. *Cement and Concrete Research*, 31(1), 25–30. [http://doi.org/10.1016/S0008-8846\(00\)00435-X](http://doi.org/10.1016/S0008-8846(00)00435-X)
- Ahmed, A., Ugai, K., & Kamei, T. (2011). Investigation of recycled gypsum in conjunction with waste plastic trays for ground improvement. *Construction and Building Materials*, 25(1), 208–217. <http://doi.org/10.1016/j.conbuildmat.2010.06.036>
- Ahmed, A. (2015). Compressive strength and microstructure of soft clay soil stabilized with recycled bassanite. *Applied Clay Science*, 104, 27–35. <http://doi.org/10.1016/j.clay.2014.11.031>
- Ahmed, A., & El Naggar, M. H. (2016). Swelling and geo-environmental properties of bentonite treated with recycled bassanite. *Applied Clay Science*, 121–122, 95–102. <http://doi.org/10.1016/j.clay.2015.11.011>
- Arakelyan, EA, (1986). Characteristic of determination of the physical properties of gypsum soils. *Soil Mech Found Eng* 23(1):27-29
- Ariffin, M. A. M., Bhutta, M. A. R., Hussin, M. W., Mohd Tahir, M., & Aziah, N. (2013). Sulfuric acid resistance of blended ash geopolymer concrete. *Construction and Building Materials*, 43, 80–86. <http://doi.org/10.1016/j.conbuildmat.2013.01.018>
- Arulrajah, A., Ali, M. M. Y., Ph, D., Disfani, M. M., & Horpibulsuk, S. (2014). Recycled-Glass Blends in Pavement Base / Subbase Applications : Laboratory and Field Evaluation. *Journal of Materials in Civil Engineering*, 26(7). [http://doi.org/10.1061/\(ASCE\)MT.1943-5533.0000966](http://doi.org/10.1061/(ASCE)MT.1943-5533.0000966).
- Bang, S. S., Galinat, J. K., & Ramakrishnan, V. (2001). Calcite precipitation induced by polyurethane-immobilized *Bacillus pasteurii*. *Enzyme and microbial technology*, 28(4), 404-409.
- Bakharev, T., (2005). Geopolymeric materials prepared using class F fly ash and elevated curing temperature, *Cement and Concrete Research*, 35, 6, 1224-1232.
- Bell, F. G., & Maud, R. R. (1994). Dispersive soils: a review from a South African perspective. *Quarterly Journal of Engineering Geology*, 27(Elges 1985), 195–210.

- Bishop, J. L., Lane, M. D., Dyar, M. D., King, S. J., Brown, A. J., & Swayze, G. A. (2014). Spectral properties of Ca-sulfates: Gypsum, bassanite, and anhydrite. *American Mineralogist*, 99(10), 2105–2115. <http://doi.org/10.2138/am-2014-4756>
- Boonserm, K., Sata, V., Pimraksa, K., & Chindapasirt, P. (2012). Improved geopolymerization of bottom ash by incorporating fly ash and using waste gypsum as additive. *Cement and Concrete Composites*, 34(7), 819–824. <http://doi.org/10.1016/j.cemconcomp.2012.04.001>
- Brough, A. R., & Atkinson, A. (2002). Sodium silicate-based, alkali-activated slag mortars - Part I. Strength, hydration, and microstructure. *Cement and Concrete Research*, 32(6), 865–879. [http://doi.org/10.1016/S0008-8846\(02\)00717-2](http://doi.org/10.1016/S0008-8846(02)00717-2)
- Brunauer, S., Emmett, P. H., & Teller, E. (1938). Adsorption of Gases in Multimolecular Layers. *J Am Chem Soc* 60:309-319
- Canakci, H., & Cabalar, A. F. (2003). Improvement of a Sand Matrice Using Biopolymer-Forming Bacteria. *Proc. of International conference on new developments in soil mechanics and geotechnical engineering*. Lefkose, N. Cyprus.
- Caterpillar. (2006). Introduction to Soil Stabilization. QEDQ 1229
- Chandrasekhar, S., & Pramada, P. N. (1999). Investigation on the synthesis of zeolite NaX from Kerala kaolin. *Journal of Porous Materials*, 6(4), 283–297. <http://doi.org/10.1023/A:1009632606671>
- Cheng, T. W., & Chiu, J. P. (2003). Fire-resistant geopolymer produce by granulated blast furnace slag. *Minerals Engineering*, 16(3), 205–210. [http://doi.org/10.1016/S0892-6875\(03\)00008-6](http://doi.org/10.1016/S0892-6875(03)00008-6)
- Chibowski, E. (2011). Flocculation and Dispersion Phenomena in Soils. In J. Gliński, J. Horabik, & J. Lipiec (Eds.), *Encyclopedia of Agrophysics* (pp. 301–304). Dordrecht: Springer Netherlands. http://doi.org/10.1007/978-90-481-3585-1_59
- Criado, M., Palomo, A., & Ferna, A. (2005). Alkali activation of fly ashes . Part 1 : Effect of curing conditions on the carbonation of the reaction products, 84, 2048–2054. <http://doi.org/10.1016/j.fuel.2005.03.030>
- Criado, M., Fernández-Jiménez, A., & Palomo, A. (2007). Alkali activation of fly ash: Effect of the SiO₂/Na₂O ratio. Part I: FTIR study. *Microporous and Mesoporous Materials*, 106(1–3), 180–191. <http://doi.org/10.1016/j.micromeso.2007.02.055>

- Czuchajowski, L., Duraj, S., & Kucharska, M. (1976). Vibrational studies of biquinonyl. *Journal of Molecular Structure*, 34(2), 187–196. [http://doi.org/10.1016/0022-2860\(76\)82004-2](http://doi.org/10.1016/0022-2860(76)82004-2)
- Das, B. M. (2010). *Principle of geotechnical engineering*. Stanford, CT: Cengage Learning.
- Davidovits, J., & Quentin, S. (1991). GEOPOLYMERS Inorganic polymeric new materials. *Journal of Thermal Analysis*, 37, 1633–1656. <http://doi.org/10.1007/BF01912193>
- Davidovits, J. (1994). Properties of Geopolymer Cements. *First International Conference on Alkaline Cements and Concretes*, 131–149.
- Davidovits, J. (1999). Chemistry of geopolymeric systems, terminology. In *Geopolymer* (Vol. 99, No. 292, pp. 9-39).
- Davidovits J. (2008). *Geopolymer chemistry and applications*, 2nd ed. Saint Quentin, France: Institute Geopolymere.
- Dejong, J. T., Fritzges, M. B., & Nusslein, K. (2006). Microbially Induced Cementation to Control Sand Response to Undrained Shear. *Journal of Geotechnical and Geoenvironmental Engineering ASCE* 1090-0241, 1381-1392.
- Dermatas, D. (1995). Ettringite-Induced Swelling in Soils: State-of-the-Art. *Applied Mechanics Reviews*, 48(10), 659–673. <http://doi.org/10.1115/1.3005046>
- Dombrowski, K., Buchwald, A., & Weil, M. (2007). The influence of calcium content on the structure and thermal performance of fly ash based geopolymers. *Journal of Materials Science*, 42(9), 3033–3043. <http://doi.org/10.1007/s10853-006-0532-7>
- Duxson, P., Fernández-Jiménez, A., Provis, J. L., Lukey, G. C., Palomo, A., & Van Deventer, J. S. J. (2007). Geopolymer technology: The current state of the art. *Journal of Materials Science*, 42(9), 2917–2933. <http://doi.org/10.1007/s10853-006-0637-z>
- Eisazadeh A (2010). Physicochemical behavior of lime and phosphoric acid stabilized clayey soil. Doctoral dissertation, Universiti Teknologi Malaysia, Faculty of Civil Engineering)

- Eisazadeh, A., Kassim, K. A., & Nur, H. (2012). Stabilization of tropical kaolin soil with phosphoric acid and lime. *Natural Hazards*, 61(3), 931–942. <http://doi.org/10.1007/s11069-011-9941-2>
- El-Alfi, E. A., & Gado, R. A. (2016). Preparation of calcium sulfoaluminate-belite cement from marble sludge waste. *Construction and Building Materials*, 113, 764–772. <http://doi.org/10.1016/j.conbuildmat.2016.03.103>
- Fernández-Jiménez, A., Vázquez, T., & Palomo, A. (2011). Effect of sodium silicate on calcium aluminate cement hydration in highly alkaline media: A microstructural characterization. *Journal of the American Ceramic Society*, 94(4), 1297–1303. <http://doi.org/10.1111/j.1551-2916.2010.04242.x>
- Firoozi, A. A., Guney Olgun, C., Firoozi, A. A., & Baghini, M. S. (2017). Fundamentals of soil stabilization. *International Journal of Geo-Engineering*, 8(1), 26. <http://doi.org/10.1186/s40703-017-0064-9>
- Jonkers, H. M., Thijssen, A., Muyzer, G., Copuroglu, O., & Schlangen, E. (2009). Application of bacteria as self-healing agent for the development of sustainable concrete. *Ecological Engineering*. <http://doi.org/10.1016/j.ecoleng.2008.12.036>, 3-6.
- Jun, Y., & Oh, J. E. (2015). Use of gypsum as a preventive measure for strength deterioration during curing in class F fly ash geopolymer system. *Materials*, 8(6), 3053–3067. <http://doi.org/10.3390/ma8063053>
- Galan, E., Aparicio, P., Miras, A., Michailidis, K., & Tsirambides, A. (1996). Technical properties of compounded kaolin sample from Griva (Macedonia, Greece). *Applied Clay Science*, 10(6), 477–490. [http://doi.org/10.1016/0169-1317\(95\)00041-0](http://doi.org/10.1016/0169-1317(95)00041-0)
- Garbev, K., Stemmermann, P., Black, L., Breen, C., Yarwood, J., & Gasharova, B. (2007). Structural features of C-S-H(I) and its carbonation in air-A Raman spectroscopic study. Part I: Fresh phases. *Journal of the American Ceramic Society*, 90(3), 900–907. <http://doi.org/10.1111/j.1551-2916.2006.01428.x>
- García-Lodeiro, I., Fernández-Jiménez, A., Blanco, M. T., & Palomo, A. (2008). FTIR study of the sol-gel synthesis of cementitious gels: C-S-H and N-A-S-H. *Journal of Sol-Gel Science and Technology*, 45(1), 63–72. <http://doi.org/10.1007/s10971-007-1643-6>

- Garcia-Lodeiro, I., Palomo, A., Fernández-Jiménez, A., & MacPhee, D. E. (2011). Compatibility studies between N-A-S-H and C-A-S-H gels. Study in the ternary diagram Na₂O-CaO-Al₂O₃-SiO₂-H₂O. *Cement and Concrete Research*, 41(9), 923–931. <http://doi.org/10.1016/j.cemconres.2011.05.006>
- Geiman, C. M. (2005). *Stabilization of Soft Clay Subgrades in Virginia Phase I laboratory Study*. Virginia Polytechnic Institute and State University.
- Guleria, S. P., & Dutta, R. K. (2011). Unconfined Compressive Strength of Fly Ash – Lime – Gypsum Composite Mixed with Treated Tire Chips. *Journal of Materials in Civil Engineering*, 23(AUGUST), 1255–1263. [http://doi.org/10.1061/\(ASCE\)MT.1943-5533.0000292](http://doi.org/10.1061/(ASCE)MT.1943-5533.0000292).
- Guleria, S. P., & Dutta, R. K. (2012). Effect of addition of tire chips on the unconfined compressive strength of fly ash-lime-gypsum mixture. *International Journal of Geotechnical Engineering*, 6(1), 1–13. <http://doi.org/10.3328/IJGE.2012.06.01.1-13>
- Guo, X., Shi, H., & Dick, W. A. (2010). Compressive strength and microstructural characteristics of class C fly ash geopolymer. *Cement and Concrete Composites*, 32(2), 142–147. <http://doi.org/10.1016/j.cemconcomp.2009.11.003>
- Guo, X., Shi, H., & Xia, M. (2016). Effect of different calcium resources on the reaction mechanism of geopolymer. *Cailiao Yanjiu Xuebao/Chinese Journal of Materials Research*, 30(5) (In Chinese). <http://doi.org/10.11901/1005.3093.2015.558>
- Gollapudi, U. K., Knutson, C. L., Bang, S. S., & Islam, M. R. (1995). A New Method For Controlling Leaching Through Permeable Channels. *Chemosphere*, Vol. 30, 695-705.
- Jha, B., & Singh, D. N. (2016). Fly Ash Zeolites, 78. <http://doi.org/10.1007/978-981-10-1404-8>
- Jha, A. K., & Sivapullaiah, P. V. (2015). Susceptibility of strength development by lime in gypsiferous soil-A micro mechanistic study. *Applied Clay Science*, 115, 39–50. <http://doi.org/10.1016/j.clay.2015.07.017>
- Jha, A., & Sivapullaiah, P. (2014). Role of gypsum on microstructure and strength of soil. *Environmental Geotechnics*, 4, 1–12. <http://doi.org/doi:10.1680/envgeo.13.00084>

- Jiang, N.-J., Du, Y.-J., Liu, S.-Y., Wei, M.-L., Horpibulsuk, S., & Arulrajah, A. (2009). Multi-scale Laboratory Evaluation of the Physical, Mechanical and Microstructural Properties of Soft Highway Subgrade Soil Stabilized with Calcium Carbide Residue. *Canadian Geotechnical Journal*, 46(12), 1461–1472. <http://doi.org/10.1139/t10-0>
- Hajimohammadi, A., Provis, J. L., & Van Deventer, J. S. J. (2008). One-part geopolymer mixes from geothermal silica and sodium aluminate. *Industrial and Engineering Chemistry Research*, 47(23), 9396–9405. <http://doi.org/10.1021/ie8006825>
- Hamzah, H. N., Al Bakri Abdullah, M. M., Cheng Yong, H., Arif Zainol, M. R. R., & Hussin, K. (2015). Review of Soil Stabilization Techniques: Geopolymerization Method one of the New Technique. *Key Engineering Materials*, 660(September), 298–304. <http://doi.org/10.4028/www.scientific.net/KEM.660.298>
- Han, J. (2015). *Principles and Practice of Ground Improvement*. John Wiley & Sons. <http://doi.org/10.1007/s13398-014-0173-7.2>
- Heah, C. Y., Kamarudin, H., Mustafa Al Bakri, A. M., Bnhussain, M., Luqman, M., Khairul Nizar, I., Liew, Y. M. (2012). Study on solids-to-liquid and alkaline activator ratios on kaolin-based geopolymers. *Construction and Building Materials*, 35, 912–922. <http://doi.org/10.1016/j.conbuildmat.2012.04.102>
- Hillier, S., & Ryan, P. C. (2002). Identification of halloysite (7 Å) by ethylene glycol solvation: the “MacEwan effect.” *Clay Minerals*, 37(3), 487–496. <http://doi.org/10.1180/0009855023730047>
- Holtz RD, Kovac WD. An introduction to geotechnical engineering. New Jersey: Prentice Hall; 1981.
- Hoy, M., Horpibulsuk, S., & Arulrajah, A. (2016). Strength development of Recycled Asphalt Pavement–Fly ash geopolymer as a road construction material. *Construction and Building Materials*, 117, 209-219.
- Hunter, D., 1988. Lime-included heave in sulfate-bearing clay soils. *J. Geotech. Eng.* 114 (2), 150-167.
- Huasmann, M.R. (1990). *Engineering Principles of Ground Modification*. McGraw-Hill, New York.

- Ikeda, K., 1998. Consolidation of mineral powders by the geopolymer binder technique for materials use. *Journal of the Mining and Materials Processing Institute of Japan* 114, 497-500 (in Japanese).
- Kapeluszna, E., Kotwica, Ł., Różycka, A., & Gołek, Ł. (2017). Incorporation of Al in C-A-S-H gels with various Ca/Si and Al/Si ratio: Microstructural and structural characteristics with DTA/TG, XRD, FTIR and TEM analysis. *Construction and Building Materials*, 155, 643–653.
<http://doi.org/10.1016/j.conbuildmat.2017.08.091>
- Karge HG. (1998). Characterization by infrared spectroscopy. *Microporous Mesoporous Mater.* 22:547–549
- Katz, L., Rauch, A., Liljestrand, H., Harmon, J., Shaw, K., & Albers, H. (2001). Mechanisms of Soil Stabilization with Liquid Ionic Stabilizer. *Transportation Research Record: Journal of the Transportation Research Board*, 1757(January 2001), 50–57. <http://doi.org/10.3141/1757-06>
- Kamtornkiat M., Mitchell R., & Yunping Xi. (2016). Fracture of Recycled Aggregate Concrete under High Loading Rates. *Journal of Materials in Civil Engineering*, 25(October), 864–870. [http://doi.org/10.1061/\(ASCE\)MT.1943-5533](http://doi.org/10.1061/(ASCE)MT.1943-5533)
- Kamei, T., Ahmed, A., & Shibi, T. (2013). The use of recycled bassanite and coal ash to enhance the strength of very soft clay in dry and wet environmental conditions. *Construction and Building Materials*, 38, 224–235.
<http://doi.org/10.1016/j.conbuildmat.2012.08.028>
- Khater, H. M. (2012). Effect of Calcium on Geopolymerization of Aluminosilicate Wastes. *Journal of Materials in Civil Engineering*, 24(1), 92–101.
[http://doi.org/10.1061/\(ASCE\)MT.1943-5533.0000352](http://doi.org/10.1061/(ASCE)MT.1943-5533.0000352)
- Khater, H. M. (2013). Effect of silica fume on the characterization of the geopolymer materials. *International Journal of Advanced Structural Engineering*, 5(1), 12.
<http://doi.org/10.1186/2008-6695-5-12>
- Kobayashi, M., Ahmed, A., & Ugai, K. (2013). Improvement Properties of Cohesion-Less Soil Using Recycled Bassanite. *Journal of Civil Engineering and Architecture*, 7(12), 1566–1573. Retrieved from
<http://www.davidpublishing.com/davidpublishing/Upfile/12/24/2013/2013122406241804.pdf>

- Komnitsas, K., & Zaharaki, D. (2007). Geopolymerisation: A review and prospects for the minerals industry. *Minerals Engineering*, 20(14), 1261–1277.
<http://doi.org/10.1016/j.mineng.2007.07.011>
- Khoury, N. N., Zaman, M., & Laguros, J. G. (2003). D050 the Use of Xrd Patterns To Evaluate the Compressive Strength of Stabilized Aggregates. *Powder Diffraction*, 18(2), 180. <http://doi.org/10.1154/1.1755145>
- Król, M., Minkiewicz, J., & Mozgawa, W. (2016). IR spectroscopy studies of zeolites in geopolymeric materials derived from kaolinite. *Journal of Molecular Structure*, 1126, 200–206. <http://doi.org/10.1016/j.molstruc.2016.02.027>
- Kumar, S., Kumar, R., & Mehrotra, S. P. (2010). Influence of granulated blast furnace slag on the reaction, structure and properties of fly ash based geopolymer. *Journal of materials science*, 45(3), 607-615.
- Kuttah, D., & Sato, K. (2015). Review on the effect of gypsum content on soil behavior. *Transportation Geotechnics*, 4, 28–37.
<http://doi.org/10.1016/j.trgeo.2015.06.003>
- Latifi, N., Meehan, C. L., Majid, M. Z. A., & Horpibulsuk, S. (2016a). Strengthening montmorillonitic and kaolinitic clays using a calcium-based non-traditional additive: A micro-level study. *Applied Clay Science*.
<http://doi.org/10.1016/j.clay.2016.06.004>
- Latifi, N., Rashid, A. S. A., Ecemis, N., Tahir, M. M., & Marto, A. (2016b). Time-dependent physicochemical characteristics of Malaysian residual soil stabilized with magnesium chloride solution. *Arabian Journal of Geosciences*, 9(1), 58.
<http://doi.org/10.1007/s12517-015-2100-4>
- Latifi, N., Rashid, A. S. A., Siddiqua, S., & Horpibulsuk, S. (2015). Micro-structural analysis of strength development in low- and high swelling clays stabilized with magnesium chloride solution — A green soil stabilizer. *Applied Clay Science*, 118, 195–206. <http://doi.org/10.1016/j.clay.2015.10.001>
- Latifi, N., Eisazadeh, A., & Marto, A. (2014). Strength behavior and microstructural characteristics of tropical laterite soil treated with sodium silicate-based liquid stabilizer. *Environmental Earth Sciences*, 72(1), 91–98.
<http://doi.org/10.1007/s12665-013-2939-1>

- Lee, S. L., & Karunaratne, G. P. (2007). Treatment of soft ground by Fibredrain and highenergy impact in highway embankment construction. *Proceedings of the ICE - Ground Improvement*, 11(4), 181–193.
<http://doi.org/10.1680/grim.2007.11.4.181>
- Little, D. N., Nair, S. (2009). *Recommended Practice for Stabilization of Subgrade Soils and Base Materials*. Washington, DC: The National Academies Press.
<https://doi.org/10.17226/22999>.
- Little, D. N., Nair, S., & Herbert, B. (2010). Addressing Sulfate-Induced Heave in Lime Treated Soils. *Journal of Geotechnical and Geoenvironmental Engineering*, 136(1), 110–118. [http://doi.org/10.1061/\(ASCE\)GT.1943-5606.0000185](http://doi.org/10.1061/(ASCE)GT.1943-5606.0000185)
- Madejov, J., Komadel, P., (2001). Base Line Studies of the Clay Minerals Society Source Clays: Infrared Methods. *Clay and Clay Minerals*, 49(5), 410–432.
<http://doi.org/10.1346/CCMN.2001.0490508>
- MacNaughton, R. B., Beauchamp, B., Dewing, K., Smith, R., Wilson, N., & Zonneveld, J. P. (2005). *Encyclopedia of sediments and sedimentary rocks*. Geoscience Canada (Vol. 32). <http://doi.org/10.1007/978-90-481-3585-1>
- Makusa, G. P. (2012). State of the Art Review Soil Stabilization Methods and Materials. *Journal of STATE OF THE ART REVIEW*, 1–30.
- Martínez, E. A., Tobón, J. I., & Morales, J. G. (2014). Coal acid mine drainage treatment using cement kiln dust. *Dyna*, 81(186), 87.
<http://doi.org/10.15446/dyna.v81n186.38834>
- Mehta P. K. (1973). Mechanism of expansion associated with ettringite formation. *Cem Concr Res* 3(1):1–6.
- Ming, D. W., & Boettinger, J. L. (2001). Zeolites in Soil Environments. *Reviews in Mineralogy and Geochemistry*, 45(1), 323–345.
<http://doi.org/10.2138/rmg.2001.45.11>
- Miranda-Trevino, J. C., & Coles, C. A. (2003). Kaolinite properties, structure and influence of metal retention on pH. *Applied Clay Science*, 23(1–4), 133–139.
[http://doi.org/10.1016/S0169-1317\(03\)00095-4](http://doi.org/10.1016/S0169-1317(03)00095-4)
- Mitchell, J.K., Soga, K., 2005. *Fundamentals of Soil Behavior* (3rd edition) John Wiley and Sons, New York.

- Mitchell, J.K. (1981). "Soil improvement—State-of-the-art report." *Proceedings of the 10th International Conference on Soil Mechanics and Foundation Engineering*, Stockholm, 4, 509–565
- Miller, G. A., & Azad, S. (2000). Influence of soil type on stabilization with cement kiln dust. *Construction and Building Materials*, 14(2), 89–97.
[http://doi.org/10.1016/S0950-0618\(00\)00007-6](http://doi.org/10.1016/S0950-0618(00)00007-6)
- Molenaar, (2005). Road Materials, Part I: Cohesive and Non-Cohesive Soils and Unbound Granular Materials for Bases and Subbases in Roads. Lecture notes, University of Stellenbosch and University of Delft, South Africa.
- Mohn, D. (2015). *Impact of Gypsum Bearing Water on Soil Subgrades Stabilized with Lime or Portland Cement*. Master Thesis, University of Akron.
- Mu, C. M., Pejčić, B., Esteban, L., Piane, C. D., Raven, M., & Mizaikoff, B. (2014). Infrared Attenuated Total Reflectance Spectroscopy : An Innovative Strategy for Analyzing Mineral Components in Energy Relevant Systems, 1–11.
<http://doi.org/10.1038/srep06764>
- Murayama, N., Yamamoto, H. and Shibata, J., Mechanism of zeolite synthesis from coal fly ash by alkali hydrothermal reaction, *International Journal of Mineral Processing*, 64, 1-17, (2002).
- Nacamoto, K. (1970). *Infrared Spectra of Inorganic and Coordinated Compounds*. Wiley, New York.
- Nath, S. K., & Kumar, S. (2013). Influence of iron making slags on strength and microstructure of fly ash geopolymer. *Construction and Building Materials*, 38, 924–930. <http://doi.org/10.1016/j.conbuildmat.2012.09.070>
- Nayak, P. S., & Singh, B. K. (2007). Instrumental characterization of clay by XRF, XRD, and FTIR. *Bulletin of Materials Science*, 30(3), 235–238.
<http://doi.org/10.1007/s12034-007-0042-5>
- Neville, A.M. (2012). *Properties of Concrete*, Trans-Atlantic Publications, Indian International Education, 5th edition, 856p.
- Nigussie, E. (2011). Evaluation of sodium silicate and its combination with cement/lime for soil stabilization. (Master Thesis). Addis Ababa University.

- Ozdogan, A. (2010). *A Study on the Triaxial Shear Behavior and Microstructure of Biologically Treated Sand Specimens*. Master Thesis. University of Delaware.
- Paiste, P., Liira, M., Heinmaa, I., Vahur, S., & Kirsimäe, K. (2016). Alkali-activated construction materials: Assessing the alternative use for oil shale processing solid wastes. *Construction and Building Materials*, 122, 458–464.
<http://doi.org/10.1016/j.conbuildmat.2016.06.073>
- Palomo, A. and Glasser, F. P., (1992). Chemically-bonded cementitious materials based on metakaolin, *British Ceramic Transactions Journal*, 91, 107-112.
- Palomo, A., Grutzeck, M. W. and Blanco, M. T., (1999a). Alkali-activated fly ashes: a cement for the future, *Cement and Concrete Research*, 29, 8, 1323-1329,
- Palomo, A., Blanco-Varela, M. T., Granizo, M. L., Puertas, F., Vazquez, T. and Grutzeck, M. W., (1999b). Chemical stability of cementitious materials based on metakaolin, *Cement and Concrete Research*, 29, 7, 997-1004,
- Pahir, J. W., (2001). Compositional effects and microstructure of fly ash-based geopolymers. Ph.D. Thesis, Department of Chemical Engineering, University of Melbourne, Victoria, Australia.
- Pavithra, P., Srinivasula Reddy, M., Dinakar, P., Hanumantha Rao, B., Satpathy, B. K., & Mohanty, A. N. (2016). Effect of the Na₂SiO₃/NaOH Ratio and NaOH Molarity on the Synthesis of Fly Ash-Based Geopolymer Mortar. *Journal of Geotechnical and Geoenvironmental Engineering*, 142(9), 336–344.
[http://doi.org/10.1061/\(ASCE\)GT.1943-5606.0001506](http://doi.org/10.1061/(ASCE)GT.1943-5606.0001506)
- Peethamparan, S., Olek, J., & Lovell, J. (2008). Influence of chemical and physical characteristics of cement kiln dusts (CKDs) on their hydration behavior and potential suitability for soil stabilization. *Cement and Concrete Research*, 38(6), 803–815. <http://doi.org/10.1016/j.cemconres.2008.01.011>
- Petry, T. M., & Little, D. N. (2002). Review of Stabilization of Clays and Expansive Soils in Pavements and Lightly Loaded Structures—History, Practice, and Future. *Journal of Materials in Civil Engineering*, 14(6), 447–460.
[http://doi.org/10.1061/\(ASCE\)0899-1561\(2002\)14:6\(447\)](http://doi.org/10.1061/(ASCE)0899-1561(2002)14:6(447))
- Phummiphan, I., Horpibulsuk, S., Sukmak, P., Chinkulkijniwat, A., Arulrajah, A., & Shen, S.-L. (2016). Stabilisation of marginal lateritic soil using high calcium fly

- ash-based geopolymer. *Road Materials and Pavement Design*, 629(January), 1–15. <http://doi.org/10.1080/14680629.2015.1132632>
- Prasad, P.S.R., Chaitanya, V.K., Prasad, K.S., and Rao, D.N. (2005). Direct formation of the γ -CaSO₄ phase in dehydration process of gypsum: In situ FTIR study. *American Mineralogist*, 90, 672–678.
- Provis, J. L., Lukey, G. C., & Van Deventer, J. S. J. (2005). Do geopolymers actually contain nanocrystalline zeolites? a reexamination of existing results. *Chemistry of Materials*, 17(12), 3075–3085. <http://doi.org/10.1021/cm050230i>
- Prusinski, J., & Bhattacharja, S. (1999). Effectiveness of Portland cement and lime in stabilizing clay soils. *Transportation Research Record*, 1652, 215-227.
- Puertas, F., & Fernández-Jiménez, A. (2003). Mineralogical and microstructural characterisation of alkali-activated fly ash/slag pastes. *Cement and Concrete Composites*, 25(3), 287–292. [http://doi.org/10.1016/S0958-9465\(02\)00059-8](http://doi.org/10.1016/S0958-9465(02)00059-8)
- Puppala AJ, Intharasombat N, Vempati RK (2005) Experimental studies on ettringite-induced heaving in soils. *Journal of Geotechnical and Geoenvironmental Engineering* 131(3):325–337.
- Ramakrishnan, V. (2007, September). Performance characteristics of bacterial concrete—a smart biomaterial. In *Proceedings of the First International Conference on Recent Advances in Concrete Technology* (pp. 67-78).
- Rashid, A. S. A., Latifi, N., Meehan, C. L., & Manahiloh, K. N. (2017). Sustainable Improvement of Tropical Residual Soil Using an Environmentally Friendly Additive. *Geotechnical and Geological Engineering*, 35(6), 2613–2623. <http://doi.org/10.1007/s10706-017-0265-1>
- Rauch, A. F., Harmon, J. S., Katz, L. E., & Liljestrang, H. M. (2002). Liquid Soil Stabilizers: Measured Effects on Engineering Properties of Clay. *Transportation Research Record: Journal of the Transportation Research Board*, 1787(2), 33–41.
- Rees, C. A., Provis, J. L., Lukey, G. C., & Van Deventer, J. S. J. (2007). Attenuated total reflectance fourier transform infrared analysis of fly ash geopolymer gel aging. *Langmuir*, 23(15), 8170–8179. <http://doi.org/10.1021/la700713g>

- Reig, L., Soriano, L., Borrachero, M. V., Monzó, J., & Payá, J. (2014). Influence of the activator concentration and calcium hydroxide addition on the properties of alkali-activated porcelain stoneware. *Construction and Building Materials*, 63, 214–222. <http://doi.org/10.1016/j.conbuildmat.2014.04.023>
- Ridtirud, C., Chindaprasirt, P., & Pimraksa, K. (2011). Factors affecting the shrinkage of fly ash geopolymers. *International Journal of Minerals, Metallurgy and Materials*, 18(1), 100–104. <http://doi.org/10.1007/s12613-011-0407-z>
- Rowles, M., & O'Connor, B. (2003). Chemical optimization of the compressive strength of aluminosilicate geopolymers synthesized by sodium silicate activation of metakaolinite. *Journal of Materials Chemistry*, 13(5), 1161–1165. <http://doi.org/10.1039/b212629j>
- San Cristóbal, A. G., Castelló, R., Martín Luengo, M. A., & Vizcayno, C. (2010). Zeolites prepared from calcined and mechanically modified kaolins. A comparative study. *Applied Clay Science*, 49(3), 239–246. <http://doi.org/10.1016/j.clay.2010.05.012>
- Sato, K., Fujikawa, T., & Oshikata, T. (2012). Plasterboard Recycle. Soil improvement effects bassanite derived from waste plaster boards. In: WASCON 2012 conference proceedings, 30 May-1 June 2012 Gothenburg, Sweden. Retrieved from <http://www.swedgeo.se/contentassets/0aee8ccd94704620b222156245b2d06d/k1a.-kenichi-sato-rev.pdf>
- Satee, J. (2003). Effects of Curing Periods on Sodium Silicate Stabilized Soil. The University of Malaysia, Faculty of Civil Engineering.
- Salisbury, J.W., Walter, L.S., Vergo, N., and D'Aria, D.M. (1991) Infrared (2.1–25 μm) Spectra of Minerals. 267 p. Johns Hopkins University Press, Baltimore.
- Singh, P. S., Bastow, T., & Trigg, M. (2005). Structural studies of geopolymers by ^{29}Si and ^{27}Al MAS-NMR. *Journal of Materials Science*, 40(15), 3951–3961. <http://doi.org/10.1007/s10853-005-1915-x>
- Sindhunata. (2006). *A Conceptual Model of Geopolymerisation*. Ph.D. Thesis, Department of Chemical and Biomolecular Engineering, University of Melbourne, Australia.

- Sivapullaiah, P. V., & Jha, A. K. (2014). Gypsum Induced Strength Behaviour of Fly Ash-Lime Stabilized Expansive Soil. *Geotechnical and Geological Engineering*, 32(5), 1261–1273. <http://doi.org/10.1007/s10706-014-9799-7>
- Smith, J.W., Comrie, D.C., 1988. Geopolymeric building materials in third world countries. In: Davidovits, J., Orlinski, J. (Eds.), Proceedings of the 1st Int. Conf. Geopolymer '88, vol. 1, Compiègne, France, 1–3 June 1988, pp. 89–92
- Suganya, K., Ph, D., Asce, S. M., & Sivapullaiah, P. V. (2016). Role of Sodium Silicate Additive in Cement-Treated Kuttanad Soil. *Journal of Materials in Civil Engineering*, 28(6), 1–6. [http://doi.org/http://dx.doi.org/10.1061/\(ASCE\)MT.1943-5533.0001538](http://doi.org/http://dx.doi.org/10.1061/(ASCE)MT.1943-5533.0001538)
- Sukmak, P., Horpibulsuk, S., Shen, S. L., Chindaprasirt, P., & Suksiripattanapong, C. (2013). Factors influencing strength development in clay-fly ash geopolymer. *Construction and Building Materials*, 47, 1125–1136. <http://doi.org/10.1016/j.conbuildmat.2013.05.104>
- Susan A. Bernal, Rodríguez, E. D., de Gutiérrez, R. M., & Provis, J. L. (2012). Performance of alkali-activated slag mortars exposed to acids. *Journal of Sustainable Cement-Based Materials*, 1(3), 138–151. <http://doi.org/10.1080/21650373.2012.747235>
- Tasong, W.A., (1999), “Mechanisms by Which Ground Granulated Blastfurnace Slag Prevents Sulphate Attack of Lime-Stabilized Kaolinite”, *Cement and Concrete Research*, Vol.29, pp.975-982.
- Tchakouté, H. K., Rüscher, C. H., Kong, S., & Ranjbar, N. (2016). Synthesis of sodium water glass from white rice husk ash as an activator to produce metakaolin-based geopolymer cement. *Journal of Building Engineering*, 6, 252–261. <http://doi.org/10.1016/j.jobbe.2016.04.007>
- Tingle, J., & Santoni, R. (2003). Stabilization of Clay Soils with Nontraditional Additives. *Transportation Research Record: Journal of the Transportation Research Board*, 72–84. <http://doi.org/10.3141/1819b-10>
- Tingle, J., Newman, J., Larson, S., Weiss, C., & Rushing, J. (2007). Stabilization Mechanisms of Nontraditional Additives. *Transportation Research Record: Journal of the Transportation Research Board*, 2007(1989), 59–67. <http://doi.org/10.3141/1989-49>

- Tran, T. D., Cui, Y. J., Tang, A. M., Audiguier, M., & Cojean, R. (2014). Effects of lime treatment on the microstructure and hydraulic conductivity of Héricourt clay. *Journal of Rock Mechanics and Geotechnical Engineering*, 6(5), 399-404.
- Tironi, A., Trezza, M. A., Scian, A. N., & Irassar, E. F. (2013). Assessment of pozzolanic activity of different calcined clays. *Cement and Concrete Composites*, 37(1), 319–327. <http://doi.org/10.1016/j.cemconcomp.2013.01.002>
- The OxyChem Sodium Silicate Handbook. (2003) Silicate Division, Specialty Business Group. Dallas, TX. The USA. Retrieved from: <http://www.ilyacorp.co.kr/product/pdf/silicate.pdf>.
- Turkoz, M., Savas, H., Acaz, A., & Tosun, H. (2014). The effect of magnesium chloride solution on the engineering properties of clay soil with expansive and dispersive characteristics. *Applied Clay Science*, 101, 1–9. <http://doi.org/10.1016/j.clay.2014.08.007>
- Uchino, T., Sakka, T., & Iwasaki, M. (1991). Interpretation of Hydrated States of Sodium Silicate Glasses by Infrared and Raman Analysis. *Journal of the American Ceramic Society*, 74(2), 306–313. <http://doi.org/10.1111/j.1151-2916.1991.tb06880.x>.
- USGS (2014). "Mineral commodity summaries," U.S Geological Survey, pp.38-39.
- Uo, M., Wada, T., & Sugiyama, T. (2015). Applications of X-ray fluorescence analysis (XRF) to dental and medical specimens. *Japanese Dental Science Review*, 51(1), 2–9. <http://doi.org/10.1016/j.jdsr.2014.07.001>
- Xu, H., & Van Deventer, J. S. J. (2000). The geopolymerisation of alumino-silicate minerals. *International Journal of Mineral Processing*, 59(3), 247–266. [http://doi.org/10.1016/S0301-7516\(99\)00074-5](http://doi.org/10.1016/S0301-7516(99)00074-5)
- Xu, H. (2001). *Geopolymerisation of Aluminosilicate Minerals*. Ph.D. Thesis, Department of Chemical Engineering, University of Melbourne, Australia.
- Van Jaarsveld, J. G. S., Van Deventer, J. S. J., & Lorenzen, L. (1997). Potential use of geopolymeric materials to immobilize toxic metals: Part I. Theory and applications. *Minerals Engineering*, 10(7), 659–669. [http://doi.org/10.1016/S0892-6875\(97\)00046-0](http://doi.org/10.1016/S0892-6875(97)00046-0)
- Waseda, Y., Matsubara, E., & Shinoda, K. (2011). *X-Ray Diffraction Crystallography; Introduction, examples and solved problems*. *Zhurnal Eksperimental'noi i Teoreticheskoi Fiziki*. <http://doi.org/10.1007/978-3-642-16635-8>

- Worasith, N., Goodman, B. A., Neampan, J., Jeyachoke, N., & Thiravetyan, P. (2011). Characterization of modified kaolin from the Ranong deposit Thailand by XRD, XRF, SEM, FTIR, and EPR techniques. *Clay Minerals*, 46(4), 539–559. <http://doi.org/10.1180/claymin.2011.046.4.539>
- Ye, S.L., Han, J., and Ye, G.B. (1994). *Ground Improvement and Underpinning Technologies*, 2nd ed. China Building Industry Press, Beijing.
- Yi, Y., Li, C., Liu, S., & Asce, M. (2010). Alkali-Activated Ground-Granulated Blast Furnace Slag for Stabilization of Marine Soft Clay. *Journal of Material in Civil Engineering*, 11(4), 246–250. [http://doi.org/10.1061/\(ASCE\)MT.1943-5533.0001100](http://doi.org/10.1061/(ASCE)MT.1943-5533.0001100).
- Yilmaz, I., & Civelekoglu, B. (2009). Gypsum: An additive for stabilization of swelling clay soils. *Applied Clay Science*, 44(1–2), 166–172. <http://doi.org/10.1016/j.clay.2009.01.020>
- Yu, P., Kirkpatrick, R. J., Poe, B., McMillan, P. F., & Cong, X. (2004). Structure of Calcium Silicate Hydrate (C-S-H): Near-, Mid-, and Far-Infrared Spectroscopy. *Journal of the American Ceramic Society*, 82(3), 742–748. <http://doi.org/10.1111/j.1151-2916.1999.tb01826.x>
- Zhang, Z., Wang, H., Yao, X., & Zhu, Y. (2012). Cement & Concrete Composites Effects of halloysite in kaolin on the formation and properties of geopolymers. *Cement and Concrete Composites*, 34(5), 709–715. <http://doi.org/10.1016/j.cemconcomp.2012.02.003>
- Zaliha, S. Z. S., Kamarudin, H., Mustafa, A. M., Bakri, A., Binhussain, M., & Salwa, M. S. S. (2013). Review on Soil Stabilization Techniques. *Australian Journal of Basic and Applied Sciences*, 7.

Appendix

PERMISSION LETTERS



Mehmet Sagnak <msagnak@udel.edu>

Copyright permission letter of a journal paper

Weeks, Jennifer <JWeeks@nas.edu>
To: "msagnak@udel.edu" <msagnak@udel.edu>

Thu, Jan 25, 2018 at 4:38 PM

Dear Mehmet Sagnak:

The Transportation Research Board grants you permission to use Figure 1, Figure 2, and Figure 4 from "Effectiveness of Portland Cement and Lime in Stabilizing Clay Soils," by J. R. Prusinski and S. Bhattacharja, in your Master's thesis at the University of Delaware, as identified in your request dated January 22, 2017, subject to the following conditions:

1. The citation should include the following information:

From Prusinski, J.R., and S. Bhattacharja. Effectiveness of Portland Cement and Lime in Stabilizing Clay Soils. *Transportation Research Record: Journal of the Transportation Research Board*, No. 1652, Vol. 1, Figure 1, p. 217, Figure 2, p. 217, and Figure 4, p. 218, 1999. Reproduced with permission of the Transportation Research Board.

2. None of this material may be presented to imply endorsement by TRB of a product, method, practice, or policy.
3. The authors of the paper should be contacted, if possible, to obtain permission to reproduce the table.

Every success with you thesis. Please let me know if you have any questions.

Sincerely,

Jennifer J. Weeks

Publishing Projects Manager

500 Fifth Street, NW

Washington, DC 20001

202-334-2984 | JWeeks@nas.edu | www.TRB.org

The National Academies of
SCIENCES • ENGINEERING • MEDICINE



From: Lamberton, Sharon
Sent: Monday, January 22, 2018 2:54 PM
To: Weeks, Jennifer
Subject: FW: Copyright permission letter of a journal paper

Hi Jennifer,

Forwarding is a request involving the *Record*.

Thanks!

Sharon

Sharon Lamberton | Editor
TRB | Cooperative Research Programs

slamberton@nas.edu | 240-351-0281

The National Academies of
SCIENCES • ENGINEERING • MEDICINE

From: Mehmet Sagnak [<mailto:msagnak@udel.edu>]
Sent: Monday, January 22, 2018 2:06 PM
To: Lamberton, Sharon
Subject: Copyright permission letter of a journal paper

[Quoted text hidden]

**SPRINGER NATURE LICENSE
TERMS AND CONDITIONS**

Jan 18, 2018

This Agreement between University of Delaware -- Mehmet Sagnak ("You") and Springer Nature ("Springer Nature") consists of your license details and the terms and conditions provided by Springer Nature and Copyright Clearance Center.

License Number	4271900883158
License date	Jan 18, 2018
Licensed Content Publisher	Springer Nature
Licensed Content Publication	Journal of Thermal Analysis
Licensed Content Title	Geopolymers
Licensed Content Author	J. Davidovits
Licensed Content Date	Jan 1, 1991
Licensed Content Volume	37
Licensed Content Issue	8
Type of Use	Thesis/Dissertation
Requestor type	academic/university or research institute
Format	electronic
Portion	figures/tables/illustrations
Number of figures/tables/illustrations	2
Will you be translating?	no
Circulation/distribution	<501
Author of this Springer Nature content	no
Title	Stabilization of bentonite and kaolinite clays using recycled gypsum and liquid sodium silicate
Instructor name	Mehmet Sagnak
Institution name	University of Delaware
Expected presentation date	Feb 2018
Portions	Figure 1
Requestor Location	University of Delaware Pierre S. Du Pont Hall, 127 The Green NEWARK, DE 19716 United States Attn: Mehmet Sagnak
Billing Type	Invoice
Billing Address	University of Delaware Pierre S. Du Pont Hall, 127 The Green NEWARK, DE 19716

United States
Attn: Mehmet Sagnak

Total 0.00 USD

Terms and Conditions

Springer Nature Terms and Conditions for RightsLink Permissions

Springer Customer Service Centre GmbH (the Licensor) hereby grants you a non-exclusive, world-wide licence to reproduce the material and for the purpose and requirements specified in the attached copy of your order form, and for no other use, subject to the conditions below:

1. The Licensor warrants that it has, to the best of its knowledge, the rights to license reuse of this material. However, you should ensure that the material you are requesting is original to the Licensor and does not carry the copyright of another entity (as credited in the published version).

If the credit line on any part of the material you have requested indicates that it was reprinted or adapted with permission from another source, then you should also seek permission from that source to reuse the material.

2. Where **print only** permission has been granted for a fee, separate permission must be obtained for any additional electronic re-use.
3. Permission granted **free of charge** for material in print is also usually granted for any electronic version of that work, provided that the material is incidental to your work as a whole and that the electronic version is essentially equivalent to, or substitutes for, the print version.
4. A licence for 'post on a website' is valid for 12 months from the licence date. This licence does not cover use of full text articles on websites.
5. Where '**reuse in a dissertation/thesis**' has been selected the following terms apply: Print rights for up to 100 copies, electronic rights for use only on a personal website or institutional repository as defined by the Sherpa guideline (www.sherpa.ac.uk/romeo/).
6. Permission granted for books and journals is granted for the lifetime of the first edition and does not apply to second and subsequent editions (except where the first edition permission was granted free of charge or for signatories to the STM Permissions Guidelines <http://www.stm-assoc.org/copyright-legal-affairs/permissions/permissions-guidelines/>), and does not apply for editions in other languages unless additional translation rights have been granted separately in the licence.
7. Rights for additional components such as custom editions and derivatives require additional permission and may be subject to an additional fee. Please apply to Journalpermissions@springernature.com/bookpermissions@springernature.com for these rights.
8. The Licensor's permission must be acknowledged next to the licensed material in print. In electronic form, this acknowledgement must be visible at the same time as the figures/tables/illustrations or abstract, and must be hyperlinked to the journal/book's homepage. Our required acknowledgement format is in the Appendix below.
9. Use of the material for incidental promotional use, minor editing privileges (this does not include cropping, adapting, omitting material or any other changes that affect the meaning, intention or moral rights of the author) and copies for the disabled are permitted under this licence.
10. Minor adaptations of single figures (changes of format, colour and style) do not require the Licensor's approval. However, the adaptation should be credited as shown in Appendix below.

Appendix — Acknowledgements:**For Journal Content:**

Reprinted by permission from [**the Licensor**]: [**Journal Publisher** (e.g. Nature/Springer/Palgrave)] [**JOURNAL NAME**] [**REFERENCE CITATION** (Article name, Author(s) Name), [**COPYRIGHT**] (year of publication)

For Advance Online Publication papers:

Reprinted by permission from [**the Licensor**]: [**Journal Publisher** (e.g. Nature/Springer/Palgrave)] [**JOURNAL NAME**] [**REFERENCE CITATION** (Article name, Author(s) Name), [**COPYRIGHT**] (year of publication), advance online publication, day month year (doi: 10.1038/sj.[**JOURNAL ACRONYM**].)

For Adaptations/Translations:

Adapted/Translated by permission from [**the Licensor**]: [**Journal Publisher** (e.g. Nature/Springer/Palgrave)] [**JOURNAL NAME**] [**REFERENCE CITATION** (Article name, Author(s) Name), [**COPYRIGHT**] (year of publication)

Note: For any republication from the British Journal of Cancer, the following credit line style applies:

Reprinted/adapted/translated by permission from [**the Licensor**]: on behalf of Cancer Research UK: : [**Journal Publisher** (e.g. Nature/Springer/Palgrave)] [**JOURNAL NAME**] [**REFERENCE CITATION** (Article name, Author(s) Name), [**COPYRIGHT**] (year of publication)

For Advance Online Publication papers:

Reprinted by permission from The [**the Licensor**]: on behalf of Cancer Research UK: [**Journal Publisher** (e.g. Nature/Springer/Palgrave)] [**JOURNAL NAME**] [**REFERENCE CITATION** (Article name, Author(s) Name), [**COPYRIGHT**] (year of publication), advance online publication, day month year (doi: 10.1038/sj.[**JOURNAL ACRONYM**])

For Book content:

Reprinted/adapted by permission from [**the Licensor**]: [**Book Publisher** (e.g. Palgrave Macmillan, Springer etc)] [**Book Title**] by [**Book author(s)**] [**COPYRIGHT**] (year of publication)

Other Conditions:

Version 1.0

Questions? customercare@copyright.com or +1-855-239-3415 (toll free in the US) or +1-978-646-2777.
